

UNCLASSIFIED

AD

**412684**

DEFENSE DOCUMENTATION CENTER

FOR

SCIENTIFIC AND TECHNICAL INFORMATION

CAMERON STATION, ALEXANDRIA, VIRGINIA



UNCLASSIFIED

NOTICE: When government or other drawings, specifications or other data are used for any purpose other than in connection with a definitely related government procurement operation, the U. S. Government thereby incurs no responsibility, nor any obligation whatsoever; and the fact that the Government may have formulated, furnished, or in any way supplied the said drawings, specifications, or other data is not to be regarded by implication or otherwise as in any manner licensing the holder or any other person or corporation, or conveying any rights or permission to manufacture, use or sell any patented invention that may in any way be related thereto.

**BLANK PAGES  
IN THIS  
DOCUMENT  
WERE NOT  
FILMED**

63-4-4

ASD-TDR-63-635

CATALOGED BY DDC  
AS AD No. 412684

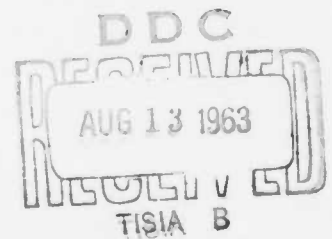
**THORIUM OXIDE - DIFFUSION OF OXYGEN,  
COMPATIBILITY WITH BORIDES,  
AND FEASIBILITY OF COATING BORIDES  
BY PYROHYDROLYSIS OF METAL HALIDES**

TECHNICAL DOCUMENTARY REPORT NO. ASD-TDR-63-635

July 1963

412684

AF Materials Laboratory  
Aeronautical Systems Division  
Air Force Systems Command  
Wright-Patterson Air Force Base, Ohio



Project No. 7350, Task No. 735001

(Prepared under Contract No. AF33(657)-8470 by General Electric Company  
Nuclear Materials and Propulsion Operation, Evendale, Ohio;  
H. S. Edwards, A. F. Rosenberg, and J. T. Bittel, Authors)



## NOTICES

When Government drawings, specifications, or other data are used for any purpose other than in connection with a definitely related Government procurement operation, the United States Government thereby incurs no responsibility nor any obligation whatsoever; and the fact that the Government may have formulated, furnished, or in any way supplied the said drawings, specifications, or other data, is not to be regarded by implication or otherwise as in any manner licensing the holder or any other person or corporation, or conveying any rights or permission to manufacture, use, or sell any patented invention that may in any way be related thereto.

Qualified requesters may obtain copies of this report from the Defense Documentation Center (DDC), (formerly ASTIA), Arlington Hall Station, Arlington 12, Virginia.

This report has been released to the Office of Technical Services, U.S. Department of Commerce, Washington 25, D.C., for sale to the general public.

Copies of this report should not be returned to the Aeronautical Systems Division unless return is required by security considerations, contractual obligations, or notice on a specific document.

## FOREWORD

This report was prepared by the Nuclear Materials and Propulsion Operation of the General Electric Company under USAF Contract No. AF 33(657)-8470. This contract was initiated under Project No. 7350, "Refractory Inorganic Nonmetallic Materials," Task No. 735001, "Refractory Inorganic Nonmetallic Materials: Non-Graphitic." This work was administered under the direction of the AF Materials Laboratory, Aeronautical Systems Division, Wright-Patterson Air Force Base, Ohio, with Mr. K. S. Mazdiasni as the project engineer.

This report covers work conducted from April 1962 to June 1963.

The authors gratefully acknowledge the contribution to this effort by R. Latta and G. Anderson for preparing the thoria spheres; by R. Wandstradt for extensive laboratory work on the coating and compatibility problems; by J. Beeler and Miss C. Menke for the computations reported in Appendix II; and by M. Cummings and J. Yalch for additional programming and computations.

## ABSTRACT

Measurements of self-diffusion of oxygen in  $\text{ThO}_2$  were complicated by slow exchange at the surface. The measured values of the diffusion coefficient,  $D$ , range from  $1.8 \times 10^{-13} \text{ cm}^2/\text{sec}$  at  $800^\circ\text{C}$  to  $3.5 \times 10^{-8} \text{ cm}^2/\text{sec}$  at  $1500^\circ\text{C}$ . The rate constant of the surface reaction,  $K$ , ranged from  $6.8 \times 10^{-10} \text{ cm/sec}$  at  $800^\circ\text{C}$  to  $1.3 \times 10^{-4} \text{ cm/sec}$  at  $1500^\circ\text{C}$ . The results may be expressed by equations of the form

$$D = D_0 \exp \left( \frac{-\Delta H_D}{RT} \right)$$

and

$$K = K_0 \exp \left( \frac{-\Delta H_K}{RT} \right)$$

Specifically

$$D = 4.4 \exp \left( \frac{-65,800}{RT} \right) \text{ cm}^2/\text{sec}$$

and

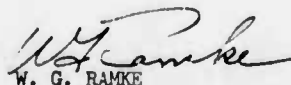
$$K = 7.6 \times 10^3 \exp \left( \frac{-63,800}{RT} \right) \text{ cm/sec}$$

The value  $D_0 = 4.4$  indicates that the diffusion was intrinsic in this temperature range.

Attempts to deposit dense impervious layers of  $\text{ThO}_2$  on selected solid borides ( $95\text{TiB}_2$  -  $5\text{CrB}_2$ ,  $\text{TiB}_2$ ,  $\text{ZrB}_2$ , and  $\text{HfB}_2$ ) by pyrohydrolysis of  $\text{ThCl}_4$  were essentially unsuccessful. The main problem was attack of the borides by  $\text{CO}_2$  in the coating gas. With further work, the pyrohydrolysis technique might prove to be an economical way to build up a coating of  $\text{ThO}_2$  that had been started by another method.

The commercially available boride samples which were tested reacted with  $\text{ThO}_2$  at temperatures in the range  $2400^\circ$  to  $2600^\circ\text{C}$ . The boride samples also reacted with graphite in the temperature range of  $2400^\circ$  to  $2700^\circ\text{C}$ . Because of these reactions, a graphite-boride-thoria system will be useful for only limited times at temperatures above  $2400^\circ\text{C}$ . While pure borides were not investigated, it is expected that their behavior would be similar to that of the commercial samples examined in this work.

This technical documentary report has been reviewed and is approved.



W. G. RAMKE  
Chief, Ceramics and Graphite Branch  
Metals and Ceramics Division  
Air Force Materials Laboratory

## CONTENTS

	Page
1. INTRODUCTION .....	1
2. OXYGEN TRANSPORT .....	2
2.1 Theory of Self-Diffusion .....	2
2.2 Mathematical Treatment .....	2
2.3 Experimental Equipment and Materials .....	6
2.4 Preliminary Evaluation of the Diffusion Apparatus .....	15
2.5 Treatment of Experimental Data and Calculation of Diffusion Coefficients .....	23
2.6 Discussion of Experimental Results .....	25
3. DEPOSITION OF COATINGS .....	35
3.1 Materials and Apparatus .....	35
3.2 Experimental Procedure and Program .....	37
3.3 Results .....	41
3.4 Conclusions .....	43
3.5 Recommendations .....	43
4. COMPATIBILITY OF ThO <sub>2</sub> WITH BORIDES .....	46
4.1 Published Data on Borides .....	46
4.2 Equipment .....	46
4.3 Materials .....	49
4.4 Experimental Program and Procedures .....	49
4.5 Reaction of Borides with Graphite .....	58
4.6 Conclusions .....	60
4.7 Recommendations .....	60
5. GENERAL RECOMMENDATIONS .....	61
APPENDIX I - Mathematical Solutions of the Diffusion Equation .....	65
APPENDIX II - Computations of Diffusion from a Limited Volume of Well-Stirred Fluid into a Sphere .....	91
APPENDIX III - Approximate Solution of Diffusion from a Limited Volume of Well- Stirred Fluid into a Sphere .....	101
APPENDIX IV - Exact Solution of Diffusion from a Limited Volume of Well-Stirred Fluid into a Sphere .....	111
APPENDIX V - Reduction of Mass Spectrometer Data .....	127
APPENDIX VI - Determination of Diffusion Coefficients with Consideration of a Phase Boundary Reaction .....	133
REFERENCES .....	141

## FIGURES

	Page
1 - Schematic diagram of diffusion apparatus .....	7
2 - Exploded view of reaction chamber .....	8
3 - Diffusion apparatus .....	9
4 - Plasma torch .....	11
5 - Particle feed system for inductively coupled plasma apparatus .....	12
6 - ThO <sub>2</sub> spheres -270/+320 mesh .....	13
7 - Behavior of $Dt/a^2$ versus $t$ .....	26
8 - Photomicrograph of spherodized thoria .....	28
9 - Arrhenius plot of uncorrected diffusion coefficients .....	31
10 - Arrhenius plot of corrected diffusion coefficients .....	32
11 - Arrhenius plot of the rate constant of the surface exchange reaction .....	33
12 - Transverse section of vapor deposited Al <sub>2</sub> O <sub>3</sub> coating on BeO .....	36
13 - Apparatus for coating BeO tubes with ThO <sub>2</sub> .....	39
14 - Apparatus for coating boride rods with ThO <sub>2</sub> .....	40
15 - BeO tube coated with vapor-deposited ThO <sub>2</sub> and an uncoated tube for comparison ...	42
16 - Transverse section of vapor deposited ThO <sub>2</sub> coating on BeO .....	42
17 - Electron microbeam probe scan across coating on ZrB <sub>2</sub> rod .....	44
18 - Appearance of boride rods before and after coating runs .....	45
19 - High-temperature tungsten tube furnaces in laboratory operation .....	48
20 - ThO <sub>2</sub> -HfB <sub>2</sub> sample after 1 hour in dry hydrogen at 2700°C .....	48
21 - Polished sections of ThO <sub>2</sub> -boride compacts after 1 hour in hydrogen of 0°C dewpoint .....	55
22 - Photomicrographs of ThO <sub>2</sub> -ZrB <sub>2</sub> compact after heating for 1 hour at 2600°C in hydrogen of 0°C dewpoint .....	56
23 - Photomicrograph of ThO <sub>2</sub> -TiB <sub>2</sub> compact after heating for 1 hour at 2600°C in hydrogen of 0°C dewpoint .....	59
24 - Ranges of validity of the exact and approximate diffusion equations .....	95
25 - Uptake by a sphere from a stirred solution of limited volume .....	96
26 - Behavior of Equation (I-117) for $F = 0.30$ and various values of $Q$ .....	123
27 - Behavior of Equation (I-117) for $F = 0.50$ and various values of $Q$ .....	124
28 - Behavior of Equation (I-117) for $F = 0.70$ and various values of $Q$ .....	125
29 - Typical mass spectrometer trace for enriched O <sub>2</sub> gas .....	128
30 - Typical mass spectrometer trace for enriched CO gas .....	129
31 - Typical mass spectrometer trace for enriched CO <sub>2</sub> gas .....	130

## LIST OF TABLES

	Page
1 - Numerical solutions of the diffusion equation for spheres with instantaneous equilibrium at the surface .....	4
2 - Precision of mass spectrometer determinations .....	14
3 - Summary of experimental diffusion runs .....	16
4 - Diffusion of $O^{16}$ into $ThO_2^{18}$ and $O^{18}$ into $ThO_2^{16}$ .....	29
5 - Description of boride rods .....	38
6 - Range of coating parameters for BeO tubes .....	41
7 - Range of coating parameters for boride rods .....	41
8 - Properties of borides .....	47
9 - Analyses of titanium diboride .....	50
10 - Analyses of zirconium and hafnium diborides .....	51
11 - Analyses of transition metal borides .....	52
12 - Analyses of rare earth metal borides .....	53
13 - Observations of $ThO_2$ pellets sintered in hydrogen and then fired in air at $1050^\circ C$ ..	57
14 - Liquefaction of borides in contact with graphite .....	57
15 - A short list of Laplace Transform pairs .....	66
16 - Comparison of $M_t/M_\infty$ computed from the exact and the approximate equations .....	93
17 - FORTRAN program for computation of diffusion into a sphere with instantaneous equilibrium at the surface .....	98
18 - Listing of FORTRAN program for computing $u/u_1$ versus $\sqrt{t}$ from Equation (I-123)..	102
19 - Sample output from FORTRAN program shown in Table 18 .....	105
20 - Listing of program for computing $M_t/M_\infty$ versus $(Dt/a^2)^{1/2}$ from Equation (I-123) .....	106
21 - Sample output from FORTRAN program shown in Table 20 .....	108
22 - Listing of FORTRAN program for computations with Equation (I-117) .....	112
23 - Sample calculations of $M_t/M_\infty$ versus $(Dt/a^2)^{1/2}$ from the program of Table 22 ....	120
24 - Sample calculation of the roots of the auxiliary equation used in obtaining Table 23..	121
25 - Sample calculation of the roots of the auxiliary equation used in obtaining Table 26..	121
26 - Sample calculation of $M_t/M_\infty$ versus $t$ from the program of Table 22 .....	122
27 - Sample gas-enrichment calculation for experiment No. 38 .....	132

## 1. INTRODUCTION

The usefulness of graphite would be markedly increased if it could be maintained in oxidizing atmospheres. It has been suggested that a high-melting boride might serve as a buffer between graphite and thorium oxide which might be protective if it could be kept from reacting with graphite. For a system of this type to be useful,  $\text{ThO}_2$  must be resistant to diffusion of oxygen, it must be capable of being applied to selected borides, and it must not react with them. The three parts of this research program, oxygen transport in thoria, deposition of coatings, and the compatibility of thoria with borides, were directed toward finding out if these aims could be achieved.

## 2. OXYGEN TRANSPORT

### 2.1 THEORY OF SELF-DIFFUSION

Diffusion is the process in which matter is transported by random molecular motion from one part of a system to another; in this study, the transport of a gas (oxygen) into a solid (thorium oxide) was investigated. The theory of gas migration through a solid has been treated by Kingery<sup>1</sup> and others<sup>2,3</sup>. The mathematics of the diffusion process is treated exhaustively by Crank<sup>4</sup> and others.<sup>5,6,7</sup> Most of the diffusion equations used in this research are derived and discussed in the appendices.

One of the simplest methods of measuring diffusion coefficients of a material is by observing the change in pressure as a gas diffuses through a membrane of this material. However, at elevated temperatures this method presents formidable obstacles partly because of difficulties in preventing gas leakage around the sample.

The approach favored by several investigators<sup>8,9</sup> has been to immerse the solid in a well-stirred gas. The mathematical equations describing this diffusion process have been solved only for solids in the form of a plane sheet, a cylinder, or a sphere. Most investigators have preferred spherical samples because they satisfy both the mathematical and the experimental needs.

The diffusion of oxygen into thoria is expected to be a two-step process, (1) oxygen exchange on the surface and (2) migration of oxygen into the solid. This second step usually is expected to be slower than the first and therefore to be the rate controlling one. The following tests can be made to gain confidence that diffusion is the rate-controlling step. The diffusion coefficient must be independent of the effective radius of the thoria spheres, the initial pressure, the initial enrichment, the molecular composition of the gas, and the time the reaction has proceeded.

### 2.2 MATHEMATICAL TREATMENT

The diffusion of a solute from a limited volume of well-stirred solution into a sphere of radius  $a$  is described by Equation (2-1). It is assumed that equilibration between the gas and the surface of the solid is instantaneous.

$$\frac{M_t}{M_\infty} = 1 - \sum_{a=1}^{\infty} \frac{6\lambda(1+\lambda)e^{-q_a^2 \frac{Dt}{a^2}}}{q_a^2 \lambda^2 + 9\lambda + 9} \quad (2-1)$$

where:

$M_t$  = amount of solute taken up by the sphere in time,  $t$

$M_\infty$  = amount of solute the sphere could take up in infinite time

$D$  = diffusion coefficient



$t$  = elapsed time  
 $a$  = radius of the sphere  
 $\lambda = (1 - F)/F$ , where  $1 - F$  = fraction of the solute remaining in the solution as  $t \rightarrow \infty$   
 $q_a$  = one of the non-zero, positive roots of  $\tan q_a = 3 q_a / (3 + q_a^2)$ .

It is often tedious and difficult to evaluate the solution to the above equation. Carman and Haul<sup>6</sup> developed an approximation to this equation which is more suited to hand calculations. This is given by Equation (2-2):

$$\frac{M_t}{M_\infty} = (1 + \alpha) \left[ 1 - \frac{\gamma_1}{\gamma_1 + \gamma_2} \text{erfc} \left( 3 \gamma_1 \frac{\sqrt{x}}{\alpha} \right) - \frac{\gamma_2}{\gamma_1 + \gamma_2} \text{erfc} \left( -3 \gamma_2 \frac{\sqrt{x}}{\alpha} \right) \right] + (\text{higher terms}) \quad (2-2)$$

where:

$$\gamma_1 = \frac{1}{2} \left[ \left( 1 + \frac{4}{3} \alpha \right)^{1/2} + 1 \right]$$

$$\gamma_2 = \gamma_1 - 1$$

$$x = \frac{Dt}{a^2}$$

$$\alpha = \frac{1 - F}{F}$$

$$\text{erfc } y \equiv (\exp y^2)(\text{erfc } y)$$

Using an IBM 7090 Computer, a program was established to:

1. Compare numerical solutions of the exact equation with numerical solutions of the Carman-Haul approximation.
2. Establish numerical values of  $M_t/M_\infty$  for  $\sqrt{Dt/a^2}$  from 0 to 0.40.

The comparison of the exact solution with the Carman-Haul approximation shows that the two equations give good agreement to five significant figures for:

$$0.02 < \left( \frac{Dt}{a^2} \right)^{1/2} < 0.10$$

For  $F > 0.75$ , the approximate equation should not be used. The  $M_t/M_\infty$  values it gives become greater than 1 and then approach 1 gradually from above with increasing  $F$ . Below values of  $(Dt/a^2)^{1/2} = 0.02$ , the program for the exact equation breaks down because only a limited number of roots can be handled conveniently, and the program for the Carman-Haul approximation has to be used.

Table 1 lists the computed values for  $M_t/M_\infty$  for  $0.0 < (Dt/a^2)^{1/2} < 0.40$  at values of the fractional uptake,  $F$ , from 0.10 to 0.90 in increments of 0.05. This group of values covers any possible experimentally useful range. A plot of the various uptake curves is given in Appendix IV.

If it is assumed that equilibration at the gas - solid interface proceeds at a finite rate, then Equation (2-3) is applicable:

$$\frac{M_t}{M_\infty} = 1 - \frac{2(1 + \lambda)}{3\lambda} \sum_{a=1}^{\infty} \frac{q_a^2 e^{-q_a^2 \frac{Dt}{a^2}}}{F \left( \frac{q_a^2 Q}{9} + \frac{1}{\lambda} \right) + F^2 + q_a^2 E^2 - \frac{2E}{\lambda}} \quad (2-3)$$

TABLE 1  
NUMERICAL SOLUTIONS OF THE DIFFUSION EQUATION FOR  
SPHERES WITH INSTANTANEOUS EQUILIBRIUM AT THE SURFACE

$(Dt/a^2)^{1/2}$	F = 0.90	F = 0.85	F = 0.80	F = 0.75	F = 0.70	F = 0.65	F = 0.60	F = 0.55
0.005	0.150	0.104	0.080	0.065	0.054	0.047	0.041	0.037
0.010	0.269	0.194	0.152	0.124	0.105	0.091	0.081	0.072
0.015	0.365	0.271	0.216	0.179	0.153	0.133	0.118	0.106
0.020	0.443	0.339	0.273	0.229	0.197	0.173	0.154	0.139
0.025	0.508	0.397	0.326	0.275	0.239	0.210	0.188	0.170
0.030	0.562	0.449	0.373	0.318	0.278	0.246	0.221	0.200
0.035	0.607	0.495	0.416	0.358	0.314	0.280	0.252	0.229
0.040	0.646	0.535	0.455	0.395	0.348	0.312	0.282	0.257
0.045	0.679	0.571	0.490	0.429	0.381	0.342	0.310	0.284
0.050	0.708	0.603	0.523	0.461	0.411	0.371	0.337	0.310
0.055	0.733	0.632	0.553	0.490	0.439	0.398	0.364	0.334
0.060	0.755	0.658	0.580	0.518	0.466	0.424	0.389	0.358
0.065	0.774	0.682	0.606	0.543	0.492	0.449	0.412	0.381
0.070	0.792	0.703	0.629	0.567	0.516	0.472	0.435	0.404
0.075	0.807	0.723	0.651	0.590	0.539	0.495	0.457	0.425
0.080	0.821	0.741	0.671	0.611	0.560	0.516	0.478	0.446
0.085	0.834	0.757	0.689	0.631	0.580	0.537	0.499	0.465
0.090	0.845	0.772	0.707	0.650	0.600	0.556	0.518	0.485
0.095	0.855	0.786	0.723	0.667	0.618	0.575	0.537	0.503
0.100	0.865	0.799	0.738	0.684	0.635	0.593	0.555	0.521
0.105	0.873	0.810	0.752	0.699	0.652	0.610	0.572	0.538
0.110	0.881	0.821	0.765	0.714	0.667	0.626	0.588	0.555
0.115	0.888	0.832	0.778	0.728	0.682	0.641	0.604	0.571
0.120	0.895	0.841	0.789	0.741	0.697	0.656	0.620	0.586
0.125	0.901	0.850	0.800	0.753	0.710	0.670	0.634	0.601
0.130	0.907	0.858	0.810	0.765	0.723	0.684	0.648	0.616
0.135	0.912	0.866	0.820	0.776	0.735	0.697	0.662	0.630
0.140	0.917	0.873	0.829	0.787	0.747	0.710	0.675	0.643
0.145	0.922	0.880	0.838	0.797	0.758	0.722	0.688	0.656
0.150	0.926	0.886	0.846	0.806	0.769	0.733	0.700	0.669
0.155	0.930	0.892	0.853	0.815	0.779	0.744	0.712	0.681
0.160	0.934	0.898	0.861	0.824	0.789	0.755	0.723	0.693
0.165	0.938	0.903	0.867	0.832	0.798	0.765	0.734	0.704
0.170	0.941	0.908	0.874	0.840	0.807	0.775	0.744	0.715
0.175	0.944	0.913	0.880	0.847	0.815	0.784	0.754	0.726
0.180	0.947	0.917	0.886	0.855	0.823	0.793	0.764	0.736
0.185	-	-	-	-	-	0.802	0.773	0.746
0.190	-	-	-	-	-	0.810	0.782	0.756
0.195	-	-	-	-	-	0.818	0.791	0.765
0.200	0.958	0.933	0.907	0.880	0.853	0.826	0.800	0.774
0.205	-	-	-	-	-	0.833	0.808	0.783
0.210	-	-	-	-	-	0.840	0.815	0.791
0.215	-	-	-	-	-	0.847	0.823	0.799
0.220	-	-	-	-	-	0.854	0.830	0.807
0.225	-	-	-	-	-	0.860	0.837	0.815
0.230	-	-	-	-	-	0.866	0.844	0.822
0.250	0.975	0.960	0.944	0.926	0.908	0.888	0.869	0.849
0.300	0.986	0.977	0.967	0.956	0.944	0.931	0.917	0.903
0.350	0.993	0.988	0.982	0.975	0.968	0.959	0.950	0.941
0.400	0.996	0.994	0.991	0.987	0.983	0.978	0.972	0.966

TABLE 1 (Cont.)

NUMERICAL SOLUTIONS OF THE DIFFUSION EQUATION FOR  
SPHERES WITH INSTANTANEOUS EQUILIBRIUM AT THE SURFACE

$(Dt/a^2)^{1/2}$	F = 0.50	F = 0.45	F = 0.40	F = 0.35	F = 0.30	F = 0.25	F = 0.20	F = 0.15	F = 0.10
0.01	0.065	0.060	0.055	0.051	0.047	0.044	0.042	0.039	0.037
0.02	0.126	0.116	0.107	0.099	0.093	0.087	0.082	0.078	0.073
0.03	0.183	0.169	0.157	0.146	0.137	0.128	0.121	0.115	0.109
0.04	0.236	0.219	0.203	0.190	0.179	0.168	0.159	0.151	0.143
0.05	0.286	0.266	0.248	0.233	0.219	0.207	0.196	0.186	0.177
0.10	0.491	0.464	0.440	0.418	0.398	0.379	0.363	0.348	0.334
0.15	0.640	0.613	0.588	0.565	0.543	0.523	0.504	0.487	0.470
0.20	0.749	0.726	0.703	0.682	0.661	0.642	0.623	0.605	0.588
0.25	0.830	0.811	0.792	0.773	0.755	0.738	0.721	0.705	0.689
0.30	0.889	0.874	0.859	0.844	0.830	0.815	0.801	0.787	0.773
0.35	0.931	0.920	0.909	0.898	0.887	0.875	0.863	0.852	0.840
0.40	0.959	0.952	0.944	0.936	0.928	0.920	0.911	0.902	0.893

where the symbols different from those in Equation (2-1) are:

$$q_a = \text{one of the non-zero, positive roots of } \tan q_a = \frac{q_a E}{F}$$

$$E = \frac{1}{\lambda} - \frac{Q}{9} q_a^2$$

$$F = \frac{1}{\lambda} + \frac{QN}{9} q_a^2$$

This F should not be confused with the fractional uptake.

$$N = \frac{3}{Q} - 1$$

$$Q = \frac{DS}{K}$$

$$S = \text{surface-to-volume ratio. For a sphere, } S = \frac{3}{a}$$

K = rate constant of the surface exchange reaction, in cm/sec.

The behavior of Equation (2-3) is discussed in Appendix IV.

## 2.3 EXPERIMENTAL EQUIPMENT AND MATERIALS

### Diffusion Apparatus

The experimental equipment for the determination of the diffusion coefficient of  $O_2$  in  $ThO_2$  is shown in Figures 1, 2, and 3. Its main part is a Vycor reaction vessel, 40 mm in diameter by approximately 200 mm long. The vessel is connected to a manifold that also has five double sample containers and a mercury manometer attached. One leg of the manifold contains an electro-magnetically operated miniature pump which enhances the gas circulation through the reaction vessel and the manifold. One end of the manifold is connected to a Toepler pump. To one leg of the Toepler pump, a 500 ml bulb containing the undiluted  $O_2^{18}$  is attached; to the other leg, a 1000 ml bulb that holds the used  $O_2^{18}$  is attached. In this way, most of the used  $O_2^{18}$  can be recovered and stored for further use. The entire system is connected to a mechanical vacuum pump for evacuation.

The reaction vessel has an optically flat Vycor window at one end to allow undistorted viewing and temperature measurements with an optical pyrometer.\* A 21-turn coil of 3/16-inch tubing, wound around the reaction chamber, is connected to a 2.5-KVA induction heater to heat a cylindrical susceptor inside the reaction vessel. Figure 2 is an exploded view of the reaction vessel and its contents. The  $ThO_2$  spheres are placed in a boat inside the susceptor along with some black body tubes to facilitate accurate temperature measurements.

Two susceptors were used during this investigation. A heavy-walled 50Pt - 50Rh susceptor of 3/4-inch diameter with 1/8-inch wall thickness was used for temperatures up to 1100°C. For temperatures above 1100°C, a 1/2-inch-diameter platinum tube with a 0.010-inch wall thickness was used. This tube had better coupling characteristics in the radio frequency field and therefore was easier to heat to higher temperatures.

---

\*After experiment 37 was conducted, a 10/30 standard taper joint was attached to the reaction vessel to allow the introduction of a Pt / Pt - 10Rh thermocouple for temperature measurement below 900°C.

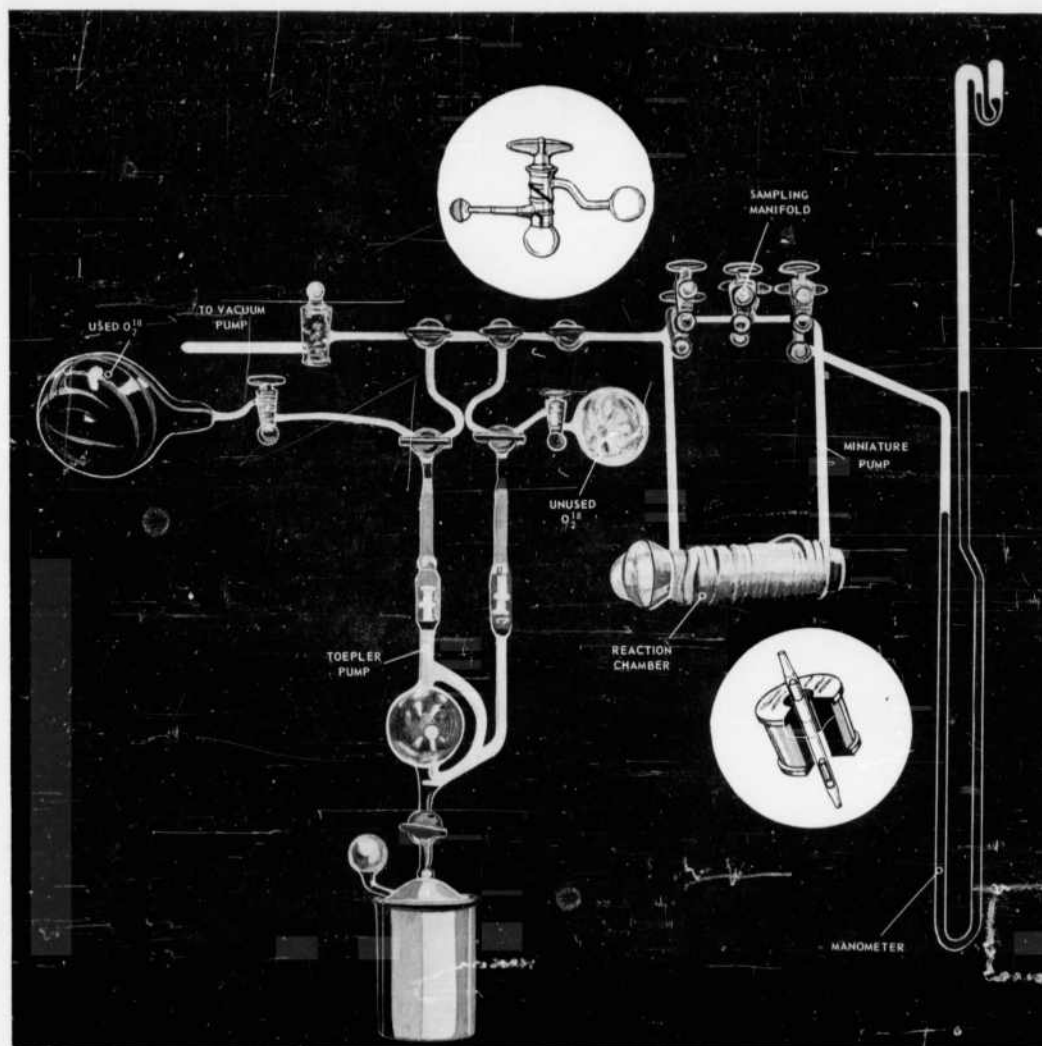


Fig. 1—Schematic diagram of diffusion apparatus—Inset: Cutaway drawings of sample bulb and electromagnetically operated miniature pump

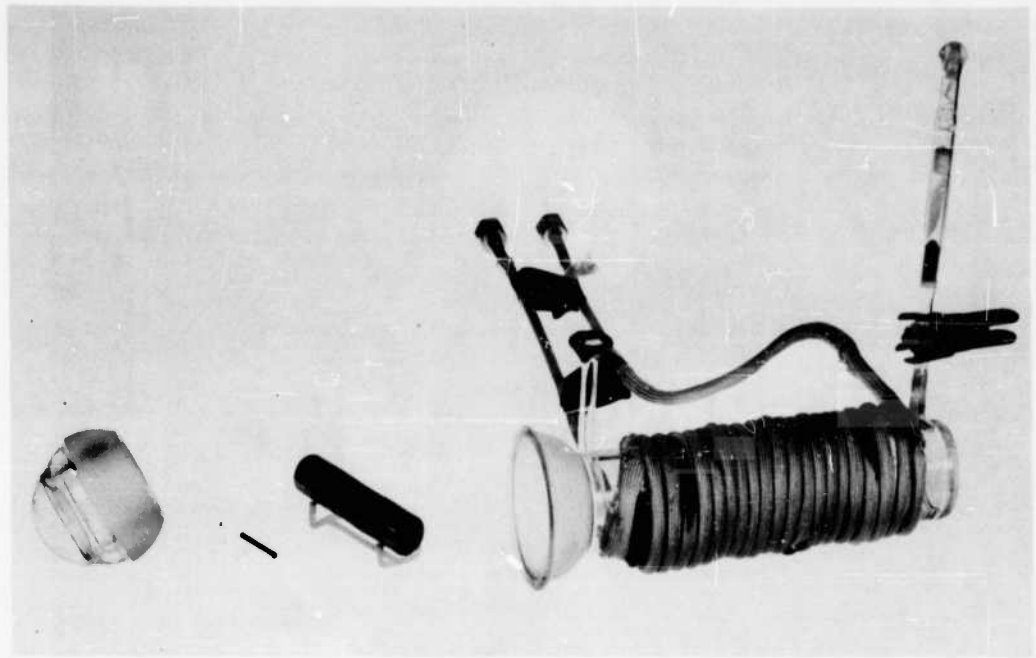


Fig. 2—Exploded view of reaction chamber (Neg. P62-8-17B)

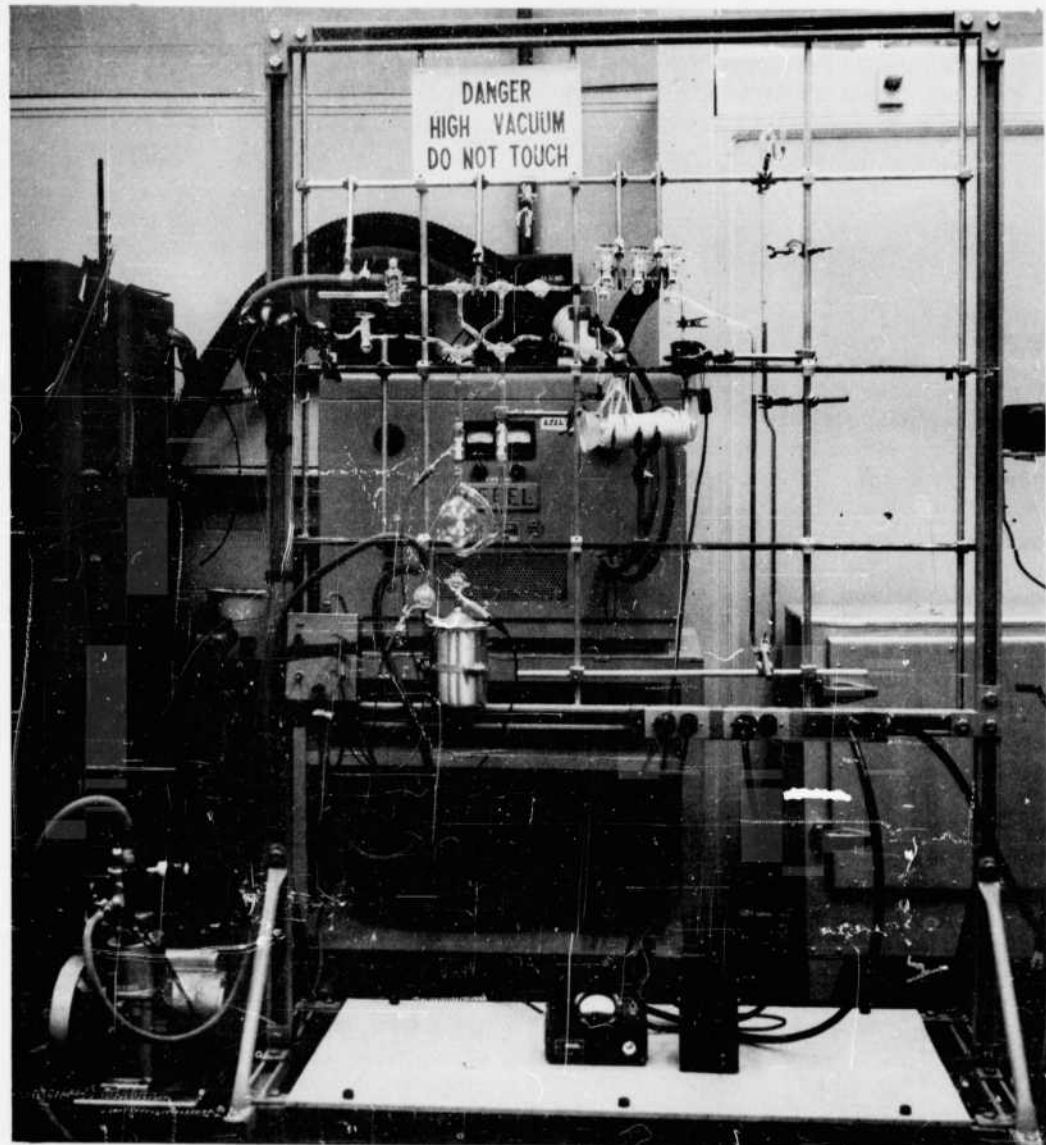


Fig. 3—Diffusion apparatus (Neg. P62-8-17a)

### Induction Coupled Plasma Torch

Spheres of relatively low melting solids are easily prepared by dropping powder through an oxygen-gas flame. Because of the short residence time in the hot zone, this method is unsuitable for refractory materials.

To prepare the diffusion samples for this work, it was necessary to heat  $\text{ThO}_2$  powder well above its melting point (approximately  $3300^\circ\text{C}$ ) and to quench the molten droplets rapidly to obtain spheres of the desired size and density. The usual techniques of resistance or induction heating will not easily produce the desired temperatures; therefore, an inductively coupled plasma apparatus was used. Drawings of this apparatus are shown in Figures 4 and 5. Reed<sup>10,11,12</sup> has discussed the theory and operation of this plasma torch in considerable detail.

After local preheating, argon can be ionized at atmospheric pressure by inductive coupling at approximately 4 megacycles or higher. The partially ionized gas then becomes electrically conductive, and approximately 50 percent of the power input of the radio frequency induction coil is transferred to the gas. This results in flames with temperatures of the order of  $15,000^\circ\text{K}$  at the center decreasing to  $5,000^\circ\text{K}$  at the outside. The  $\text{ThO}_2$  powder is swept up by a carrier gas and allowed to fall through the plasma torch where it is melted and spherodized. The spheres are then quenched in, and collected under, water. Figure 6 shows  $\text{ThO}_2$  spheres prepared this way. Several grams of spheres with diameters ranging from 44 to 74 microns have been prepared. It was thought that spheres of larger diameters could be produced in this manner. However, all attempts at making larger, dense spheres were unsuccessful.

A 300-micron-diameter powder was passed through the plasma torch repeatedly. Only partial spherodization was accomplished. Even the spheres which were made were not solid, but had central voids. The material was deemed unsuitable for use in this study.

### Mass Spectrometer

For each experiment, two samples were taken to obtain the initial gas composition. Experiments 1 through 8 were performed with gas samples containing the original 97.7 percent oxygen-18. These 15 samples were used to evaluate the performance of the mass spectrometer. The values obtained are listed in Table 2. From this table it can be seen that the precision of the mass spectrometer measurements is better than two parts per thousand at the highest enrichment. At the lowest enrichments it decreased to six parts per thousand. Actually the mass spectrometer may be capable of more precise measurements since it is quite possible that some of the samples may have contained very small amounts of air either because of insufficient initial pump-out of the diffusion apparatus or because of leakage. In any event, these data show that the mass spectrometer data are more precise than needed for this study.

### Materials

Thoria - The  $\text{ThO}_2$  used in this investigation was initially 99.7 percent pure. Spectrographic analyses revealed the following contaminants, at less than 100 ppm each: Si, Fe, Cr, Mn, Ca, Mg, Zr, Pb, and Na. The material was also examined for: Al, Ti, V, Bi, Mo, Sn, Y, Ag, Sb, As, Co, B, Zn, Ba, Sr, K, Nb, W, Li, and Cd. None of these was detected.

In preparing diffusion specimens, the fine  $\text{ThO}_2$  powder was extruded with hydroxymethyl-cellulose as a binder into 1/8-inch-diameter rods that were chopped into pellets and calcined at  $3100^\circ\text{F}$  for 4-1/2 hours in hydrogen, using molybdenum boats as containers. These pellets were then ground and sized prior to spherodizing.

Spectrographic analysis of a spherodized sample revealed less than 100 ppm each of Ca, Mg, and Fe contaminants. The material was also examined for: Si, Cr, Mn, Zr, Pb, Na, Al, Ti, Cu, Ni, V, Bi, Mo, Sn, Ag, Co, Sb, As, B, Sr, Ba, Zn, Nb, K, W, Li, and Cd. None of these was detected.



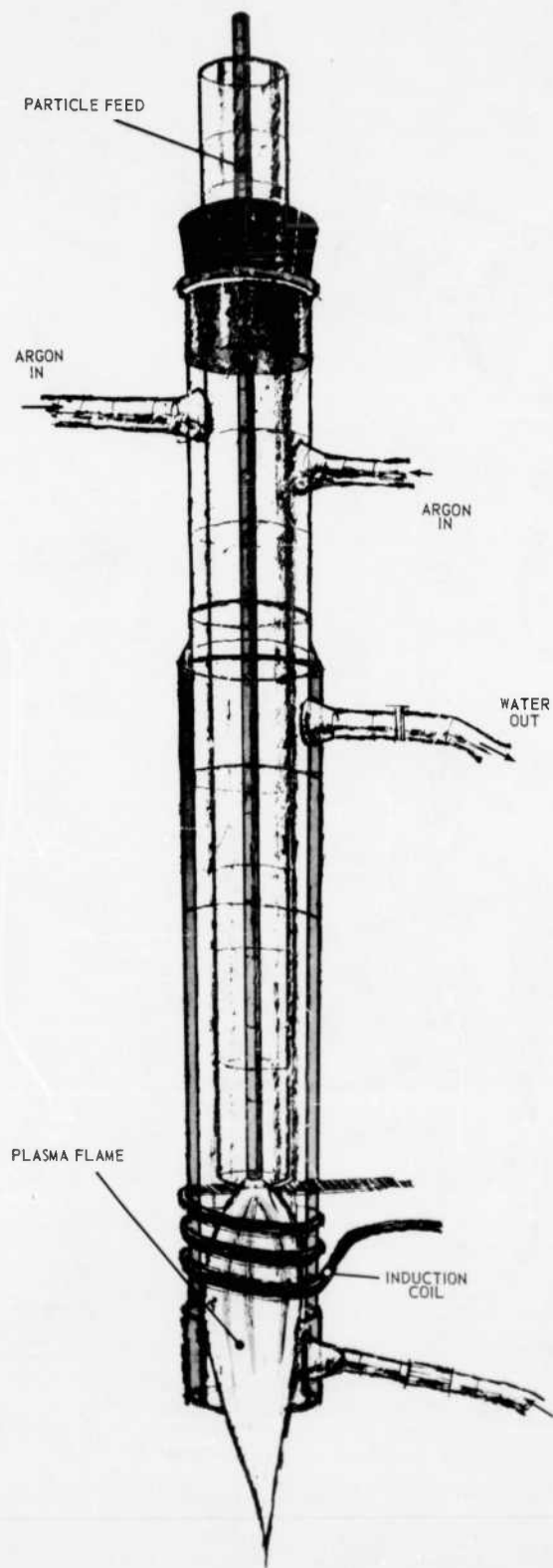


Fig. 4 - Plasma torch (AS-116)

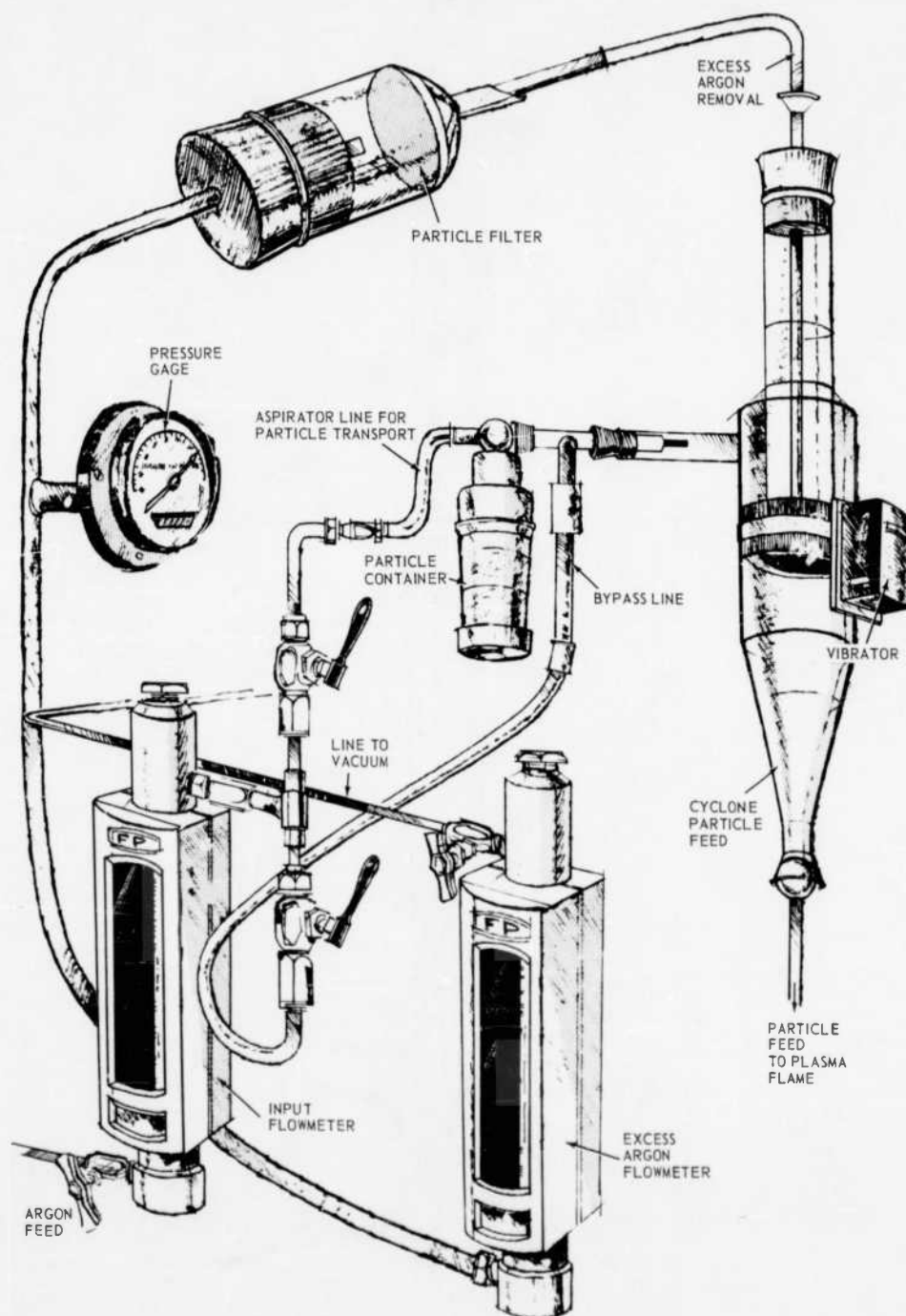
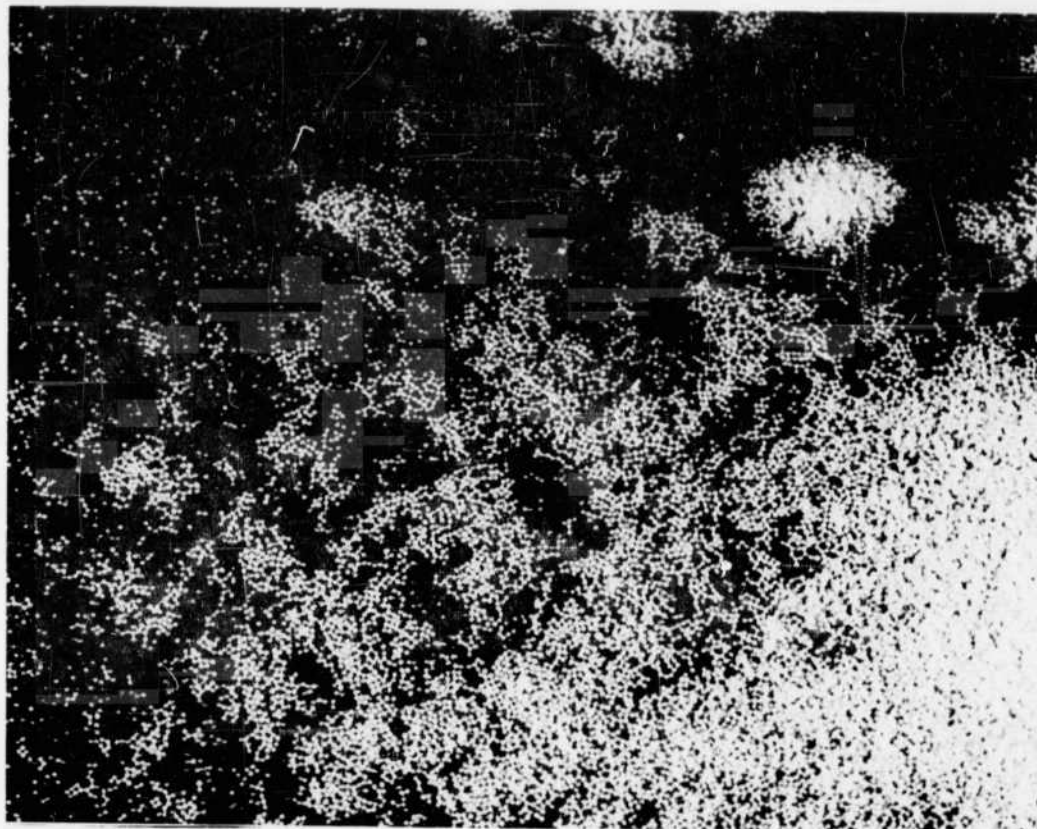


Fig. 5 - Particle feed system for inductively coupled plasma apparatus (AS-152)



Neg. P62-8-17C

Fig. 6—ThO<sub>2</sub> spheres -270/+320 mesh

40 X

TABLE 2  
PRECISION OF MASS SPECTROMETER DETERMINATIONS

Experiment No.	Sample No.	$O_2^{18}$ Content, %
I	3	97.47
	11	97.73
III	10	97.34
	15	97.29
IV	5	97.75
	15	97.72
V	5	97.73
	13	97.52
	15	97.73
VI	13	97.71
	15	97.71
VII	13	97.76
	17	97.73
VIII	E	97.73
	H	97.75
Average		97.64
Precision		$\pm 0.13\%$
Spread		97.76 - 97.29

Spectrographic analysis of the same sample after exchange with  $\text{CO}_2$  at approximately  $1000^\circ\text{C}$  (experiment 27) revealed only the same Ca, Mg, and Fe contaminants at less than 100 ppm each.

Stabilized Zirconia - A standard material with which to test and calibrate the equipment was desired. Based on the work of Kingery, et al.,<sup>8</sup> a particular formulation of stabilized zirconia ( $\text{Zr}_{0.85}\text{Ca}_{0.15}\text{O}_{1.85}$ ) appeared to be such a material. The material appears to be unexpectedly difficult to reproduce, however, and it was dropped from consideration as a standard. A given batch of stabilized zirconia would be useful for interlaboratory comparisons, but we were not able to accomplish such an intercomparison during the period of the contract.

Oxygen - The oxygen as received may have contained small amounts of carbon monoxide and carbon dioxide, but it was deemed unnecessary to use up any oxygen-18 to determine this exactly. Mass spectrometric analysis of a certified pure oxygen sample showed that small amounts of carbon monoxide and/or carbon dioxide are formed in the mass spectrometer during oxygen analysis. No other impurities were found. The distribution of oxygen isotopes was as follows: oxygen-18 = 97.7 percent, oxygen-17 = 0.4 percent, and oxygen-16 = 1.9 percent.

Carbon Dioxide - The as-received carbon dioxide may have contained small amounts of carbon monoxide, but no other impurities were detected by mass spectrometric analysis. The oxygen isotopic distribution was as follows: oxygen-18 = 89.4 percent, oxygen-17 plus oxygen-16 = 10.6 percent. The exact amount of oxygen-17 is difficult to determine since  $\text{C}^{12}\text{O}^{16}\text{O}^{17}$  has the same mass as  $\text{C}^{13}\text{O}_2^{16}$  and therefore gives rise to the same peaks in the mass spectrometer.

Carbon Monoxide - No impurities were detected by mass spectrometric analysis. The oxygen isotopic distribution was as follows: oxygen-18 = 76.8 percent, oxygen-17 = 0.9 percent, and oxygen-16 = 22.3 percent.

All the gases were reused, and after the initial use they contained varying amounts of CO and  $\text{CO}_2$  and had lower enrichments of oxygen-18 than indicated in the above listing. The starting composition of the gas for each experiment is listed in Table 3.

#### 2.4 PRELIMINARY EVALUATION OF THE DIFFUSION APPARATUS

It was deemed necessary to evaluate the design of the diffusion apparatus and to determine its usefulness in the determination of the diffusion coefficient of oxygen in  $\text{ThO}_2$ .

##### Gas Transfer

Since Toepler pumps are not normally operated at pressures envisaged for this study, the effectiveness of the Toepler pump in moving the gas into the storage bulb was checked. It was found that gas up to pressures of  $1/2$  atmosphere (the maximum expected to be encountered) could be moved conveniently.

##### Temperature Control and Temperature Measurements

The control of temperature over a long period of time was checked. It was found that the radio frequency generator tended to drift, but it was easily controlled manually. Temperature measurements at an indicated temperature of  $1060^\circ\text{C}$  were made for 2 hours; on one spot of the susceptor, the temperature remained constant at an indicated  $1060^\circ\text{C} \pm 5^\circ\text{C}$  during this time.

It is essential to know the exact test temperature. To determine the exact temperature with an optical pyrometer, it is necessary to have an object which has black body characteristics. For this purpose two  $1/16$ -inch-diameter holes were drilled into the heavy-walled susceptor parallel to the long axis of the cylindrical susceptor; one hole was  $5/8$ -inch deep and the other  $5/16$ -inch deep. A third hole was drilled  $1/16$ -inch wide by  $3/16$ -inch long by  $5/8$ -inch deep. When the temperature of the susceptor was maintained at approximately  $1000^\circ\text{C}$ , the apparent temperature of the three holes was the same within experimental reading error ( $\pm 3^\circ\text{C}$ ). This agreement indicates black body conditions in all three holes.

TABLE 3  
SUMMARY OF EXPERIMENTAL DIFFUSION RUNS

Experiment	Temperature, °C	Time, sec	Solid $O^{18}$ Enrichment, <sup>a</sup>		Gas $O^{18}$ Enrichment		$M_L$ $M_e$	$F$	Particle Size, $\mu$	Uncorrected $D$ , cm <sup>2</sup> /sec	Corrected $D$ , cm <sup>2</sup> /sec	$K$ , cm/sec
			m moles	%	Composition	m moles	%					
1	1000	0	3.825	N	$O_2^{18}$	1.943	97.60	-	0.682	24	-	-
		$5.4 \times 10^3$					41.63	0.859			$5.1 \times 10^{-11}$	-
		5.4					41.73	0.858			5.1	-
		12.6					33.85	0.990			-	-
5	1224	0	0.666	N	$O_2^{18}$	1.920	97.31	-	0.257	26	-	-
		$1.2 \times 10^5$					73.74	0.942			$6.7 \times 10^{-10}$	-
		1.2					73.57	0.949			9.0	-
		2.4					71.66	1.0			-	-
		2.4					71.34	1.0			-	-
		3.6					70.36	1.0			-	-
4	1005	0	1.208	N	$O_2^{18}$	2.363	97.73	-	0.336	24	-	-
		$1.6 \times 10^3$					81.94	0.477			$5.0 \times 10^{-11}$	-
		1.6					81.66	0.460			4.9	-
		3.6					77.03	0.625			5.2	-
		3.6					77.04	0.625			5.2	-
		5.4					73.43	0.734			5.8	-
5	1228	0	1.365	N	$O_2^{18}$	2.572	97.65	-	0.346	24	-	-
		$0.63 \times 10^{-3}$					99.29	0.657			$6.0 \times 10^{-10}$	-
		0.63					99.21	0.639			6.1	-
		1.11					96.05	0.932			6.0	-
		1.11					96.05	0.932			6.0	-
		5.4					73.49	0.732			5.7	-
6	1012	0	1.150	N	$O_2^{18}$	2.122	97.71	-	0.351	24	-	-
		$1.8 \times 10^3$					87.74	0.290			$1.4 \times 10^{-11}$	-
		1.8					87.78	0.289			1.4	-
		5.6					83.43	0.415			1.6	-
		5.6					83.59	0.411			1.6	-
		4.8					80.98	0.467			1.8	-
7	1026	0	0.461	N	$O_2^{18}$	1.226	97.75	-	0.281	34.5	-	-
		$1.2 \times 10^3$					91.96	0.211			$1.2 \times 10^{-11}$	-
		1.2					91.97	0.211			1.2	-
		2.22					90.68	0.257			0.95	-
		2.22					90.34	0.270			1.1	-
		5.3					57.73	1.0			-	-
8	1300	0	1.408	N	$O_2^{18}$	2.121	97.74	-	0.396	54.5	-	-
		$0.96 \times 10^3$					75.73	0.566			$2.5 \times 10^{-10}$	-
		0.96					76.25	0.552			2.4	-
		1.8					61.35	0.935			0.98	-
		1.8					61.88	0.922			0.89	-
		2.4					60.16	0.966			0.92	-
9	1229	0	1.123	N	$O_2^{18}$	2.216	97.73	-	0.339	34.5	-	-
		$0.6 \times 10^3$					55.42	0.661			$7.3 \times 10^{-10}$	-
		0.6					55.36	0.663			7.5	-
		1.2					61.34	0.830			8.4	-
		1.2					-	-			-	-
		1.8					49.62	0.901			8.6	-
10	842	0	0.980	N	$O_2^{18}$	2.448	97.73	-	0.266	24	-	-
		$1.8 \times 10^3$					71.98	-			-	-
		1.8					71.23	0.035			$18 \times 10^{-14}$	-
		3.0					71.26	0.035			-	-
		5.0					71.50	0.033			10.8	-
		4.2					71.55	0.030			8.4	-
11	1010	0	1.236	N	$O_2^{18}$	1.249	97.73	-	0.499	24	-	-
		$0.9 \times 10^5$					72.03	-			-	-
		0.9					67.73	0.054			$2.2 \times 10^{-12}$	-
		1.5					66.22	0.161			2.5	-
		1.5					66.29	0.159			2.6	-
		2.1					-	-			-	-
12	1012	0	1.046	N	$O_2^{18}$	1.169	64.19	0.216	0.470	24	-	-
		$1.2 \times 10^3$					64.19	0.216			-	-
		1.2					66.96	0.149			$3.0 \times 10^{-12}$	-
		2.4					66.93	0.151			3.1	-
		2.4					63.96	0.236			4.6	-
		2.4					62.49	0.295			4.9	-
		5.6					61.60	0.308			5.4	-
		5.6					61.64	0.307			5.4	-
		4.6					59.51	0.370			8.4	-
		4.6					59.53	0.369			6.3	-
		4.6					-	-			-	-
		4.6					-	-			-	-

TABLE 3 (Cont.)  
SUMMARY OF EXPERIMENTAL DIFFUSION RUNS

Experiment	Temperature, °C	Time, sec	Solid $O^{18}$ Enrichment, <sup>a</sup>		Gas $O^{18}$ Enrichment		$M_L$ $M_m$	F	Particle Size, $\mu$	Uncorrected $D$ , cm <sup>2</sup> /sec	Corrected $D$ , cm <sup>2</sup> /sec	K, cm/sec
			m moles	%	Composition	m moles						
13	1043	0	1.202	N	$O_2^{16}$	3.334	71.32	-	0.276	24	-	-
		$1.8 \times 10^3$					66.14	0.263			$1.3 \times 10^{-11}$	-
		1.6					66.43	0.246			1.1	-
		3.6					64.12	0.366			1.4	-
		3.6					64.11	0.366			1.4	-
		5.4					62.21	0.463			1.7	-
		6.4					62.10	0.468			1.7	-
		7.2					60.68	0.641			1.9	-
		7.2					60.67	0.541			1.9	-
14	620	0	0.732	N	$O_2^{16}$	1.611	64.54	-	0.329	20	-	-
		$1.8 \times 10^3$					63.88	-			-	-
		1.6					63.77	0.034			$10.2 \times 10^{-14}$	-
		3.6					63.75	-			-	-
		3.6					63.81	0.036			5.9	-
		6.4					63.72	-			-	-
		6.4					63.79	0.037			4.1	-
		7.2					63.77	-			-	-
		7.2					63.64	0.040			3.7	-
15	830	0	0.763	N	$O_2^{18}$	1.476	64.53	-	0.343	20	-	-
		$1.8 \times 10^3$					63.99	0.012			$1.4 \times 10^{-14}$	-
		1.6					64.00	0.012			1.4	-
		3.6					63.87	0.015			1.1	-
		3.6					63.87	0.015			1.1	-
		5.4					63.89	-			-	-
		7.2					63.78	-			-	-
		7.2					63.82	-			-	-
17	1464	0	1.001	N	$O_2^{18}$	1.802	64.36	-	0.360	34.5	-	-
		$1.0 \times 10^3$					40.52	-			-	-
		1.0					40.47	0.572			$2.8 \times 10^{-10}$	-
		1.8					40.46	-			-	-
		1.8					40.28	0.575			1.6	-
		2.7					40.27	0.577			1.1	-
		2.7					-	-			-	-
		3.6					40.10	-			-	-
		3.6					40.19	0.581			0.8	-
18	1400	0	0.921	N	$O_2^{18}$	1.615	64.60	-	0.366	34.5	-	-
		215					-	-			-	-
		228					48.81	0.752			$2.9 \times 10^{-9}$	-
		562					-	-			-	-
		585					41.98	0.957			3.8	-
		756					40.89	1.0			-	-
		770					40.88	1.0			-	-
		900					40.46	1.0			-	-
		911					40.44	1.0			-	-
19	1351	0	1.129	N	$O_2^{18}$	1.527	61.80	-	0.438	34.5	-	-
		502					37.97	-			-	-
		510					38.41	0.871			$2.1 \times 10^{-9}$	-
		692					36.48	-			-	-
		703					38.77	0.929			2.3	-
		998					-	-			-	-
		1010					35.17	0.982			2.5	-
		1331					34.89	-			-	-
		1344					35.14	0.991			-	-
20	1220	0	0.921	N	$O_2^{18}$	1.632	52.41	-	0.364	34.5	-	$7 \times 10^{-10}$
		$0.6 \times 10^3$					36.07	-			-	$3.0 - 6.1 \times 10^{-5}$
		0.6					36.80	0.702			$9.4 \times 10^{-10}$	-
		1.2					34.04	-			-	-
		1.2					34.25	0.819			7.6	-
		1.8					32.94	-			-	-
		1.6					33.04	0.671			6.6	-
		2.4					32.30	0.900			6.0	-
		2.4					32.39	-			-	-
21	1220	0	1.136	N	$O_2^{18}$	1.773	51.37	-	0.394	34.5	-	$10 \times 10^{-10}$
		$0.6 \times 10^3$					39.35	0.594			$4.6 \times 10^{-10}$	$2.9 \times 10^{-6}$
		0.6					-	-			-	-
		1.2					34.76	-			-	-
		1.2					34.73	0.821			7.3	-
		1.8					32.44	-			-	-
		1.6					32.57	0.932			9.7	-
		2.4					31.54	-			-	-
		2.4					31.76	0.974			9.4	-
22	1030	0	0.606	N	$O_2^{18}$	1.479	51.56	-	0.357	34.5	-	$8 - 10 \times 10^{-11}$
		$0.9 \times 10^3$					47.05	0.214			$2.1 \times 10^{-11}$	$7.0 - 6.7 \times 10^{-7}$
		0.9					-	-			-	-
		1.6					45.57	-			-	-
		1.6					45.27	0.335			3.7	-
		2.7					43.70	-			-	-
		2.7					43.35	0.436			4.9	-
		3.6					42.17	-			-	-
		3.6					41.89	0.520			5.9	-

TABLE 3 (Cont.)  
SUMMARY OF EXPERIMENTAL DIFFUSION RUNS

Experiment	Temperature, °C	Time, sec	Solid		Composition	Gas		$M_L$ $M_\infty$	F	Particle Size, $\mu$	Uncorrected $D_1$ cm <sup>2</sup> /sec	Corrected $D_1$ cm <sup>2</sup> /sec	K, cm/sec
			$O^{18}$ m moles	Enrichment, <sup>a</sup> %		$O^{18}$ m moles	Enrichment %						
23	1025	0	1.250	N	$O_2^{18}$	1.233	51.33	-	0.306	34.3	-	$6 - 8 \times 10^{-11}$	$7.3 - 9.9 \times 10^{-7}$
		$0.9 \times 10^3$					45.86	0.311			$4.0 \times 10^{-11}$		
		0.9					45.31						
		1.8					41.87	0.392			3.6		
		1.6					40.96						
		2.7					39.09	0.479			4.1		
		2.7					38.01						
24	910	0	1.017	N	$O_2^{18}$	1.839	51.62	-	0.359	24	-	$4 - 3 \times 10^{-12}$	$1.4 - 2.6 \times 10^{-8}$
		$1.8 \times 10^3$					50.66	0.094			$3.9 \times 10^{-13}$		
		1.6					50.36						
		4.1					49.96	0.094			5.1		
		4.1					49.87						
		6.5					48.96	0.141			7.2		
		6.5					49.03						
25	1320	0	0.886	N	$CO_2^{18}$	1.647	80.41	-	0.341	34.6	-	$3.5 - 3 \times 10^{-9}$	$1.2 - 1.7 \times 10^{-5}$
		250					66.93	0.736			$2.3 \times 10^{-9}$		
		293					63.63	0.780			2.6		
		453					52.63	0.877			2.9		
		635					60.64	0.943			3.2		
		675					69.61	0.975			3.6		
		890					69.04	0.996			-		
28	1220	0	1.012	N	$CO_2^{18}$	1.587	89.39	-	0.389	34.5	-	$2 - 3.6 \times 10^{-9}$	$1.3 - 4.3 \times 10^{-6}$
		460					63.37	0.692			$1.0 \times 10^{-9}$		
		470					64.97	0.703			1.0		
		520					62.49	0.774			1.1		
		530					62.16	0.780			1.1		
		806					60.29	0.834			1.2		
		813					60.24	0.839			1.2		
27	1045	0	1.032	N	$CO_2^{18}$	1.663	89.49	-	0.394	34.3	-	$5 \times 10^{-11}$	$4.3 - 3.4 \times 10^{-7}$
		$0.9 \times 10^3$					82.68	0.196			$1.9 \times 10^{-11}$		
		0.9					82.50						
		1.6					79.13	0.300			2.6		
		1.8					76.66						
		2.7					75.13	0.406			3.6		
		2.7					73.21						
28	925	0	1.052	N	$CO_2^{18}$	1.603	89.27	-	0.368	24	-	$1.5 \times 10^{-12}$	$2.7 - 3.6 \times 10^{-8}$
		$4.0 \times 10^3$					86.04	0.096			$3.2 \times 10^{-13}$		
		4.0					66.05						
		8.4					84.39	0.149			6.2		
		8.4					84.38						
		13.2					62.69	0.201			7.6		
		13.2					-				-		
29	1045	0	1.070	N	$CO^{16}$	1.601	76.72	-	0.402	34.5	-	$6 - 10 \times 10^{-11}$	$1.7 - 2.9 \times 10^{-7}$
		$0.76 \times 10^{-3}$					72.05	0.151			$1.3 \times 10^{-11}$		
		0.76					72.06						
		1.3					69.20	0.245			1.9		
		1.3					69.13						
		2.1					67.15	0.311			2.4		
		2.1					67.13						
30	1425	0	1.097	N	$CO^{18}$	1.661	76.66	-	0.386	34.5	-	$3 \times 10^{-9}$	$2.6 - 7.5 \times 10^{-3}$
		90					60.28	0.337			$3.0 \times 10^{-9}$		
		135					57.63	0.639			2.7		
		205					53.19	0.724			2.7		
		290					33.47	0.785			2.6		
		308					53.01	0.600			2.6		
		333					31.90	0.636			2.7		
31	1225	0	1.261	N	$CO^{16}$	1.666	76.91	-	0.430	34.3	-	$10 \times 10^{-10}$	$4.3 - 3.8 \times 10^{-5}$
		195					63.91	0.393			$4.3 \times 10^{-10}$		
		240					62.36	0.441			4.7		
		345					59.26	0.303			4.5		
		473					56.39	0.621			4.3		
		545					33.16	0.656			6.6		
		702					32.66	0.728			7.3		
		823					50.09	0.812			6.4		
		934					50.02	0.814			6.4		



TABLE 3 (Cont.)  
SUMMARY OF EXPERIMENTAL DIFFUSION RUNS

SUMMARY OF EXPERIMENTAL DIFFUSION RUNS															
Experiment	Temperature, °C	Time, sec	Solid		Composition	Gas		$M_2$	$\lambda$	Particle Size, $\mu$	Uncorrected $D$ , cm <sup>2</sup> /sec	Corrected $D$ , cm <sup>2</sup> /sec	$K$ , cm/sec		
			m moles	<sup>18</sup> O Enrichment, %		m moles	<sup>18</sup> O Enrichment %								
32	925	0	1.110	N	CO <sup>18</sup>	1.606	61.28	-	0.413	24	-	4 - 6 x 10 <sup>-12</sup>	4.2 - 5.2 x 10 <sup>-9</sup>		
		3.84 x 10 <sup>3</sup>					80.14	0.045			9.8 x 10 <sup>-14</sup>				
		7.2					69.91	0.058			8.8				
		10.9					59.42	0.073			9.8				
		14.4					68.92	0.093			11.6				
		16.0					67.96	0.131			19.2				
		22.3					57.06	0.166			25.3				
		26.8					58.36	0.195			30.4				
28.8	58.36	0.195	30.4												
33	1535	0	1.017	N	CO <sup>18</sup>	1.696	61.22	-	0.374	50	-	8 - 9 x 10 <sup>-9</sup>	7.5 - 13.5 x 10 <sup>-5</sup>		
		45					50.64	0.467			7.1 x 10 <sup>-9</sup>				
		76					48.72	0.646			6.8				
		110					46.85	0.637			7.0				
		175					44.21	0.743			7.4				
		215					43.28	0.784			7.3				
		245					42.58	0.815			7.5				
		267					42.08	0.837			7.7				
280	41.83	0.847	7.8												
34	1117	0	1.530	N	O <sub>2</sub> <sup>18</sup>	1.598	95.72	-	0.493	34.5	-	-	-		
		130					93.07	0.056			0.18 x 10 <sup>-11</sup>			-	-
		280						0.118			0.59			-	-
		480					85.72	0.212			1.3			-	-
		690						0.279			2.0			-	-
		915					72.99	0.481			6.4			-	-
		1165						-			-			-	-
		1480					99.05 <sup>b</sup>	0.135			2.8 x 10 <sup>-11</sup>			-	-
1820	0.256	4.9	-	-											
35	1120	0	1.530	49.52	O <sub>2</sub> <sup>18</sup>	2.203	99.05 <sup>b</sup>	-	0.12	34.5	-	3 - 4 x 10 <sup>-10</sup>	7.5 - 12 x 10 <sup>-7</sup>		
		0.27 x 10 <sup>3</sup>					96.32 <sup>b</sup>	0.135			2.8 x 10 <sup>-11</sup>				
		0.66					93.87 <sup>b</sup>	0.256			4.9				
		1.13					92.07 <sup>b</sup>	0.346			5.6				
		1.5					91.06 <sup>b</sup>	0.394			5.8				
		2.0					89.59 <sup>b</sup>	0.468			8.9				
		2.8					87.84 <sup>b</sup>	0.555			8.8				
		3.3					88.45 <sup>b</sup>	0.624			9.6				
4.1	85.01 <sup>b</sup>	0.695	10.9												
36	1120	0	1.530	N	O <sub>2</sub> <sup>18</sup>	2.854	75.79	-	0.367	34.5	-	10 x 10 <sup>-10</sup>	1.2 - 2.5 x 10 <sup>-6</sup>		
		0.3 x 10 <sup>3</sup>					71.07	0.172			4.8 x 10 <sup>-11</sup>				
		0.7					67.26	0.307			7.9				
		1.2					64.06	0.422			9.9				
		1.8					61.12	0.528			12				
		2.55					57.92	0.643			15				
		3.5					55.38	0.734			17				
		4.7					52.17	0.850			24				
6.2	49.94	0.930	29												
37A	917	0	1.530	51.41	O <sub>2</sub> <sup>18</sup>	0.721	98.06 <sup>b</sup>	-	0.703	34.5	-	5 - 6 x 10 <sup>-13</sup>	1.2 - 1.7 x 10 <sup>-9</sup>		
		0.47 x 10 <sup>3</sup>					97.14 <sup>b</sup>	0.029			1.6 x 10 <sup>-13</sup>				
		0.95					96.78 <sup>b</sup>	0.040			1.6				
		1.46					96.54 <sup>b</sup>	0.048			1.5				
		2.11					96.36 <sup>b</sup>	0.053			1.4				
		2.85					95.93 <sup>b</sup>	0.066			1.7				
		3.8					95.39 <sup>b</sup>	0.083			2.0				
		5.1					94.87 <sup>b</sup>	0.099			1.7				
		6.9					94.47 <sup>b</sup>	0.112			2.0				
		9.3					93.50 <sup>b</sup>	0.142			2.2				
12.7	92.46 <sup>b</sup>	0.175	2.5												
37B	1125	0	1.530	33.48	O <sub>2</sub> <sup>18</sup>	0.989	98.45 <sup>b</sup>	-	0.638	34.5	-	3 x 10 <sup>-10</sup>	4.3 - 6.5 x 10 <sup>-7</sup>		
		125					96.04 <sup>b</sup>	0.120			1.8 x 10 <sup>-11</sup>				
		340					93.30 <sup>b</sup>	0.257			1.8				
		700					90.16 <sup>b</sup>	0.413			8.3				
		1.2 x 10 <sup>3</sup>					87.35 <sup>b</sup>	0.553			8.7				
		1.79					85.12 <sup>b</sup>	0.665			10.7				
		2.55					83.06 <sup>b</sup>	0.767			13.8				
		3.3					81.75 <sup>b</sup>	0.833			15.9				
		4.4					80.45 <sup>b</sup>	0.898			18.8				
		5.6					79.77 <sup>b</sup>	0.931			19.7				
7.4	79.01 <sup>b</sup>	0.970	23.2												
37C	1256	0	1.530	21.14	O <sub>2</sub> <sup>18</sup>	1.738	98.90 <sup>b</sup>	-	0.490	34.5	-	1 - 2 x 10 <sup>-9</sup>	1.7 - 5.0 x 10 <sup>-6</sup>		
		30					96.76 <sup>b</sup>	0.202			4.6 x 10 <sup>-10</sup>				
		107					95.54 <sup>b</sup>	0.323			3.9				
		300					93.69 <sup>b</sup>	0.507			4.6				
		528					92.00 <sup>b</sup>	0.674			6.3				
		710					91.17 <sup>b</sup>	0.757			7.2				
		900					90.65 <sup>b</sup>	0.808			7.5				
		1.2 x 10 <sup>3</sup>					89.85 <sup>b</sup>	0.867			9.0				
1.6	89.35 <sup>b</sup>	0.937	9.8												
2.1	88.99 <sup>b</sup>	0.972	10.3												
2.6	88.72 <sup>b</sup>	0.999	-												
38	1127	0	1.313	N	O <sub>2</sub> <sup>18</sup>	1.639	47.48	-	0.443	34.5	-	5 - 8 x 10 <sup>-10</sup>	4.3 - 20 x 10 <sup>-7</sup>		
		1.2 x 10 <sup>3</sup>					33.48	0.666			3.0 x 10 <sup>-10</sup>				
		5.0					28.64 <sup>i</sup>	0.989			5.1				
		5.0					26.70 <sup>i</sup>	-			-				

TABLE 3 (Cont.)  
SUMMARY OF EXPERIMENTAL DIFFUSION RUNS

SUMMARY OF EXPERIMENTAL DIFFUSION RUNS																	
Experiment	Temperature, °C	Time, sec	Solid		Composition	Gas		$\frac{M_1}{M_2}$	F	Particle Size, $\mu$	Uncorrected $D_1$ , cm <sup>2</sup> /sec	Corrected $D_1$ , cm <sup>2</sup> /sec	K, cm/sec				
			m moles	<sup>18</sup> O Enrichment, <sup>a</sup> %		m moles	<sup>18</sup> O Enrichment %										
38B	1127	0	1.313	26.45	O <sub>2</sub> <sup>18</sup>	2.406	99.80 <sup>b</sup>	-	0.354	34.5	-	3 x 10 <sup>-10</sup>	2.6 x 10 <sup>-7</sup>				
		1.2 x 10 <sup>3</sup>					94.52 <sup>b</sup>	0.570			2.3 x 10 <sup>-10</sup>						
		4.5					91.61 <sup>b</sup>	0.894			3.1						
		4.6					91.53 <sup>b</sup>	0.692			3.1						
		4.6					91.70 <sup>b</sup>	0.874			2.8						
39	1124	0	1.313	0.48	O <sub>2</sub> <sup>18</sup>	3.187	47.83	-	0.289	34.5	-	5 x 10 <sup>-10</sup>	1.2 - 1.7 x 10 <sup>-6</sup>				
		0.3 x 10 <sup>3</sup>					44.30	0.255			1.5 x 10 <sup>-10</sup>						
		0.7					42.16	0.410			1.9						
		1.2					38.98	0.641			2.5						
		1.8															
		2.5									3.2						
		3.3									3.4						
		4.6					35.29	0.908			3.8						
		lost															
39B	1128	0	1.313	34.01	O <sub>2</sub> <sup>18</sup>	2.586	99.79 <sup>b</sup>	-	0.339	34.5	-	-	-				
		0.3 x 10 <sup>3</sup>															
		0.7															
		1.2															
		1.2															
		1.99															
		2.5															
		4.5					80.04 <sup>b</sup>	0.851			2.5 x 10 <sup>-10</sup>	-	-				

<sup>a</sup>N = natural abundance = 0.20%.

<sup>b</sup>In these cases the percentages refer to the diffusing species,  $O_2^{18}$ .

Another black body was made by drilling a 1/16-inch-diameter hole 1-inch deep into the end of a 1/8-inch-diameter platinum rod. This rod was moved longitudinally through the susceptor and its temperature compared with that indicated by the holes in the end of the susceptor. At 1000°C, the maximum difference was 4°C lower on the inside than on the outside. This indicates that uniform temperature throughout the length of the susceptor has been attained.

#### Gas Mixing Tests

If gas mixing were slow, an important error could occur because the change in concentration of the  $O_2^{18}$  occurs at the  $ThO_2$  in the reaction chamber and the samples for analysis are removed at the manifold.

The following experiment was performed to establish the speed of mixing. At room temperature, the apparatus was evacuated and then repressured to approximately 120 mm with pure  $N_2$ . The electromagnetically operated double-check-valve pump in one leg of the manifold was started; at a chosen time zero, an amount of  $O_2$  sufficient to raise the pressure by about 12 mm was quickly added. Gas samples were taken from the manifold after elapsed times of 0 second, 10 seconds, 30 seconds, 1 minute, 2 minutes, 3 minutes, 5 minutes, 10 minutes, and 30 minutes. The  $N_2:O_2$  ratio of the gas samples was determined with a mass spectrometer. The composition of the gas throughout the reaction system became homogeneous in less than 3 minutes. In a heated system thermal convection will improve gas mixing.

#### Error Analysis

The calculated diffusion coefficients could be affected by errors in determining the following quantities:

1. Initial pressure of the gas
2. Volume of the system
3. Weight of the solid material
4. Composition of the gas samples
5. Length of time the diffusion reaction has proceeded
6. Particle size of the solid material
7. Temperature measurement
8. Graphical conversion from  $M_t/M_\infty$  and  $F$  to values of  $(Dt/a^2)^{1/2}$
9. Withdrawal of gas samples.

The first four sources of errors listed affect the calculated values of  $F$  and  $M_t/M_\infty$ . Therefore, a given error will influence the calculated value of  $D$  depending on the magnitude of  $M_t/M_\infty$ .

Initial Gas Pressure and System Volume - The measurements of the gas pressure are accurate to within  $\pm 2$  mm of Hg. The volume of the system is known to within  $\pm 5$  milliliters. Both measurement errors have the same effect and are of comparable magnitude. The error is largest for the largest values of  $M_t/M_\infty$ , but at reasonable values for the fractional uptake,  $F$ , the relative error in  $Dt/a^2$  is still less than 1 percent when  $M_t/M_\infty = 0.900$ . Therefore, these errors can be neglected.

Weight of the Solid Material - The thoria spheres were weighed to the nearest one-tenth milligram. An error in the weight of thoria will have the same effect on the calculated diffusion coefficient as an error in the determination of the available gas. Since the weighing error is smaller than the error in the pressure measurement, it can be neglected.

Composition of the Gas Samples - Errors in the gas analysis can be caused by either leakage of air into the gas sample or by errors made during the mass spectrometric analysis of the samples. Gross air leakage into the sample is readily detected and the analysis of that sample can then be ignored. Undetected amounts of air could produce only inconsequential errors.

The precision of the mass spectrometric gas analysis is discussed in section 2.3. An error

of  $\pm 0.2$  percent in determining the initial oxygen-18 concentration could result in a sizable error in the calculated value for the diffusion coefficient when the change in the oxygen-18 concentration is small. The actual magnitude of the error produced in the diffusion coefficient by an error of 0.2 percent in the oxygen-18 concentration depends on the values of other parameters, such as  $M_t/M_\infty$ , amount of gas present,  $F$ , etc. However, for most values of the variables used in these experiments the error in the diffusion coefficient that could be caused by an error of 0.2 percent absolute in the oxygen-18 concentration does not exceed  $\pm 5$  percent relative.

Time of Diffusion Reaction - An error in specifying the elapsed time attributed to a specific gas composition can arise because of (1) the undefined time required for the gas to move from the reaction site to the sampling point, (2) the selection of the time at which the desired temperature was reached, and (3) the diffusion and exchange which occurred prior to reaching this desired temperature.

The error caused by a lag in the gas mixing is largest at the lowest temperature, and decreases with increasing temperature. When the error in fixing the starting time is largest, the elapsed time also is large and the net effect on the calculated diffusion coefficient is negligible.

The second possible source of error can be neglected since the time at which the desired temperature was reached can be determined to  $\pm 3$  seconds. The last possible source of error can also be ignored since the rate of the diffusion reaction decreases rapidly with decreasing temperature and the rate of heating was high.

At higher temperatures where short reaction times were employed, it was necessary to know the elapsed time accurately since any given error in it produces a proportional error in the diffusion coefficient. A plot of  $Dt/a^2$  versus  $t$  for the data obtained from experiment 33 missed the origin by 3 seconds, indicating that elapsed times could be determined accurately, even when the total time was short.

The diffusion coefficient  $D$  is inversely proportional to  $t$ , the time the reaction has proceeded; therefore, the percentage error in the calculated diffusion coefficient is of the same magnitude as the percentage error in the measured time. At the lower temperature where the error is the largest, the reaction was observed for several thousand seconds; the error was less than 3 percent. At the higher temperature where the diffusion reaction was observed for only several hundred seconds, the error could be as large as 100 percent, but as mentioned above the actual error is much smaller.

Particle Size of the Solid Material - The diffusion coefficient,  $D$ , is directly proportional to the square of the radius,  $a$ , of the spheres employed; therefore, any relative error in the radius will give rise to approximately twice that error in the diffusion coefficient.

The thoria spheres were sieved into as small a range as commercially available sieves allowed. Microscopic examination of the spheres showed that almost all of the particles fell within the indicated range, and that within that range the distribution appeared to be nearly uniform. It was assumed that the root-mean-square average diameter was equal to the average of the hole sizes of the sieves used in making the sphere separation. Permissible screen tolerances could lead to errors of about  $\pm 15$  percent in the square of the diameter.

Temperature Measurement - An error in the temperature measurement will not affect the calculated value of the diffusion coefficient. It will, however, affect the calculation of the activation energy from the diffusion coefficients. During a diffusion experiment the temperature varies by as much as  $\pm 10^\circ\text{C}$ . Calibration errors of the optical pyrometer and varying deposits on the viewing window also could give rise to a  $\pm 10^\circ\text{C}$  error.

Graphical Conversion - The errors caused by converting values of  $M_t/M_\infty$  and  $F$  to values for  $(Dt/a^2)^{1/2}$  are probably very small. They are caused by interpolating between the available curves for  $F$  values and by possible errors in the curves themselves. The errors in  $D$  from this source

should not exceed  $\pm 5$  percent. The form of the solution of the diffusion equation made it necessary to program the computer to calculate values of  $M_t/M_\infty$  from assumed sets of values of  $(Dt/a^2)^{1/2}$  and  $F$ . It was not possible to eliminate the graphical interpolation errors by direct computation of  $(Dt/a^2)^{1/2}$  from experimentally obtained values of  $F$  and  $M_t/M_\infty$ .

Withdrawal of Gas Samples - The removal of gas samples for analysis could cause an error in  $M_t/M_\infty$  by changing the amount of gas available for exchange. A total of 10 samples of approximately 3 milliliters each is withdrawn during an experiment. Two samples are taken before the pressure measurement at the beginning of the experiment and two are taken at the end; therefore, these four do not contribute to any possible error. The other six samples have a combined volume of 18 ml. The system volume is approximately 400 ml; therefore, the maximum possible error from this source would be a change of up to 4.5 percent in the calculated  $M_\infty$ .

The effect of sample withdrawals was checked in experiments 38 and 39. The diffusion coefficient,  $D$ , was determined at approximately 1125°C. Six samples were withdrawn during the course of one 4500-second run. In the other run of the same duration, samples were taken at 1200 and 4500 seconds. No difference was detected in the diffusion coefficients calculated from the two runs.

## 2.5 TREATMENT OF EXPERIMENTAL DATA AND CALCULATION OF DIFFUSION COEFFICIENTS

### Calculation of $M_t/M_\infty$

Gas samples withdrawn from the apparatus during a diffusion run were analyzed by the mass spectrometer and the mole percent of the desired isotope (usually  $O^{18}$ ) in each sample was determined as discussed in Appendix V. The results for experiment 38 determined in this manner are given below. Following that is a summary of the other parameters measured during the experiment and a sample calculation of  $M_t/M_\infty$ .

Sample Number	Elapsed Time, seconds	Percent Of $O_2^{18}$
A	0	47.48 av.
C	0	
D	1200	33.48
B	5000	26.64
14	5000	26.70

### Sample Calculation

Data from experiment 38:

Volume of system = 382 ml.

Pressure of  $O_2$  gas = 80.5 mm Hg

Temperature = 27.8°C

$$\text{m moles } ^* O_2 \text{ gas} = \frac{382 \text{ ml}}{22.4 \text{ ml/m mole}} \times \frac{273^\circ\text{K}}{300.8^\circ\text{K}} \times \frac{80.5 \text{ mm Hg}}{760 \text{ mm Hg}} = 1.639 \text{ m moles } O_{2(g)}$$

\* m moles  $\equiv$  millimoles

$$\begin{aligned} \text{m moles O}^{18} &= \left(0.4748 \text{ O}^{18}_{(g)}\right) \left(1.639 \text{ m moles gas}\right) + \left(0.0020^* \text{ O}^{18}_{(s)}\right) (1.313 \text{ m moles solid}) \\ &= 0.7810 \end{aligned}$$

$$\begin{aligned} \text{m moles O}^{16} &= \left(0.5252 \text{ O}^{16}_{(g)}\right) \left(1.639 \text{ m moles gas}\right) + \left(0.9980 \text{ O}^{16}_{(s)}\right) (1.313 \text{ m moles solid}) \\ &= 2.1717 \end{aligned}$$

$$\text{Total m moles O}_2 = 2.9527$$

$$\text{mole fraction O}^{18} = \frac{0.7810}{2.9527} = \frac{\text{O}^{18}}{\text{O}^{18} + \text{O}^{16}} = 0.2645$$

$$\begin{aligned} M_{\infty} &= (\text{mole fraction O}^{18})(\text{m moles O}_{(s)}) - \text{initial m moles O}^{18}_{(s)} = 0.2645 (1.313) - 0.0026 \\ &= 0.3448 \end{aligned}$$

$$F = \frac{M_{\infty}}{\text{m moles O}^{18}_{(g)}} = \frac{0.3448}{0.7784} = 0.443$$

$$\text{Weight of ThO}_2 = 346.7 \text{ mg}$$

$$\text{m moles O}_2 \text{ solid} = \frac{346.7 \text{ mg}}{264 \text{ mg/m mole}} = 1.313 \text{ m moles O}_{2(s)}$$

$$\text{Average radius of thoria spheres} = 34.5 \mu = 3.45 \times 10^{-3} \text{ cm}$$

For sample D:

$$\text{O}_2^{18}_{(s)} = \left(\text{conc. O}_2^{18}_{(g)t=0} - \text{conc. O}_2^{18}_{(g)t=t}\right) \times \text{m moles O}_{2(g)} = [(0.4748) - (0.3348)] \times$$

$$1.639 = 0.229^5 = M_t$$

$$\frac{M_t}{M_{\infty}} = \frac{0.229^5}{0.344^8} = 0.666$$

#### Calculation of Diffusion Coefficients

For a first trial calculation, it is convenient to assume that the rate of exchange at the surface of the spheres has no effect on the measurement of D. If the values of D found in this way are not constant, then one tries to find both a D and a K which together give agreement between theory and experiment.

When the surface reaction is assumed to have no effect on the measurements, the known values of F and  $M_t/M_{\infty}$  are used to find  $(Dt/a^2)^{1/2}$  from the graph shown in Figure 24 of Appendix II. As an example, for experiment 35 (Sample D)  $M_t/M_{\infty} = 0.666$  and  $F = 0.443$ . This leads to  $(Dt/a^2)^{1/2} = 0.175$ , then

$$\begin{aligned} D &= \left[ \left( \frac{Dt}{a^2} \right)^{1/2} \right]^2 \frac{a^2}{t} \\ &= \frac{(0.175)^2 (3.45 \times 10^{-3})^2}{1.2 \times 10^3} \end{aligned}$$

$$D = 3.0 \times 10^{-10}$$

\*Natural abundance

If a plot of  $(Dt)$  versus  $t$  or  $(Dt/a^2)$  versus  $t$  is a straight line passing through the origin, as shown in Figure 7a, then the value of  $K$  is assumed to be so large that the measurements are not influenced by any finite rate of exchange at the surface. In many of the experiments conducted, particularly those at the lower temperatures, the plots of  $Dt/a^2$  versus  $t$  showed positive curvature as shown in Figure 7b. These experiments required further treatment of the data.

When it appears that the surface reaction is important, the experimental variation of  $M_t/M_\infty$  with time must be compared with the computed behavior of  $M_t/M_\infty$  when various pairs of values of  $D$  and  $K$  or  $D$  and  $Q$  are chosen. The best fit of chosen values with the experiment is achieved by successive trials. The problem is to choose the trial pairs of  $D$  and  $K$  as efficiently as possible.

An attractive way to choose the trial pairs of  $D$  and  $K$  would be to apply the approximate equation discussed in section I.6 of Appendix I and in Appendices III and VI. In this case, an attempt is made to match the experimentally determined variation of enrichment of the gas with time against one of the tabulated columns of values. If a match is found, the values of  $\alpha$  and  $\beta$  for the tabular column lead to values of  $D$  and  $K$ . Before such an attempt is made, one must determine that the exact and approximate equations match satisfactorily over the desired range of times. Since the value of  $F$  (or  $\lambda$ ) is known from the experimental conditions, such information can be obtained roughly from the graphs in Appendix IV. As  $F$  increases, the exact and the approximate equations are in disagreement down to smaller values of time.

Both the experimental and the calculated behaviors may show a point of inflection. Such points of inflection were marked in the tables to aid in selecting columns for more detailed comparison with the experimental values. Even with this added criterion, it frequently was not possible to choose  $\alpha$  and  $\beta$  with the desired accuracy. Overall, the approximate equation was not found to be as useful as it originally was thought to be.

A second method for approximating the value of  $D$  is to calculate it from the limiting slope of a plot such as shown in Figure 7b. This is possible because the surface reaction will have progressively less influence on diffusion in the solid as  $M_t/M_\infty \rightarrow 1$ .

Once a trial value of  $D$  has been obtained, it is used in conjunction with various assumed values of  $Q$  to produce sets of  $M_t/M_\infty$  as a function of  $t$ . The same procedure is used with at least one value of  $D$  greater than the best trial value and one value of  $D$  which is smaller. Comparison of this group of calculations with the experimental set of calculations either permits the decision that  $D$  and  $K$  have been determined within achievable accuracy or it permits the choice of new trial values of  $D$ .

When a set of values of  $D$  and  $K$  has been obtained for a group of measurements over a range of temperatures, linear plots should be obtained for  $\log D$  versus  $1/T$  and for  $\log K$  versus  $1/T$ ; unless there is reason to think, for example, that both intrinsic and extrinsic behavior are being observed.

## 2.6 DISCUSSION OF EXPERIMENTAL RESULTS

A total of 42 diffusion experiments were attempted using  $O_2$ ,  $CO$ , or  $CO_2$  as the source of oxygen-18. Omitting four experiments that were failures, there were 29 with  $O_2$  as the source of oxygen-18, 5 with  $CO$ , and 4 with  $CO_2$ . In experiment 16 the apparatus failed before any samples were taken. In experiments 8 and 34 known malfunctions occurred during the runs. Experiment 17 stopped at 50 percent completion. Subsequent experiments indicated that this unique behavior was caused by a weighing error or that a substantial part of the sample was lost. The remaining 38 experiments can not be evaluated equally because various samples taken during a run were lost or were removed after diffusion had proceeded too far to yield usable data. Experiments 11 and 12 were performed with thoria which was spherodized in a hydrogen - argon atmosphere. This particular batch was black after passage through the plasma flame, indicating that the thoria had been made substoichiometric. Therefore, the spheres were oxidized overnight in oxygen at  $800^\circ C$  and

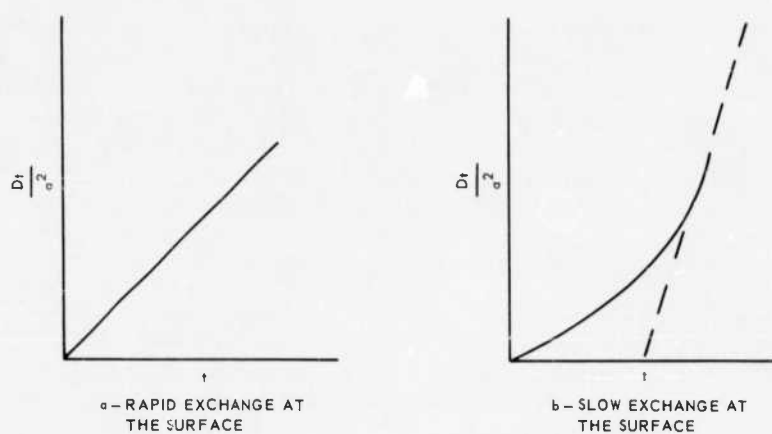


Fig. 7 - Behavior of  $\frac{D_t}{a^2}$  versus  $t$



were equilibrated with air at approximately 1500°C before use. The air equilibration was followed with all subsequent experiments.

The first ten experiments were performed with ThO<sub>2</sub> which was spherodized in small experimental batches during attempts to determine the best way to make spheres with the inductively coupled plasma torch. Some of these preparations were made in hydrogen - argon atmosphere and others were made in oxygen - argon atmosphere. In all of the first ten experiments, the spheres were used without further treatment, since it had not yet been realized that nonstoichiometry might be a problem. The first batches were not markedly discolored; therefore, the errors in the first ten runs due to nonstoichiometry probably were minor. Experiments 13 through 39 were performed with samples from a single batch of thorium which was spherodized in an oxygen - argon atmosphere. Microscopic examination of this batch of spheres (Figure 8) showed that approximately one-half of the spheres were transparent and the other half were cloudy. The sample also contained some large irregular unfused particles. By examination of etched sections, the transparent spheres were seen to be single crystals, while the cloudy spheres were polycrystalline. Not all of the spheres were solid. Some showed small central voids that were thought to be due to the unavoidable shrinkage caused by the rapid quenching during the spherodizing process.

#### Measured Diffusion Coefficients

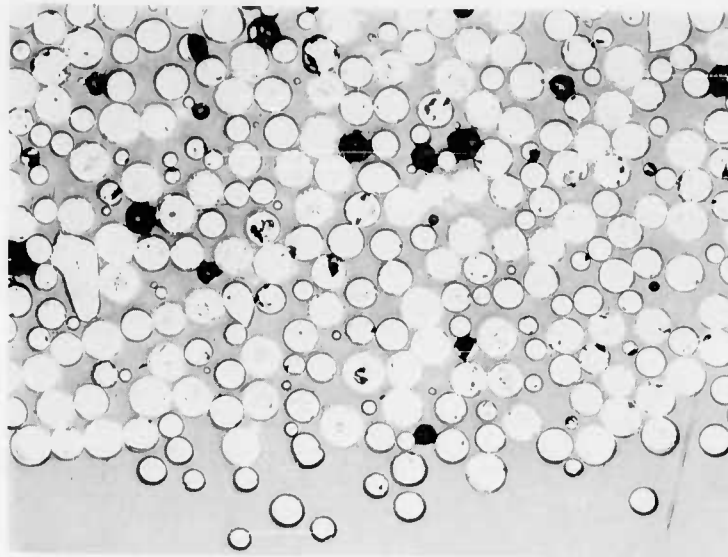
It is necessary to show that the measured diffusion coefficients are independent of certain experimental parameters. Such checks do not prove conclusively that the measurements are free of systematic error, but the variety of tests discussed below rule out a very wide range of such errors. The diffusion coefficient,  $D$ , should be independent of:

1. The radius of the spheres
2. The pressure of the gas used
3. The composition of the gas used
4. The initial concentration of the diffusing isotope
5. The particular isotope used
6. The fractional uptake,  $F$
7. The elapsed time.

For obvious experimental reasons it was not possible to vary some of these parameters as widely as would be desirable. Unless it is otherwise noted, "uncorrected diffusion coefficients" (defined on page 30) are used in the following discussions.

Radius of the Spheres - The diffusion coefficient can be shown to be independent of the thorium sphere diameter by utilizing spheres of different sizes. At approximately 1000°C (experiments 1, 4, 6, 7, and 13) using 48-micron-diameter spheres,  $D$  varied from 1.0 to 5.7 x 10<sup>-11</sup>; using 79-micron-diameter spheres (experiments 22 and 23),  $D$  varied from 2.1 to 5.9 x 10<sup>-11</sup>. At 1200°C two experiments (3 and 5) were performed using 48-micron-diameter spheres;  $D$  varied from 8.0 to 9.0 x 10<sup>-10</sup>. Using 79-micron-diameter spheres, at the same temperature, three experiments (9, 20, and 21) were performed;  $D$  varied from 6.0 to 9.7 x 10<sup>-10</sup>. These data indicate that the diffusion coefficient is independent of the diameter of the spheres used.

Pressure of the Gas Used - To test the independence of the diffusion coefficient from the gas pressure, the pressure of the gas was varied by a factor of two. At approximately 1000°C and an oxygen pressure of 158 mm (experiment 13),  $D$  varied from 1.1 to 1.9 x 10<sup>-11</sup>; at an oxygen pressure of 59 mm (experiment 23),  $D$  varied from 4.0 to 5.1 x 10<sup>-11</sup>. At approximately 1200°C and an oxygen pressure of 157 mm (experiment 5),  $D$  was 8.0 x 10<sup>-10</sup>; at an oxygen pressure of 75 mm (experiment 20),  $D$  varied from 6.0 to 9.4 x 10<sup>-10</sup>. These data indicate that the calculated diffusion coefficient is independent of the gas pressure.



Neg. 1930

100 X

Fig. 8—Photomicrograph of spherodized thoria

Composition of the Gas Used - To examine the independence of the diffusion coefficient of oxygen in thoria from the composition of the gas used, experiments (25-33) were performed with CO and CO<sub>2</sub>. The calculated diffusion coefficients in the temperature range of 900° to 1300°C using CO, CO<sub>2</sub>, or O<sub>2</sub> as the source of oxygen-18 yielded comparable diffusion coefficients. This indicated that the diffusion coefficient is independent of the gas used.

Initial Concentration of the Diffusing Isotope - To examine the independence of the diffusion coefficient from the initial oxygen-18 enrichment of the gas, similar experiments were performed using different oxygen-18 concentrations. At approximately 1000°C and 98 percent O<sub>2</sub><sup>18</sup> (experiment 6) the calculated diffusion coefficient varied from 1.4 to 1.8 x 10<sup>-11</sup>; with 71 percent O<sub>2</sub><sup>18</sup> (experiment 13), D varied from 1.1 to 1.9 x 10<sup>-11</sup>; and with 52 percent O<sub>2</sub><sup>18</sup> (experiment 22), D varied from 2.1 to 5.9 x 10<sup>-11</sup>. At approximately 1200°C and 98 percent O<sub>2</sub><sup>18</sup> (experiment 5), D was 8.0 x 10<sup>-10</sup>; with 72 percent O<sub>2</sub><sup>18</sup> (experiment 9), D varied from 7.3 to 8.7 x 10<sup>-10</sup>; and with 52 percent O<sub>2</sub><sup>18</sup> (experiment 20), D varied from 6.0 to 9.4 x 10<sup>-10</sup>. These data show that the diffusion coefficient is satisfactorily independent of the initial oxygen-18 concentration in the gas.

Particular Isotope Used - To show nondependence of the measurements on the particular isotope used, experiments 34 through 37 were performed as follows: O<sup>18</sup> was diffused into ThO<sub>2</sub><sup>16</sup> and the sample was allowed to come to equilibrium with the gas. The sample was then immersed in O<sub>2</sub><sup>16</sup> and the diffusion coefficient for the diffusion of O<sup>16</sup> into ThO<sub>2</sub><sup>18</sup> was measured. Since only part of the O<sup>18</sup> diffuses out of the ThO<sub>2</sub>, the sample was allowed to equilibrate with the surrounding gas and another measurement of the diffusion coefficient was made. As can be seen from the data in Table 4, the diffusion of oxygen into thoria is reversible and, therefore, independent of the oxygen isotope used.

TABLE 4  
DIFFUSION OF O<sup>16</sup> INTO ThO<sub>2</sub><sup>18</sup> AND O<sup>18</sup> INTO ThO<sub>2</sub><sup>16</sup>

Experiment No.	Temperature, °C	D, cm <sup>2</sup> /sec	
35	1120	2.8 - 10.9 x 10 <sup>-11</sup>	O <sup>16</sup> → ThO <sub>2</sub> <sup>18</sup>
36	1120	4.8 - 29 x 10 <sup>-11</sup>	O <sup>18</sup> → ThO <sub>2</sub> <sup>16</sup>
37A	917	1.4 - 2.5 x 10 <sup>-13</sup>	O <sup>16</sup> → ThO <sub>2</sub> <sup>18</sup>
37B	1125	1.8 - 23 x 10 <sup>-11</sup>	O <sup>16</sup> → ThO <sub>2</sub> <sup>18</sup>
37C	1256	6.3 - 10.3 x 10 <sup>-10</sup>	O <sup>16</sup> → ThO <sub>2</sub> <sup>18</sup>

Fractional Uptake - To test the independence of the diffusion coefficient from the fractional uptake, F, one can vary F by changing the relative amounts of thoria and O<sub>2</sub><sup>18</sup> gas present in the system. However, to maintain reasonable enrichments, gas pressures, and accurately weighable amounts of thoria, F can be varied over only a fairly narrow range. At approximately 1000°C (experiment 1) and F = 0.663, the calculated diffusion coefficient was 5.1 x 10<sup>-11</sup>; for F = 0.337 (experiment 4), D = 4.9 to 5.7 x 10<sup>-11</sup>. This shows that the diffusion coefficient is independent of F.

Elapsed Time - To show that the diffusion coefficient is independent of the elapsed time, t, Dt/a<sup>2</sup> versus t can be plotted. This plot should be linear and should go through the origin. This appeared to be the case for some of the experiments which were performed at the higher temperatures; but from measurements at low temperatures, the plots showed positive curvature. This observation led to the choice of a mathematical model which assumed a finite rate of exchange at the gas-solid interface. Diffusion coefficients calculated on this latter basis showed satisfactory independence of elapsed time.

The experimental results are summarized as Arrhenius plots in Figures 9, 10, and 11. Figure 9 is a plot of the values of  $D$  obtained from all 38 experiments under the assumption that instantaneous equilibration at the surface occurred. In general, this assumption was not valid. Figures 10 and 11 show the values of  $D$  and  $K$  obtained when a finite rate of exchange at the surface was assumed, and Equation 2-3 was used to analyze experiment 20 and the ones following it. The data from earlier runs did not appear to be complete enough to warrant this treatment.

For convenience, the  $D$ 's calculated under the assumption of instantaneous surface equilibrium are called "uncorrected diffusion coefficients," and those obtained from the more elaborate treatment are called "corrected diffusion coefficients."

The corrected  $D$ 's were divided into a high-temperature group and a low-temperature group of eleven each. Average values of  $\log D$  and  $1/T$  for the two groups were:  $\log D = -10.532$ , and  $1/T = 7.78 \times 10^{-4}$ ; and  $\log D = -8.832$ ,  $1/T = 6.59 \times 10^{-4}$ . The straight line in Figure 10 is drawn through these two average points. The same line is shown on Figure 9 to illustrate the effects of the alternative method of interpreting the data.

When the two average points were used to fit the data to an equation of the form,

$$D = D_0 \exp \left( - \frac{\Delta H_D}{RT} \right)$$

the values obtained were

$$D_0 = 4.4 \frac{\text{cm}^2}{\text{sec}}$$

and

$$\Delta H_D = 65,800 \frac{\text{calories}}{\text{mole}}$$

A  $D_0$  of this magnitude is indicative of intrinsic diffusion as opposed to an impurity-controlled process.

The activation energy is of the same order of magnitude as the 63.5 kcal heat of activation measured by Auskern and Belle<sup>9</sup> for the diffusion of oxygen through stoichiometric  $\text{UO}_2$ . Independent measurements of the diffusion coefficient of oxygen in thoria by C. S. Morgan and C. S. Yust led to an activation energy for diffusion of 14.7 kcal/mole. Private communication with one of the authors (C. S. Morgan) revealed that they used polycrystalline particles of 10- to 60-micron diameter and with total impurities less than 500 ppm. The crystallite size in their particles was of the order of 500 Angstrom units. This suggests that their measurements were influenced by grain boundary diffusion more than would be the case in the measurements reported here.

When the values of  $K$  shown in Figure 11 were similarly treated, the average points obtained were:  $\log K = -6.945$ ,  $1/T = 7.78 \times 10^{-4}$ ; and  $\log K = -5.292$ ,  $1/T = 6.59 \times 10^{-4}$ . The line passing through these points is shown on the figure.

When the values of  $K$  were fitted to an equation of the form:

$$K = K_0 \exp \left( - \frac{\Delta H_K}{RT} \right),$$

use of the average points led to  $K_0 = 7.6 \times 10^3$  cm/sec and  $\Delta H_K = 63,800$  calories/mole.

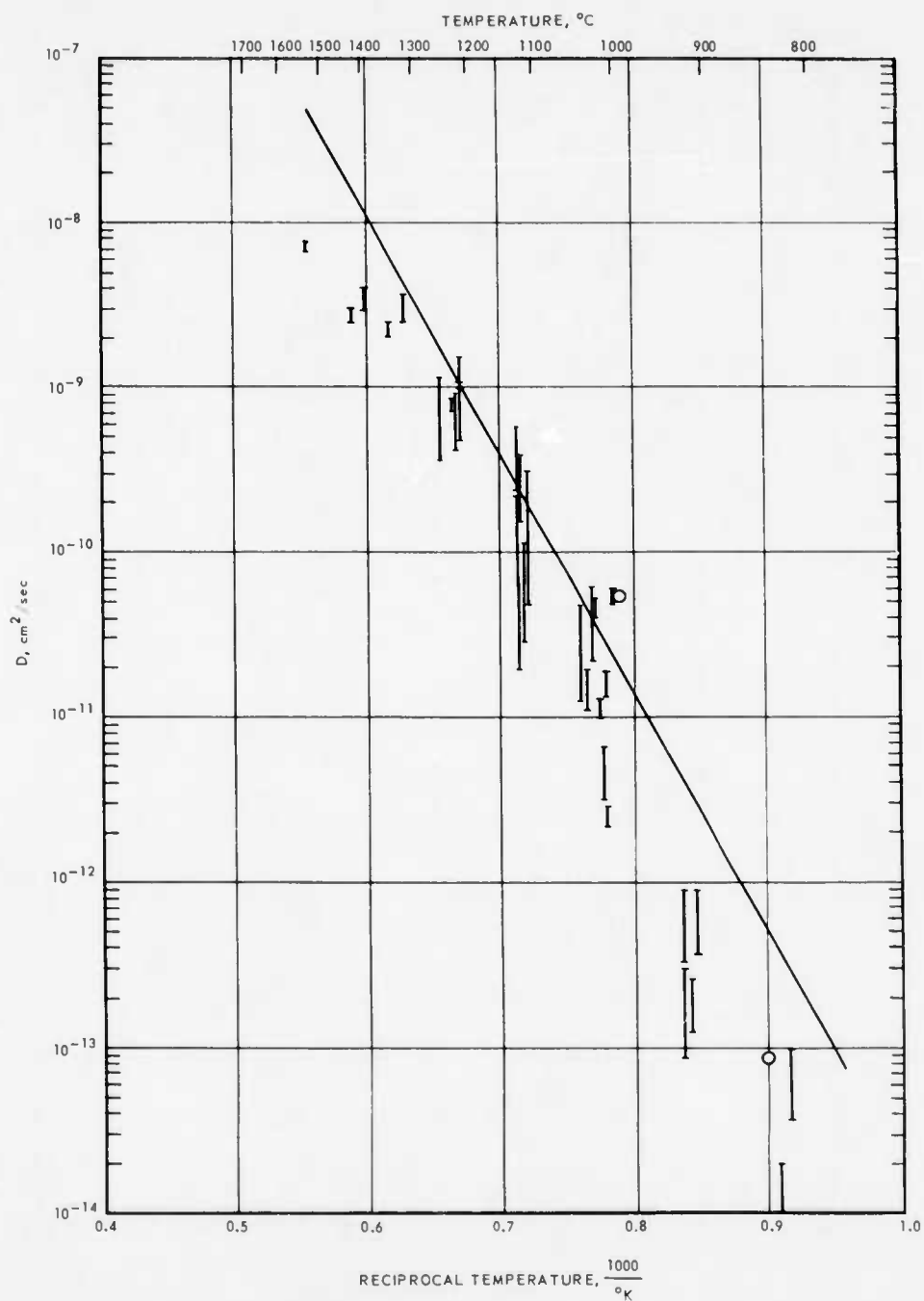


Fig. 9—Arrhenius plot of uncorrected diffusion coefficients

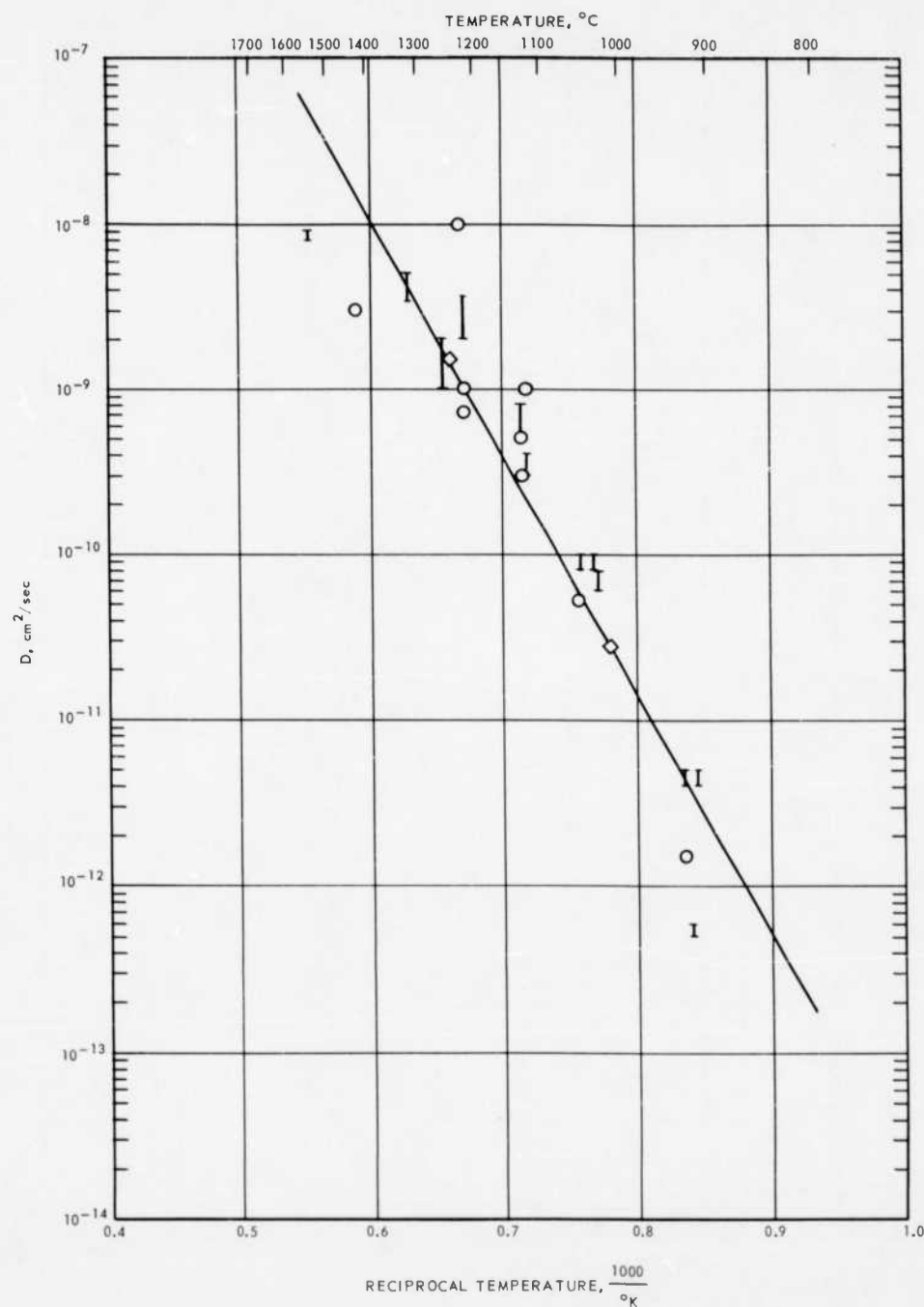


Fig. 10 - Arrhenius plot of corrected diffusion coefficients

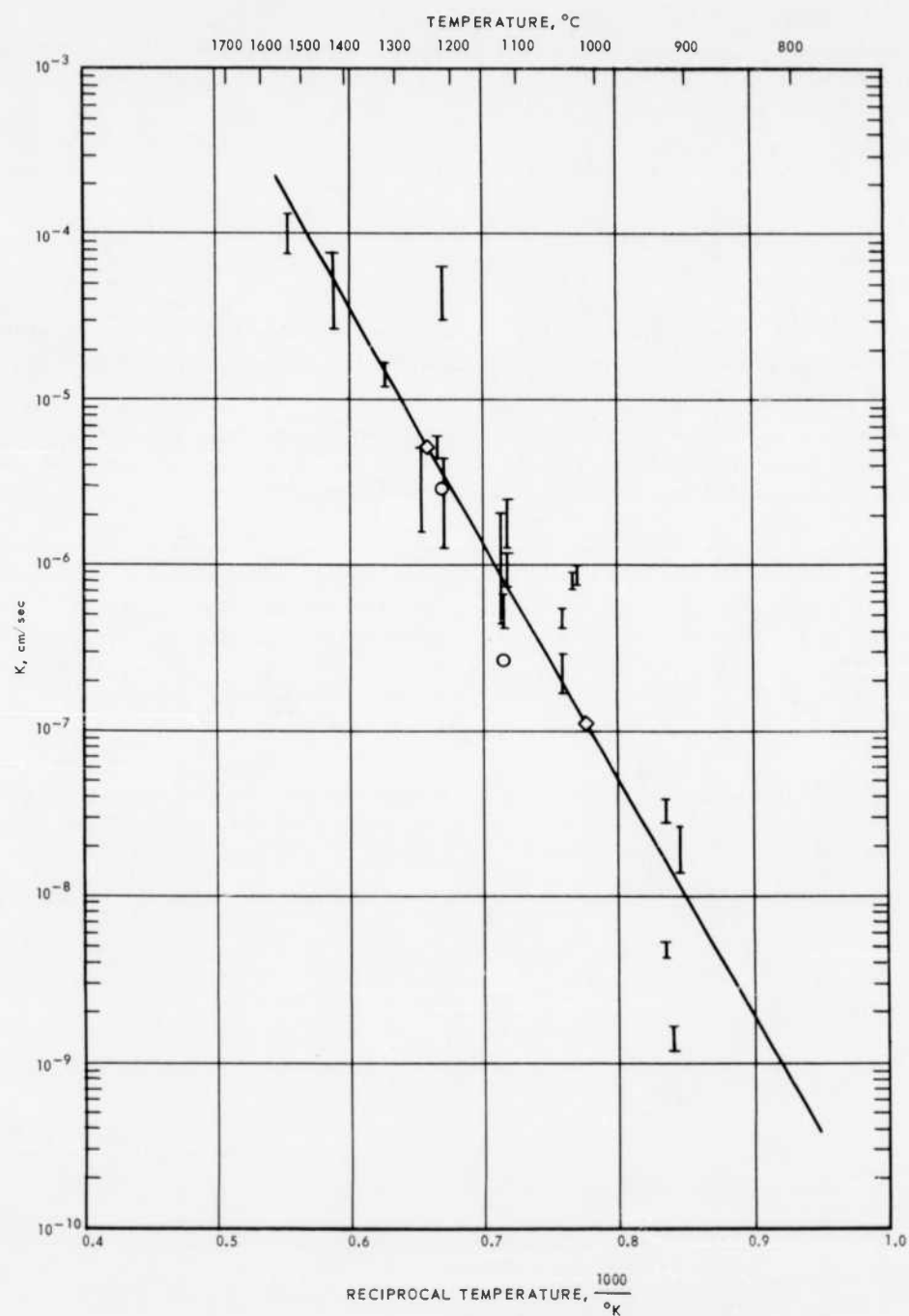


Fig. 11 - Arrhenius plot of the rate constant of the surface exchange reaction

### Conclusions

Measurements of the self-diffusion coefficient of oxygen in thoria had to take into account a finite rate of exchange at the gas-solid interface. For the temperature range 800° to 1500°C, the data are described by the equations:

$$D = 4.4 \exp \left( \frac{-65,800}{RT} \right) \text{ cm}^2/\text{sec}$$

and

$$K = 7.6 \times 10^3 \exp \left( \frac{-63,800}{RT} \right) \text{ cm/sec}$$

where  $D$  is the self-diffusion coefficient of oxygen in thoria and  $K$  is the rate constant of the exchange reaction at the gas-solid interface. The diffusion process appears to be intrinsic rather than impurity-controlled in this temperature range.

Since no standard samples exist with which to calibrate the apparatus used in these measurements, it is impossible to specify the accuracy of the results. It is expected, however, that values of the diffusion coefficient calculated from the equation:

$$D = 4.4 \exp \left( \frac{-65,800}{RT} \right)$$

or as read from the straight line of Figure 10 will be accurate within a factor of two for the temperature range 800° to 1500°C. Values of  $K$  probably depend on the past history of the sample tested.

The high self-diffusion coefficient ( $10^{-8}$  cm<sup>2</sup>/sec at approximately 1400°C) indicates that thoria is relatively permeable to oxygen, and as a coating would provide only very limited oxidation protection.

### Recommendations

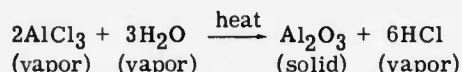
Properly doped thoria might show a much lower diffusion coefficient of oxygen than pure thoria. Additions of oxides of elements of Group V and Group VI of the Periodic Table should be studied to see if they have the desired effect.

Additional effort should be made to develop standard calibration samples for diffusion measurements.

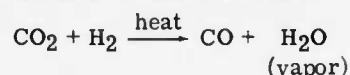


### 3. DEPOSITION OF COATINGS

The operation of components in high-temperature applications often requires a protective coating for the matrix material. A vapor-deposition or vapor-plating technique can be utilized to apply this protective coating. This technique consists of reacting or decomposing the vapors of a volatile compound upon the heated surface of the material to be coated. Dense oxide coatings can be vapor-deposited by the pyrohydrolysis of volatile metal halides. At GE-ANPD, tubular BeO pieces were successfully coated, both internally and externally, with  $\text{Al}_2\text{O}_3$  by the reaction:

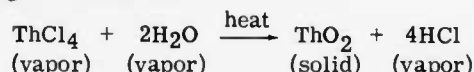


The water was supplied by the reaction:

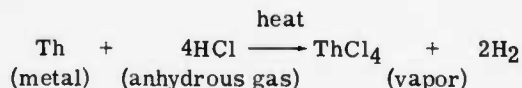


Process conditions were achieved which produced an  $\text{Al}_2\text{O}_3$  coating approximately 0.001 inch thick in one hour. Figure 12 is a photomicrograph of a polished cross section of this coating.

It appeared reasonable to believe that  $\text{ThO}_2$  coatings could be applied in a similar manner; i. e., according to the reaction:



In vapor-deposition utilizing volatile metal halides, the metal halide vapor can be supplied by heating the anhydrous salt (in this case,  $\text{ThCl}_4$ ). Another convenient method is the direct chlorination of the metal:



This latter technique sometimes provides a more readily controlled halide vapor flow than that obtained from the direct use of the anhydrous salt.

#### 3.1 MATERIALS AND APPARATUS

##### Materials

BeO Tubes - In the initial effort, BeO tubes approximately 4 inches long with an outside diameter of one-third inch were used. The tubes were fabricated from UOX grade\* BeO by extrusion; they were sintered to near theoretical density in hydrogen at  $1550^\circ\text{C}$  for 2 hours. These specimens were chosen to demonstrate  $\text{ThO}_2$  coating feasibility for the following reasons:

1. The thermal coefficients of expansion of BeO and  $\text{ThO}_2$  are nearly equal.
2. A supply of BeO tubes was available.
3. Considerable experience had been accumulated in coating BeO tubes and, therefore, apparatus design and technique could readily be applied to the  $\text{ThO}_2$  effort.

\*Brush Beryllium Corp., Cleveland, Ohio

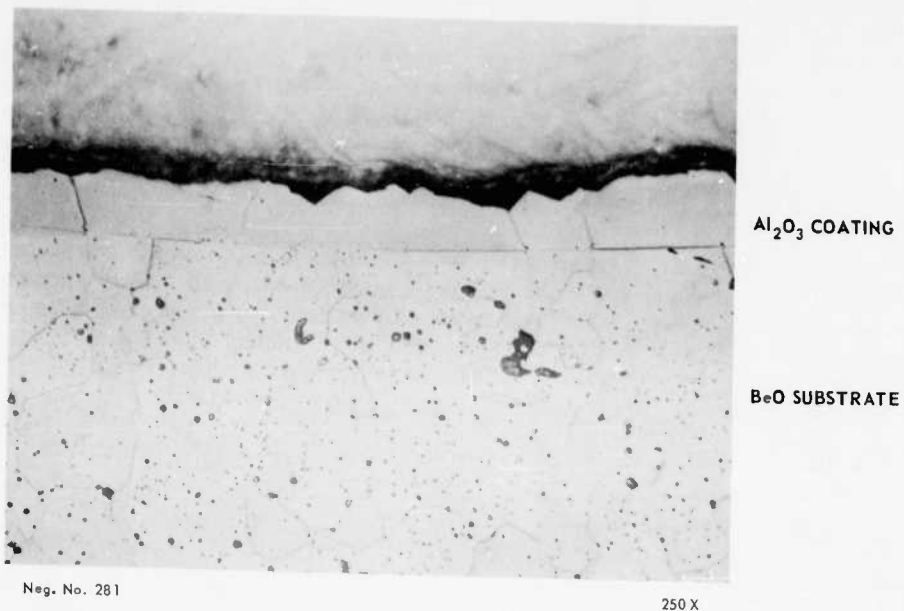


Fig. 12 - Transverse section of vapor deposited Al<sub>2</sub>O<sub>3</sub> coating on BeO

Boride Rods - In the second phase of the effort, boride rods of various compositions and sizes were used as specimens for the coating experiments. A description of these rods is presented in Table 5.

Thorium - Thorium metal turnings were used as the source of  $\text{ThCl}_4$  vapor by the  $\text{HCl}$  reaction described above. Analysis of these turnings revealed no metallic impurities in quantities greater than 0.01 percent.

Gases - The gases used were of the usual commercial grades.

### Apparatus

As shown in Figure 13, the  $\text{BeO}$  tubular specimen was held on a graphite resistance heater along the axis of the reactor tube.

Although either resistance or induction heating could be used for specimen heating, it was found in previous efforts that resistance heating provided the best method for coating the external surface of small  $\text{BeO}$  tubes. The resistance heater consists of a 3/16-inch rod of spectrographic grade graphite which fits into the bore of these  $\text{BeO}$  tubes.

Vycor tubes were used as a reaction chamber in the  $\text{BeO}$ -tube coating effort; a quartz tube was used in the boride-rod coating program.

Since calculations showed that extremely high amperage would be needed for resistance heating of boride rods, because of their high conductivities, induction heating was used. A 7.5-kva, 450-kilocycle Lepel generator was used for this purpose. A coating apparatus was designed and assembled according to Figure 14.

All of the gases used were metered into the system through Fischer-Porter flowmeters. Argon and  $\text{HCl}$  were passed into the hot bed of thorium chips while  $\text{H}_2$  and  $\text{CO}_2$  went directly into the coating chamber.

## 3.2 EXPERIMENTAL PROCEDURE AND PROGRAM

### Coating Procedure

The procedure for coating a  $\text{BeO}$  specimen consisted of cleaning, weighing, and then mounting the specimen on the graphite heater rod. The thorium holder was charged with clean, fresh thorium chips and the rest of the apparatus assembled. After the specimen had been brought to temperature in flowing argon, the coating gases were introduced into the reaction chamber. The specimen temperature and gas flow rates were monitored during the run to maintain them at the desired levels. At the end of a run, the specimen was allowed to cool and then was removed for examination.

The boride rods were given an overnight pretreatment in a vacuum oven at  $120^\circ\text{C}$  to remove absorbed moisture. The coating procedure consisted of mounting a rod in the quartz stand of the coating apparatus shown in Figure 14, and the rest of a run proceeded as described above.

### Program

Twenty-one experimental coating runs were made with  $\text{BeO}$  tubes. The coating process conditions were varied within the limits listed in Table 6. The first eight runs were preliminary experiments to test the general operation of the equipment. In the following 13 runs, various combinations of the operating parameters were tried. All runs of the latter group were reasonably successful in producing coatings.

TABLE 5  
DESCRIPTION OF BORIDE RODS

Material	TiB <sub>2</sub>	95TiB <sub>2</sub> <sup>a</sup> +5CrB <sub>2</sub>	ZrB <sub>2</sub>	HfB <sub>2</sub>
Length, in.	4	4	4	4
Diameter, in.	3/4	3/8	3/8	3/8
Analysis, %				
Ti	67.97	65.11	0.05	0.30
Zr	ND <sup>b</sup>	0.16	77.96	1.5
Hf	ND	ND	1.83	79.11
Cr	0.01	2.83	0.05	0.33
B	31.06	30.38	19.22	12.00
C	0.28	0.52	0.15	0.25
N	0.0062	0.0066	0.0054	0.0092
O	0.0375	0.0126	0.055	0.0100
Al	0.007	0.01	0.002	0.01
Co	ND	0.10	0.02	0.71
Cu	0.02	0.02	0.003	0.01
Fe	0.66	0.62	0.50	1.03
Mg	0.003	0.001	0.001	0.001
Mn	0.005	0.01	0.001	0.005
Mo	ND	0.01	-	0.07
Nb	0.005	0.10	0.05	0.01
Ni	ND	0.06	0.06	0.11
Si	0.007	0.007	0.005	0.05
V	0.003	0.003	0.003	0.005
W	ND	<1.0	ND	4.88
Total	100.1	<101.	100.0	100.4

<sup>a</sup>Sample was not homogeneous.

<sup>b</sup>ND = not detected.

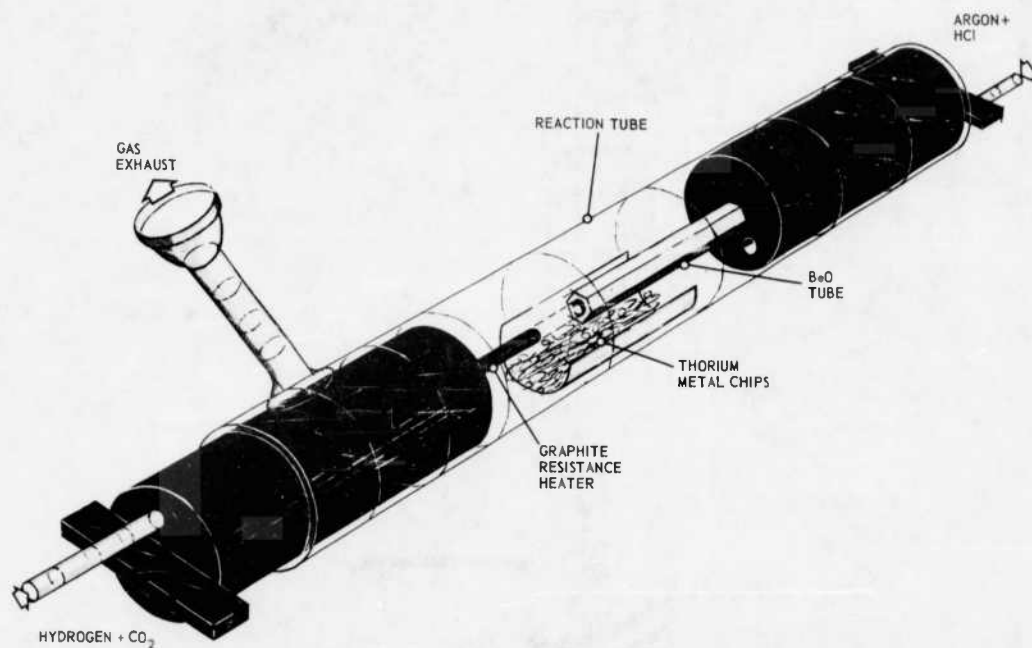


Fig. 13 - Apparatus for coating BeO tubes with  $\text{ThO}_2$  (AS-151)

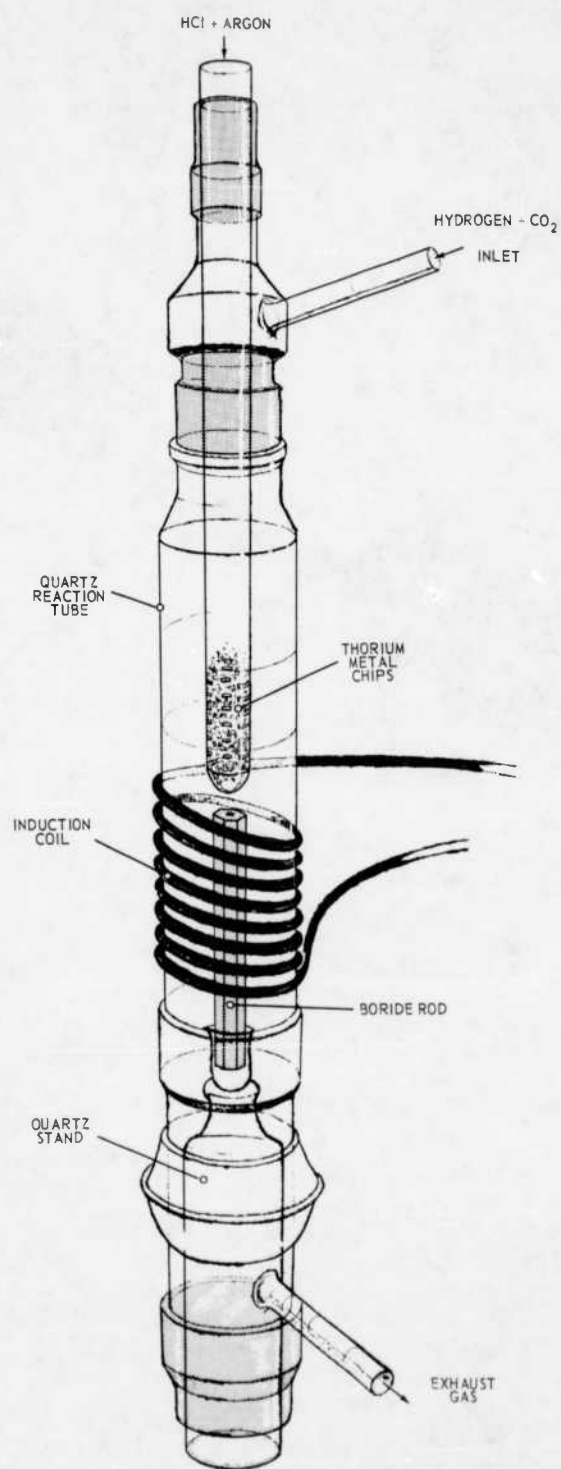


Fig. 14 - Apparatus for coating boride rods with  $\text{ThO}_2$  (AS-150)

TABLE 6  
RANGE OF COATING PARAMETERS FOR BeO TUBES

Specimen temperature, °C	1300 - 1600
Run time, min	30 - 120
H <sub>2</sub> flow, standard ml/min	160 - 240
CO <sub>2</sub> flow, standard ml/min	80 - 110
HCl flow, standard ml/min	37
Argon flow, standard ml/min	120 - 270

The best coating was obtained with the following conditions:

Specimen temperature	1600°C
Run time	60 minutes
H <sub>2</sub> flow	240 std ml/min
CO <sub>2</sub> flow	110 std ml/min
HCl flow	37 std ml/min
Argon flow	120 std ml/min

Twenty-three experimental runs were made with boride rods. The coating process conditions were varied within the limits given in Table 7. Three runs were made in which H<sub>2</sub>O vapor was introduced directly instead of being generated from H<sub>2</sub> and CO<sub>2</sub>. Seven additional experiments were performed to test compatibility of various boride compositions with the coating gases.

TABLE 7  
RANGE OF COATING PARAMETERS FOR BORIDE RODS

Specimen temperature, °C	1400 - 1750
Run time, hr	1 - 4.5
H <sub>2</sub> flow, standard ml/min	240 - 480
CO <sub>2</sub> flow, standard ml/min	20 - 750
HCl flow, standard ml/min	37 - 100
Argon flow, standard ml/min	100 - 270

### 3.3 RESULTS

#### Coating of BeO Tubes

Coatings were deposited over the entire external surface of 4-inch-long BeO tubes. Fluffy deposits found in the apparatus and on the coating surface were identified as ThO<sub>2</sub> by X-ray diffraction. Electron microprobe scanning showed the coatings to be high in thorium with no chlorine being detected; the detection limit for chlorine is about one percent. The coating also showed a fluorescence characteristic of ThO<sub>2</sub>.

Coating adherence on the BeO substrate was variable, but only fair to good at best. Coverage was good but thickness uniformity was poor. It was felt, however, that this marginal quality, in respect to uniformity and adherence, was sufficient to satisfy process feasibility requirements. The uncoated tubes used were dark. The uniform light color of the coated tube shown in Figure 15 indicates the completeness of coverage of the substrate. Figure 16 is a photomicrograph of a cross section of a ThO<sub>2</sub>-coated BeO tube.

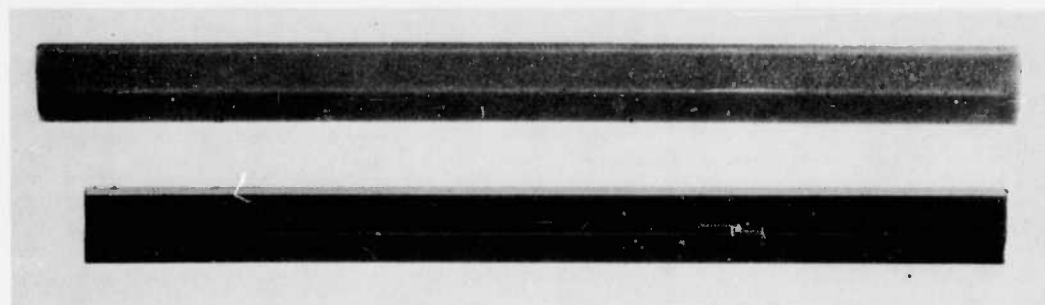
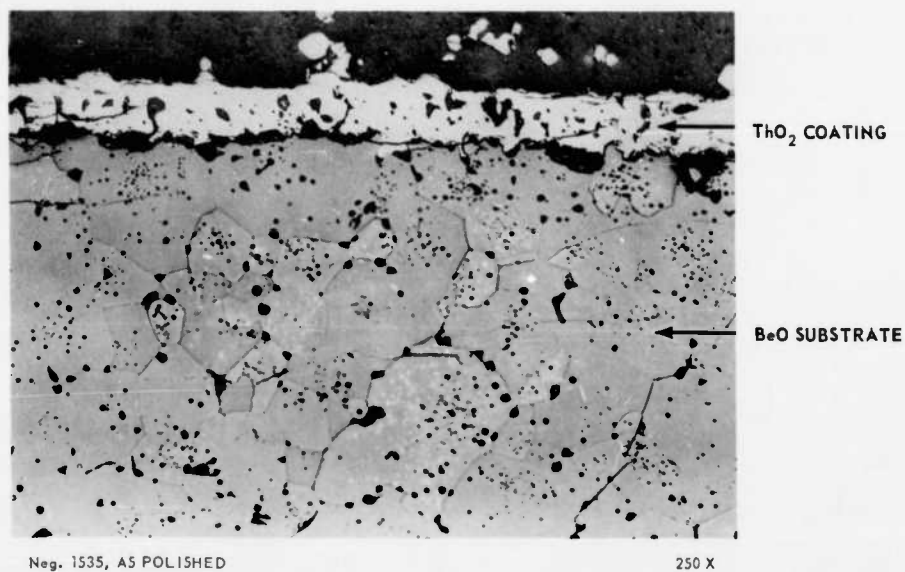


Fig. 15 – Top: BeO tube coated with vapor-deposited  $\text{ThO}_2$   
Bottom: Uncoated tube for comparison (Neg. P62-9-11A)



Neg. 1535, A5 POLISHED

250 X

Fig. 16 – Transverse section of vapor deposited  $\text{ThO}_2$  coating on BeO



### Coating of Boride Rods

In general, attempts to coat boride rods with  $\text{ThO}_2$  were unsuccessful. The rod usually became coated with a dark layer varying from a discoloration to a heavy crust. In the worst cases a substantial portion of the rod was eaten away.

In one case an attempt was made to apply a  $\text{ThO}_2$  coating on a  $\text{ZrO}_2$  coating which had been produced on a  $\text{ZrB}_2$  rod in a previous test. After a 4-hour coating run, the specimen was sectioned about 1 inch from the end. Metallographic examination showed a two-layer deposit which was porous and poorly adherent. Electron microbeam probe scans across the coating revealed an outer layer of  $\text{ThO}_2$  of variable thickness over an intermediate layer of  $\text{ZrO}_2$ , as shown in Figure 17. The abscissas of Figure 17 are proportional to the distance along the scanned path and the ordinates are roughly proportional to the concentrations of the indicated elements. In this specific scan, the  $\text{ThO}_2$  coating was about 25 microns thick.

### Compatibility of Borides with Coating Gases

When various combinations of coating gases were passed over heated boride rods,  $\text{CO}_2$  was always present when the most severe corrosive attack occurred. It had been supposed that  $\text{HCl}$  gas would be the most corrosive, but that gas alone did not cause significant damage.

Hafnium diboride was much more resistant to corrosive attack than  $\text{TiB}_2$ ,  $95\text{TiB}_2 - 5\text{CrB}_2$ , or  $\text{ZrB}_2$ . Under coating conditions where the latter materials were severely attacked,  $\text{HfB}_2$  merely showed surface discoloration.

### 3.4 CONCLUSIONS

Attempts to coat boride rods with  $\text{ThO}_2$  by vapor deposition from an atmosphere containing  $\text{ThCl}_4$  were essentially unsuccessful. The main problem was attack of the rods by the coating atmosphere. It appears that the worst damage occurred when  $\text{CO}_2$  was introduced into the coating gas;  $\text{HCl}$  gas proved to be relatively harmless. Hafnium diboride was much more resistant to corrosive attack than  $\text{TiB}_2$ ,  $95\text{TiB}_2 - 5\text{CrB}_2$ , or  $\text{ZrB}_2$ . Figure 18 shows rods which were exposed to coating gases, in comparison with untreated specimens.

$\text{BeO}$  bodies were successfully coated with  $\text{ThO}_2$ , thereby demonstrating feasibility of the coating process itself. The process was repeated sufficiently to show that a measure of control and reproducibility could be achieved, but the coating quality was not as good as would be desired if coated  $\text{BeO}$  were the goal.

In one trial,  $\text{ThO}_2$  was deposited on an intermediate layer of  $\text{ZrO}_2$  on a  $\text{ZrB}_2$  rod.

The use of  $\text{H}_2\text{O}$  vapor directly in place of the  $\text{H}_2 + \text{CO}_2 \rightarrow \text{H}_2\text{O} + \text{CO}$  reaction showed some promise of providing a coating atmosphere which would be effective and would eliminate the corrosion attributed to  $\text{CO}_2$ .

### 3.5 RECOMMENDATIONS

An attractive feature of the coating method investigated in this work is the possibility of obtaining nearly theoretically dense coatings at relatively low temperatures. If some other method, such as the pyrolysis of an organometallic compound, were successful in forming an initial protective oxide layer on the boride, then the pyrohydrolysis of  $\text{ThCl}_4$  might be the most economical way to build up the coating to the desired thickness.

If the pyrohydrolysis method is to be investigated further, continued work on the direct use of  $\text{H}_2\text{O}$  vapor is advisable.

An examination of the relative reactivities of  $\text{HfB}_2$ ,  $\text{ZrB}_2$ , and  $\text{TiB}_2$  with  $\text{CO}$  and  $\text{CO}_2$  may be of value in a study of the chemistry of borides.

In view of the results reported in Section 4 regarding the temperature limits of borides in contact with graphite, it may be profitable to investigate oxide coatings that are less refractory than  $\text{ThO}_2$ .

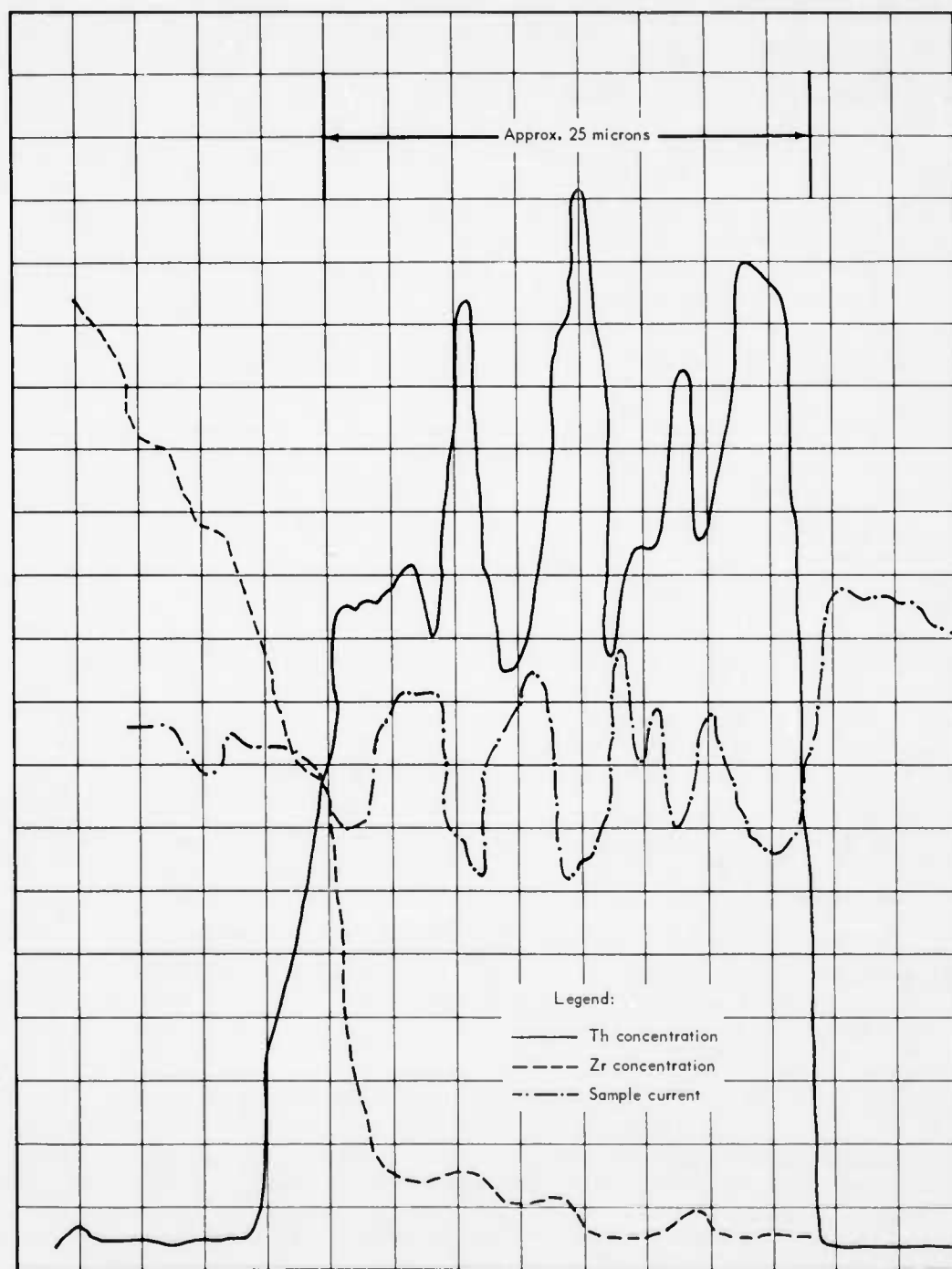


Fig. 17 - Electron microbeam probe scan across coating on  $\text{ZrB}_2$  rod

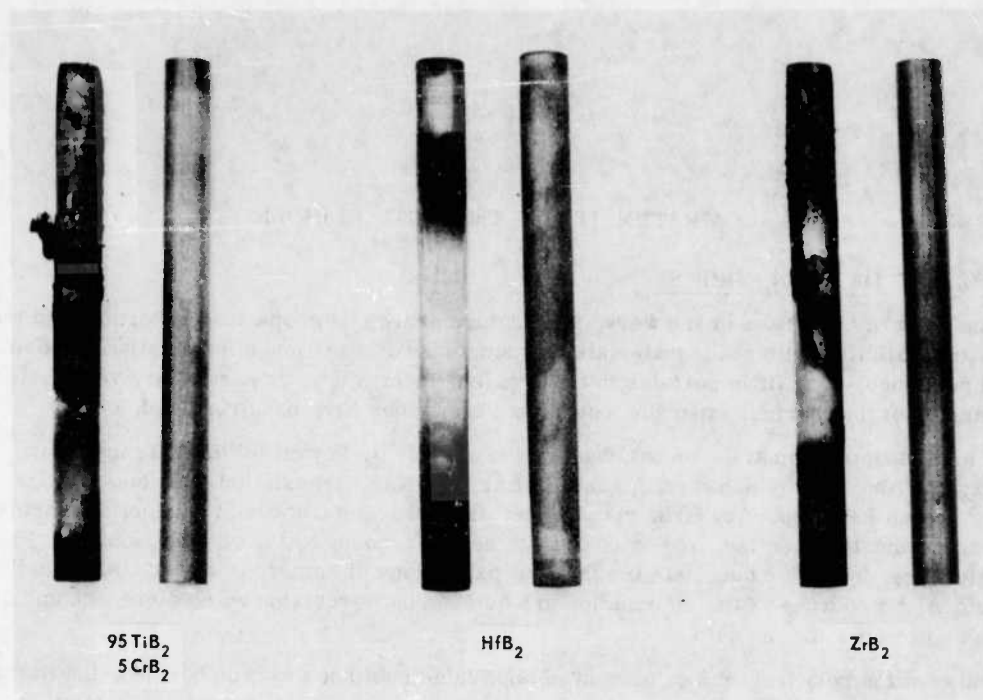


Fig. 18 - Appearance of boride rods before and after coating runs (Neg. P63-2-10)

## 4. COMPATIBILITY OF $\text{ThO}_2$ WITH BORIDES

### 4.1 PUBLISHED DATA ON BORIDES

At the start of this phase of the work, a literature search on properties of borides and their chemical compatibility with other materials was started. Although much information on borides has been published, very little pertains to the problem under study. In particular, very few measurements of the thermal expansion coefficient of borides have been reported.

The most useful summaries on borides are the chapter by Powell in "High Temperature Technology,"<sup>13</sup> the book by Schwarzkopf and Kieffer,<sup>14</sup> a NASA translation of a Russian journal article,<sup>15</sup> and an AEC report by Krikorian.<sup>16</sup> The first three references give general information, some physical properties, and extensive further references to the original sources. The fourth reference, by Krikorian, lists the thermal expansions of numerous materials, including eight borides. No sources of the information are quoted, but a revision with references and discussion was promised by the author.

Because of the relatively minor amount of applicable published data on borides, the literature searching was reduced to a minimum, and more emphasis was placed on laboratory tests.

Table 8 lists some pertinent properties of borides which were considered in this research. Both original and secondary sources of information are shown. The original references were not all available for verification.

### 4.2 EQUIPMENT

The only unusual pieces of equipment used in this part of the work were the high-temperature furnaces, which are described briefly below.

#### Tungsten Tube Furnace

In order to obtain temperatures up to  $2800^\circ\text{C}$  and  $3000^\circ\text{C}$ , the tungsten tube furnaces shown in Figure 19 were developed at GE-NMPO. The heating element is a tungsten tube, resistively heated by a 150-kilowatt, 10,000-ampere saturable-reactor-controlled power source. The power is routed to the furnace by a heavy copper bus system connected to the water-cooled copper electrodes. The tungsten tube is fastened at the top with stranded copper cable. The bottom end dips into a pool of gallium-indium-tin liquid eutectic alloy which provides electrical contact and allows for thermal expansion of the element.

A tungsten tube surrounding the heating element is used as a thermal radiation barrier. The space between this barrier and the outer shell is filled with unstabilized zirconia for thermal insulation. The outer shell and covers are double-walled, water-cooled stainless steel. The furnace is ordinarily filled with hydrogen, a small flow being maintained to insure a slight positive internal pressure. The furnace is operated similarly when a helium atmosphere is used. A closed-end molybdenum muffle is available for performing tests in a vacuum.

A quartz window at the top of the furnace allows use of an optical pyrometer for temperature measurements.

The life of the tungsten heating element is dependent on operating temperature. The element may reasonably be expected to last for 75 to 100 hours at  $2500^\circ\text{C}$  and for 25 to 40 hours at  $2800^\circ\text{C}$ .

TABLE 6  
PROPERTIES OF BORIDES

Material	Melting Point, °C	Reference <sup>a</sup>	Range Of Stability, °C	Reference <sup>a</sup>	Coefficient Of Thermal Expansion Per Degree C	Reference <sup>a</sup>	Percent Expansion 25° To			Reference <sup>a</sup>
							500°	1000°	1500°C	
ThO <sub>2</sub>	3300 ± 100	13, p. 74; 17					0.41	0.92	1.46	13, p. 50; 18; 16
TiB <sub>2</sub>	2790 2600 2980	19; 20 13, p. 141; 22; 23 15, pp. 239, 250; 24; 25	Up to melting point 20 to 2600 ± 30	19 15, p. 250; 26	6.1 x 10 <sup>-6</sup> (Room temperature to 1000°C) 6.1 x 10 <sup>-6</sup> (25° to 1300°C) 6.3 x 10 <sup>-8b</sup> 5.5 x 10 <sup>-6</sup> 7.3 x 10 <sup>-6</sup> 6.1 x 10 <sup>-6b</sup>	21 27 22 21 22				
ZrB <sub>2</sub>	2990 - 3000 3040 ± 100	13, p. 141; 23; 28 15, pp. 239, 252; 29; 20	Up to melting point 20 to 3040	19 15, p. 252; 26			0.27	0.64	1.03	16
HfB <sub>2</sub>	3000 3082 3250 ± 100	22 13, p. 141; 23 14, p. 65; 15, p. 253; 30	20 to 3250	15, p. 253; 26	5.6 x 10 <sup>-6</sup> (Room temperature to 1000°C) 5.3 x 10 <sup>-8</sup>	14, p. 285 15, p. 253; 30	0.25	0.54		16
VB	2100 ± 60	14, p. 267; 31								
VB <sub>2</sub>	2400 ± 50	15, p. 239; 26; 20	Decomposes to VB + B on melting 20 to 2400	13, p. 142; 19 15, p. 239; 26						
NbB <sub>2</sub>	3000 ± 50	15, p. 239; 32; 20	Decomposes to NbB + B on melting Decomposes above 2900 20 to 3000	13, p. 142; 19 15, p. 239; 26 14, p. 290; 19 15, p. 239; 26						
TaB <sub>2</sub>	3000 3100 ± 50	14, p. 295 15, p. 256; 26	Decomposes to TaB + B on melting 20 to 3100	13, p. 142; 19 15, p. 256; 26						
CrB <sub>2</sub>	1850 1900 ± 50 2150 ± 50	14, p. 299; 31 15, p. 258; 26	20 to 1850	15, p. 256; 26						
MoB	2160 2160 2100 2325 - 2374	13, p. 141; 33 14, p. 303; 34 15, p. 262; 26 15, p. 262; 35	Up to 2000 20 to 2160 αMoB 2000 to 2160 βMoB	13, p. 141; 33 15, p. 262; 26						
MoB <sub>2</sub>	2100 2100 ± 50	14, p. 303; 34 20								
WB	2920 ± 50 2860 2400 ± 100 2660 ± 60	13, p. 141 14, p. 306; 31 15, p. 264; 26 20	Up to 2040 20 to 2400	13, p. 141; 36 15, p. 264; 26						
LaB <sub>6</sub>	2210	37					0.23	0.56	-	16
CeB <sub>6</sub>	2190	37					0.30	0.65	-	16
SmB <sub>6</sub>	2400 ± 100	37					0.28	0.63	-	16
GdB <sub>6</sub>	>2150	37								
ThB <sub>4</sub>	>2500 2500	14, p. 306; 38 22								

<sup>a</sup>Reference numbers refer to those listed in the reference section.

<sup>b</sup>These are quoted as per degree Fahrenheit.

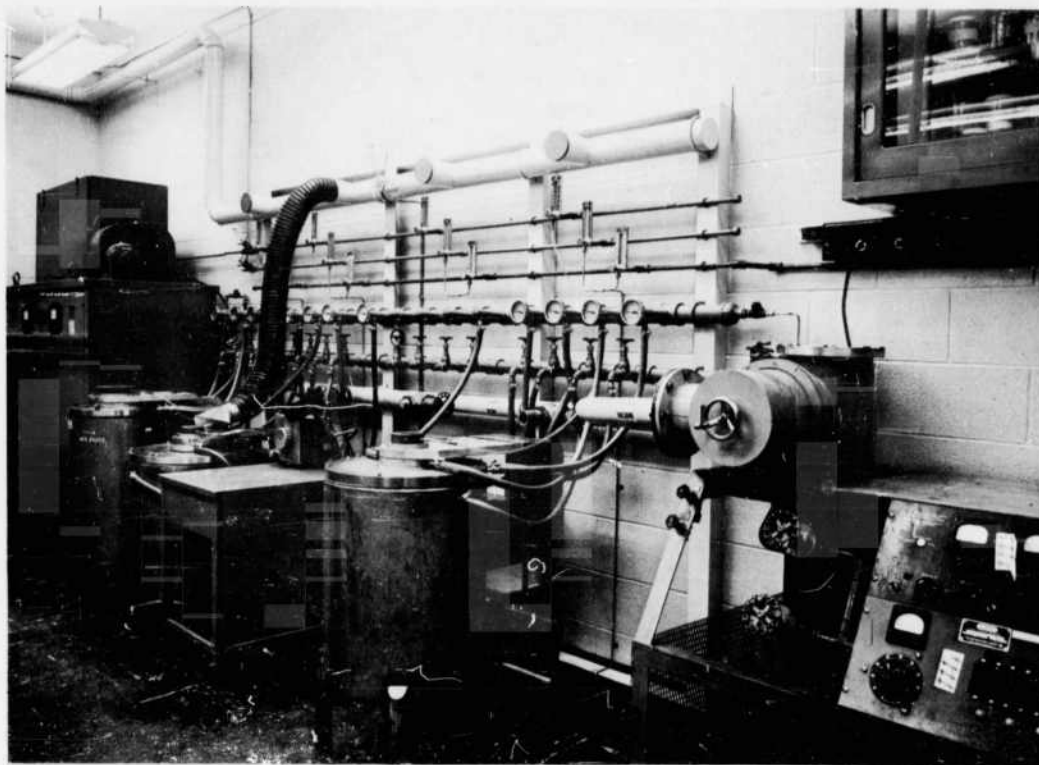


Fig. 19 - High-temperature tungsten tube furnaces in laboratory operation  
(Neg. P62-4-3A)

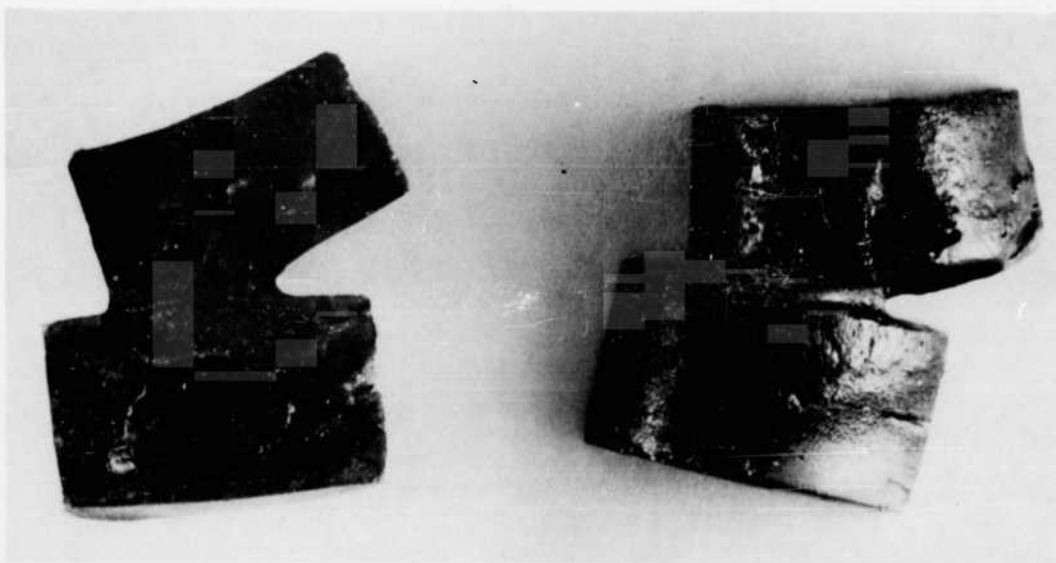


Fig. 20 -  $\text{ThO}_2\text{-HfB}_2$  sample after 1 hour in dry hydrogen at  $2700^\circ\text{C}$   
(Neg. P62-9-12)

### 4.3 MATERIALS

#### Thoria

The thoria used in these tests is the 99.7 percent pure powder mentioned in section 2.

#### Borides

Commercially available boride powders were used. The following samples were obtained:

<u>Vendor</u>	<u>Borides</u>
American Potash and Chemical Corp.	TiB <sub>2</sub> , YB <sub>6</sub> , LaB <sub>6</sub> , CeB <sub>6</sub> , PrB <sub>6</sub> , NdB <sub>6</sub> , SmB <sub>6</sub> , GdB <sub>6</sub> .
The Carborundum Co.	TiB <sub>2</sub> , ZrB <sub>2</sub> , and HfB <sub>2</sub>
National Carbon Co.	TiB <sub>2</sub>
U. S. Borax Research Co.	TiB <sub>2</sub> , ZrB <sub>2</sub> , VB <sub>2</sub> , NbB <sub>2</sub> , CrB <sub>2</sub> , MoB <sub>2</sub> , MoB, WB
Borides already on hand at GE-NMPO. These are mostly of European manufacture.	TiB <sub>2</sub> , ZrB <sub>2</sub> , MoB <sub>2</sub> , WB, TaB, EuB <sub>6</sub>

The compositions of the borides purchased are shown in Tables 9, 10, 11, and 12. These tables illustrate the general quality levels of borides commercially available in the fall of 1962. Since manufacturers are continually improving their products, these results may not be representative of currently available materials. To avoid unwarranted comparisons, the names of vendors are omitted from the tables.

To test compatibility, thoria-boride compacts were prepared by partially loading a die with ThO<sub>2</sub> powder and tamping it to leave a cup-shaped depression in the center. A powdered boride was poured into the depression through a small funnel. The rest of the ThO<sub>2</sub> was added and cold pressing was completed.

The cold-pressed samples were sintered in hydrogen at 1700°C for 4 hours or more to strengthen them for further handling. The shrinkage during this step frequently revealed flaws before testing at high temperatures.

### 4.4 EXPERIMENTAL PROGRAM AND PROCEDURES

The objective of this program was to determine if selected high-melting borides react with ThO<sub>2</sub> when the two materials are heated together in reducing, neutral, or oxidizing atmospheres. In an oxidizing atmosphere, the boride would have to be surrounded and protected by a layer of ThO<sub>2</sub>. Since it was desired to avoid any synthesis of pure borides, the purest commercially available borides and thoria were used. The work was conducted to eliminate, if possible, any further contamination of the starting materials.

#### Preparation of Specimens

The thoria powder was readily compacted into 1/2-inch or 1-inch diameter pellets by cold pressing in a steel die at an indicated 10,000 psi. Some pellets were further compacted by hydrostatic pressing at 25,000 psi or higher. A thin film of stearic acid was used to lubricate the die, but no binder was necessary. The larger ThO<sub>2</sub> setting pieces which were used to isolate the test specimens from contact with crucibles were made in the same general way.

#### Tests Under Reducing Conditions

In the first high-temperature tests, ThO<sub>2</sub> pellets (without boride added) were sintered in dry hydrogen (with -40°C dewpoint) for 1 hour at 2000°C. Additional samples were heated at 2200°C,

TABLE 9  
ANALYSES OF TITANIUM DIBORIDE

Nominal formula	TiB <sub>2</sub>				
Theoretical composition, %					
Ti	68.88				
B	31.12				
Analysis	No. 5	No. 6	No. 7	No. 21	No. 23
Major elements, %					
Ti	68.28	68.33	68.89	68.91	67.29
B	29.84	30.98	29.50	30.68	29.66
C	0.51	0.49	0.24	0.063	0.75
O	0.25	0.29	0.50	0.49	1.50
N	0.59	0.50	0.04	0.03	1.78
Trace elements, ppm					
Al	100	100	200	ND <sup>a</sup>	3000
Co	200	ND	ND	ND	ND
Cr	700	100	ND	50	ND
Cu	ND	30	ND	ND	-
Fe	2000	300	4000	100	100
Mg	10	500	10	10	50
Mn	20	ND	30	ND	ND
Mo	100	ND	ND	ND	ND
Na	20	20	20	10	20
Ni	70	ND	ND	50	ND
Si	20	100	30	30	200
Zr	200	30	200	ND	ND
K	20	20	50	20	20
Total	99.81	100.7	99.6	100.2	101.3
B/Ti atom ratio	1.93	2.00	1.89	1.96	1.95

<sup>a</sup>Not detected.



TABLE 10  
ANALYSES OF ZIRCONIUM AND HAFNIUM DIBORIDES

Nominal formula	ZrB <sub>2</sub>	ZrB <sub>2</sub>	ZrB <sub>2</sub>	HfB <sub>2</sub>
Theoretical composition, %				
M	80.83	80.83	80.83	89.19
B	19.17	19.17	19.17	10.81
Analysis	No. 4	No. 8	No. 22	No. 9
Major elements, %				
Zr	80.47	81.40	78.73	4.30
Hf	1.55	- <sup>a</sup>	1.68	85.30
B	17.64	18.41	19.13	9.93
C	0.15	0.26	0.11	0.50
O	0.77	0.35	0.79	0.59
N	0.13	0.02	1.09	0.18
Trace elements, ppm				
Al	ND <sup>b</sup>	100	3000	100
Ca	ND	1000	500	ND
Co	500	ND	ND	ND
Fe	500	3000	4000	300
Hf	-	100	-	-
Mg	20	200	1000	50
Mn	ND	20	100	10
Mo	500	ND	70	700
Na	70	30	20	20
Si	200	200	700	200
Ti	700	100	3000	200
K	20	20	20	20
V	ND	50	ND	ND
Total	101.0	100.9	102.8	101.0
B/M atom ratio	1.83	1.91	2.03	1.75

<sup>a</sup>Analysis not performed.

<sup>b</sup>Not detected.

TABLE 11

## ANALYSES OF TRANSITION METAL BORIDES

Nominal formula	MoB <sub>2</sub>	MoB <sub>2</sub>	MoB	VB <sub>2</sub>	NbB <sub>2</sub>	WB	WB	TaB	CrB <sub>2</sub>
Theoretical composition, %									
M	81.60	81.60	89.87	70.19	81.11	94.44	94.44	94.36	70.62
B	18.40	18.40	10.13	29.81	18.89	5.56	5.56	5.64	29.38
Analysis	No. 1	No. 17	No. 25	No. 2	No. 3	No. 18	No. 26	No. 19	No. 24
Major elements, %									
M	80.53	76.52	89.02	69.67	80.85	93.38	95.67	94.18	67.37
B	17.89	16.63	9.25	28.52	17.83	5.48	3.57	5.25	28.76
C	0.048	0.01	0.04	0.27	0.029	0.01	0.013	0.04	0.08
O	1.24	3.73	0.84	1.07	0.66	0.77	0.34	0.29	0.39
N	0.02	0.06	0.01	0.01	0.01	0.03	0.00	0.04	0.43
Trace elements, ppm									
Al	ND <sup>a</sup>	ND	ND	ND	ND	50	ND	30	100
Co	200	ND	70	ND	200	ND	ND	ND	100
Cr	100	100	300	200	700	50	50	200	- <sup>b</sup>
Cu	30	70	-	ND	ND	70	-	ND	-
Fe	700	1000	1000	2000	2000	300	300	500	1000
Mg	ND	ND	ND	ND	ND	500	ND	ND	30
Mn	ND	300	ND	ND	ND	200	ND	ND	50
Mo	-	-	-	ND	1000	100	100	200	500
Na	30	10	30	15	20	20	20	20	50
Nb	ND	ND	-	ND	-	ND	-	2000	-
Ni	30	100	100	50	100	50	50	ND	300
Si	ND	150	ND	50	ND	50	20	100	ND
Ta	ND	ND	-	ND	1000	ND	-	-	-
Ti	2000	1000	1000	200	500	100	200	30	700
V	ND	ND	ND	-	3000	50	ND	100	300
Zr	4000	50	300	100	300	ND	100	ND	2000
K	20	20	30	20	20	20	20	20	20
Total	100.4	97.2	99.4	99.8	100.3	99.8	99.7	100.1	97.5
B/M atom ratio	1.97	1.93	0.92	1.93	1.90	0.997	0.634	0.94	-

<sup>a</sup>Not detected.<sup>b</sup>Analysis not performed.

TABLE 12  
ANALYSES OF RARE EARTH METAL BORIDES

Nominal formula	YB <sub>6</sub>	LaB <sub>6</sub>	CeB <sub>6</sub>	PrB <sub>6</sub>	NdB <sub>6</sub>	SmB <sub>6</sub>	GdB <sub>6</sub>	EuB <sub>6</sub>
Theoretical composition, %								
M <sup>a</sup>	57.80	68.15	68.33	68.46	68.96	69.84	70.78	70.07
B	42.20	31.85	31.67	31.54	31.04	30.16	29.22	29.93
Analysis	No. 10	No. 11	No. 12	No. 13	No. 14	No. 15	No. 16	No. 20
Major elements, %								
M	61.89	67.00	66.95	68.32	68.07	67.47	73.09	64.69
B	36.74	30.11	30.45	28.31	28.49	29.41	25.37	29.24
C	0.41	0.29	0.28	0.31	0.66	0.32	0.24	0.96
O	<sup>b</sup>	-	-	-	-	-	-	1.48
N	-	-	-	-	-	-	-	1.28
Trace elements, ppm								
Al	100	1000	ND <sup>c</sup>	ND	-	-	-	-
Cr	ND	500	50	ND	1000	500	700	30
Fe	2000	1000	300	1000	1000	1000	3000	1000
Mg	50	100	30	ND	ND	ND	ND	1000
Mn	-	-	-	-	ND	ND	ND	100
Mo	-	-	-	-	ND	ND	ND	100
Na	30	10	20	20	20	10	20	30
Ni	50	500	ND	ND	-	-	-	-
Si	ND	20	ND	ND	ND	ND	ND	100
K	50	20	20	20	20	20	20	20
Ti	100	20	ND	ND	-	-	-	-
V	30	ND	ND	ND	-	-	-	-
Y	-	500	500	ND	ND	500	ND	ND
Eu	200	50	ND	ND	-	-	-	-
La	ND	-	500	ND	-	-	-	-
Total	(99.3)	(97.8)	(97.8)	(97.0)	(97.0)	(97.4)	(99.1)	97.9
B/M atom ratio	4.88	5.77	5.89	5.77	5.99	6.06	5.05	6.35

<sup>a</sup>Rare earth metal.

<sup>b</sup>Analysis not performed.

<sup>c</sup>Not detected.

2400<sup>o</sup>, and 2800<sup>o</sup>C. After the densities had been determined, the pellets were heated in air for 24 hours at 1050<sup>o</sup>C to remove what appeared to be films of tungsten or rhenium from the crucibles. The dark surfaces were lightened to yellow or tan by this treatment, but weight changes were insignificant. When the pellets were cut in half, several were noted to have black centers. Table 13 summarizes some of the observations on these pellets.

A sectioned half of one of the pellets heated at 2800<sup>o</sup>C was again heated in air at 1050<sup>o</sup>C. In 1 hour, the black area bleached to a pale gray and after four hours the entire cut surface was white. The black-and-white cut face and the air-fired white face were both examined by X-ray fluorescence spectroscopy. The recorded spectra were the same for each sample.

These observations suggested that a substoichiometric material ( $\text{ThO}_{2-x}$ ) had been formed in some of the specimens.

One of the 2800<sup>o</sup>C black-centered pieces was metallographically polished and examined. Shiny metallic particles up to 10 microns in diameter were observed in the center, but not in the white rim. Examination by the electron microprobe indicated that the particles contained about 10 percent higher thorium than the surrounding oxide, thus, confirming that they were thorium metal.

The most reasonable conclusion from these tests is that thorium heated in dry hydrogen in the temperature range of 2200<sup>o</sup> to 2800<sup>o</sup>C is converted to a substoichiometric oxide which disproportionates on cooling to form thorium metal and a more nearly stoichiometric thorium oxide.

In other tests, samples of  $\text{ThO}_2$ ,  $\text{ThO}_2$  with  $\text{HfB}_2$  centers, and  $\text{ThO}_2$  with  $\text{ZrB}_2$  centers were placed on a  $\text{ThO}_2$  disk in a rhenium crucible and heated in hydrogen for 1 hour at 2700<sup>o</sup>C. The thorium turned gray or black; the  $\text{ThO}_2$ -boride samples showed extensive deformation and incipient melting. Figure 20 shows the  $\text{ThO}_2$ - $\text{HfB}_2$  sample after heating. Originally, this was a stack of two  $\text{ThO}_2$  pellets with  $\text{HfB}_2$  centers.

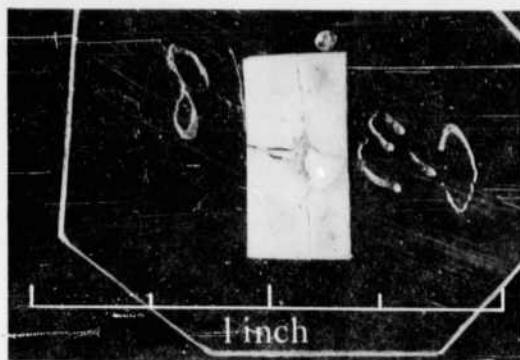
In a test at a lower temperature, dry hydrogen at 2500<sup>o</sup>C converted  $\text{ThO}_2$  to a black-coated, gray friable mass. The  $\text{ThO}_2$ - $\text{ZrB}_2$  compacts did not appear to melt under these conditions but the  $\text{ThO}_2$ - $\text{HfB}_2$  again showed melting.

Since the tests in dry hydrogen showed uniformly unfavorable results, a shift to a relatively more oxidizing atmosphere was made.

#### Tests in Moist Hydrogen

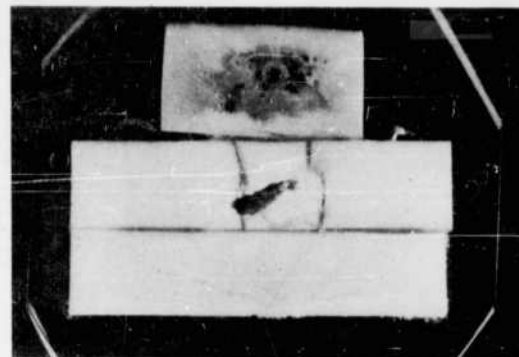
Moistening of the hydrogen atmosphere had a markedly beneficial effect on the behavior of  $\text{ThO}_2$  at high temperatures. When the hydrogen entering the furnace was bubbled through water at 0<sup>o</sup>C,  $\text{ThO}_2$  pellets heated at 2700<sup>o</sup>C for 1 hour remained dense and white and free from cracks. This beneficial effect did not extend to the oxide-boride compacts. A glassy phase appeared in the  $\text{ThO}_2$ - $\text{ZrB}_2$  and  $\text{ThO}_2$ - $\text{HfB}_2$  samples heated for 1 hour in moist hydrogen at 2400<sup>o</sup>C or at 2600<sup>o</sup>C. At the higher temperature, the boride completely disappeared, leaving a cavity, while at the lower temperature a residue, lighter in color than the original boride, remained. In the case of  $\text{ThO}_2$ - $\text{TiB}_2$  heated at 2600<sup>o</sup>C, a different behavior was observed. The entire pellet turned black; and while a cavity marked the original position of the boride, no accumulation of a glassy phase was evident. Figure 21 shows the destructive reaction between  $\text{ThO}_2$  and the borides in these specimens.

Visual and microscopic examination of polished sections of these  $\text{ThO}_2$ -boride specimens revealed a porous  $\text{ThO}_2$  body with a large cavity where the boride had been. Near the cavities in the  $\text{ThO}_2$ - $\text{ZrB}_2$  and the  $\text{ThO}_2$ - $\text{HfB}_2$  couples, there were dense, non-porous areas which appeared to have melted and resolidified. Figure 22 shows the microstructures of the  $\text{ThO}_2$ - $\text{ZrB}_2$  sample heated for 1 hour at 2600<sup>o</sup>C in hydrogen of 0<sup>o</sup>C dewpoint. (This same specimen is shown in Figure 21b.) Figure 22a shows the dense layer lining the cavity and Figure 22b shows another region



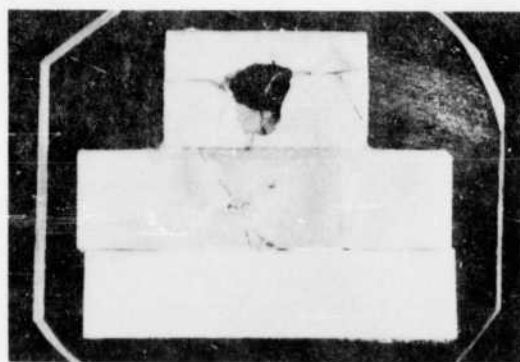
Neg. P63-1-38B

a -  $\text{ThO}_2\text{-ZrB}_2$ , 2400°C



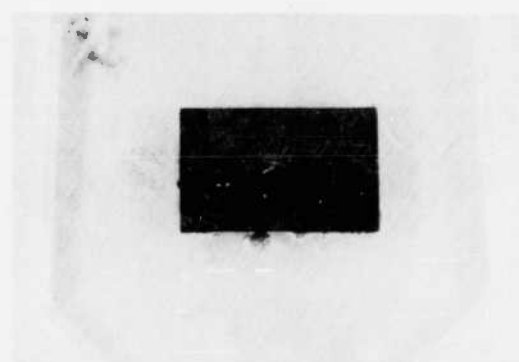
Neg. P63-1-38C

b -  $\text{ThO}_2\text{-ZrB}_2$ , 2600°C



Neg. P63-1-38A

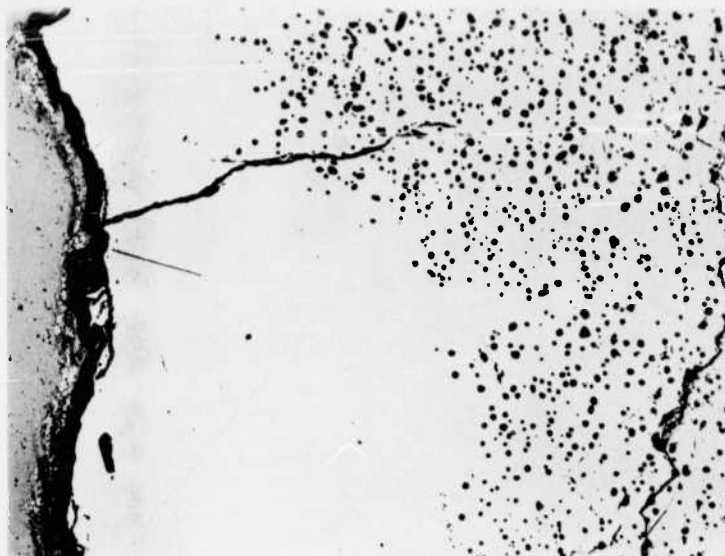
c -  $\text{ThO}_2\text{-HfB}_2$ , 2600°C



Neg. P63-1-38D

d -  $\text{ThO}_2\text{-TiB}_2$ , 2600°C

Fig. 21 - Polished sections of  $\text{ThO}_2$ -Boride compacts after 1 hour in hydrogen at 0°C dewpoint



Neg. 1886

100 X



Neg. 1887

100 X

Fig. 22 - Photomicrographs of  $\text{ThO}_2\text{-ZrB}_2$  compact after heating for 1 hour at  $2600^\circ\text{C}$  in hydrogen of  $0^\circ\text{C}$  dewpoint

**TABLE 13**  
OBSERVATIONS OF ThO<sub>2</sub> PELLETS SINTERED IN HYDROGEN  
AND THEN FIRED IN AIR AT 1050°C

Sintering Temperature, °C	Cold Pressed, psi	Apparent Density After Sintering, percent of theoretical	Appearance Of Cut Surface
2000	11,000	99 <sup>a</sup>	White
	25,000	95	White
2200	11,000	95	White
	25,000	98	Black center, 2-3 mm white rim
2400	11,000	96	White
	25,000	100	Black center, 1.5-2 mm white rim
2800	11,000	101.5	Black center, 0.5-1 mm white rim
	25,000	99	

<sup>a</sup>This measurement is believed to be too high. The sample appears porous.

**TABLE 14**  
LIQUEFACTION OF BORIDES IN CONTACT WITH GRAPHITE

Boride	Published Melting Point, °C	Liquefaction Temperature, °C	Sample Type
TiB <sub>2</sub>	2790 - 2980	2550 - 2600	Chip
		2500	Powder
ZrB <sub>2</sub>	2990 - 3040	2475 - 2525	Chip
		2425	Chip
		2400	Powder
HfB <sub>2</sub>	3062 - 3250	2600	Powder
WB	2400 - 2900	2375 - 2425	Powder
TaB	>2000	2725	Powder
NbB <sub>2</sub>	3000	2525 - 2550	Powder

where material has flowed to fill a T-shaped crack. Figure 22 is typical of areas observed on the  $\text{ThO}_2\text{-ZrB}_2$  and  $\text{ThO}_2\text{-HfB}_2$  samples.

The different behavior of the  $\text{ThO}_2\text{-TiB}_2$  specimen (Figure 21d) is illustrated in the photomicrograph shown in Figure 23. No dense layer is observed at the boundary of the cavity in this case. Examination of the specimen revealed small amounts of a second phase which had selectively collected at grain boundaries.

The results of microprobe examination of the samples of Figure 21 may be summarized as follows:

1. Only traces of tungsten were found in the samples. This indicates that the observed behavior was that of the samples and was not caused by contamination and fluxing by tungsten oxides from the crucible or heating element.
2. Insignificant amounts of Zr or Hf from the corresponding borides were found in the main body of the  $\text{ThO}_2$ . This indicates that no great transport of these ions by diffusion from their original locations occurred.
3. At the dense, non-porous areas, the sample current increased and the concentration of thorium fell off. The indication of Zr or Hf was high at the edge of such regions but was low inside them. Since higher sample current is characteristic of areas of lower average atomic weight, these observations are consistent with the assumption that the borides had been converted to borates which melted and flowed away, leaving the large cavities. Boron and oxygen are not directly observable by this technique.
4. The second phase in the heated  $\text{ThO}_2\text{-TiB}_2$  compact was high in Ti and low in Th. Except for these isolated regions, Ti was not detected in the  $\text{ThO}_2$  body of this sample.

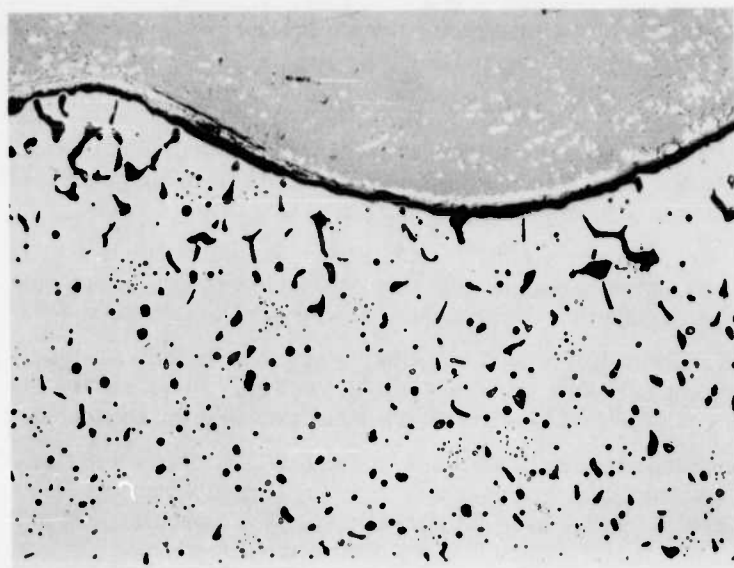
#### 4.5 REACTION OF BORIDES WITH GRAPHITE

Several sources refer to reaction of borides with graphite at  $2200^\circ$  to  $2500^\circ\text{C}$ . Feisel<sup>39</sup> stated that a  $\text{ZrB}_2$  compact reacted with a graphite container at  $2500^\circ\text{C}$  to produce a liquid phase. Jackson and Palmer<sup>40</sup> in their description of hot pressing techniques, note that "A liquid phase was produced, however, during the pressing of both zirconium boride and titanium boride at temperatures of the order of  $2300^\circ\text{C}$ . This is rather surprising since it has been shown by Glaser that the borides of zirconium and titanium are stable in the presence of carbon at temperatures up to their melting points ( $3040^\circ\text{C}$  and  $2980^\circ\text{C}$ , respectively). It would appear, nevertheless, that some decomposition of the boride or interaction with the die was taking place." Mr. A. A. R. Wood<sup>41</sup> related that, in his experience,  $\text{TiB}_2$ ,  $\text{ZrB}_2$ , and  $\text{TaB}_2$  all form liquid phases in contact with graphite at  $2200^\circ$  to  $2300^\circ\text{C}$ . Mr Wood indicated a report by Chown and Deacon<sup>42</sup> in which the melting temperatures were stated to be in the range  $2300^\circ$  to  $2500^\circ\text{C}$ .

#### Tests of Compatibility of Borides with Graphite

For these tests, a graphite crucible insulated with carbon black was induction heated in a slow flow of tank argon. Each boride sample was held in a small cavity drilled in a short piece of 1/2-inch-diameter spectrographic-grade graphite rod which was heated inside the larger crucible. A graphite cover with a 1/8-inch viewing opening was placed on the larger crucible. With practice, even though near black-body conditions prevailed inside the crucibles, the liquefaction of the samples could be readily observed through the pyrometer telescope. The results of the tests are summarized in Table 14. They confirm the observations of others that borides react with graphite at temperatures far below their melting points. Since the liquefaction temperature must depend strongly on the intimacy of contact of the boride with graphite and on the duration of preheating at temperatures where carbon diffusion can occur, these results probably would not be reproducible





Neg. 1888

100 X

Fig. 23—Photomicrograph of  $\text{ThO}_2\text{-TiB}_2$  compact after heating for 1 hour at  $2600^\circ\text{C}$  in hydrogen of  $0^\circ\text{C}$  dewpoint

in other experimental set-ups. It seems probable that bonded coatings would liquefy at lower temperatures than were observed in these experiments where the borides were in loose contact with the graphite.

#### 4.6 CONCLUSIONS

This research is considered to be a preliminary survey of the problem of compatibility of  $\text{ThO}_2$  with borides, rather than a comprehensive investigation. It did not indicate that thorium would protect borides from oxidation at high temperatures.

Thorium heated in dry hydrogen ( $-40^\circ\text{C}$  dewpoint) becomes substoichiometric  $\text{ThO}_{2-x}$  at approximately  $2200^\circ\text{C}$  and higher. This material may be friable. Thorium heated with  $\text{ZrB}_2$ ,  $\text{HfB}_2$ , or  $\text{TiB}_2$  in dry hydrogen produces a liquid phase in the temperature range of  $2500^\circ$  to  $2700^\circ\text{C}$ .

Thorium heated in moist hydrogen ( $0^\circ\text{C}$  dewpoint) is stable to at least  $2700^\circ\text{C}$ . When it is heated in this atmosphere in contact with  $\text{ZrB}_2$ ,  $\text{HfB}_2$ , or  $\text{TiB}_2$ , a liquid phase is formed at temperatures around  $2400^\circ$  to  $2600^\circ\text{C}$ . The first two borides probably are converted to borates.

These experiments indicated that thorium and commercial borides react at about  $2500^\circ\text{C}$ . This reaction may have been influenced by impurities or by the oxygen potential of the test atmosphere; however, it is not believed that the gross attack observed should be attributed to these effects. Rather, it is believed that thorium and the borides react with each other.

Various borides heated in contact with graphite in an argon atmosphere formed liquid phases at temperatures several hundred degrees below their melting points. This additional problem, the reaction of borides with graphite, indicates that the  $\text{ThO}_2$ -boride reaction may not be the factor which limits  $\text{ThO}_2$  as a protective coating.

#### 4.7 RECOMMENDATIONS

The recommendations that would be applicable to this portion of the work have been incorporated in the general recommendations of section 5.

## 5. GENERAL RECOMMENDATIONS

The objective of this work was to acquire information bearing on the feasibility of protecting graphite from oxidation at high temperature by covering it with an impervious layer of  $\text{ThO}_2$ . Reaction of graphite with  $\text{ThO}_2$  would be prevented by a buffer layer of a boride with a high melting point.

When this work was started, the limited information available indicated that borides would be stable in contact with graphite at temperatures up to their melting points. Evidence from this work and from recently available publications indicates that this premise is not correct if heating times of at least a few minutes are contemplated. If this protection scheme is to be investigated further, the first effort should be a re-examination of the compatibility of borides with graphite at high temperatures. The purity of the borides and the intimacy of their contact with graphite would be important parameters to consider in such tests.

If some borides appear to be compatible with graphite at desired temperatures, the next problem to consider is the protective qualities of a  $\text{ThO}_2$  layer. If the diffusion coefficients of oxygen in  $\text{ThO}_2$  as reported in section 2 are used as a basis for extrapolation to higher temperatures, a  $\text{ThO}_2$  diffusion barrier a few mils thick will not offer much protection at temperatures above  $2000^\circ\text{C}$ . With carefully controlled doping it might be possible to decrease the diffusion coefficient of oxygen in thoria by one or more orders of magnitude without lowering its melting point too drastically. If the maximum temperatures of acceptable boride-graphite compatibility are low enough, other oxides may be substituted for  $\text{ThO}_2$ .

Any further investigation of the feasibility of coating borides with an oxide will be seriously hampered unless thermal expansion coefficients are determined for the materials in the temperature ranges involved. With further development, deposition of  $\text{ThO}_2$  by pyrohydrolysis of  $\text{ThCl}_4$  might prove to be the most economical way to build up a coating on an initial layer applied by some other method. If the pyrohydrolysis method is to be investigated further, coating gases which omit  $\text{CO}_2$  should lessen the corrosion problem.

The above recommendations apply if relatively long-term protection is desired. If protection for only a few seconds to a minute were sufficient, then a much more elaborate program to investigate the kinetics of the destructive changes and the effects of thermal shock would be needed.

APPENDIXES I THROUGH VI

## APPENDIX I

### MATHEMATICAL SOLUTIONS OF THE DIFFUSION EQUATION

The diffusion coefficients reported in section 2 of this report were obtained by adjusting the parameters of an appropriate solution of the diffusion equation to give the best fit between experimentally determined quantities and the predictions of the mathematical model. A number of these solutions have been available for some time. These were rederived to check on the assumptions made in their formulation and to give assurance that typographical errors had not crept into the published versions. Other solutions are derived here for the first time.

Several techniques are available for solving linear partial differential equations together with specified initial and boundary conditions. The technique chosen here was the Laplace transform method. A brief discussion of Laplace transforms is included for readers who are not familiar with them. Following this discussion the various solutions are derived.

Many of the solutions, particularly those in the form of infinite series, are not convenient for numerical calculations. Appendices II, III, and IV present the details of the digital computer programs which have been prepared. Included are useful tables and graphs which simplify the work of obtaining the desired values of the diffusion coefficients.

#### I.1 THE LAPLACE TRANSFORM METHOD

This section is intended as a rapid review for those who have had some acquaintance with Laplace transforms or as a very brief introduction for those who are unfamiliar with this technique. For proofs, existence theorems, and detailed derivations the reader is referred to the various texts on the subject. Churchill<sup>43</sup>, McLachlan<sup>44</sup>, and Carslaw and Jaeger<sup>45</sup> are suitable. The text by McLachlan is particularly valuable for the problems treated here.\* A second book by Carslaw and Jaeger<sup>46</sup> has solutions of heat conduction problems which can be applied to diffusion problems by redefining the variables.

Before the utility of the Laplace transform method can be demonstrated, the transform must be defined and several of its properties described.

If  $f(x)$  is defined for all positive values of  $x$ , and if the function meets certain conditions that insure the existence of the following integral,

$$\bar{f}(p) = \int_0^{\infty} f(x) e^{-px} dx \quad (I-1)$$

then  $f(x)$  and  $\bar{f}(p)$  are said to be a Laplace transform pair. In particular,  $\bar{f}(p)$  is the (direct) transform of  $f(x)$  and  $f(x)$  is the inverse transform of  $\bar{f}(p)$ . Where no confusion should arise, the functions are referred to as  $f$  and  $\bar{f}$ . Similarly,  $\bar{x}$  is the transform of  $x$ , etc. Simple transforms may be derived by direct integration. For example, if  $f(x) = 1$ , then  $\bar{f}(p) = \int_0^{\infty} e^{-px} dx = 1/p$ . By such integrations and other methods, extensive tables of transform pairs have been computed. Refer-

\*This text employs a different definition of the Laplace transform.

ence to these tables frequently reduces the labor of applying the transform method. A small selection of transform pairs is shown in Table 15.

TABLE 15  
A SHORT LIST OF LAPLACE  
TRANSFORM PAIRS

$\bar{f}(p)$	$f(x)$
$\frac{1}{p}$	1
$\frac{1}{p^2}$	x
$\frac{1}{p^2 - m^2}$	$\frac{1}{m} \sinh mx$
$\frac{p}{p^2 - m^2}$	$\cosh mx$
$\frac{1}{p^{1/2} + a}$	$(\pi x)^{-1/2} - a e^{a^2 x} \operatorname{erfc}(ax^{1/2})^*$ $= (\pi x)^{-1/2} - a \operatorname{erfc}(ax^{1/2})^*$

\* $\operatorname{erfc} x \equiv 1 - \operatorname{erf} x$

$\operatorname{eerfc} x \equiv e^{x^2} \operatorname{erfc} x$

Several numerical tables of the error function ( $\operatorname{erf} x$ ) and the complementary error function ( $\operatorname{erfc} x$ ) are available.

A second point to be covered is the correspondence between certain operations on  $f(x)$  and  $\bar{f}(p)$ . If we adopt the symbolism,  $L[f(x)] = \bar{f}(p)$ , and use primes to indicate differentiation with respect to  $x$ , then integration by parts in Equation (I-1) leads to

$$L[f'(x)] = p\bar{f}(p) - f(0+), \quad (\text{I-2})$$

and

$$L[f''(x)] = p^2 \bar{f}(p) - pf(0+) - f'(0+). \quad (\text{I-3})$$

The quantity  $f(0+)$  is defined as the limit, as  $x$  approaches zero through positive values, of  $f(x)$ . This distinction is important when  $f(x)$  is discontinuous at  $x = 0$ .

With these preliminaries completed, let us solve a simple differential equation.

Given:

$$\frac{d^2 x(t)}{dt^2} - m^2 x(t) = 0$$

$$x(0+) = a \quad (\text{I-4})$$

$$x'(0+) = b,$$

where  $a$ ,  $b$ , and  $m$  are constants.

If we transform the equation term by term we obtain

$$p^2 \bar{x} - p x(0+) - x'(0+) - m^2 \bar{x} = 0 \quad (I-5)$$

$$(p^2 - m^2) \bar{x} = p a + b$$

$$\bar{x} = \frac{p a + b}{p^2 - m^2}$$

$$\bar{x} = a \left( \frac{p}{p^2 - m^2} \right) + b \left( \frac{1}{p^2 - m^2} \right) \quad (I-6)$$

By reference to the table of transforms,  $x = a \cosh mt + b/m \sinh mt$ .

If  $A \equiv b/m$  and  $B \equiv a$ , we reduce the solution to the familiar form

$$x(t) = A \sinh mt + B \cosh mt. \quad (I-7)$$

With a table of transforms available, the differential equation was solved by ordinary algebraic manipulations.

In the case of partial derivatives, one makes the transformation with respect to only one variable with each application of the transformation process. For example, given  $f(x, t)$  then transformation with respect to  $t$  leads to  $\bar{f}(x, p)$ . Also, with the proper restrictions on  $f(x, t)$  it can be shown that transformation with respect to  $t$  gives

$$L \left[ \frac{\partial}{\partial t} f(x, t) \right] = p \bar{f}(x, p) - f(x, 0+), \quad (I-8)$$

$$L \left[ \frac{\partial}{\partial x} f(x, t) \right] = \frac{d}{dx} \bar{f}(x, p), \quad (I-9)$$

and

$$L \left[ \frac{\partial^2}{\partial x^2} f(x, t) \right] = \frac{d^2}{dx^2} \bar{f}(x, p). \quad (I-10)$$

Frequently, including most of the cases treated in this Appendix, the inversion of the transform cannot be obtained by reference to available tables. In those cases, the Inversion Theorem may be used. This states that if

$$\bar{f}(p) = \int_0^\infty e^{-pt} f(t) dt, \quad p > 0,$$

then

$$f(t) = \frac{1}{2\pi i} \lim_{\beta \rightarrow \infty} \int_{\gamma - i\beta}^{\gamma + i\beta} e^{\lambda t} \bar{f}(\lambda) d\lambda \quad (I-11)$$

where  $\gamma$  is a constant greater than the real part of any singularity of  $\bar{f}(\lambda)$ . Application of the Inversion Theorem requires familiarity with complex variable theory and the evaluation of integrals by the residue theorem. These applications will be treated individually as special cases when they arise.

Finally, Theorem XI given on page 256 of reference 45 will be useful in later work. In the symbolism of this Appendix, the theorem states that if  $\bar{x}(0+)$  exists and if  $p \rightarrow 0$  through positive real values, then

$$\lim_{p \rightarrow 0} p \bar{x}(p) = \lim_{t \rightarrow \infty} x(t) \quad (I-12)$$

The restrictions on  $x(t)$  are ones which have already been assumed in this Appendix.

## I. 2 DIFFUSION FROM A LIMITED VOLUME OF WELL-STIRRED FLUID INTO A PLANE SLAB (INSTANTANEOUS EQUILIBRIUM AT THE SURFACE IS ASSUMED)

Assume that a plane slab of thickness  $2\ell$  is located in a coordinate system so that the faces of the slab lie in the planes  $x = \ell$  and  $x = -\ell$ . Also, assume that all of each face is exposed to a fixed volume of an aqueous dye solution. If the slab extends far enough in the  $y$  and  $z$  directions, the concentration gradient of dye diffusing into the solid will be  $\partial C / \partial x$ , a function of  $x$  only. If the diffusion coefficient,  $D$ , of the dye diffusing into the slab is independent of concentration,  $C$ , then Fick's second law of diffusion may be written

$$\frac{\partial^2 C}{\partial x^2} - \frac{1}{D} \frac{\partial C}{\partial t} = 0 \quad (\text{I-13})$$

where  $0 < x < \ell$ .

The concentration is a function of  $x$  and  $t$ . If  $C$  is measured in moles/cm<sup>3</sup> and  $t$  is in seconds, the diffusion coefficient,  $D$ , has the dimensions cm<sup>2</sup>/sec.

Now assume the same geometry, but replace the liquid with a well-mixed gas which is enriched in an isotope of oxygen. This isotope is to diffuse into the solid and displace a different isotope of the same element. For example, the gas may be enriched in O<sup>18</sup> which will diffuse into a solid oxide and displace O<sup>16</sup>.

In following the course of such an experiment, certain complications arise because it is much more convenient to deal with isotopic enrichment (mole fraction of the isotope) in the gas and in the solid than it is to compute concentrations (e.g. in moles/cm<sup>3</sup>). For the solid, let  $n_s^1$  = total moles per cubic centimeter of the element under consideration and let  $v(x, t)$  be the enrichment of the diffusing isotope. For example,  $n_s^1$  might be the moles of oxygen (total of all isotopes) per cubic centimeter and  $v(x, t)$  might be mole fraction of O<sup>18</sup>.

Since  $C = n_s^1 v$  and  $n_s^1$  is a constant, it follows that

$$\frac{\partial C}{\partial t} = n_s^1 \frac{\partial v}{\partial t}$$

and

$$\frac{\partial^2 C}{\partial x^2} = n_s^1 \frac{\partial^2 v}{\partial x^2}$$

Therefore, from Fick's second law we can derive the convenient expression

$$\frac{\partial^2 v}{\partial x^2} - \frac{1}{D} \frac{\partial v}{\partial t} = 0, \quad (\text{I-14})$$

where  $0 < x < \ell$ .

We turn now to Fick's first law

$$J = -D \frac{\partial C}{\partial x}. \quad (\text{I-15})$$

This relates the flux,  $J$ , of a material diffusing through an interface to the concentration gradient at the interface.

If  $C$  is in moles/cm<sup>3</sup>, then the unit of  $J$  will be moles/cm<sup>2</sup>-sec. Again, we must adapt this equation to the use of mole fractions. Assume that the volume of the solid is  $V$ , its total area exposed to the gas is  $A$ , and that it contains  $n_s$  moles of O. Since

$$\frac{\partial C}{\partial x} = n_s \frac{\partial v}{\partial x}$$



and

$$n_s = \frac{n_g}{V},$$

then

$$\frac{\partial C}{\partial x} = \frac{n_s}{V} \frac{\partial v}{\partial x}.$$

Also, if there are  $n_g$  moles of O in the gas and the enrichment of O in the isotope which is diffusing is  $u$ , then the amount per second of isotope leaving the gas is  $n_g(\partial u/\partial t)$ . This is equal to the total area times the flux per unit area. Therefore, at  $x = \ell$ ,

$$n_g \frac{\partial u}{\partial t} = JA = -DA \frac{\partial C}{\partial x} = -AD \frac{n_s}{V} \frac{\partial v}{\partial x}$$

The minus sign is needed in this equation because  $\partial u/\partial t$  is numerically negative and  $\partial v/\partial x$  is numerically positive at  $x = \ell$ . Let  $\lambda \equiv n_g/n_s$ , i.e.,  $\lambda$  is the ratio of moles of O in the gas to moles of O in the solid, without regard to isotopic composition. Also let  $S$  be the surface-to-volume ratio for the solid.

$$S = \frac{A}{V} \tag{I-16}$$

In the case of this slab,

$$S = \frac{A}{A\ell} = \frac{1}{\ell}$$

If areas are in  $\text{cm}^2$  and volumes in  $\text{cm}^3$ , then  $S$  has the dimension  $\text{cm}^{-1}$ . When these newly defined quantities are used,

$$\frac{\partial u}{\partial t} = -\frac{SD}{\lambda} \frac{\partial v}{\partial x} \tag{I-17}$$

when  $x = \ell$ , and  $t > 0$ .

Furthermore, from conditions of geometrical symmetry, there will be no net flow of isotope across the central plane of the slab. Therefore  $\partial C/\partial x = 0$ ,  $x = 0$ , and  $t \geq 0$  or

$$\frac{\partial v}{\partial x} = 0 \tag{I-18}$$

where  $x = 0$  and  $t \geq 0$ .

The assumption of isotopic equilibrium between the gas and the surface of the solid may be expressed by

$$u = v \tag{I-19}$$

for  $x = \ell$  and  $t \geq 0$ .

Finally, the values of  $u$  and  $v$  at the start of the experiment are specified as:

$$u = u_1 \tag{I-20}$$

when  $t = 0$  and

$$v = v_1 \tag{I-21}$$

when  $t = 0$  and  $0 \leq x \leq \ell$ .

In setting  $v = v_1$  it is assumed that at the start of the experiment the solid may already contain a uniform distribution of the isotope which will diffuse in. Also, the previous assumption that  $\partial v / \partial x$  is positive at  $x = \ell$  implies that  $u_1 > v_1$ .

To start the solution, transform the terms of Equation (I-14) to

$$\frac{d^2 \bar{v}}{dx^2} - \frac{1}{D}(p \bar{v} - v_1) = 0 \quad (I-22)$$

If we define

$$q^2 = \frac{p}{D} \quad (I-23)$$

where  $p$  is the Laplace transform variable and  $D$  is the diffusion coefficient, then

$$\frac{d^2 \bar{v}}{dx^2} - q^2 \bar{v} = -\frac{v_1}{D} \quad (I-24)$$

This has reduced the partial differential equation in the variable  $v(x, t)$  to an ordinary differential equation in the variable  $\bar{v}(x)$ . Until we are ready to make the inverse transformation,  $p$  is considered to be a parameter of the equation in the variable  $\bar{v}$ . The homogeneous equation corresponding to Equation (I-24) has the solution (see Equation I-7),

$$\bar{v} = A \sinh qx + B \cosh qx$$

Since  $v_1/p$  is a particular integral of Equation (I-24), the general solution of Equation (I-24) is

$$\bar{v} = A \sinh qx + B \cosh qx + \frac{v_1}{p} \quad (I-25)$$

We now particularize the solution by applying the restrictions of the various boundary conditions. From Equation (I-18)

$$\left. \frac{d\bar{v}}{dx} \right|_{x=0} = q (A \cosh 0 + B \sinh 0) = 0$$

Since  $\cosh 0 = 1$  and  $\sinh 0 = 0$ , for Equation (I-18) to be valid we must have  $A = 0$ , and

$$\bar{v} = B \cosh qx + \frac{v_1}{p} \quad (I-26)$$

If we define

$$M \equiv \frac{SD}{\lambda} \quad (I-27)$$

and use  $\bar{v}$  from Equation (I-26), then Equation (I-17) transforms to

$$p \bar{u} - u_1 = -MBq \sinh q \ell \quad (I-28)$$

From Equation (I-19),  $u = v$  at  $x = \ell$ . It follows that  $\bar{u} = \bar{v}$  at  $x = \ell$ , and

$$p \bar{v} - u_1 = -MBq \sinh q \ell \quad (I-29)$$

If we insert  $\bar{v}$  from Equation (I-26) and solve for B we find that

$$B = \frac{u_1 - v_1}{p \cosh q\ell + Mq \sinh q\ell} \quad (\text{I-30})$$

and thus from Equation (I-26) that

$$\bar{v} = \frac{(u_1 - v_1) \cosh qx}{p \cosh q\ell + Mq \sinh q\ell} + \frac{v_1}{p} \quad (\text{I-31})$$

Finally, since  $\bar{u} = \bar{v}$  at  $x = \ell$ , we have

$$\bar{u} = \frac{(u_1 - v_1) \cosh q\ell}{p \cosh q\ell + Mq \sinh q\ell} + \frac{v_1}{p} \quad (\text{I-32})$$

The next step will be to invert  $\bar{u}$  and thus find  $u(t)$ , the variation of enrichment of the gas as a function of time. The latter quantity  $u(t)$  can be determined by experiment.

First, however, let us examine a way to make the subsequent algebraic manipulations simpler. If we adopt the symbolism  $L^{-1}[\bar{f}(p)] = f(x)$  to indicate the operation of performing the inverse transformation and if we temporarily transform only the second term of  $\bar{u}$ , then

$$\frac{u - v_1}{u_1 - v_1} = L^{-1} \left( \frac{\cosh q\ell}{p \cosh q\ell + Mq \sinh q\ell} \right) \quad (\text{I-33})$$

The quantity in parentheses is exactly the transform of  $u/u_1$  that would have been obtained if we had assumed  $v_1 = 0$  in Equation (I-21). This can be shown to be true in all cases discussed in this Appendix by making a simple transformation of the variables, e.g.,  $u^* = u - v_1$ ,  $v^* = v - v_1$ . For convenience, in the derivations in this Appendix we will first assume  $v_1 = 0$  and then generalize the result to apply when  $v_1$  is a constant.

The remaining problem is to find the inverse transformation of

$$\bar{u} = \frac{u_1 \cosh q\ell}{p \cosh q\ell + Mq \sinh q\ell} \quad (\text{I-34})$$

Tables are inadequate for this purpose, so the Inversion Theorem, Equation (I-11), must be used.

For convenience, we divide both sides of Equation (I-34) by  $u_1$  and divide the numerator and denominator of the right hand side by  $\cosh q\ell$ . Then

$$\frac{u}{u_1} = \frac{1}{2\pi i} \int_{\gamma-i\infty}^{\gamma+i\infty} \frac{e^{pt} dp}{p + Mq \tanh q\ell} \quad (\text{I-35})$$

We now find the values of  $p$  which make the denominator of the integrand zero and then find the residues of the integrand at these values of  $p$ . When  $p = 0$ , then  $q \equiv \sqrt{p/D} = 0$ , also. The denominator will be zero for  $p = 0$  and for additional values of  $p$  which make  $(1 + Mq/p \tanh q\ell)$  equal to zero. McLachlan, in Chapter III of reference 44, has a good discussion of the evaluation of such integrals. The integrand is of the form  $f(p)/pg(p)$  and its singularities are simple poles.

For this discussion, the formula which applies is

$$\frac{1}{2\pi i} \int_{\gamma-i\infty}^{\gamma+i\infty} \frac{f(p) dp}{p g(p)} = \frac{f(0)}{g(0)} + \sum_{m=1}^{\infty} \frac{f(a_m)}{a_m g'(a_m)}, \quad (\text{I-36})$$

where

$$g'(a_m) = \left[ \frac{d}{dp} g(p) \right]_{p=a_m}$$

From Equation (I-35),

$$f(p) = e^{pt}$$

and

$$g(p) = 1 + \frac{Mq}{p} \tanh q^\ell$$

Since  $p = Dq^2$  and  $M \equiv \frac{SD}{\lambda}$ ,

$$g(p) = 1 + \frac{SDq}{\lambda Dq^2} \tanh q^\ell = 1 + \frac{S}{\lambda} \frac{\tanh q^\ell}{q}$$

$$\lim_{q \rightarrow 0} \frac{\tanh q^\ell}{q} = \lim_{q \rightarrow 0} \frac{1}{q} \left( q^\ell - \frac{(q^\ell)^3}{3} + \frac{2(q^\ell)^5}{15} - \dots \right) = \ell$$

Also,  $S = 1/\ell$

Therefore  $g(0) = 1 + 1/\lambda$ ,  $f(0) = 1$ ,

$$\text{and } \frac{f(0)}{g(0)} = \frac{\lambda}{1 + \lambda}. \quad (\text{I-37})$$

In the derivations which follow this one, it is much more difficult to evaluate  $f(0)/g(0)$ . To show how an alternative method works, we apply it to arrive at Equation (I-37).

Recalling Theorem XI as expressed in Equation (I-12), we note that

$$\frac{f(0)}{g(0)} = \lim_{p \rightarrow 0} p \frac{\bar{u}(p)}{u_1} = \lim_{t \rightarrow \infty} \frac{u(t)}{u_1} = \frac{u(\infty)}{u_1}. \quad (\text{I-38})$$

At  $t = 0$  there are  $n_g u_1 + 0 n_s$  moles of isotope. As  $t \rightarrow \infty$ ,  $u \rightarrow v \rightarrow u(\infty)$  and there are  $(n_s + n_g) u(\infty)$  moles of isotope. Since none of the isotope is formed nor destroyed,

$$\begin{aligned} n_g u_1 &= (n_s + n_g) u(\infty) \\ \frac{u(\infty)}{u_1} &= \frac{n_g}{n_s + n_g} = \frac{n_g/n_s}{\frac{n_s}{n_s} + \frac{n_g}{n_s}} = \frac{\lambda}{1 + \lambda} \end{aligned} \quad (\text{I-39})$$

We see that Equation (I-39) is the residue of the integrand of Equation (I-35) for  $p = 0$ .

To find the zeroes of  $g(p)$ , set

$$p + Mq \tanh q^\ell = 0 \quad (\text{I-40})$$

With

$$p = q^2 D$$

and

$$M = \frac{SD}{\lambda} = \frac{D}{\lambda^\ell},$$

Equation (I-40) is satisfied when

$$\tanh q^\ell = -\lambda q^\ell \quad (\text{I-41})$$

For convenience, we can convert to circular functions by recalling the identity:  $\tanh ix = i \tan x$  and by setting  $q = i q_n$ .

$$\tanh i q_n^\ell = -i q_n \lambda^\ell$$

$$i \tan q_n^\ell = -i q_n \lambda^\ell$$

$$\tan q_n^\ell = -q_n \lambda^\ell$$

Define  $q_a \equiv q_n^\ell$ , then

$$\tan q_a = -q_a \lambda \quad (\text{I-42})$$

Equation (I-42) gives the values of  $q_a$  at which we must evaluate

$$\sum_{a=1}^{\infty} \left[ \frac{f(p)}{p g'(p)} \right]_{q_a}$$

From  $Dq^2 = p$ , it follows that

$$\frac{dp}{dq} = \frac{1}{2 Dq}$$

Calculations are simplified if we note that

$$\begin{aligned} p \frac{d}{dp} g(p) &= p \frac{d}{dq} g(p) \frac{dq}{dp} = \frac{q}{2} \frac{d}{dq} g(p) \\ p \frac{d}{dp} g(p) &= \frac{q}{2} \frac{d}{dq} g(Dq^2) \end{aligned} \quad (\text{I-43})$$

When the differentiation is performed and terms collected

$$p \frac{d}{dp} g(Dq^2) = \frac{1}{2} \left[ \frac{1}{\lambda} (1 - \tanh^2 q^\ell) - \frac{\tanh q^\ell}{q} \right]$$

With the substitution  $\tanh q^\ell = \tanh i q_a = i \tan q_a = -i q_a \lambda$ , then

$$p \frac{d}{dp} g(p) = \frac{1}{2\lambda} (q_a^2 \lambda^2 + \lambda + 1).$$

Also,  $f(q) = e^{-pt} = e^{-Dq^2 t} = e^{-\frac{Dq_a^2 t}{\ell^2}}$

Therefore

$$\frac{u}{u_1} = \frac{\lambda}{1+\lambda} + 2\lambda \sum_{a=1}^{\infty} \frac{e^{-\frac{Dq_a^2 t}{\ell^2}}}{q_a^2 \lambda^2 + \lambda + 1} \quad (\text{I-44})$$

The solution is often presented in an alternative form in terms of  $M_t/M_{\infty}$ .

$$\frac{M_t}{M_{\infty}} = \frac{\text{mass of isotope which has left the gas after time } t}{\text{mass of isotope which would leave gas as } t \rightarrow \infty} \quad (\text{I-45})$$

$$\begin{aligned} &= \frac{n_g u_1 - n_g u(t)}{n_g u_1 - n_g u(\infty)} \\ &= \frac{1 - \frac{u(t)}{u_1}}{1 - \frac{u(\infty)}{u_1}} \end{aligned} \quad (\text{I-46})$$

$\frac{u(t)}{u_1}$  is given by Equation (I-41) and  $\frac{u(\infty)}{u_1} = \frac{\lambda}{1+\lambda}$  from Equation (I-39).

Therefore,

$$\begin{aligned} \frac{M_t}{M_{\infty}} &= \frac{1 - \frac{u(t)}{u_1}}{1 - \frac{\lambda}{1+\lambda}} \\ &= 1 + \lambda - (1 + \lambda) \frac{u(t)}{u_1} \end{aligned} \quad (\text{I-47})$$

$$\frac{M_t}{M_{\infty}} = 1 - \sum_{a=1}^{\infty} \frac{2\lambda(1+\lambda) e^{-q_a^2 \frac{Dt}{\ell^2}}}{q_a^2 \lambda^2 + \lambda + 1} \quad (\text{I-48})$$

The  $q_a$ 's are the positive non-zero roots of the equation  $\tan q_a = -q_a \lambda$ . This form of the solution is shown on page 53 of reference 4.

### I. 3 DIFFUSION FROM A LIMITED VOLUME OF A WELL-STIRRED FLUID INTO A PLANE SLAB (EQUILIBRATION AT THE SURFACE PROCEEDS AT A FINITE RATE.)

Much of the discussion of Section I. 2 applies to this case. If  $u$  = enrichment in the gas and  $v$  = enrichment in the solid, then

$$\frac{\partial^2 v}{\partial x^2} - \frac{1}{D} \frac{\partial v}{\partial t} = 0 \quad (\text{I-49})$$

when  $0 \leq x \leq \ell$  and  $t > 0$ , and

$$\frac{\partial u}{\partial t} = -\frac{SD}{\lambda} \frac{\partial v}{\partial x} \quad (\text{I-50})$$

when  $x = \ell$  and  $t = 0$ .

When  $x = 0$  and  $t > 0$

$$\frac{\partial v}{\partial x} = 0; \quad (I-51)$$

when  $t = 0$

$$u = u_1; \quad (I-52)$$

when  $0 \leq x \leq \ell$  and  $t = 0$

$$v = 0; \quad (I-53)$$

and when  $x = \ell$  and  $t > 0$

$$K(u - v) - D \frac{\partial v}{\partial x} = 0. \quad (I-54)$$

Since it was shown in section I.2 that  $v_1$  may be set equal to zero with no loss in generality, Equations (I-49) to (I-53) are valid for the reasons presented in the previous section. Equation (I-54) needs further justification. If Equation (I-54) is solved for  $D(\partial v / \partial x)$  and that value is inserted in Equation (I-50), we obtain

$$\frac{\partial u}{\partial t} = - \frac{KS(u - v)}{\lambda} \quad (I-55)$$

when  $x = \ell$  and  $t > 0$ .

This equation merely indicates that the rate of decrease of enrichment of the gas is directly proportional to the surface-to-volume ratio, is directly proportional to the instantaneous difference between the enrichment of the gas and the enrichment of the surface of the solid exposed to the gas, and is inversely proportional to  $n_g/n_s$ .  $K$  is a proportionality constant with the dimensions cm/sec. Equation (I-54) or (I-55) is regarded as representing a reasonable assumption. Haul, Dumbgen, and Just<sup>7</sup> present a kinetic derivation of Equation (I-54).

The solution of Equation (I-49) through (I-54) proceeds along familiar lines. The transform of Equation (I-49) with  $v_1 = 0$  and  $q^2 = p/D$  is

$$\frac{d^2 \bar{v}}{dx^2} - q^2 \bar{v} = 0. \quad (I-56)$$

From Equation (I-7) we have

$$\bar{v} = A \sinh qx + B \cosh qx \quad (I-57)$$

From  $\frac{d \bar{v}}{dx} = 0$ , then  $\frac{d \bar{v}}{dx} = 0$ ;

and, as before,  $A = 0$  if this condition is to hold. So

$$\bar{v} = B \cosh qx \quad (I-58)$$

Equation (I-50) may be rearranged to  $\frac{\lambda}{S} \frac{\partial u}{\partial t} + D \frac{\partial v}{\partial x} = 0$

and transformed to  $\frac{\lambda}{S} [p \bar{u} - u(0)] + D \frac{d\bar{v}}{dx} = 0$ , or

$$\frac{\lambda}{S} p \bar{u} + D \frac{d\bar{v}}{dx} = \frac{\lambda u_1}{S} \quad (\text{I-59})$$

where  $x = \ell$  and  $t > 0$ .

Equation (I-54) transforms to

$$K(\bar{u} - \bar{v}) - D \frac{d\bar{v}}{dx} = 0 \quad (\text{I-60})$$

where  $x = \ell$  and  $t > 0$ .

If  $\bar{v} = B \cosh qx$  and  $d\bar{v}/dx = qB \sinh qx$  are inserted in Equations (I-59) and (I-60), we get, after gathering terms in  $\bar{u}$  and  $B$ ,

$$\begin{cases} \frac{\lambda p}{S} \bar{u} + (Dq \sinh q\ell) B = \frac{\lambda u_1}{S} \\ K\bar{u} - (K \cosh q\ell + Dq \sinh q\ell) B = 0 \end{cases} \quad (\text{I-61})$$

By Cramer's rule

$$\begin{aligned} \bar{u} &= \frac{\begin{vmatrix} \frac{\lambda u_1}{S} & Dq \sinh q\ell \\ 0 & -(K \cosh q\ell + Dq \sinh q\ell) \end{vmatrix}}{\begin{vmatrix} \frac{\lambda p}{S} & Dq \sinh q\ell \\ K & -(K \cosh q\ell + Dq \sinh q\ell) \end{vmatrix}} \\ \bar{u} &= u_1 \frac{K \cosh q\ell + Dq \sinh q\ell}{Kp \cosh q\ell + \left(p + \frac{KS}{\lambda}\right) Dq \sinh q\ell} \end{aligned}$$

Define  $N \equiv \frac{KS}{\lambda}$ . Divide numerator and denominator by  $\cosh q\ell$ .

$$\frac{\bar{u}}{u_1} = \frac{K + Dq \tanh q\ell}{Kp + (p + N) Dq \tanh q\ell} \quad (\text{I-62})$$

To find  $u/u_1$ , the Inversion Theorem, Equation (I-11) must be used.

$$\frac{u}{u_1} = \frac{1}{2\pi i} \int_{\gamma - i\infty}^{\gamma + i\infty} \frac{e^{pt} (K + Dq \tanh q\ell) dp}{Kp + (p + N) Dq \tanh q\ell} \quad (\text{I-63})$$



There are singular points of the integrand for  $p = 0$  and for values of  $p$  that satisfy

$$\tanh q^\ell = - \frac{Kp}{(p+N) Dq} \quad (I-64)$$

The integrand is of the form  $f(p)/p g(p)$  and the treatment of section I. 2 applies. By the same arguments that led to Equations (I-38) and (I-39), the residue for  $p = 0$  is  $\lambda/(1+\lambda)$ .

For the zeroes of  $g(p)$ , we start with Equation (I-64), and proceed to circular functions through the identity:  $\tanh ix = i \tan x$  and by use of the definitions  $q \equiv iq_n \equiv i q_a S$ . We find that

$$\tan q_a = \frac{q_a}{\frac{DS}{K} q_a^2 - \frac{1}{\lambda}}$$

The quantity  $DS/K$  is an important dimensionless ratio which is designated  $Q$ . If we designate  $T \equiv Qq_a^2 - 1/\lambda$ , the auxiliary equation may be written

$$\tan q_a = \frac{q_a}{Qq_a^2 - \frac{1}{\lambda}} = \frac{q_a}{T} \quad (I-65)$$

To evaluate the residues for  $p \neq 0$  we need

$$p \frac{d}{dp} \left[ K + (p+N) \frac{Dq}{p} \tanh q^\ell \right]$$

From Equation (I-43), this is equal to

$$\frac{q}{2} \frac{d}{dq} \left( K + \frac{Dq^2 + N}{q} \tanh q^\ell \right)$$

When the differentiation is performed,

$$p g'(p) = \frac{q}{2} \left[ \left( \frac{Dq^2 + N}{q} \right) (1 - \tanh^2 q^\ell)^\ell + (\tanh q^\ell) \left( \frac{Dq^2 - N}{q^2} \right) \right] \quad (I-66)$$

With the various substitutions,

$$q = iq_n = i q_a S$$

$$q^\ell = i q_a$$

$$N = \frac{KS}{\lambda}$$

and

$$\tan q_a = \frac{q_a}{T}$$

one can arrive at

$$p g'(p) = - \frac{K}{2T} \left[ T^2 + q_a^2 + T + \frac{2}{\lambda} \right] \quad (I-67)$$

The algebra for these steps is quite tedious. One should make every effort to identify such dimensionless groups as  $Q$ ,  $N$ ,  $T$ , etc. and carry them through the manipulations.

Similarly,

$$\begin{aligned} f(p) &= (K + Dq \tanh q \ell) e^{pt} \\ &= \left[ K + (D i q_a S) \left( \frac{i q_a}{T} \right) \right] e^{Dq^2 t} \\ f(p) &= -\frac{K}{T\lambda} e^{-q_a^2 \frac{Dt}{\ell^2}} \end{aligned} \quad (I-68)$$

$$\frac{f(p)}{p g'(p)} = \frac{\frac{2}{\lambda} e^{-q_a^2 \frac{Dt}{\ell^2}}}{T^2 + q_a^2 + T + \frac{2}{\lambda}} \quad (I-69)$$

We complete the inversion of  $\bar{u}$  by evaluating the series indicated in Equation (I-36).

$$\frac{u}{u_1} = \frac{\lambda}{1 + \lambda} + \frac{2}{\lambda} \sum_{a=1}^{\infty} \frac{e^{-q_a^2 \frac{Dt}{\ell^2}}}{T^2 + q_a^2 + T + \frac{2}{\lambda}} \quad (I-70)$$

By use of Equation (I-47), this result may be expressed as

$$\frac{M_t}{M_{\infty}} = 1 - \frac{2(1 + \lambda)}{\lambda} \sum_{a=1}^{\infty} \frac{e^{-q_a^2 \frac{Dt}{\ell^2}}}{T^2 + q_a^2 + T + \frac{2}{\lambda}} \quad (I-71)$$

In Equations (I-70) and (I-71), the  $q_a$ 's are the non-zero, positive roots of

$$\tan q_a = \frac{q_a}{T} = \frac{q_a}{Q q_a^2 - \frac{1}{\lambda}}$$

If one substitutes  $Q q_a^2 - 1/\lambda$  for  $T$ , expands, and collects terms, Equation (I-70) reduces to Equation (11) of the article by Haul, Dömbgen, and Just.

One of the reasons for carrying out the derivation in section I.2 is that it represents the limiting case of I.3 as  $K \rightarrow \infty$ . This provides useful checks on the algebraic manipulations. For example, Equation (I-62) may be rewritten as

$$\begin{aligned} \frac{\bar{u}}{u_1} &= \frac{1 + \frac{Dq}{K} \tanh q \ell}{p + \left( p + \frac{KS}{\lambda} \right) \frac{Dq}{K} \tanh q \ell} \\ \lim_{K \rightarrow \infty} \frac{\bar{u}}{u_1} &= \frac{1}{p + \frac{DSq}{\lambda} \tanh q \ell} \end{aligned} \quad (I-72)$$

Equation (I-72) is identical with Equation (I-34) of section I. 2. Similarly the equation for  $\tan q_a$  and the equation for  $u/u_1$  in section I. 3 are reduced to their counterparts in section I. 2 as  $K \rightarrow \infty$  (or as  $Q \rightarrow 0$ ).

#### I. 4 DIFFUSION FROM A LIMITED VOLUME OF WELL-STIRRED FLUID INTO A SPHERE (INSTANTANEOUS EQUILIBRIUM AT THE SURFACE IS ASSUMED)

Assume that a sphere of radius  $a$  is immersed in a limited volume of well-stirred gas which is enriched in an isotope of element O. This isotope is to diffuse into the solid sphere and displace a different isotope of the same element. We wish to derive a mathematical expression for the enrichment of the gas as a function of time. Most of the quantities used have been defined in section I. 2, and much of the preliminary discussion of that section applies to this case, also.

In general coordinates, Fick's second law may be written

$$\frac{\partial C}{\partial t} = D \nabla^2 C \quad (\text{I-73})$$

It is assumed that  $D$  is constant.

If the center of the sphere is chosen as the center of a system of spherical coordinates, and if  $C$  exhibits radial symmetry in the solid, then Equation (I-73) may be written

$$\frac{\partial^2 C}{\partial r^2} + \frac{2}{r} \frac{\partial C}{\partial r} - \frac{1}{D} \frac{\partial C}{\partial t} = 0 \quad (\text{I-74})$$

where  $0 \leq r \leq a$  and  $t > 0$ .

By the arguments that led to Equation (I-14), Equation (I-74) reduces to

$$\frac{\partial^2 v}{\partial r^2} + \frac{2}{r} \frac{\partial v}{\partial r} - \frac{1}{D} \frac{\partial v}{\partial t} = 0 \quad (\text{I-75})$$

where  $0 \leq r \leq a$  and  $t > 0$ . Also,

$$\frac{\partial u}{\partial t} = - \frac{DS}{\lambda} \frac{\partial v}{\partial r} \quad (\text{I-76})$$

where  $r = a$  and  $t > 0$

Here,  $\lambda = \frac{n_g}{n_s}$  still, but

$$S = \frac{A}{V} = \frac{4\pi a^2}{\frac{4}{3}\pi a^3} = \frac{3}{a}$$

Further, when  $r = a$  and  $t > 0$

$$u = v; \quad (\text{I-77})$$

when  $t = 0$

$$u = u_1; \quad (\text{I-78})$$

when  $0 \leq r \leq a$  and  $t = 0$

$$v = 0; \quad (I-79)$$

and when  $t \geq 0$

$$v \text{ is finite at } r = 0. \quad (I-80)$$

To start the solution for this case, note that

$$\frac{\partial^2 (r v)}{\partial r^2} - \frac{1}{D} \frac{\partial (r v)}{\partial t} = 0, \quad (I-81)$$

where  $0 \leq r \leq a$  and  $t > 0$ , is equivalent to Equation (I-75). This can be established by carrying out the indicated differentiations.

The transform of Equation (I-81) is

$$\begin{aligned} \frac{d^2 (r \bar{v})}{dr^2} - \frac{1}{D} \left[ p(r \bar{v}) - (r \bar{v})_{t=0} \right] &= 0 \\ \frac{d^2 (r \bar{v})}{dr^2} - q^2 (r \bar{v}) &= 0 \end{aligned} \quad (I-82)$$

where  $q^2 \equiv \frac{p}{D}$ .

The solution to this familiar equation is

$$(r \bar{v}) = A \sinh qr + B \cosh qr$$

For  $r = 0$ ,  $v$  was assumed to be finite. At that point,  $\bar{v}$  is finite also and  $r \bar{v} = 0$

$$0 = A \sinh 0 + B \cosh 0$$

when  $r = 0$ .

Since  $\cosh 0 = 1$ , to satisfy the boundary conditions we must have  $B = 0$ .

$$r \bar{v} = A \sinh q r$$

$$\bar{v} = \frac{A}{r} \sinh q r \quad (I-83)$$

$$\frac{d \bar{v}}{dr} = \frac{r q A \cosh q r - A \sinh q r}{r^2} \quad (I-84)$$

Next, transform Equation (I-76):

$$p \bar{u} - u(0) = - \frac{DS}{\lambda} \frac{d \bar{v}}{dr} \quad (I-85)$$

when  $r = a$ .

Since  $u(0) = u_1$  and  $\bar{u} = \bar{v}$  at  $r = a$ ,

$$p\bar{v} - u_1 = -\frac{DS}{\lambda} \frac{d\bar{v}}{dr}$$

when  $r = a$ .

Insert  $\bar{v}$  and  $d\bar{v}/dr$  from Equations (I-83) and (I-84), expand, and collect terms.

$$\begin{aligned} A &= \frac{u_1}{\left(\frac{p}{a} - \frac{DS}{\lambda a^2}\right) \sinh qa + \frac{DSq}{\lambda a} \cosh qa} \\ \left[\bar{u} = \bar{v}\right]_{r=a} &= \frac{A}{a} \sinh qa \\ &= \frac{u_1}{a} \frac{\sinh qa}{\left(\frac{p}{a} - \frac{DS}{\lambda a^2}\right) \sinh qa + \frac{DSq}{\lambda a} \cosh qa} \end{aligned} \quad (I-86)$$

This can be reduced to

$$\frac{\bar{u}}{u_1} = \frac{\lambda}{\left(p\lambda - \frac{DS}{a}\right) + DSq \coth qa} \quad (I-87)$$

The next step is to find  $\frac{u}{u_1}$  from Equation (I-87) by application of the Inversion Theorem.

$$\frac{u}{u_1} = \frac{1}{2\pi i} \int_{\gamma-i\infty}^{\gamma+i\infty} \frac{\lambda e^{pt} dp}{\left(p\lambda - \frac{DS}{a}\right) + DSq \coth qa} \quad (I-88)$$

The denominator is zero for  $p = 0$  and for values of  $p$  that satisfy the equation

$$\tanh qa = \frac{-DSq}{p\lambda - \frac{DS}{a}} \quad (I-89)$$

(We have chosen to write Equation (I-89) in terms of  $\tanh qa = 1/\coth qa$ .) The process of inversion proceeds in a way very similar to that for Equations (I-35) or (I-63).

As in the previous cases, the residue for  $p = 0$  is  $\lambda/(1+\lambda)$ . Equation (I-89) is converted to circular functions for convenience. Use of  $S = 3/a$  leads to

$$\tan q_a = \frac{3q_a}{q_a^2 \lambda + 3} \quad (I-90)$$

We must sum the values of

$$\frac{f(p)}{p g'(p)} \text{ for the values of } q_a \text{ from Equation (I-90).}$$

$$\begin{aligned}
p \frac{d}{dp} g(p) &= p \frac{d}{dp} \left[ \left( \lambda - \frac{DS}{ap} \right) + \frac{DSq}{p} \coth qa \right] \\
&= \frac{q}{2} \frac{d}{dq} \left[ \left( \lambda - \frac{DS}{aDq^2} \right) + \frac{DSq}{Dq^2} \coth qa \right] \\
&= \frac{3}{a^2 q^2} \left[ 2 + q^2 a^2 (1 - \coth^2 qa) - qa \coth qa \right]
\end{aligned} \tag{I-91}$$

From Equation (I-90) and by use of the identity  $\coth ix = -i \cot ix$ , we have

$$\coth qa = -i \left( \frac{q_a^2 \lambda + 3}{3q_a} \right) \tag{I-92}$$

$q_a$  was defined so that  $\coth qa = \coth iq_a$ .

When Equation (I-92) is inserted into Equation (I-91), the result is

$$p \frac{d}{dp} g(p) = \frac{1}{6} \left[ q_a^2 \lambda^2 + 9\lambda + 9 \right] \tag{I-93}$$

Also

$$\begin{aligned}
f(p) &= \lambda e^{pt}; \\
p = Dq^2 &= D \left( \frac{iq_a}{a} \right)^2 = - \frac{Dq_a^2}{a^2}; \\
f(p) &= \lambda e^{-q_a^2 \frac{Dt}{a^2}}
\end{aligned} \tag{I-94}$$

Evaluation of the series indicated in Equation (I-36) leads to

$$\frac{u}{u_1} = \frac{\lambda}{1 + \lambda} + \sum_{a=1}^{\infty} \frac{6\lambda e^{-q_a^2 \frac{Dt}{a^2}}}{q_a^2 \lambda^2 + 9\lambda + 9} \tag{I-95}$$

If  $v_1 \neq 0$  then we replace

$$\frac{u}{u_1} \text{ by } \frac{u - v_1}{u_1 - v_1}$$

By application of Equation (I-47), Equation (I-95) may be written in the familiar alternative form

$$\frac{M_t}{M_{\infty}} = 1 - \sum_{a=1}^{\infty} \frac{6\lambda(1 + \lambda) e^{-q_a^2 \frac{Dt}{a^2}}}{q_a^2 \lambda^2 + 9\lambda + 9} \tag{I-96}$$

For Equations (I-95) or (I-96), the  $q_a$ 's are the positive, non-zero roots of

$$\tan q_a = \frac{3q_a}{q_a^2 \lambda + 3}$$

Equation (I-96) is the form of the solution which is given by Crank on page 88 of reference 4.

Appendix II presents a digital computer program for evaluating Equation (I-96). A table of computed values and a convenient graphical presentation of the results are included.

#### I.5 DIFFUSION FROM A LIMITED VOLUME OF WELL-STIRRED FLUID INTO A SPHERE (EQUILIBRATION AT THE SURFACE PROCEEDS AT A FINITE RATE)

Assume that a sphere of radius  $a$  is immersed in a limited volume of well-stirred gas which is enriched in an isotope of element O. This isotope is to diffuse into the solid sphere and displace a different isotope of the same element. We wish to derive a mathematical expression for the enrichment of the gas as a function of time. It is assumed that isotopic exchange at the surface of the sphere proceeds at a finite rate.

This case is mathematically similar to that discussed in section I.4, but Equation (I-77) must be replaced by Equation (I-54) from section I.3.

The set of equations to be solved is:

$$\frac{\partial^2 v}{\partial r^2} + \frac{2}{r} \frac{\partial v}{\partial r} - \frac{1}{D} \frac{\partial v}{\partial t} = 0 \quad (\text{I-97})$$

where  $0 \leq r \leq a$  and  $t > 0$ , and

$$\frac{\partial u}{\partial t} = -\frac{DS}{\lambda} \frac{\partial v}{\partial r} \quad (\text{I-98})$$

when  $r = a$  and  $t > 0$ .

When  $t = 0$

$$u = u_1; \quad (\text{I-99})$$

when  $0 \leq r \leq a$  and  $t = 0$

$$v = 0; \quad (\text{I-100})$$

and when  $r = a$  and  $t > 0$

$$K(u - v) - D \frac{\partial v}{\partial r} = 0. \quad (\text{I-101})$$

The arguments that led to Equations (I-83) and (I-84) still apply, so that

$$\bar{v} = \frac{A}{r} \sinh qr \quad (\text{I-102})$$

$$\frac{d\bar{v}}{dr} = \frac{r q A \cosh qr}{r^2} - \frac{A \sinh qr}{r^2} \quad (\text{I-103})$$

Transform Equation (I-98), with  $v(0) = v_1$ , and transform Equation (I-101) to give

$$\left\{ \begin{array}{l} \frac{\lambda p}{S} \bar{u} + D \frac{d\bar{v}}{dr} = \frac{\lambda}{S} u_1 \\ K(\bar{u} - \bar{v}) - D \frac{d\bar{v}}{dr} = 0 \end{array} \right\} \quad r = a \quad \text{and } t > 0 \quad (\text{I-104})$$

Insert  $\bar{v}$  and  $d\bar{v}/dr$  from Equation (I-102) and (I-103) into Equation (I-104). Set  $r = a$ , and collect terms in  $\bar{u}$  and in  $A$ .

$$\left\{ \begin{array}{l} \frac{p\lambda}{S} \bar{u} + \left( \frac{Dq}{a} \cosh qa - \frac{D}{a^2} \sinh qa \right) A = \frac{\lambda u_1}{S} \\ K\bar{u} + \left[ \left( \frac{D}{a^2} - \frac{K}{a} \right) \sinh qa - \frac{Dq}{a} \cosh qa \right] A = 0 \end{array} \right\} \quad (\text{I-105})$$

By application of Cramer's rule

$$\bar{u} = \frac{\begin{vmatrix} \frac{\lambda u_1}{S} & (qa \cosh qa - \sinh qa) \\ 0 & - \left[ qa \cosh qa + \left( \frac{Ka}{D} - 1 \right) \sinh qa \right] \end{vmatrix}}{\begin{vmatrix} \frac{p\lambda}{S} & (qa \cosh qa - \sinh qa) \\ \frac{D}{a^2} & K - \left[ qa \cosh qa + \left( \frac{Ka}{D} - 1 \right) \sinh qa \right] \end{vmatrix}} \quad (\text{I-106})$$

This may be written as

$$\frac{\bar{u}}{u_1} = \frac{qa \cosh qa + \left( \frac{Ka}{D} - 1 \right) \sinh qa}{\left( p + \frac{KS}{\lambda} \right) qa \cosh qa + \left[ p \left( \frac{Ka}{D} - 1 \right) - \frac{KS}{\lambda} \right] \sinh qa} \quad (\text{I-107})$$

Since  $a = \frac{3}{S}$ ,

$$\left( \frac{Ka}{D} - 1 \right) = \left( \frac{3K}{DS} - 1 \right)$$

The quantity  $DS/K$  is an important dimensionless group, which is designated by  $Q$ . We also define  $N$  so that

$$N \equiv \left( \frac{Ka}{D} - 1 \right) \equiv \left( \frac{3}{Q} - 1 \right)$$



With these substitutions, and after division of numerator and denominator on the right by  $\cosh qa$ ,

$$\frac{\bar{u}}{u_1} = \frac{qa + N \tanh qa}{\left(p + \frac{KS}{\lambda}\right) qa + \left(pN - \frac{KS}{\lambda}\right) \tanh qa} \quad (I-108)$$

Application of the Inversion Theorem, Equation(I-11), leads to

$$\frac{u}{u_1} = \frac{1}{2\pi i} \int_{\gamma-i\infty}^{\gamma+i\infty} \frac{e^{pt}(qa + N \tanh qa) dp}{\left(p + \frac{KS}{\lambda}\right) qa + \left(pN - \frac{KS}{\lambda}\right) \tanh qa} \quad (I-109)$$

The inversion proceeds as in the cases discussed earlier in this Appendix. The integrand has a singularity at  $p = 0$  and the residue at that point is  $\lambda/(1 + \lambda)$ .

Since  $p = Dq^2$ , the other singularities occur when

$$\tanh qa = - \frac{\left(Dq^2 + \frac{KS}{\lambda}\right) qa}{Dq^2 N - \frac{KS}{\lambda}} \quad (I-110)$$

By using the identity:  $\tanh ix = i \tan x$  and defining  $q \equiv i q_a S/3$ , we can pass to the equivalent condition in terms of circular functions,

$$\tan q_a = \frac{q_a \left(\frac{1}{\lambda} - \frac{Q}{9} q_a^2\right)}{\frac{1}{\lambda} + \frac{QN}{9} q_a^2} \quad (I-111)$$

It is convenient to define

$$E \equiv \frac{1}{\lambda} - \frac{Q}{9} q_a^2 \quad (I-112)$$

and

$$F \equiv \frac{1}{\lambda} + \frac{QN}{9} q_a^2 \quad (I-113)$$

so that

$$\tan q_a = \frac{q_a E}{F} \quad (I-114)$$

In evaluating the residues of the integrand,  $pg'(p)$  corresponds to

$$\begin{aligned} p \frac{d}{dp} \left[ \left(p + \frac{KS}{\lambda}\right) \frac{qa}{p} + \frac{1}{p} \left(pN - \frac{KS}{\lambda}\right) \tanh qa \right] \\ = \frac{q}{2} \frac{d}{dq} \left[ \left(Dq^2 + \frac{KS}{\lambda}\right) \frac{a}{Dq} + \frac{1}{Dq^2} \left(Dq^2 N - \frac{KS}{\lambda}\right) \tanh qa \right] \end{aligned}$$

Similarly,  $f(p)$  corresponds to

$$\begin{aligned} (qa + N \tanh qa) e^{pt} \\ = q \left( \frac{3}{S} + \frac{N}{q} \tanh qa \right) e^{pt} \end{aligned}$$

Therefore  $\frac{f(p)}{pg'(p)}$  corresponds to

$$\frac{2\left(\frac{3}{S} + \frac{N}{q} \tanh qa\right) e^{pt}}{\frac{3}{SDq^2} \left(Dq^2 - \frac{KS}{\lambda}\right) + \frac{3}{S} \left(N - \frac{KS}{Dq^2\lambda}\right) (1 - \tanh^2 qa) + \frac{2KS}{Dq^3\lambda} \tanh qa} \quad (I-115)$$

From the identity:  $\tanh ix = i \tan x$  and Equation (I-114),

$$\tanh qa = \tanh i q_a = i q_a \frac{E}{F}.$$

When the substitution is made for  $\tanh qa$  in Equation (I-115) we find that the term to be evaluated at each value of  $q_a$  is:

$$\frac{2q_a^2}{3\lambda} \frac{e^{pt}}{F\left(\frac{q_a^2 Q}{9} + \frac{1}{\lambda}\right) + F^2 + q_a^2 E^2 - \frac{2E}{\lambda}}$$

Since  $pt = -q_a^2 \frac{Dt}{a^2}$ , then

$$\frac{u}{u_1} = \frac{\lambda}{1 + \lambda} + \frac{2}{3\lambda} \sum_{a=1}^{\infty} \frac{q_a^2 e^{-q_a^2 \frac{Dt}{a^2}}}{F\left(\frac{q_a^2 Q}{9} + \frac{1}{\lambda}\right) + F^2 + q_a^2 E^2 - \frac{2E}{\lambda}} \quad (I-116)$$

By applying Equation (I-47), this solution can be put in the alternative form:

$$\frac{M_t}{M_{\infty}} = 1 - \frac{2(1 + \lambda)}{3\lambda} \sum_{a=1}^{\infty} \frac{q_a^2 e^{-q_a^2 \frac{Dt}{a^2}}}{F\left(\frac{q_a^2 Q}{9} + \frac{1}{\lambda}\right) + F^2 + q_a^2 E^2 - \frac{2E}{\lambda}} \quad (I-117)$$

The  $q_a$ 's are the non-zero, positive roots of

$$\left\{ \begin{array}{l} E \equiv \frac{1}{\lambda} - \frac{Q}{9} q_a^2 \\ F \equiv \frac{1}{\lambda} + \frac{QN}{9} q_a^2 \\ N \equiv \frac{3}{Q} - 1 \\ Q \equiv \frac{DS}{K} \end{array} \right.$$

If we make all of the indicated substitutions in Equation (I-117), multiply, and collect the coefficients of powers of  $q_a$ , the result is

$$\frac{M_t}{M_\infty} = 1 - \frac{2(1+\lambda)}{3\lambda} \sum_{a=1}^{\infty} \frac{e^{-q_a^2 \frac{D_t}{a^2}}}{q_a^4 \left(\frac{Q}{81}\right) + q_a^2 \left(\frac{1}{9} - \frac{Q}{27} - \frac{2Q}{9\lambda}\right) + \left(\frac{1}{\lambda} + \frac{1}{\lambda^2}\right)} \quad (\text{I-118})$$

As  $K \rightarrow \infty$ , then  $Q \rightarrow 0$  and Equation (I-118) should reduce to the case for equilibrium at the surface of the sphere. Equation (I-118) does reduce to Equation (I-96) under these circumstances.

Equation (I-117) has been programmed for high-speed digital computation. The program is shown in Appendix IV. Equation (I-117) contains too many parameters for convenient tabulation of numerical values, but some information on its behavior also appears in Appendix IV.

#### 1.6 SOLUTIONS WHICH ARE VALID FOR SMALL VALUES OF THE TIME

Haul, Dumbgen, and Just<sup>7</sup> state, without derivation, two approximate diffusion equations which are useful if the elapsed time is short enough. Their Equation (13), if applicable, would be particularly valuable in supplying approximate values of  $D$  and  $K$ . Such values could be tested for agreement with experiment by making computations with the exact solutions.

The equations of Haul, Dumbgen, and Just were rederived and examined for applicability to our measurements.

#### Diffusion From a Limited Volume of Well-Stirred Fluid Into a Plane Slab (Equilibration at the Surface Proceeds at a Finite Rate)

We start with Equation (I-62). It is pointed out in various texts on Laplace transforms, that with the proper restrictions on  $x(t)$  and  $\bar{x}(p)$  then,

$$\lim_{p \rightarrow \infty} p \bar{x}(p) = \lim_{t \rightarrow 0} x(t).$$

With this in mind we examine the behavior of Equation (I-62) for values of  $p$  large enough to make  $(\tanh q \ell) \rightarrow 1$ . Under these conditions

$$\frac{\bar{u}}{u_1} = \frac{K + Dq}{Kp + (p + N) Dq} \quad (\text{I-119})$$

From the definition,  $q = \frac{p^{1/2}}{D^{1/2}}$ ,

$$\frac{\bar{u}}{u_1} = \frac{p^{1/2} + \frac{K}{D^{1/2}}}{p^{1/2} \left( p + \frac{K}{D^{1/2}} p^{1/2} + \frac{KS}{\lambda} \right)} \quad (\text{I-120})$$

The denominator will be zero for  $p = 0$  and for

$$p^{1/2} = \frac{-\frac{K}{\sqrt{D}} \pm \sqrt{\frac{K^2}{D} - \frac{4KS}{\lambda}}}{2}$$

$$p^{1/2} = -\frac{K}{2\sqrt{D}} \pm \frac{K}{2\sqrt{D}} \left( \sqrt{1 - \frac{4DS}{K\lambda}} \right)$$

If  $\alpha \equiv \frac{K}{2\sqrt{D}}$  and  $\beta \equiv \sqrt{1 - \frac{4DS}{K\lambda}}$ ,

$$\frac{\bar{u}}{u_1} = \frac{p^{1/2} + 2\alpha}{p^{1/2} [p^{1/2} + \alpha(1 - \beta)] [p^{1/2} + \alpha(1 + \beta)]} \quad (1-121)$$

Since the transform for  $(p^{1/2} + a)^{-1}$  is available from Table 16, this expression for  $\frac{\bar{u}}{u_1}$  can be inverted by the partial fraction technique.

$$\begin{aligned} \frac{\bar{u}}{u_1} = & \frac{-\alpha(1 - \beta) + 2\alpha}{[-\alpha(1 - \beta)] [-\alpha(1 - \beta) + \alpha(1 + \beta)]} \cdot \frac{1}{p^{1/2} + \alpha(1 - \beta)} \\ & + \frac{-\alpha(1 + \beta) + 2\alpha}{[-\alpha(1 + \beta)] [-\alpha(1 + \beta) + \alpha(1 - \beta)]} \cdot \frac{1}{p^{1/2} + \alpha(1 + \beta)} \end{aligned}$$

+ a third term associated with the residue at  $p = 0$ . This is ruled out because it was assumed that  $p > 0$ . (I-122)

By use of the table of transforms,

$$\begin{aligned} \frac{u}{u_1} = & \frac{(-\alpha + \alpha\beta + 2\alpha) [-\alpha(1 - \beta)]}{[-\alpha(1 - \beta)] (-\alpha + \alpha\beta + \alpha + \alpha\beta)} \text{erfc} [(1 - \beta)\alpha\sqrt{t}] \\ & + \frac{(-\alpha - \alpha\beta + 2\alpha) [-\alpha(1 + \beta)]}{[-\alpha(1 + \beta)] (-\alpha - \alpha\beta + \alpha - \alpha\beta)} \text{erfc} [(1 + \beta)\alpha\sqrt{t}] \\ \frac{u}{u_1} = & \frac{1 + \beta}{2\beta} \text{erfc} [(1 - \beta)\alpha\sqrt{t}] \\ & - \frac{1 - \beta}{2\beta} \text{erfc} [(1 + \beta)\alpha\sqrt{t}] \end{aligned} \quad (I-123)$$

Some terms involving  $\frac{1}{\sqrt{\pi t}}$  have been omitted because they rapidly become negligible as  $t$  increases.

The potential usefulness of Equation (I-123) is made apparent if we solve for  $D$  and  $K$  in terms of  $\alpha$  and  $\beta$ .

$$\begin{cases} K = 2\alpha\sqrt{D} \\ K = \frac{4DS}{\lambda(1 - \beta^2)} \end{cases}$$

From these equations,

$$\begin{cases} \sqrt{D} = \frac{\lambda\alpha(1 - \beta^2)}{2S} \\ K = 2\alpha\sqrt{D} \end{cases} \quad (I-124)$$

Therefore, if we are able to match the experimental values of  $u/u_1$  as a function of  $t$  with a set of values of  $u/u_1$  calculated by assigning specific numerical values to  $\alpha$  and  $\beta$ , then we can arrive at approximate values of  $D$  and  $K$  for the experiment.

To find the range of times for which Equation (I-123) represents a good approximation to Equation (I-117), we can proceed as follows:

From the definition of  $Q$ ,

$$K = \frac{DS}{Q} = \frac{3D}{aQ}.$$

Insertion of this value of  $K$  into the definition of  $\alpha$  leads to  $\alpha = \frac{3}{2} \frac{\sqrt{D}}{aQ}$

Thus,  $\alpha\sqrt{t} = \frac{3}{2Q} \frac{\sqrt{Dt}}{a}$  or

$$\left(\frac{Dt}{a^2}\right)^{1/2} = \frac{2}{3} Q (\alpha\sqrt{t}) \quad (\text{I-125})$$

On the basis of the above considerations, we can compare Equation (I-123) with Equation (I-117) by the following steps:

1. Choose values of  $\lambda$  and  $Q$
2. By using Equation (I-117) calculate a set of values of  $M_t/M_\infty$  corresponding to a set of values of  $(Dt/a^2)^{1/2}$
3. From the chosen  $\lambda$  and  $Q$ , calculate  $\beta$ .
4. Given  $\beta$ , calculate values of  $u/u_1$  corresponding to a set of values of  $(\alpha\sqrt{t})$
5. Calculate a set of values of

$$\frac{M_t}{M_\infty} = (1 + \lambda) \left(1 - \frac{u}{u_1}\right)$$

6. For each value of  $(\alpha\sqrt{t})$  calculate

$$\left(\frac{Dt}{a^2}\right)^{1/2} = \frac{2Q}{3} (\alpha\sqrt{t})$$

7. For a given value of  $(Dt/a^2)^{1/2}$  compare the values of  $M_t/M_\infty$  calculated from the two equations.

The results of such a comparison are discussed in Appendix III.

#### Diffusion From a Limited Volume of Well-Stirred Fluid Into a Sphere (Equilibration at the Surface Proceeds at a Finite Rate)

This derivation starts from Equation (I-108), which may be rewritten as

$$\frac{\bar{u}}{u_1} = \frac{qa + \left(\frac{Ka}{D} - 1\right) \tanh qa}{\left(p + \frac{KS}{\lambda}\right) qa + \left[p \left(\frac{Ka}{D} - 1\right) - \frac{KS}{\lambda}\right] \tanh qa} \quad (\text{I-126})$$

Again, assume that  $p$  is large enough to make  $(\tanh qa) \rightarrow 1$ .

If we substitute  $a = \frac{3}{S}$  and  $q = \frac{p^{1/2}}{D^{1/2}}$ , then

$$\frac{\bar{u}}{u_1} = \frac{\frac{3p^{1/2}}{SD^{1/2}} + \frac{3K}{SD} - 1}{\left(p + \frac{KS}{\lambda}\right) \frac{3p^{1/2}}{SD^{1/2}} + p \left(\frac{3K - DS}{DS}\right) - \frac{KS}{\lambda}}$$

$$\frac{\bar{u}}{u_1} = \frac{p^{1/2} + \left( \frac{K}{\sqrt{D}} - \frac{S\sqrt{D}}{3} \right)}{p^{3/2} + p \left( \frac{K}{\sqrt{D}} - \frac{S\sqrt{D}}{3} \right) + p^{1/2} \left( \frac{KS}{\lambda} \right) - \frac{KS^2\sqrt{D}}{3\lambda}} \quad (\text{I-127})$$

Since the denominator can be considered to be a cubic in  $p^{1/2}$ , the denominator will be zero for  $p^{1/2} = z_1, z_2, z_3$  where the  $z$ 's are the roots of

$$z^3 + z^2 \left( \frac{K}{\sqrt{D}} - \frac{S\sqrt{D}}{3} \right) + z \left( \frac{KS}{\lambda} \right) - \frac{KS^2\sqrt{D}}{3\lambda} = 0$$

A partial fraction expansion resolves the transform into three terms.

If  $X \equiv \left( \frac{K}{\sqrt{D}} - \frac{S\sqrt{D}}{3} \right)$ , then

$$\begin{aligned} \frac{\bar{u}}{u_1} &= \frac{z_1 + X}{(z_1 - z_2)(z_1 - z_3)} \cdot \frac{1}{p^{1/2} - z_1} \\ &+ \frac{z_2 + X}{(z_2 - z_1)(z_2 - z_3)} \cdot \frac{1}{p^{1/2} - z_2} \\ &+ \frac{z_3 + X}{(z_3 - z_1)(z_3 - z_2)} \cdot \frac{1}{p^{1/2} - z_3} \end{aligned} \quad (\text{I-128})$$

The inverse transform of  $\frac{1}{p^{1/2} + a}$  is  $\frac{1}{\sqrt{\pi t}} - a \operatorname{erfc}(at^{1/2})$

Therefore,

$$\begin{aligned} \frac{u}{u_1} &= \frac{z_1 (z_1 + X)}{(z_1 - z_2)(z_1 - z_3)} \operatorname{erfc}(-z_1 \sqrt{t}) \\ &+ \frac{z_2 (z_2 + X)}{(z_2 - z_1)(z_2 - z_3)} \operatorname{erfc}(-z_2 \sqrt{t}) \\ &+ \frac{z_3 (z_3 + X)}{(z_3 - z_1)(z_3 - z_2)} \operatorname{erfc}(-z_3 \sqrt{t}) \\ &+ \frac{3}{\sqrt{\pi t}} \end{aligned} \quad (\text{I-129})$$

For useful values of  $t$ , the last term usually is negligible.

## APPENDIX II

### COMPUTATIONS OF DIFFUSION FROM A LIMITED VOLUME OF WELL-STIRRED FLUID INTO A SPHERE

In the computation of diffusion from a limited volume of well-stirred fluid into a sphere,\* the sphere is assumed to occupy the space  $r < a$ , which is immersed in a bath of solution with volume  $V$  (excluding the space occupied by the sphere). Further assumptions are that the sphere is initially free from solute and that the concentration of the solute in the solution is always uniform and initially  $C_0$ . Equation (II-1) expresses the total amount of solute,  $M_t$ , in the sphere at time,  $t$ , as a fraction of  $M_\infty$ , the corresponding quantity after infinite time:<sup>4,47</sup>

$$\frac{M_t}{M_\infty} = 1 - \sum_{n=1}^{\infty} \frac{6 \alpha (\alpha + 1) e^{-Z_n^2 x}}{9 + 9\alpha + Z_n^2 \alpha^2} \quad (\text{II-1})$$

where  $\alpha$  is the ratio of the volumes of solution and sphere divided by the partition factor,  $Y$ :

$$\alpha = \frac{3V}{(4\pi a^3 Y)} \quad (\text{II-2})$$

$$x = \frac{Dt}{a^2}$$

and  $Z_n$  is the  $n$ -th non-zero root of the equation:

$$G(Z) = \tan Z - \frac{3Z}{3 + \alpha Z^2} \quad (\text{II-3})$$

$D$  is the diffusion coefficient of the solute in the sphere.

Equation (II-4) expresses  $\alpha$  in terms of the final fractional uptake,  $F$ , of the solute by the sphere.

$$F = \frac{M_\infty}{VC_0} = \frac{1}{1 + \alpha} \quad (\text{II-4})$$

As the value of  $M_t/M_\infty$  decreases, the number of terms required increases rapidly. It is then preferable to use an alternative solution, Equation (II-5), the Carman-Haul approximation,<sup>6</sup> which is a series of error functions suitable for numerical evaluation at small times, i. e., small values of  $M_t/M_\infty$ .

---

\*Instantaneous equilibrium at the surface is assumed.

$$\begin{aligned} \frac{M_t}{M_\infty} = (1 + \alpha) & \left[ 1 - \left( \frac{\gamma_1}{\gamma_1 + \gamma_2} \right) \operatorname{erfc} \left( 3 \gamma_1 \frac{\sqrt{x}}{\alpha} \right) \right. \\ & \left. - \left( \frac{\gamma_2}{\gamma_1 + \gamma_2} \right) \operatorname{erfc} \left( -3 \gamma_2 \frac{\sqrt{x}}{\alpha} \right) \right] \\ & + (\text{higher terms}) \end{aligned} \quad (\text{II-5})$$

where  $\gamma_1 = [(1 + 4\alpha/3)^{1/2} + 1]/2$ ,  $\gamma_2 = \gamma_1 - 1$ , and  $\operatorname{erfc} y = (\exp y^2) (\operatorname{erfc} y)$ .

An IBM 7090 program was written to determine the extent of agreement between the exact and the approximate equations and in what regions, if any, the approximate calculations are invalid.

#### COMPUTATIONAL PROCEDURE

A  $\beta$  is calculated:

$$\beta = \frac{1}{F} - 1$$

This value is then compared with  $\alpha$  values obtained from the root table in Crank.<sup>4</sup> By interpolation, a first estimate of the root corresponding to the calculated  $\beta$  is determined. This root value is placed into Equation (II-3) and examined to see if the result is sufficiently close to zero, i.e.,  $\leq 10^{-5}$ . If not, Equation (II-3) is solved by Newton's method, i.e., by successively computing

$$Z_n^{(m)} = Z_n^{(m-1)} - \frac{G Z_n^{(m-1)}}{G' Z_n^{(m-1)}} \quad (\text{II-6})$$

until  $F(Z)$  becomes sufficiently close to zero.

$$G'(Z) = \sec^2 Z - \frac{3}{(3 + \alpha Z^2)} + \frac{6\alpha Z^2}{(3 + \alpha Z^2)^2} \quad (\text{II-7})$$

Equation (II-1) now can be computed by solving the summation equation for values of  $Z_n$  over the range 1 to NM, an input value, then subtracting this summation from 1. Equation (II-5) is solved by placing the value  $\beta$  for  $\alpha$  into the Carman-Haul equation.

#### SUMMARY OF NUMERICAL RESULTS

In Table 16 the sorption fraction given by the Carman-Haul approximation for spherical geometry is compared to six significant figures with the exact solution given by Wagner and by Crank. The comparison was made for  $0.0001 \leq Dt/a^2 \leq 0.64$  and  $0.1 \leq F \leq 0.9$  where  $D$  is the diffusion coefficient,  $t$  is the time,  $a$  is the sphere radius, and  $F$  is the fractional solute uptake by the sphere in an infinite time. The Carman-Haul approximation is accurate to five significant figures for  $0.1 \leq F \leq 0.75$  and  $0.0004 < Dt/a^2 < 0.09$ .

For values of  $Dt/a^2 < 0.0004$ , the results of the exact equation are not accurate unless more than 50 roots are used for the computation. For values of  $Dt/a^2 > 0.09$  and  $0.1 < F < 0.75$ , the deviation between the exact and approximate solutions increases and the exact equation is preferred for reliability. For  $F > 0.75$ , the approximate solution becomes either unreliable or gives nonphysical results, i.e.,  $M_t/M_\infty > 1$ ; therefore, the use of the exact equation is essential. The regions of agreement and disagreement are mapped out in Figure 24. Figure 25 is a large-scale plot of the computed values.



TABLE 16

COMPARISON OF  $M_t/M_\infty$  COMPUTED FROM THE EXACT AND THE APPROXIMATE EQUATIONS

$(Dt/a^2)^{1/2}$	F = 0.1		F = 0.15		F = 0.20		F = 0.25	
	Exact	Approx.	Exact	Approx.	Exact	Approx.	Exact	Approx.
0.01	-	0.037170	-	0.039289	-	0.041864	-	0.044344
0.02	0.073463	0.037170	0.077519	0.039289	0.082049	0.041664	0.087141	0.044344
0.03	0.108890	0.037170	0.114711	0.039289	0.121189	0.041664	0.128442	0.128441
0.04	0.143481	0.143462	0.150885	0.039289	0.159116	0.041664	0.168294	0.128441
0.05	0.177189	0.143462	0.186059	0.039289	0.195880	0.041664	0.206745	0.128441
0.10	0.333520	0.143462	0.347575	0.039289	0.362838	0.041664	0.379467	0.128441
0.15	0.470213	0.470214	0.486679	0.039289	0.504264	0.041864	0.523075	0.128441
0.20	0.588348	0.470214	0.605200	0.039289	0.622912	0.041664	0.641526	0.128441
0.25	0.688884	0.688865	0.704708	0.039289	0.721093	0.041664	0.738019	0.128441
0.30	0.772597	-	0.786540	-	0.800732	-	0.815142	-
0.35	0.840296	-	0.851868	-	0.863456	-	0.875018	-
0.40	0.892827	-	0.901899	-	0.910830	-	0.919581	-
0.45	0.931538	-	0.938251	-	0.944741	-	0.950980	-
0.50	0.958453	-	0.963136	-	0.967578	-	0.971761	-
0.55	0.976068	-	0.979146	-	0.982006	-	0.984642	-
0.60	0.986918	-	0.988824	-	0.990557	-	0.992117	-
0.65	0.993215	-	0.994327	-	0.995314	-	0.996182	-
0.70	0.998861	-	0.997272	-	0.997802	-	0.998255	-
0.75	0.998441	-	0.998758	-	0.999025	-	0.999247	-
0.80	0.999309	-	0.999464	-	0.999591	-	0.999694	-

$(Dt/a^2)^{1/2}$	F = 0.30		F = 0.35		F = 0.40		F = 0.45	
	Exact	Approx.	Exact	Approx.	Exact	Approx.	Exact	Approx.
0.01	-	0.047393	-	0.050892	-	0.054949	-	0.059708
0.02	0.092908	0.092906	0.099487	0.050892	0.107070	0.054949	0.115903	0.059708
0.03	0.136616	0.136615	0.145896	0.050892	0.156527	0.054949	0.168823	0.059708
0.04	0.178592	0.178591	0.190224	0.050892	0.203470	0.054949	0.218686	0.059708
0.05	0.218904	0.218902	0.232568	0.050892	0.248039	0.054949	0.265692	0.059708
0.10	0.379648	0.397646	0.417593	0.050892	0.439563	0.054949	0.463861	0.059708
0.15	0.543228	0.543227	0.564846	0.050892	0.588067	0.054949	0.613034	0.059708
0.20	0.661087	0.661085	0.681628	0.050892	0.703184	0.054949	0.725769	0.059708
0.25	0.755476	0.755475	0.773439	0.050892	0.791876	0.054949	0.810734	0.059708
0.30	0.829732	-	0.844449	-	0.859233	-	0.874007	-
0.35	0.886508	-	0.897867	-	0.909036	-	0.919943	-
0.40	0.928110	-	0.936369	-	0.944312	-	0.951889	-
0.45	0.956937	-	0.962582	-	0.967887	-	0.972822	-
0.50	0.975670	-	0.979289	-	0.982607	-	0.985614	-
0.55	0.987048	-	0.989222	-	0.991163	-	0.992874	-
0.60	0.993506	-	0.994729	-	0.995790	-	0.996698	-
0.65	0.996934	-	0.997577	-	0.998119	-	0.998569	-
0.70	0.998637	-	0.998954	-	0.999212	-	0.999420	-
0.75	0.999429	-	0.999575	-	0.999691	-	0.999780	-
0.80	0.999975	-	0.999838	-	0.999886	-	0.999922	-

$(Dt/a^2)^{1/2}$	F = 0.50		F = 0.55		F = 0.60		F = 0.65	
	Exact	Approx.	Exact	Approx.	Exact	Approx.	Exact	Approx.
0.01	-	0.065369	-	0.072215	-	0.080663	-	0.091346
0.02	0.126321	0.065369	0.138793	0.072215	0.153989	0.080663	0.172909	0.091346
0.03	0.183207	0.065369	0.200256	0.072215	0.220783	0.080663	0.245961	0.091346
0.04	0.236343	0.065369	0.257074	0.072215	0.281747	0.080663	0.311582	0.091346
0.05	0.286018	0.065369	0.309663	0.072215	0.337493	0.080663	0.370692	0.091346
0.10	0.490846	0.065369	0.520946	0.072215	0.554660	0.080663	0.592569	0.091346
0.15	0.639893	0.065369	0.668786	0.072215	0.699837	0.080663	0.733127	0.091346
0.20	0.749381	0.749380	0.773984	0.072215	0.799505	0.080663	0.825809	0.091348
0.25	0.829935	0.749380	0.849377	0.072215	0.868921	0.080663	0.888391	0.091346
0.30	0.888679	-	0.903139	-	0.917261	-	0.930900	-
0.35	0.930510	-	0.940654	-	0.950285	-	0.959313	-
0.40	0.959046	-	0.965734	-	0.971904	-	0.977515	-
0.45	0.977363	-	0.981488	-	0.985181	-	0.988434	-
0.50	0.988304	-	0.990676	-	0.992733	-	0.994485	-
0.55	0.994359	-	0.995628	-	0.996692	-	0.997566	-
0.60	0.997462	-	0.998092	-	0.998602	-	0.999006	-
0.65	0.998934	-	0.999225	-	0.999452	-	0.999624	-
0.70	0.999583	-	0.999707	-	0.999801	-	0.999869	-
0.75	0.999847	-	0.999897	-	0.999933	-	0.999958	-
0.80	0.999948	-	0.999966	-	0.999979	-	0.999987	-

TABLE 18 (Cont.)

COMPARISON OF $M_t/M_\infty$ COMPUTED FROM THE EXACT AND THE APPROXIMATE EQUATIONS								
$(Dt/a^2)^{1/2}$	F = 0.70		F = 0.75		F = 0.80		F = 0.85	
	Exact	Approx.	Exact	Approx.	Exact	Approx.	Exact	Approx.
0.01	-	0.105288	-	0.124244	-	0.151501	-	0.194013
0.02	0.197105	0.197104	0.229120	0.124244	0.273427	0.151501	0.338621	0.194013
0.03	0.277550	0.197104	0.318309	0.124244	0.372789	0.372788	0.448954	0.194013
0.04	0.348348	0.348347	0.394689	0.124244	0.454700	0.372788	0.534909	0.194013
0.05	0.410916	0.348347	0.460527	0.124244	0.522946	0.372788	0.603127	-
0.10	0.635321	0.348347	0.883589	0.124244	0.737948	0.372788	0.798587	-
0.15	0.768661	0.348347	0.806301	0.124244	0.845688	0.372788	0.888121	-
0.20	0.852681	0.348347	0.879806	0.879805	0.906743	-	0.932920	-
0.25	0.907564	0.348347	0.926176	0.926174	0.943920	-	0.980487	-
0.30	0.943898	-	0.956087	-	0.967303	-	0.977394	-
0.35	0.967648	-	0.975211	-	0.981935	-	0.987775	-
0.40	0.982531	-	0.986930	-	0.990704	-	0.993863	-
0.45	0.991246	-	0.993624	-	0.995590	-	0.997169	-
0.50	0.995945	-	0.997135	-	0.998079	-	0.998805	-
0.55	0.998267	-	0.998816	-	0.999233	-	0.999539	-
0.60	0.999317	-	0.999550	-	0.999719	-	0.999838	-
0.65	0.999752	-	0.999843	-	0.999908	-	0.999948	-
0.70	0.999917	-	0.999949	-	0.999971	-	0.999985	-
0.75	0.999974	-	0.999985	-	0.999992	-	0.999998	-
0.80	0.999993	-	0.999998	-	0.999998	-	0.999999	-

$(Dt/a^2)^{1/2}$	F = 0.90	
	Exact	Approx.
0.01	-	0.269378
0.02	0.443288	0.269378
0.03	0.581611	0.269378
0.04	0.845729	0.269378
0.05	0.707787	-
0.10	0.884736	-
0.15	0.926444	-
0.20	0.957654	-
0.25	0.975495	-
0.30	0.988244	-
0.35	0.992718	-
0.40	0.996433	-
0.45	0.998401	-
0.50	0.999347	-
0.55	0.999757	-
0.60	0.999918	-
0.65	0.999975	-
0.70	0.999993	-
0.75	0.999998	-
0.80	1.	-

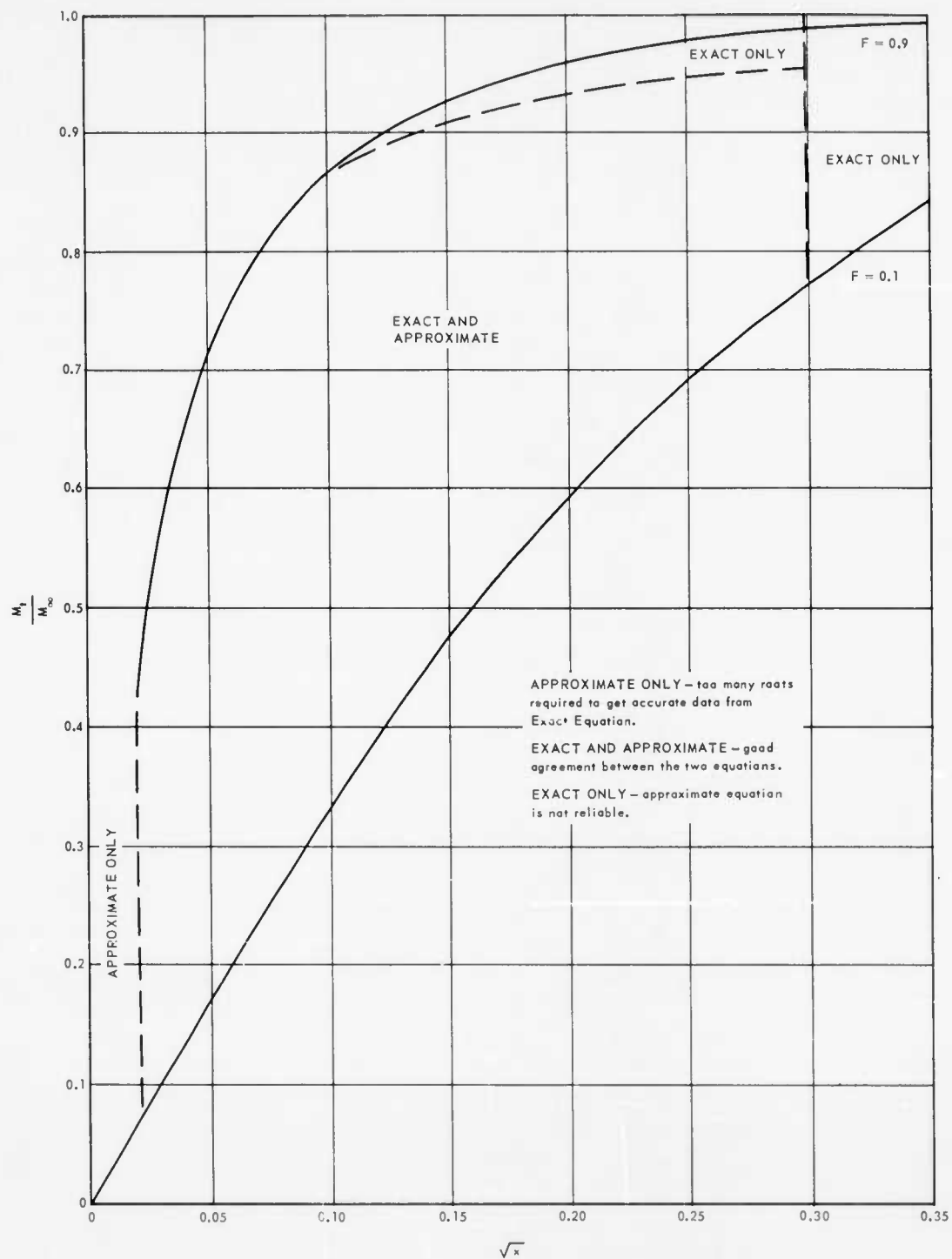
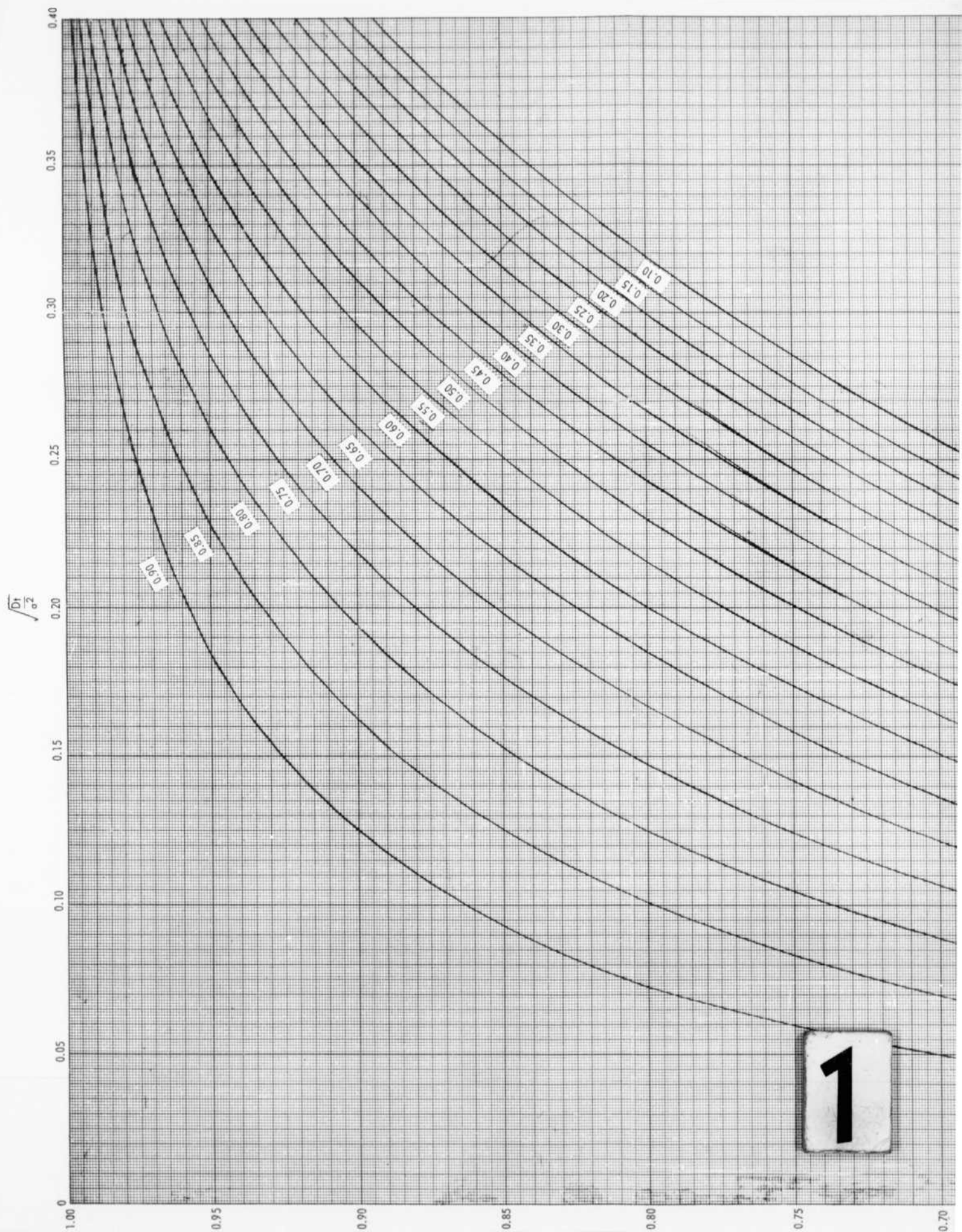
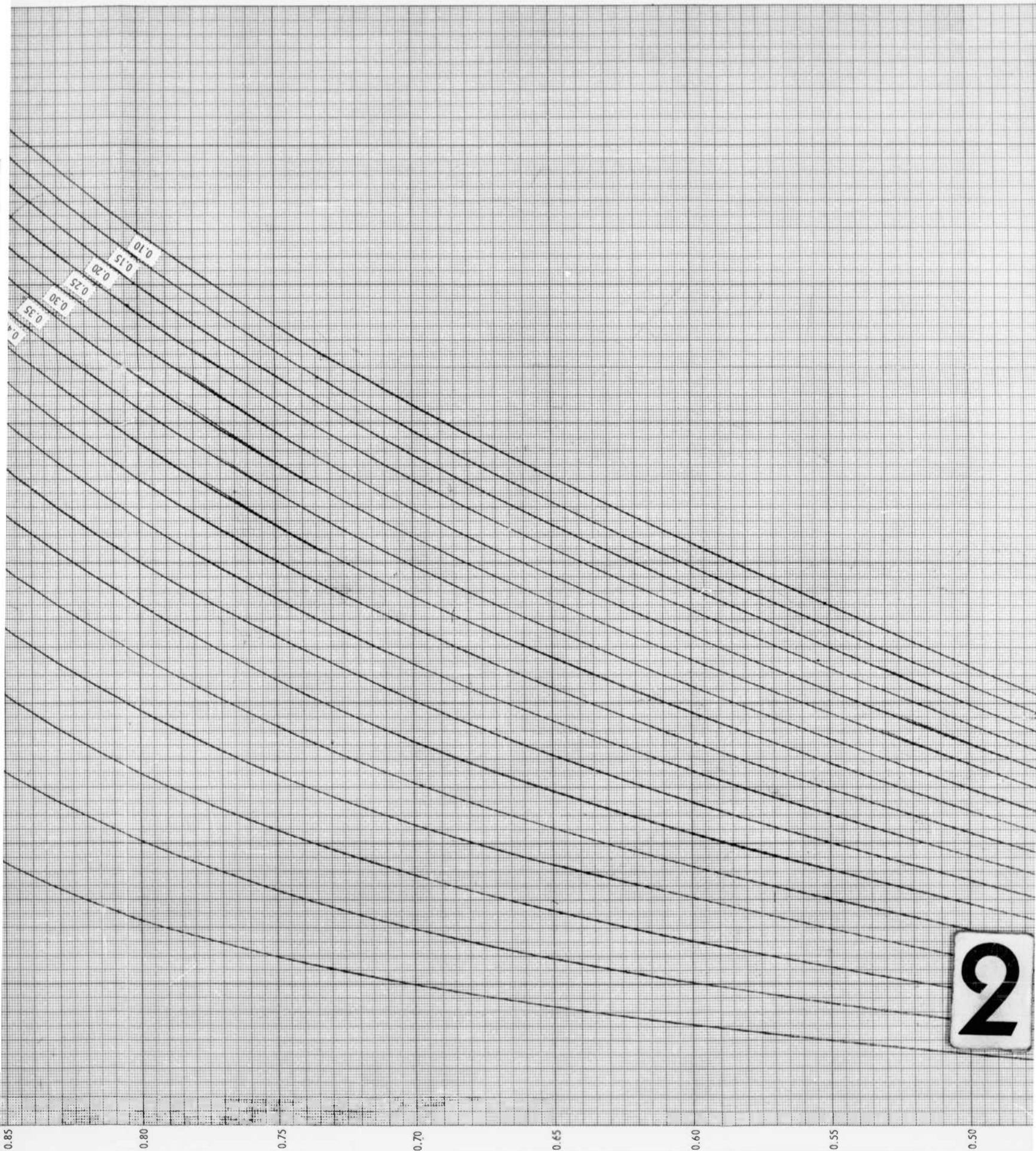


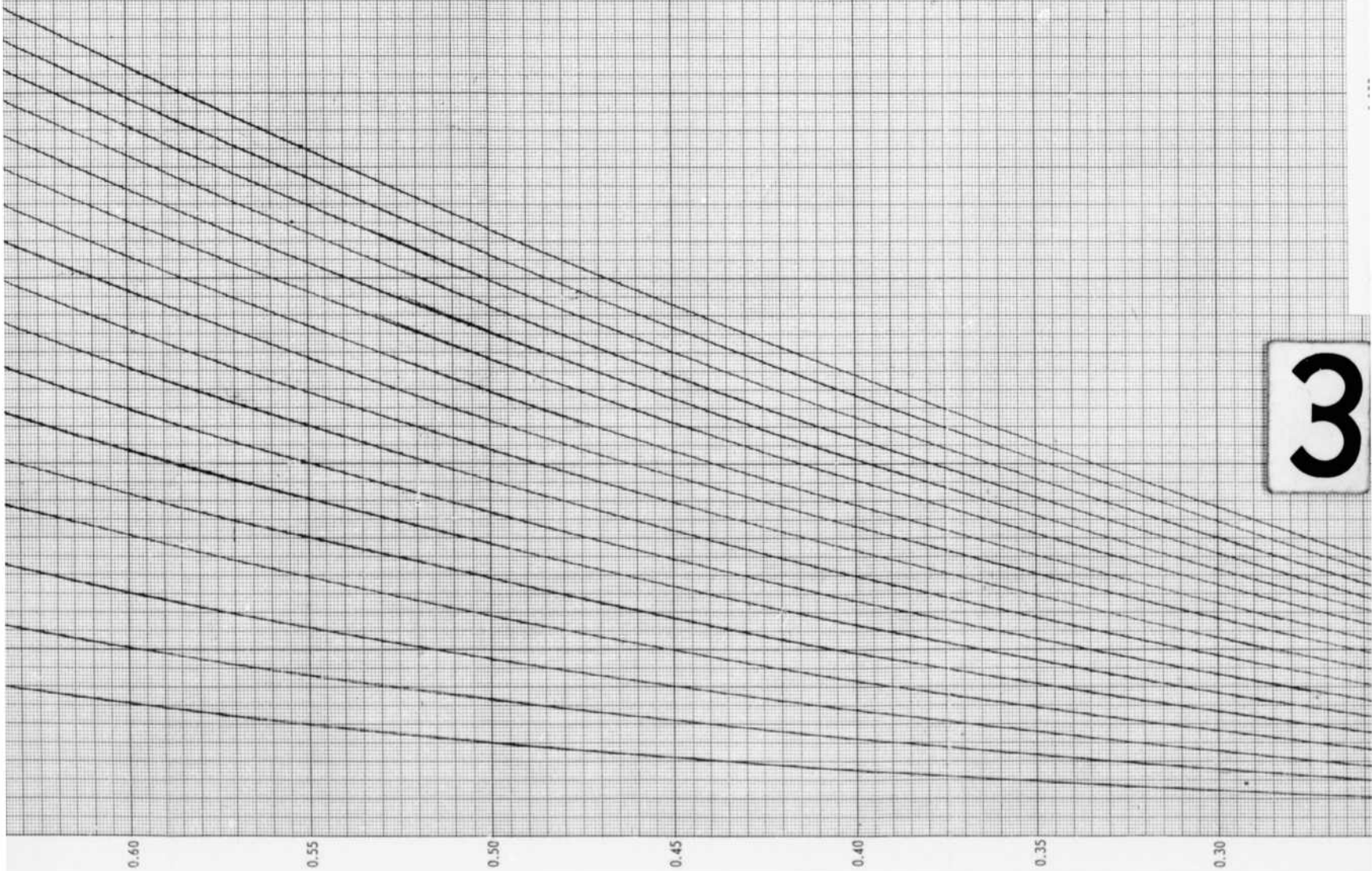
Fig. 24 - Ranges of validity of the exact and approximate diffusion equations



1







$$\frac{M_t}{M_\infty} = 1 - \sum_{n=1}^{\infty} \frac{6\alpha(\alpha+1)e^{-Z_n^2 X}}{9 + \alpha + Z_n^2 \alpha^2}$$

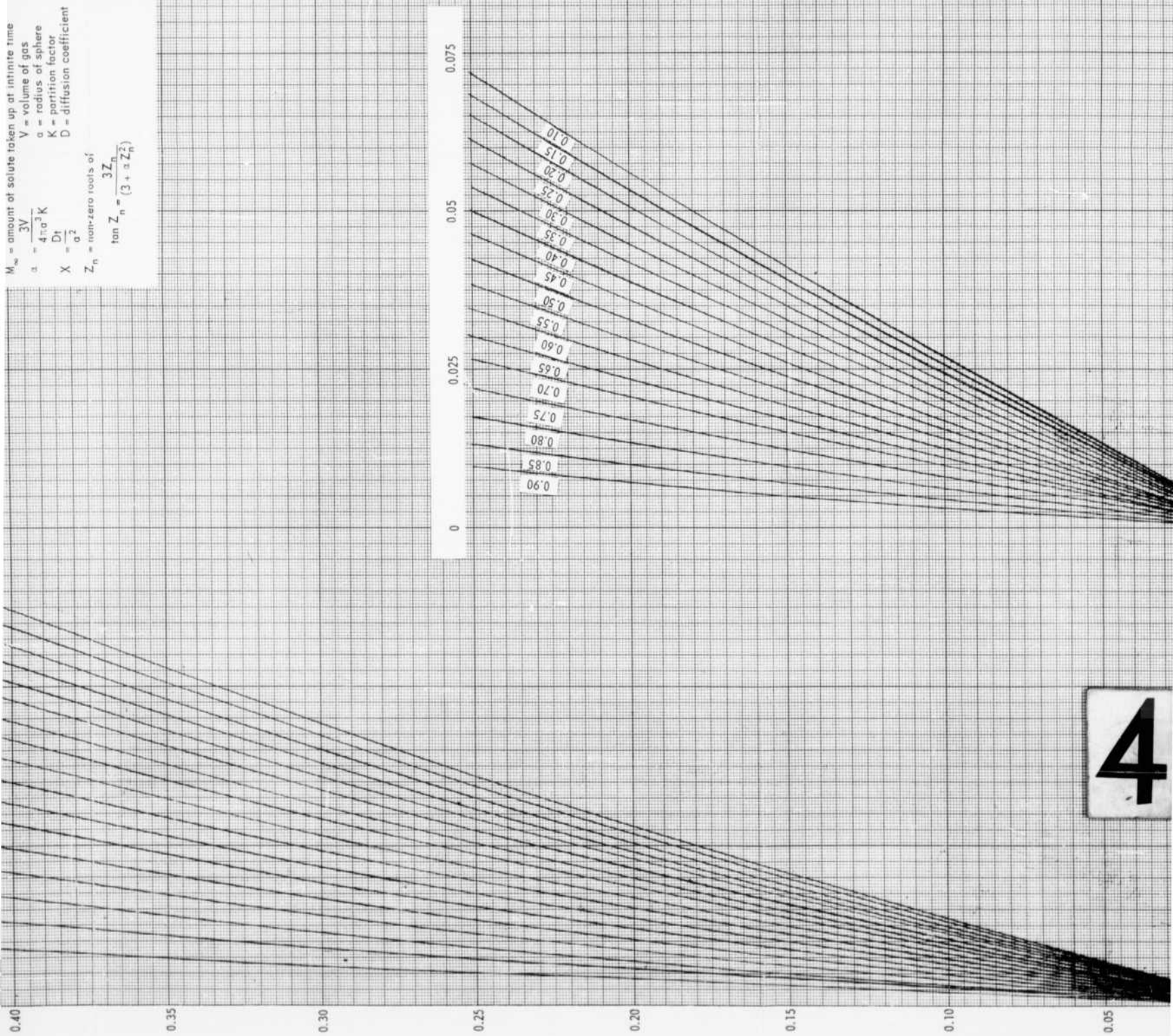
$M_t$  = amount of solute taken up at time  $t$   
 $M_\infty$  = amount of solute taken up at infinite time  
 $V$  = volume of gas  
 $a$  = radius of sphere  
 $K$  = partition factor  
 $D$  = diffusion coefficient

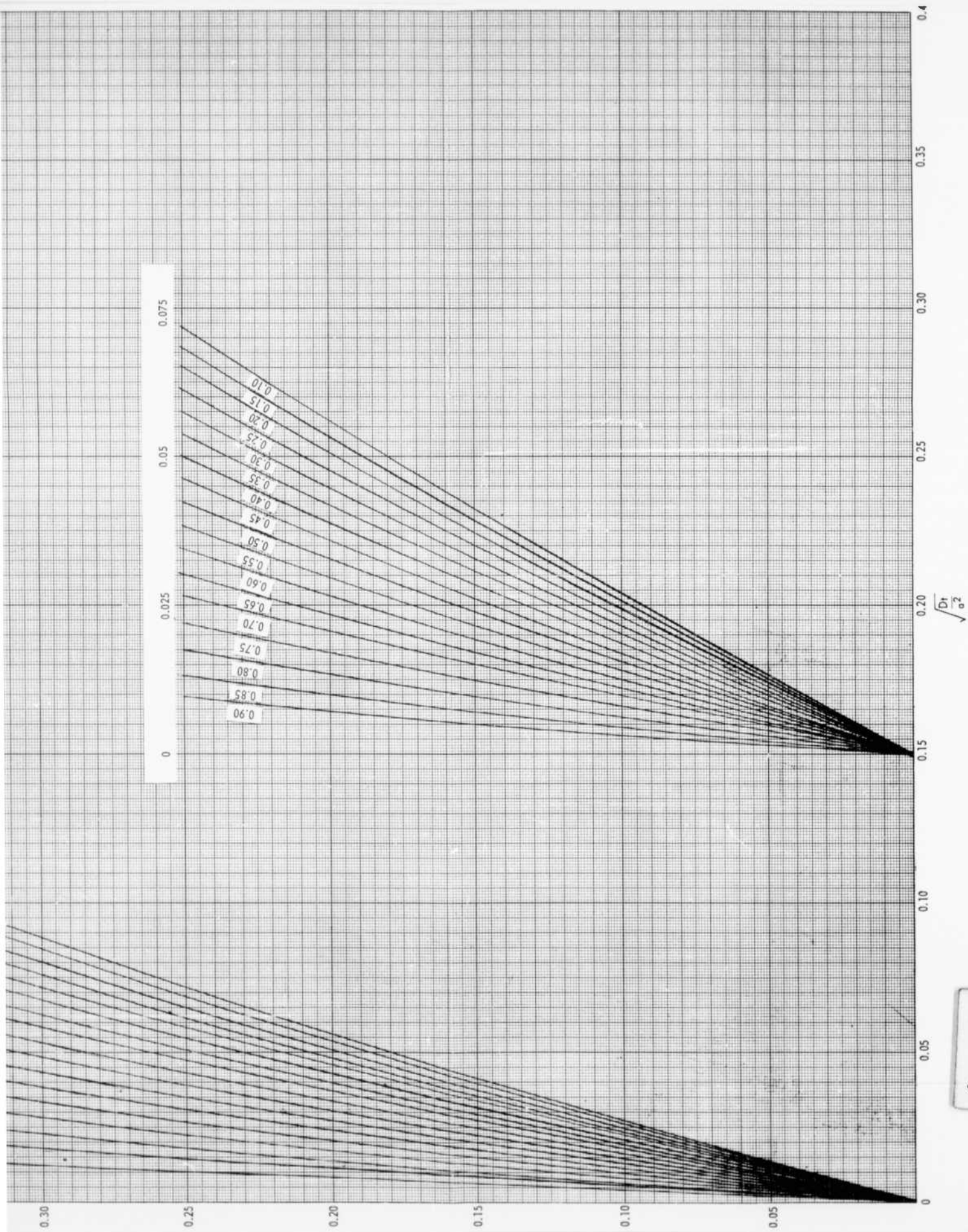
$\alpha = \frac{4\pi a^3 K}{D t}$   
 $X = \frac{D t}{a^2}$   
 $Z_n$  = non-zero roots of

$$\tan Z_n = \frac{3Z_n}{(3 + \alpha Z_n^2)}$$



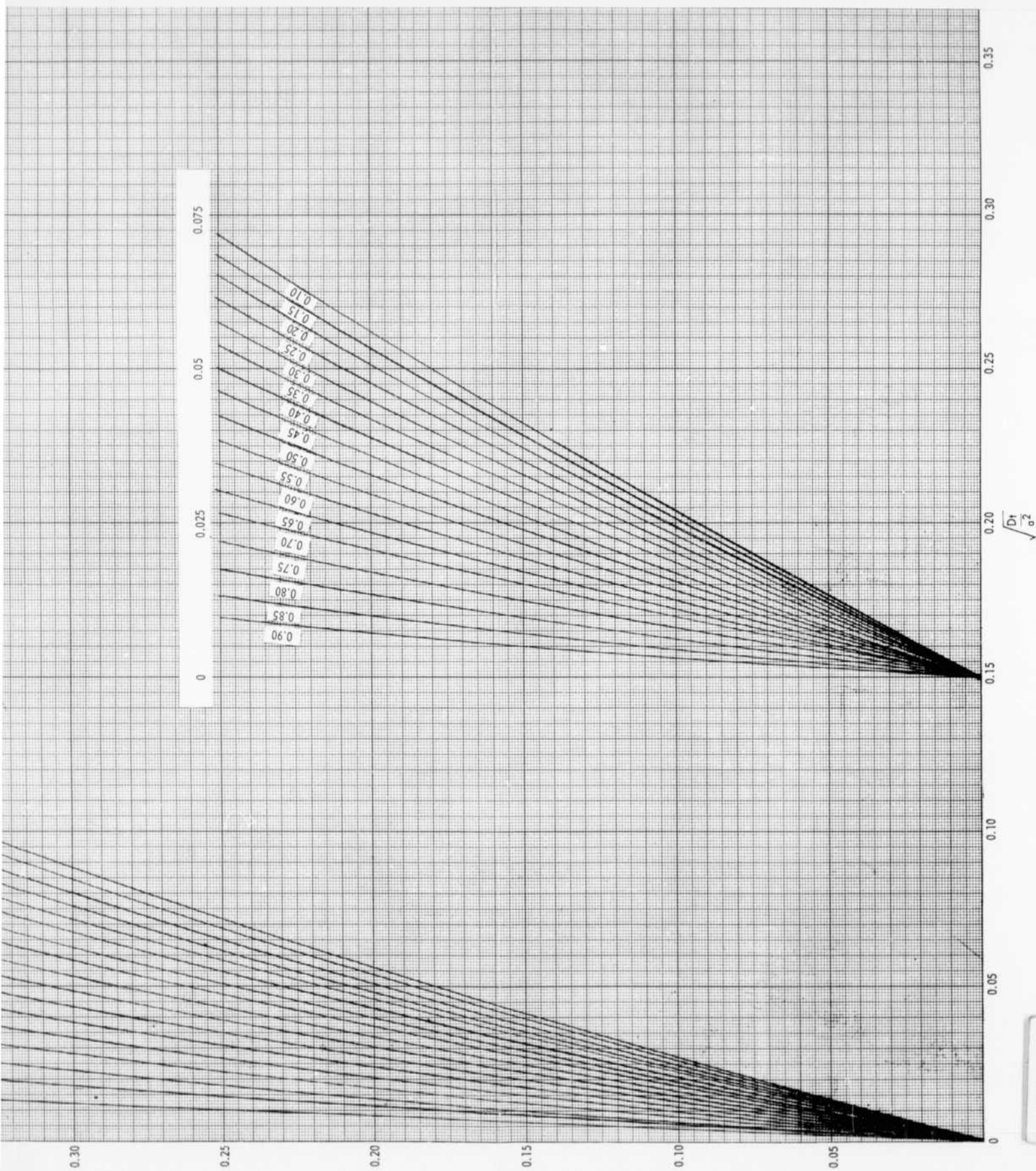
$M_\infty$  = amount of solute taken up at infinite time  
 $a = \frac{3V}{4\pi a^3 K}$   
 $a$  = volume of gas  
 $a$  = radius of sphere  
 $K$  = partition factor  
 $D$  = diffusion coefficient  
 $X = \frac{D t}{a^2}$   
 $Z_n$  = non-zero roots of  
 $\tan Z_n = \frac{3Z_n}{(3 + a^2 Z_n^2)}$





Uptake by a sphere from a stirred solution of limited volume.  
Numbers on curves show fraction of solute finally taken up by sphere.





Uptake by a sphere from a stirred solution of limited volume.  
Numbers on curves show fraction of solute finally taken up by sphere.

Fig. 25 - Uptake by a sphere from a stirred solution of limited volume

## PROGRAM PARAMETERS

### Input

- F - the fraction of the solute taken up by a sphere of radius  $a$  after an infinitely long immersion.
- NM - the number of roots,  $Z_n$ , to be determined for solving Equation (II-1).
- DELTA - tolerance on solutions to Equation (II-3).  $Z$  is taken to be a root if  $G(Z) \leq \text{DELTA}$ .
- SRX - the initial value of  $(Dt/a^2)^{1/2}$  for which  $M_t/M_\infty$  is to be computed.
- SRXS - the maximum value of  $(Dt/a^2)^{1/2}$
- DSRX - the interval width between successive values of  $(Dt/a^2)^{1/2}$ .

### Output

F

Number of Roots

Square Root of  $Dt/a^2$

Exact  $M_t/M_\infty$

Approximate  $M_t/M_\infty$

ALPHA - corresponds to calculated  $\beta$ -value

Z - list of all roots calculated by program for solution of the exact equation

X - value of  $Dt/a^2$

GAMO

UO } - parameters used in calculation of approximate equation

UT }

A copy of the FORTRAN program is shown in Table 17.

TABLE 17

**FORTRAN PROGRAM FOR COMPUTATION OF DIFFUSION INTO A  
SPHERE WITH INSTANTANEOUS EQUILIBRIUM AT THE SURFACE**

```

10 READ DIP F,SRXS,OSRX,NM,DELTA,SRX
15 WRITE OUTPUT TAPE 3,5
20 N=1
   M=1
30 BETA=(1./F)-1.
   WRITE OUTPUT TAPE 3,2,BETA,F,NM
   WRITE OUTPUT TAPE 3,1
40 DIMENSION ALPHA(1000),ZO(1000),FZ(1000),FZP(1000),
   LAM(1000),ZN(1000)
41 TABLE ALPHA(10.0,9.0,4.0,2.3333,1.5,1.0,.6667,
   1.4286,.25,.1111,0.0),ZO(3.1416,3.241,3.3485,3.465,
   23.5909,3.7264,3.8711,4.0236,4.1811,4.3395,4.4934)
44 DO 47 K=1,11
45 IF(BETA-ALPHA(K))47,46,48
47 CONTINUE
46 Z=ZO(K)
   GO TO 50
48 AX=ALPHA(K-1)-ALPHA(K)
   ZX=ZO(K)-ZO(K-1)
   BX=BETA-ALPHA(K)
   Y=8X*ZX/AX
49 Z=ZO(K)-Y
50 FZ=SINF(Z)/COSF(Z)-3.*Z/(3.+BETA*Z**2)
   IF(ABS(FZ)-DELTA)90,90,60
60 F/P=(1./COSF(Z)**2)-(3./(3.+BETA*Z**2))
   1+(6.*BETA*Z**2)/(3.+BETA*Z**2)**2
65 ZM(M)=Z
   FZ(M)=FZ
   FZP(M)=FZP
70 M=M+1
80 ZM(M)=ZM(M-1)-FZ(M-1)/FZP(M-1)
85 Z=ZM(M)
   GO TO 50
90 ZN(N)=Z
   WRITE OUTPUT TAPE 3,6,ZN(N)
95 IF(N-NM)100,120,10
100 N=N+1
   PI=3.14159
110 ZN(N)=ZN(N-1)+PI
   Z=ZN(N)
   GO TO 50
120 X=SRX**2
140 SUM=0.0
   DO 142 N=1,NM
142 SUM=SUM+(6.*BETA*(BETA+1.)*EXP(-((ZN(N)**2)*X))
   1/(9.+9.*BETA+(ZN(N)**2)*BETA**2)
145 EM=1.-SUM
150 GAMO=.5*((1.+4.*BETA/3.)**.5)+1.
160 GAMT=GAMO-1.
170 UO=(3.*GAMO/BETA)*SRX
180 UI=(3.*GAMT/BETA)*SRX
   IF((UO**2)-88.028)190,185,185
185 WRITE OUTPUT TAPE 3,9,SRX,EM
186 GO TO 205
190 AX=(1.+BETA)*(1.-((GAMO/(GAMO+GAMT)))*

```

TABLE 17 (Cont.)

```

1EXPF(UO**2)*(1.-ERF(UO)))-
2((GAMT/(GAMO+GAMT))*EXPF(UT**2)*(1.+ERF(UT)))
WRITE OUTPUT TAPE 3,3
200 WRITE OUTPUT TAPE 3,4,SRX,EM,AM
5 FORMAT
  RESTORE

  SPACE3

  SPACE2
    ALPHA
    END OF FORMAT
  2 FORMAT
    -E6
    END OF FORMAT
  1 FORMAT
    Z
    END OF FORMAT
  6 FORMAT
    -E6
    END OF FORMAT
  3 FORMAT
    SPACE
    SQ. ROOT OF OT/A**2
    EXACT MT/MI
    APPROX. MT/MI
    END OF FORMAT
  4 FORMAT
    -E6
    -E6
    -E6
    SPACE
    END OF FORMAT
  7 FORMAT
    SUM
    GAMO
    UO
    UT
    X
    -E6
    -E6
    -E6
    -E6
    -E4
    SPACE2
    END OF FORMAT
  9 FORMAT
    SPACE
    SQ. ROOT OF OT/A**2
    EXACT MT/MI
    -E6
    -E6
    END OF FORMAT
205 WRITE OUTPUT TAPE 3,7,SUM,GAMO,UO,UT,X
  IF(SRX-SRXS)210,220,10
210 SRX=SRX+OSRX
  GO TO 120
220 GO TO 10
  END(1,1,0,1,0,1,1,1,0,1,0,0,0,0,0)

```

### APPENDIX III

#### APPROXIMATE SOLUTION OF DIFFUSION FROM A LIMITED VOLUME OF WELL-STIRRED FLUID INTO A SPHERE

Although Equation (I-123) of Appendix I was derived for slab geometry, the suggestion has been made that it is also a satisfactory short-time approximation for the spherical case.

The equation is repeated below

$$\frac{u}{u_1} = \frac{1 + \beta}{2\beta} \operatorname{erfc} [(1 - \beta) \alpha \sqrt{t}] - \frac{1 - \beta}{2\beta} \operatorname{erfc} [(1 + \beta) \alpha \sqrt{t}]$$

where,

$u$  = concentration (mole fraction) of isotope in the gas at time  $t$

$u_1$  = concentration of isotope in the gas at  $t = 0$

$$\alpha = \frac{K}{2\sqrt{D}}$$

$$\beta = \sqrt{1 - \frac{4DS}{K\lambda}} = \sqrt{1 - \frac{4Q}{\lambda}}$$

$D$  = diffusion coefficient,  $\text{cm}^2/\text{sec}$

$K$  = rate constant of surface exchange reaction,  $\text{cm}/\text{sec}$

$S$  = surface-to-volume ratio of the solid. For a sphere of radius  $a$ ,

$$S = \frac{3}{a}$$

$$\lambda = \frac{\text{moles of diffusing element in the gas}}{\text{moles of diffusing element in the solid.}}$$

A FORTRAN program for computing  $u/u_1$  is given in Table 18 below. A sample of the calculation is shown in Table 19.

It also was desired to compare this approximate equation with the exact one. The FORTRAN program was modified to produce values of  $M_t/M_\infty$  and the corresponding values of  $(Dt/a^2)^{1/2}$ . This modified program is given in Table 20. The subroutine for the function  $\operatorname{erfc}$  from the original program is needed in this modified program also, but it was not recopied. Following the program is a sample table of results (Table 21).

TABLE 18

LISTING OF FORTRAN PROGRAM FOR COMPUTING  $u/u_1$   
VERSUS  $\sqrt{t}$  FROM EQUATION (I-123)

C000749 DIFFUSION INTO A PLATE WITH BOUNDARY REACTION, APPROX. SOL.  
C CODED BY JOHN YALCH FEBRUARY 1963

C  
C DIMENSION ALPHA(40),SRT(50),RATIO(40,50,10),  
1 SYMTAB(22),NSRT(50),BETA(10),DSRT(50),S(50)

C  
C TABLE SYMTAB(7,\$ (NPAGE,NA,NB,NT,BETA,ALPHA,SRT))

C  
C NPAGE=1

1 CALL DING(SYMTAB,1)

C  
C CALCULATE

K=1

21 N=1

22 DO 2 M=1,NA

BP=1.+BETA(K)

BM=1.-BETA(K)

BPAT=BP\*ALPHA(M)\*SRT(N)

BMAT=BM\*ALPHA(M)\*SRT(N)

RATIO(M,N,K)=(BP\*EERFC(BMAT)-BM\*EERFC(BPAT))/(2.\*BETA(K))

2 CONTINUE

N=N+1

IF(NT-N)23,22,22

23 K=K+1

IF(NB-K)24,21,21

24 CONTINUE

C  
C FIND INFLECTION POINTS

C  
C DO 30 N=2,NT

30 DSRT(N-1)=SRT(N)-SRT(N-1)

C  
C K=1

31 M=1

32 DO 33 N=2,NT

33 S(N-1)=(RATIO(M,N,K)-RATIO(M,N-1,K))/DSRT(N-1)

DO 34 N=3,NT

34 S(N-2)=S(N-2)-S(N-1)

N=4

35 IF(S(N-3)\*S(N-2))36,36,37

36 RATIO(M,N-2,K)=RATIO(M,N-2,K)+4.

37 N=N+1

IF(NT-N)38,35,35

38 M=M+1

IF(NA-M)39,32,32

39 K=K+1

IF(NB-K)40,31,31

40 CONTINUE

C  
C DO 3 N=1,NT

3 NSRT(N)=SRT(N)

C  
C PRINT OUT

K=1

20 NAS=1

TABLE 18 (Cont.)

```

      NAE=10
10  IF(NA-NAE)11,11,12
11  NAE=NA
12  WRITE OUTPUT TAPE 3,100,NPAGE,BETA(K),(ALPHA(M),M=NAS,NAE)
      WRITE OUTPUT TAPE 3,400
      NPAGE=NPAGE+1
C
      N=1
4   L=5
5   WRITE OUTPUT TAPE 3,200,NSRT(N),(RATIO(M,N,K),M=NAS,NAE)
      L=L-1
      IF(L)6,6,7
6   WRITE OUTPUT TAPE 3,300
      L=5
7   N=N+1
      IF(N-N)8,5,5
8   IF(NA-NAE)13,13,9
9   NAS=NAE+1
      NAE=NAE+10
      GO TO 10
13  K=K+1
      IF(NB-K)1,20,20
C
100 FORMAT
    RESTORE
      DIFFUSION INTO A PLATE WITH BOUNDARY REACTION          PAGE   -1
    SPACE
      BETA   -OPF3
      ALPHA  -F3   -F3   -F3   -F3   -F3   -F3   -F3   -F3   -F3   -F3
    END OF FORMAT
400 FORMAT
    TIME
    END OF FORMAT
200 FORMAT
      -I     -OPF3   -F3   -F3   -F3   -F3   -F3   -F3   -F3   -F3   -F3
    END OF FORMAT
300 FORMAT
    SPACE
    END OF FORMAT
    END

```

TABLE 18 (Cont.)

```

CEERFC
  FUNCTION EERFC(X)
    DIMENSION A(5,31),B(31)
    TABLE B(1.0,0.8965,0.8090,0.7346,0.6708,0.6157,0.5678,0.5259,
    10.4891,0.4565,0.4276,0.4017,0.3785,0.3576,0.3387,0.3216,0.3060,
    20.2917,0.2786,0.2665,0.2554,0.2451,0.2356,0.2267,0.2185,0.2108,
    30.2036,0.1969,0.1905,0.1846,0.1790)
    IF(X-3.1)1,2,2
  C COMPUTE EERFC BY INTERPOLATION
    1 IF(FN-30.)5,11,5
  C
    5 K=0
    6 FN=K
    K=K+1
    XZ=FN/10.
    XZS=XZ*XZ
    A(1,K)=-XZ
    A(2,K)=(2.*XZS-1.)/3.
    A(3,K)=((-2.*XZS+3.)*XZ)/6.
    A(4,K)=(((XZS-3.)*4.*XZS)+3.)/30.
    A(5,K)=((((XZS+5.)*4.*XZS-15.)*XZ)/90.
    IF(K-31)6,7,7
  100 FORMAT
    RESTORE
    COEFFICIENTS USED IN INTERPOLATION FOR EERFC
    SPACE 2
    A(1,K)    A(2,K)    A(3,K)    A(4,K)    A(5,K)
    SPACE
    -1PE3      -E3      -E3      -E3      -E3
    REPEAT 1
    END OF FORMAT
    7 WRITE OUTPUT TAPE 3,100,((A(I,K),I=1,5),K=1,31)
  C
    11 K=10.*X
    XZ=K
    XZ=XZ/10.
    H=X-XZ
    K=1+K
    S=(1.+(A(1,K)+(A(2,K)+(A(3,K)+(A(4,K)+A(5,K)*H)*H)*H)*H)*H
    EERFC=EXP(H*(2.*XZ+H))*(B(K)-2.*.56418958*S)
    GO TO 10
  C COMPUTE EERFC BY SERIES
    2 EERFC=1.
    TN=1.
    FACT=-.5/(X*X)
    K=1
    T=-1.
    3 T=T+2.
    TN=FACT*TN*T
    EERFC=EERFC+TN
    K=1+K
    IF(5-K)4,3,3
    4 EERFC=.56418958*EERFC/X
  10 RETURN

```



TABLE 19

SAMPLE OUTPUT FROM FORTRAN PROGRAM SHOWN IN TABLE 18

DIFFUSION INTO A PLATE WITH BOUNDARY REACTION

PAGE 120

BETA	0.610										
ALPHA	0.031	0.032	0.033	0.034	0.035	0.036	0.037	0.038	0.039	0.040	
$\sqrt{TIME}$											
30	0.812	0.805	0.798	0.791	0.784	0.777	0.771	0.764	0.757	0.751	
60	0.624	0.614	0.604	0.595	0.586	0.577	0.568	0.559	0.551	0.543	
90	0.495	0.485	0.475	0.466	0.456	0.448	0.439	0.431	0.423	0.415	
120	0.405	0.396	0.387	0.378	0.370	0.362	0.354	0.347	0.340	0.333	
150	0.342	0.333	0.325	0.317	0.309	0.302	0.295	0.289	0.282	0.276	
180	0.294	0.286	0.279	0.271	0.265	0.258	0.252	0.246	0.241	0.235	
210	0.257	0.250	0.244	0.237	0.231	0.225	0.220	0.214	0.209	0.205	
240	0.228	0.222	0.216	0.210	0.205	0.199	0.194	0.190	0.185	0.181	
270	0.205	0.199	0.194	0.188	0.183	0.179	0.174	0.170	0.166	0.162	
300	0.186	0.181	0.176	0.171	0.166	0.162	0.158	0.154	0.150	0.146	
330	0.170	0.165	0.161	0.156	0.152	0.148	0.144	0.140	0.137	0.134	
360	0.157	0.152	0.148	0.144	0.140	0.136	0.132	0.129	0.126	0.123	
390	0.145	0.141	0.137	0.133	0.129	0.126	0.123	0.119	0.116	0.114	
420	0.135	0.131	0.127	0.124	0.120	0.117	0.114	0.111	0.108	0.106	
450	0.127	0.123	0.119	0.116	0.113	0.110	0.107	0.104	0.101	0.099	
480	0.119	0.115	0.112	0.109	0.106	0.103	0.100	0.098	0.095	0.093	
510	0.112	0.109	0.106	0.102	0.100	0.097	0.094	0.092	0.090	0.087	
540	0.106	0.103	0.100	0.097	0.094	0.092	0.089	0.087	0.085	0.083	
570	0.101	0.098	0.095	0.092	0.089	0.087	0.085	0.082	0.080	0.078	
600	0.096	0.093	0.090	0.087	0.085	0.083	0.080	0.078	0.076	0.074	

TABLE 20

LISTING OF FORTRAN PROGRAM FOR COMPUTING  $M_t/M_\infty$   
VERSUS  $(Dt/a^2)^{1/2}$  FROM EQUATION (I-123)

```

C000751 FRACTIONAL DIFFUSION INTO A PLATE WITH BOUNDARY REACTION,
C APPROXIMATE SOLUTION.
C CODED BY JOHN YALCH MAY 1963
C
C DIMENSION Q(10),F(20),XAMDA(20),BETA(10,20),
1 ASRT(40),FRDI(40,10,20),S(25),SRDTA(40,10)
C
C TABLE S(8,S(Q,F,ASRT,IM,JM,KM,NPAGE,PUNCH))
C
C NPAGE=1
1 CALL DING(S,1)
C
C INITIALIZE
C
C K=1
2 J=1
3 BETA(J,K)=-0.0
i=1
4 FRDI(I,J,K)=-0.0
I=I+1
IF(I-IM)4,4,5
5 J=J+1
IF(J-JM)3,3,6
6 K=K+1
IF(K-KM)2,2,7
7 CONTINUE
C
C CALCULATE
K=1
11 XAMDA(K)=1.0/F(K)-1.0
J=1
12 BETA(J,K)=1.0-4.0*Q(J)/XAMDA(K)
IF(BETA(J,K))18,15,13
13 BETA(J,K)=SQRTF(BETA(J,K))
15 BP=1.0+BETA(J,K)
BM=1.0-BETA(J,K)
DO 16 I=1,IM
BMA=BM*ASRT(I)
BPA=BP*ASRT(I)
16 FRDI(I,J,K)=(1.0+XAMDA(K))*(1.0-(BP*EERFC(BMA)
1-BM*EERFC(BPA))/(2.0*BETA(J,K)))
18 J=J+1
IF(J-JM)12,12,19
19 K=K+1
IF(K-KM)11,11,20
20 CONTINUE
C
C
DO 21 J=1,JM
DO 21 I=1,IM
21 SRDTA(I,J)=2.0*Q(J)*ASRT(I)/3.0
C
C PRINT OUT
C
C SPACE
ALPHA SQ ROOT
SQ ROOT OF DT
OF TIME OVER A
C SPACE
END OF FORMAT
C

```

FRACTIONAL DIFFUSION

TABLE 20 (Cont.)

600	FORMAT	-1PE3	-E3	-0PF3	-F3	-F3	-F3	-F3
	END OF FORMAT							
C								
700	FORMAT	-1PE3	-E3	-E3	-E3	-E3	-E3	-E3
	END OF FORMAT							
C								
	END							
	J=1							
30	KS=1							
	KE=5							
31	IF(KM-KE)32,32,33							
32	KE=KM							
33	WRITE OUTPUT TAPE 3,100,NPAGE,Q(J),(BETA(J,K),K=KS,KE)							
	WRITE OUTPUT TAPE 3,200,(F(K),K=KS,KE)							
	WRITE OUTPUT TAPE 3,300,(XAMDA(K),K=KS,KE)							
	NPAGE=NPAGE+1							
	WRITE OUTPUT TAPE 3,500							
C								
	I=1							
34	L=5							
35	WRITE OUTPUT TAPE 3,600,ASRT(I),SRDTA(I,J),(FRDI(I,J,K),K=KS,KE)							
	L=L-1							
	IF(L)36,36,37							
36	WRITE OUTPUT TAPE 3,400							
	L=5							
37	I=I+1							
	IF(IM-I)38,35,35							
38	IF(KM-KE)40,40,39							
39	KS=KE+1							
	KE=KE+5							
	GO TO 31							
40	J=J+1							
	IF(JM-J)41,30,30							
C								
C	PUNCH OUTPUT							
C								
	41 IF(PUNCH-6HYES )1,42,1							
	42 PUNCH 700,(((SRDTA(I,J),FRDI(I,J,K),I=1,IM),K=1,KM),J=1,JM)							
	GO TO 1							
C								
100	FORMAT							
	RESTORE							
	SPACE 5							
	FRACTIONAL DIFFUSION INTO A PLATE WITH BOUNDARY REACTION						PAGE	-1
	SPACE 1							
	Q	-1PE3						
	BETA	-E3	-E3	-E3	-E3	-E3		
	END OF FORMAT							
C								
200	FORMAT							
	F	-E3	-E3	-E3	-E3	-E3		
	END OF FORMAT							
C								
300	FORMAT							
	LAMBDA	-E3	-E3	-E3	-E3	-E3		
	END OF FORMAT							
C								
400	FORMAT							
	SPACE							
	END OF FORMAT							
C								
500	FORMAT							

TABLE 21

SAMPLE OUTPUT FROM FORTRAN PROGRAM SHOWN IN TABLE 20

FRACTIONAL DIFFUSION INTO A PLATE WITH BOUNDARY REACTION PAGE 5

Q	10.000-02					
8ETA	9.103-01	8.858-01	8.563-01	8.202-01	7.746-01	
F	0.300-00	0.350-00	0.400-00	0.450-00	0.500+00	
LAMBDA	0.233+01	0.186+01	0.150+01	0.122+01	0.100+01	

ALPHA SQ ROOT OF TIME	SQ ROOT OF DT OVER A	FRACTIONAL DIFFUSION				
3.750-01	2.500-02	0.050	0.054	0.058	0.063	0.069
7.500-01	5.000-02	0.141	0.151	0.162	0.175	0.190
1.125+00	7.500-02	0.240	0.256	0.273	0.293	0.316
1.500+00	10.000-02	0.340	0.359	0.381	0.406	0.433
1.875+00	1.250-01	0.437	0.459	0.484	0.511	0.541
2.250+00	1.500-01	0.530	0.554	0.580	0.607	0.638
2.625+00	1.750-01	0.619	0.643	0.669	0.696	0.725
3.000+00	2.000-01	0.704	0.727	0.752	0.777	0.804
3.375+00	2.250-01	0.785	0.807	0.829	0.852	0.875
3.750+00	2.500-01	0.862	0.881	0.901	0.920	0.939
4.125+00	2.750-01	0.936	0.952	0.968	0.983	0.997
4.500+00	3.000-01	1.006	1.018	1.030	1.041	1.050
4.175+00	2.783-01	0.945	0.961	0.976	0.991	1.004
5.250+00	3.500-01	1.136	1.140	1.143	1.143	1.142
5.625+00	3.750-01	1.197	1.196	1.193	1.189	1.182
6.000+00	4.000-01	1.255	1.249	1.241	1.231	1.219
6.375+00	4.250-01	1.310	1.299	1.286	1.271	1.253
6.750+00	4.500-01	1.363	1.347	1.328	1.307	1.285
7.125+00	4.750-01	1.414	1.392	1.367	1.342	1.314
7.500+00	5.000-01	1.463	1.434	1.405	1.374	1.341
7.875+00	5.250-01	1.509	1.475	1.440	1.404	1.366
8.625+00	5.750-01	1.596	1.551	1.505	1.458	1.412
9.375+00	6.250-01	1.677	1.619	1.562	1.506	1.451

TABLE 21 (Cont.)

FRACTIONAL DIFFUSION INTO A PLATE WITH BOUNDARY REACTION PAGE 6

		Q	10.000-02			
		BETA	7.149-01	6.325-01	5.071-01	2.582-01 -2.000-01
		F	0.550+00	0.600+00	0.650+00	0.700+00 0.750+00
		LAM8DA	0.818+00	0.667+00	0.538+00	0.429-00 0.333-00
ALPHA SQ ROOT OF TIME	SQ ROOT OF DT OVER A	FRACTIONAL DIFFUSION				
3.750-01	2.500-02	0.076	0.086	0.097	0.112	-0.*
7.500-01	5.000-02	0.209	0.231	0.258	0.292	-0.
1.125+00	7.500-02	0.342	0.374	0.411	0.456	-0.
1.500+00	10.000-02	0.465	0.501	0.543	0.591	-0.
1.875+00	1.250-01	0.574	0.611	0.653	0.699	-0.
2.250+00	1.500-01	0.671	0.706	0.745	0.785	-0.
2.625+00	1.750-01	0.756	0.788	0.822	0.856	-0.
3.000+00	2.000-01	0.831	0.859	0.887	0.913	-0.
3.375+00	2.250-01	0.898	0.920	0.941	0.961	-0.
3.750+00	2.500-01	0.957	0.974	0.989	1.001	-0.
4.125+00	2.750-01	1.010	1.021	1.030	1.036	-0.
4.500+00	3.000-01	1.057	1.062	1.065	1.065	-0.
4.875+00	2.783-01	1.016	1.027	1.035	1.040	-0.
5.250+00	3.500-01	1.138	1.132	1.124	1.113	-0.
5.625+00	3.750-01	1.173	1.162	1.148	1.132	-0.
6.000+00	4.000-01	1.205	1.189	1.170	1.150	-0.
6.375+00	4.250-01	1.234	1.213	1.190	1.165	-0.
6.750+00	4.500-01	1.261	1.235	1.208	1.179	-0.
7.125+00	4.750-01	1.285	1.255	1.224	1.192	-0.
7.500+00	5.000-01	1.308	1.273	1.238	1.203	-0.
7.875+00	5.250-01	1.328	1.290	1.252	1.213	-0.
8.625+00	5.750-01	1.365	1.320	1.275	1.231	-0.
9.375+00	6.250-01	1.398	1.346	1.295	1.247	-0.

\* The quantity -0.0 is printed when  $\beta$  is imaginary

**APPENDIX IV**  
**EXACT SOLUTION OF DIFFUSION FROM A LIMITED VOLUME OF**  
**WELL-STIRRED FLUID INTO A SPHERE**

Numerical values were desired from Equation (I-117) of Appendix I. This equation is repeated below.

$$\frac{M_t}{M_\infty} = 1 - \frac{2(1+\lambda)}{3\lambda} \sum_{a=1}^{\infty} \frac{q_a^2 e^{-q_a^2 \frac{2Dt}{a^2}}}{F \left( \frac{q_a^2 Q}{9} + \frac{1}{\lambda} \right) + F^2 + q_a^2 E^2 - \frac{2E}{\lambda}}$$

The  $q_a$ 's are the positive, non-zero roots of

$$\tan q_a = \frac{q_a \left( \frac{1}{\lambda} - \frac{Q}{9} q_a^2 \right)}{\frac{1}{\lambda} + \frac{QN}{9} q_a^2} = \frac{q_a E}{F}$$

$$N \equiv \frac{3}{Q} - 1$$

$$Q \equiv \frac{DS}{K}$$

$D$  = diffusion coefficient

$S$  = surface-to-volume ratio for a sphere.  $S = 3/a$ , where  $a$  = radius of the sphere.

$K$  = rate constant of the surface exchange reaction.

$$\lambda = \frac{\text{moles of diffusing element in the gas}}{\text{moles of diffusing element in the solid}}$$

$$\frac{M_t}{M_\infty} = \frac{\text{mass of isotope which has left the gas after time } t}{\text{mass of isotope which would leave gas as } t \rightarrow \infty}$$

A Fortran program for calculating  $M_t/M_\infty$  from Equation (I-117) is given in Table 22. (In the input to this program, the radius of the spheres is expressed in microns.) Samples of the output formats are given in Tables 23, 24, 25, and 26.

Figures 26, 27, and 28 show plots of  $M_t/M_\infty$  versus  $(Dt/a^2)^{1/2}$  when the other parameters have the fixed values specified on the graphs.

**TABLE 22**  
**LISTING OF FORTRAN PROGRAM FOR COMPUTATIONS**  
**WITH EQUATION (I-117)**

```
*F2864A00
      DIMENSION TEMP(200),DA(25),TIME(2000),DDK(25),AK(25),RK(25)
      DIMENSION R(2000),SYMTAB(200),FJ(200),DENOM(2000),
      1KNT(2000), Q(25),F(25),D(2000),DTAK(2000),ELAMB(25),DTAK1(2000)
      TABLE SYMTAB(65,$(R,Q,F,DTA,DTAMAX,DELTAD,NGN;AINCR,DINCR,AMAX,
      1LOOP,TO,TMAX,DELTAT,NOPLT,DDK,NDS,RK,NRADUS,SX,SY,
      20A,ROOT,XK1,XK2,XK3,XK4,TOL,XJMAX,SUMTOL,DMAX,AMIN,DMIN))
      DIMENSION TITA(5),TITB(2),TITD(10),TITE(4),TITG(4),TITC(2)
      TABLE TITA(21HSQUARE ROOT OF DT/A*A)
      TABLE TITB(9HMT/MT-INF),TITC(4HTIME)
      TABLE TITG(13HCONCENTRATION),TITE(16HRADIUS RATIO R/A)
      NTA=-21
      NTB=9
      NTC=-4
      CALL MAB(BITS)
10    DO 110 I=1,2000
      NOPLT=2
110   R(I)=BITS
      DO 1 I=1,25
      F(I)=BITS
1    Q(I)=BITS
      NO=0
      KIM=1
      SUMTOL=.0000001
      LOOP=0
      DELTAD=.05
      DTA=.02
      DTAMAX=2.
      TO=1.
      TMAX=3600.
      NF=0
      NO=1
      AMIN=20.
      AMAX=30.
      DMAX=1.E-8
      DMIN=1.E-16
      DINCR=100.
      AINCR=2.
      DELTAT=BITS
      AN=0.
      QA=3.142
      ROOT=3.142
      XK1=0.
      XK2=-0.1
      XK3=0.
      XK4=0.1
      TOL=.0001
      XJMAX=31.
      NGN=94
      N=0
      NOPLT=1
      LOOP=1
      NRADUS=1
      CALL DING(SYMTAB,1)
      NOPLT=NOPLT
```

TABLE 22 (Cont.)

```

DTAM=DTA
NGN=NGN
NDTA=(DTAMAX-DTA)/DELTAD+1.
DO 2 I=1,25
  IF (F(I)-BITS) 2,3,2
2  NF=NF+1
3  DO 4 I=1,NF
4  ELAMB(I)=(1.-F(I))/F(I)
  DO 5 I=1,25
  IF (Q(I)-BITS) 5,50,5
5  NQ=NQ+1
50 N1=1
   N2=1
   IF (DELTAT-BITS) 101, 6, 101
101 NO=2
   TIME(1)=TO
   NTIME=(TMAX-TO)/DELTAT+1.
   N1=NRADUS
   N2=NDS
   NDTA=NTIME
6  DO 600 J=1,NF
   AMBDA=1./ELAMB(J)
   BC=2.*(AMBDA+1.)/3.
   DO 60C KKKK=1,NQ
   Q1=Q(KKKK)/9.
   Q2=(3.-Q(KKKK))/9.
   K=0
61 RCAL=0.
   IF (R(1)-BITS) 8,7,8
7  CALL FINDER(R,XK1,XK2,XK3,XK4,TOL,XJMAX,FJ,AMBDA,Q1,Q2,QA,
1ROOT,NGN)
   WRITE (3,22) Q(KKKK),F(J),ELAMB(J),(R(I),FJ(I),I=1,NGN)
   RCAL=1.
   GO TO 9
8  NGN=0
   DO 200 I=1,2000
   IF (R(I)-BITS) 200,9,200
200 NGN=NGN+1
9  DO 11 I=1,NGN
   EA=R(I)*R(I)
   EB=AMBDA-Q1*EA
   EC=AMBDA+Q2*EA
   ED=AMBDA+Q1*EA
   DEMON=BC*EA/(EC*(EC+ED)+EB*(EB*EA-2.*AMBDA))
   IF (DEMON) 27,27,11
27 WRITE (3,26) R(I),EB,EC,ED,BC,DEMON
   GO TO 11
11 DENOM(I)=DEMON
   DO 15 KKK=1,N1
   AA=RK(KKK)*.0001
   DO 15 KKL=1,N2
   DD=DDK(KKL)
   K=K+1
60 AK(K)=3.*DD/(AA*Q(KKKK))
   TIME(KIN)=TO

```



TABLE 22 (Cont.)

```

DO 15 KK=1,NDTA
GO TO (303,304),NO
303 DTA1=DTA*DTA
GO TO 305
304 DTA1=DD*TIME(KIM)/(AA*AA)
305 NN=0
SUM=0.
DO 12 I=1,NQN
NN=NN+1
SUM1=EXP(- (DTA1*R(I)*R(I)))*DENOM(I)
IF (SUM1-SUMTOL)13,13,12
12 SUM=SUM+SUM1
13 D(KIM)=1.-SUM
DTAK1(KIM)=DTA1
DTAK(KIM)=SQRTF(DTA1)
KNT(KIM)=NN-1
GO TO (306,307),NO
306 IF (DTAK(KIM)-DTAMAX) 14,14,15
14 DTA=DTAK(KIM)+DELTAD
GO TO 15
307 TIME(KIM+1)=TIME(KIM)+DELTAT
15 KIM=KIM+1
IF(RCAL-1.) 130,129,130
129 R(1)=BITS
130 CONTINUE
DTA=DTAM
GA=ROOT
600 CONTINUE
K1=1
K2=NDTA
GO TO (501,1000),NO
501 DO 700 J=1,NF
DO 700 K=1,NQ
WRITE (3,21) F(J),ELAMB(J),Q(K),(DTAK(I),DTAK1(I),D(I),KNT(I),
1I=K1,K2)
WRITE (3,23)
K1=K2+1
K2=K2+NDTA
700 CONTINUE
GO TO (701,702),NOPLOT
701 CALL APLLOT(DTAK,D,Q,TITA,TITB,F,1.,0.,1.,DUM1,DUM2,C.,10.,10.,NF,
1NQ,NTA,NTB,1,0.0,1.0,NDTA,.25)
702 MM=0
1000 K1=1
K2=NDTA
IF (LOOP) 1111,10,1111
1111 KKK=0
DO 2000 M=1,2
DO 2000 L=1,NF
DO 2000 KKKK=1,NQ
DO 2000 KK=1,N1
DO 2000 K=1,N2
GO TO (1112,1113),M
1112 CONTINUE
KKK=KKK+1

```

TABLE 22 (Cont.)

```

WRITE (3,24) DDK(K),RK(KK) ,AK(KKK),Q(KKKK),F(L),ELAMB(L),
1(TIME(I),D(I),DTAK(I),DTAK1(I),KNT(I),I=K1,K2)
1008 K1=K2+1
      K2=K2+NDTA
      WRITE (3,23)
      GO TO 2000
1113 CONTINUE
      GO TO (2003,10),NOPLOT
2003 CALL APLOT(TIME,D,DDK,TITC,TITB,RK,TMAX,0.,1.,F(L),Q(KKKK),0.,SX,
1SY,NRADUS,NDS,NTC,NTB,3,0.,1.,NDTA,.25)
2000 CONTINUE
      GO TO 10
20 FORMAT
      ROOTS OF TANGENT EQUATION AND
      THE PARAMETERS Q=      -F5      F=      -F5      LAMBDA=      -F5
      -F8      -F8      -F8      -F8      -F8
      REPEAT 1
      END OF FORMAT
21 FORMAT
      RESTORE
      DIFFUSION FROM A LIMITED VOLUME OF WELL STIRRED FLUID
      INTO A SOLID SPHERE WITH FINITE REACTION RATE AT THE SURFACE
      FOR THE PARAMETERS F=      -F5      LAMBDA=      -F5      Q=      -F5
      (DT/A**A)**.5      (DT/A**A)      MT/M-INF      NO OF TERMS USED
      -F5      -F5      -F5      -1
      REPEAT 1
      END OF FORMAT
22 FORMAT
      RESTORE
      ROOTS OF TANGENT EQUATION AND THEIR ERRORS
      FOR THE PARAMETERS Q=      -F5      F=      -F5      LAMBDA=      -F5
      ROOT      ERROR      ROOT      ERROR      ROOT      ERROR
      -0PF5      -1PE4      -0PF5      -1PE4      -0PF5      -1PE4
      REPEAT 1
      END OF FORMAT
23 FORMAT
      SPACE 6
      (DT/A**A)=DIFFUSION COEFFICIENT D TIMES TIME (T) DIVIDED BY THE
      RADIUS (A) SQUARED.
      (DT/A**A)**.5=SQUARE ROOT OF (DT/A**A)
      MT/M-INF=COMPOSITION OF GAS AS A FUNCTION OF TIME
      Q=DS/K THE DIFFUSION COEFFICIENT TIMES THE RATIO OF THE SURFACE TO
      VOLUME RATIO (3/A) AND THE RATE CONSTANT OF SURFACE REACTION
      VALUES OF F,DT/A**A,AND Q ARE ASSUMED TO BE KNOWN
      END OF FORMAT
24 FORMAT
      RESTORE
      DIFFUSION FROM A LIMITED VOLUME OF WELL STIRRED FLUID
      INTO A SOLID SPHERE WITH FINITE REACTION RATE AT THE SURFACE
      D=      -1PE3 A=      -0PF2 K=      -1PE3 Q=      -0PF4 F=      -F2 LAMBDA=      -F4
      TIME(SEC)      MT/M-INF      (DT/A**A)**.5      (DT/A**A)      NO. OF TERMS
      -1PE4      -0PF5      -F5      -F5      -1
      REPEAT 1
      END OF FORMAT
25 FORMAT
      RESTORE
      DIFFUSION FROM A LIMITED VOLUME OF WELL STIRRED FLUID
      INTO A SOLID SPHERE WITH FINITE REACTION RATE AT THE SURFACE
      FOR THE PARAMETERS F=      -F5      LAMBDA=      -F5      Q=      -F5
      (DT/A**A)**.5      (DT/A**A)      MT/M-INF      NO OF TERMS USED
      -F5      -F5      -F5      -F0
      REPEAT 1
      END OF FORMAT

```

TABLE 22 (Cont.)

```

26 FORMAT
  RESTORE
  ROOT          -F5  E          -F5  F          -F5
  F PRIME       -F5  COEF.      -F5  FACTOR      -F5
  END OF FORMAT
  END

*F2864A00
*SUBROUTINE TO PLOT DATA FROM DIFFUSION STUDY.
*
  SUBROUTINE APL0T(AX,AY,Q,TITA,TITB,F,  XMAX,XMIN,YMAX,ALPHA,BETA,
  1YMIN, SX,SY,NF,NQ,NA,NB,NC,AAX, AAY,NAX,X)
*
  DIMENSION AX(1),AY(1),Q(1),TITA(1),TITB(1),TITD(20),TITE(5),
  ITITG(5)
  DIMENSION XX(100),YY(100)
  DIMENSION TEMP1(25),F(1),TEMP(2000)
  DIMENSION TITH(10),TITJ(10),TITK(10)
*
  TABLE TITD(60)HDIFFUSION FROM A WELL-STIRRED FLUID INTO A SOLID SPH
  1ERE FOR )
  TABLE TITE(22)HF OF      AND VARYING Q)
  TABLE TITG(24)HQ OF      AND VARYING F)
  TABLE TITH(52)HF OF      ,Q OF      ,A OF      MICRONS AND VARYING D
  1)
  TABLE TITJ(48)HF OF      ,Q OF      ,LOG D OF      AND VARYING A)
  TABLE TITK(46)HF OF      ,Q OF      ,AND VARYING (DT/A*A)**.5)
*
  NAAA=2
  NAAB=5
  AAA=.78
  AAR=.90
  AAC=.78
  DO 2 KK=1,2
  KKS=KKS+KK
  IF (KKS-1) 8100,8100,8200
8100 REWIND 10
8200 CONTINUE
  GO TO (803,800),KK
*
  *Q IS PRINTED OUT AS TITLE IDENTIFICATION,Y VALUES
  *MUST BE REARRANGE SO THAT WE HAVE A RANGE OF LAMBDA S
  *FOR EACH Q
*
  800 I=I
  IF (NF-1) 8101,2,8101
8101 NAF=NQ
  NAQ=NF
*
  DO 806 KJ=I,NQ
806  TEMPI(KJ)=Q(KJ)
  J=1
  DO 801 L=1,NQ
  DO 801 M=1,NF
  J=((M-1)*NQ+(L-1))*NAX+1
  DO 801 N=1,NAX
  TEMP(I)=AY(J)
  J=J+1
801 I=I+1
*
  *COMPLETE TITLE OF PAGE AND SET NUMBER OF DECIMAL PLACES
  *DESIRED P AND NUMBER OF CHARACTERS IN TITLE

```

TABLE 22 (Cont.)

```

*
701 J=11
GO TO (7001,71,7002),NC
7001 DO 703 K=1,4
TITD(J)=TITG(K)
703 J=J+1
NTD=84
NAAC=5
GO TO 804
*
7002 DO 7003 K=1,9
TITD(J)=TITJ(K)
7003 J=J+1
AAC=1.104
NAAC=1
NTD=108
GO TO 804
*
*F IS PRINTED OUT FOR TITLE IDENTIFICATION,Y VALUES
*ARE IN CORRECT ORDER
*
803 CONTINUE
IF (NQ=1) 8031,2,8031
8031 J=11
GO TO (8001,8004,8002),NC
8001 DO 704 K=1,4
TITD(J)=TITE(K)
704 J=J+1
NTD=82
NAAC=2
GO TO 8006
*
8002 DO 8003 K=1,9
TITD(J)=TITH(K)
8003 J=J+1
AAC=1.068
NTD=112
NAAC=0
GO TO 8006
*
8004 DO 8005 K=1,9
TITD(J)=TITK(K)
8005 J=J+1
NTD=106
*
8006 DO 807 KJ=1,NF
807 TEMP1(KJ)=F(KJ)
NAF=NF
NAQ=NQ
J=NF*NQ*NAX+1
DO 805 I=1,J
805 TEMP(I)=AY(I)
*
804 CONTINUE
IA=1

```

TABLE 22 (Cont.)

```

      NCHNG=1
*
*REVERSE X TABLE FOR PLOTTING BACKWARDS.
*
      NR=NAX
      DO 100 I=1,NAX
      XX(I)=AX(NR)
      100 NR=NR-1
*
      JA=1
*
*SCALE DATA.
*
      CALL SCALEM(XMAX,XMIN,YMAX,YMIN,SX,SY)
*
      DO 2 J=1,NAF
*
*DRAW AND LABEL X-AXIS AND Y-AXIS ON NEGATIVE SIDES.
*
      CALL XAXIS(0.,0.,TITA,NA,SX,0.)
      CALL YAXIS(0.,0.,TITB,NB,SY,90.)
*
*LABEL EACH PLOT WITH CORRECT Q OR F INSERTED IN TITLE
*
      CALL SYMBL(AAX,AAY,.14,TITD,0.,NTD)
      QN=TEMP1(J)
*
      GO TO (9002,9000,9000),NC
9000 AB=(AAX+AAA)*SX
      NDP=NAAA
      CALL NUMBRA(AB,10.,.14,ALPHA,0.,NDP)
*
9001 AB=(AAX+AAB)*SX
      NDP=NAAAB
      CALL NUMBRA(AB,10.,.14,BETA ,0.,NDP)
      GO TO (9003,9003,9010),NC
9010 GO TO (9011,9002),KK
9011 QN=LOGF(QN)*C.434294482
*
9002 AB=(AAX+AAC)*SX
      NDP=NAAC
      CALL NUMBRA(AB,10.,.14,QN,0.,NDP)
*
9003 DO 1 I=1,NAG
      NN=0
      GO TO (12,13),NCHNG
      12 NCHNG=2
*
*PLOT CURVE IN FORWARD DIRECTION.
*
      CALL LINE(AX(1),TEMP(JA),NAX,1)
      GO TO 1
*
      13 NCHNG=1
      NR=JA+NAX-1

```

TABLE 22 (Cont.)

```

DO 200 K=1,NAX
  YY(K)=AY(NR)
200 NR=NR-1
*
*PLOT CURVE IN REVERSE DIRECTION.
*
  CALL LINE(XX(1),YY(1),NAX,1)
  1 JA=JA+NAX
*
*THIS APPROACH OF FORWARD AND BACKWARDS ALTERNATELY
*SHOULD SAVE TIME ON MOST PLOTS.
*
  CALL RESTOR
  2 CONTINUE
  71 CONTINUE
  RETURN
  END

*FINDERCO
  SUBROUTINE FINDER(R,XK1,XK2,XK3,XK4,TOL,XJMAX,FJK,AMBDA,O1,Q2,QA,
  1ROOT,NQN)
  DIMENSION XJ(8),R(200),FJK(200)
  DO 5 K=1,NQN
  DO 4 I=1,8
  4 XJ(I)=0.
    GOWHER= 6HBLANK1
    GOBACK= 6HGOBACK
  1 ALPHA=AMBDA-O1*QA*QA
    BETA=AMBDA+Q2*QA*QA
    FJ=BETA*SINF(QA)-QA*ALPHA*COSF(QA)
    FJPRIM=(BETA-ALPHA+2.*Q1*QA*QA)*COSF(QA)+(QA*ALPHA+2.*Q2*QA)*
  1SINF(QA)
    XK1=-1./FJPRIM
    XK2=0.
    XK3=-1./FJPRIM
  7777 XK4=0.
    IF (ABSF(FJ/FJPRIM)-TOL*0.1) 31,31,30
  30 CALL QIRE(QA,FJ,XK1,XK2,XK3,XK4,TOL,XJMAX,XJ,GOWHER)
    IF (GOWHER-GOBACK) 31,1,31
  31 FJK(K)=-FJ/FJPRIM
    R(K)=QA
  5 QA=QA+ROOT
  RETURN
  END

```

TABLE 23  
SAMPLE CALCULATIONS OF  $M_t/M_\infty$  VERSUS  $(Dt/a^2)^{1/2}$   
FROM THE PROGRAM OF TABLE 22

DIFFUSION FROM A LIMITED VOLUME OF WELL STIRRED FLUID  
INTO A SOLID SPHERE WITH FINITE REACTION RATE AT THE SURFACE  
FOR THE PARAMETERS  $F= 0.50000$      $\Lambda= 1.00000$      $Q= 1.00000$

$(Dt/a^2)^{1/2}$	$(Dt/a^2)$	$M_t/M_\infty$	NO OF TERMS USED
0.05000	0.00250	0.03982	15
0.07500	0.00562	0.08375	11
0.10000	0.01000	0.13868	9
0.12500	0.01562	0.20119	7
0.15000	0.02250	0.26829	6
0.17500	0.03062	0.33740	6
0.20000	0.04000	0.40643	5
0.22500	0.05062	0.47371	4
0.25000	0.06250	0.53797	4
0.27500	0.07562	0.59830	4
0.30000	0.09000	0.65411	3
0.32500	0.10562	0.70503	3
0.35000	0.12250	0.75092	3
0.37500	0.14062	0.79176	3
0.40000	0.16000	0.82770	3
0.42500	0.18062	0.85893	3
0.45000	0.20250	0.88575	2
0.47500	0.22562	0.90849	2
0.50000	0.25000	0.92753	2
0.52500	0.27562	0.94326	2
0.55000	0.30250	0.95609	2
0.57500	0.33062	0.96641	2
0.60000	0.36000	0.97461	2
0.62500	0.39062	0.98103	2
0.65000	0.42250	0.98599	2
0.67500	0.45562	0.98978	2
0.70000	0.49000	0.99263	2
0.72500	0.52562	0.99475	1
0.75000	0.56250	0.99630	1
0.77500	0.60062	0.99743	1
0.80000	0.64000	0.99823	1
0.82500	0.68062	0.99880	1
0.85000	0.72250	0.99919	1
0.87500	0.76562	0.99947	1
0.90000	0.81000	0.99965	1
0.92500	0.85562	0.99977	1
0.95000	0.90250	0.99985	1
0.97500	0.95062	0.99991	1
1.00000	1.00000	0.99994	1

$(Dt/a^2)$ =DIFFUSION COEFFICIENT D TIMES TIME (T) DIVIDED BY THE  
RADIUS (A) SQUARED.  
 $(Dt/a^2)^{1/2}$ =SQUARE ROOT OF  $(Dt/a^2)$   
 $M_t/M_\infty$ =COMPOSITION OF GAS AS A FUNCTION OF TIME  
 $Q=DS/K$  THE DIFFUSION COEFFICIENT TIMES THE RATIO OF THE SURFACE TO  
VOLUME RATIO  $(3/A)$  AND THE RATE CONSTANT OF SURFACE REACTION  
VALUES OF  $F$ ,  $Dt/a^2$ , AND  $Q$  ARE ASSUMED TO BE KNOWN

TABLE 24

SAMPLE CALCULATION OF THE ROOTS OF THE  
AUXILIARY EQUATION USED IN OBTAINING TABLE 23

ROOTS OF TANGENT EQUATION AND THEIR ERRORS FOR THE PARAMETERS C= 1.00000 F= 0.50000 LAM8DA= 1.00000					
ROOT	ERROR	ROOT	ERROR	ROOT	ERROR
3.08484	-9.3944-07	5.28715	-9.8738-07	8.14835	8.3706-08
11.19243	-1.3130-06	14.28575	-2.7097-08	17.39842	9.4355-08
20.52067	1.7682-07	23.64838	1.4426-07	26.77950	6.8397-08
29.91291	-7.0563-06	33.04792	-4.2806-06	36.18411	-2.5125-06
39.32117	-1.5239-06	42.45893	-1.1433-06	45.59721	-5.4198-07
48.73593	-3.9886-07	51.87501	-4.2429-07	55.01437	-3.4987-07
58.15398	1.8531-07	61.29379	6.1507-08	64.43378	3.8754-07
67.57392	-1.0805-07	70.71419	7.5457-07	73.85457	5.4663-07
76.99505	5.5256-07	80.13562	4.3132-07	83.27626	6.9985-07
86.41698	4.7038-07	89.55776	6.4469-08	92.69859	7.8092-07
95.83947	4.6826-09	98.98040	5.8206-07	102.12137	2.3686-07
105.26237	3.3926-08	108.40341	5.3580-07	111.54449	7.6044-07
114.68559	5.0820-08	117.82671	8.6283-07	120.96786	1.9355-07
124.10904	9.3419-09	127.25023	5.6002-07	130.39144	1.2808-06
133.53267	8.1647-07	136.67392	1.7527-06	139.81519	1.0424-06
142.95646	1.4820-06	146.09776	2.2659-07	149.23906	2.4018-07
152.38037	7.2006-07	155.52170	9.5058-07		

TABLE 25

SAMPLE CALCULATION OF THE ROOTS OF THE AUXILIARY EQUATION  
USED IN OBTAINING TABLE 26

ROOTS OF TANGENT EQUATION AND THEIR ERRORS FOR THE PARAMETERS C= 0.25000 F= 0.36400 LAM8DA= 1.74725					
ROOT	ERROR	ROOT	ERROR	ROOT	ERROR
3.35536	-C.	6.05738	3.9202-08	8.89595	3.0638-08
11.83076	-6.7097-06	14.82730	-1.2359-06	17.86362	-4.6924-08
20.92624	8.0727-08	24.00681	9.5887-08	27.10005	6.4582-08
30.20249	2.8343-08	33.31180	1.2437-07	36.42634	1.3959-07
39.54497	3.7214-07	42.66683	7.5689-08	45.79130	3.2678-07
48.91790	1.8381-08	52.04626	-9.6134-06	55.17609	-7.3708-06
58.30715	-5.4362-06	61.43926	-4.1952-06	64.57228	-2.7817-06
67.70608	-2.0218-06	70.84057	-2.0727-06	73.97564	-1.0567-06
77.11125	-7.4124-07	80.24731	-5.7480-07	83.38379	-5.9635-07
86.52063	-1.7859-07	89.65781	-2.4237-07	92.79528	-4.5653-07
95.93302	-3.0938-08	99.07100	-3.0123-07	102.20920	4.4644-07
105.34760	-1.4873-07	108.48619	-2.9387-07	111.62494	-9.5189-08
114.76385	1.0933-07	117.90290	4.4881-07	121.04208	4.2845-07
124.18139	6.4729-07	127.32080	7.7260-07	130.46032	3.4729-07
133.59994	1.5969-06	136.73965	1.6979-06	139.87944	2.9708-07
143.01931	1.4108-06	146.15926	-1.6849-08	149.29927	9.2357-07
152.43935	-3.4041-08	155.57949	8.3495-07		



TABLE 26

SAMPLE CALCULATIONS OF  $M_t/M_\infty$  VERSUS  $t$   
FROM THE PROGRAM OF TABLE 22

DIFFUSION FROM A LIMITED VOLUME OF WELL STIRRED FLUID  
INTO A SOLID SPHERE WITH FINITE REACTION RATE AT THE SURFACE

D= 4.000-10 A= 34.50 K=4.969-07 C= 0.2500 F= 0.36 LAMBCA= 1.7473

TIME(SEC)	$M_t/M_\infty$	$(Dt/A^2)^{0.5}$	$(Dt/A^2)$	NO. OF TERMS
3.0000+02	0.26122	0.10041	0.01008	10
4.5000+02	0.33785	0.12298	0.01512	8
6.0000+02	0.39595	0.14200	0.02016	7
7.5000+02	0.45208	0.15876	0.02520	6
9.0000+02	0.49684	0.17391	0.03025	6
1.0500+03	0.53592	0.18785	0.03529	6
1.2000+03	0.57046	0.20082	0.04033	5
1.3500+03	0.60129	0.21300	0.04537	5
1.5000+03	0.62902	0.22452	0.05041	5
1.6500+03	0.65414	0.23548	0.05545	4
1.8000+03	0.67700	0.24595	0.06049	4
1.9500+03	0.69791	0.25599	0.06553	4
2.1000+03	0.71710	0.26566	0.07057	4
2.2500+03	0.73479	0.27498	0.07561	4
2.4000+03	0.75114	0.28400	0.08066	4
2.5500+03	0.76628	0.29274	0.08570	4
2.7000+03	0.78034	0.30123	0.09074	4
2.8500+03	0.79343	0.30948	0.09578	3
3.0000+03	0.80563	0.31752	0.10082	3
3.1500+03	0.81701	0.32536	0.10586	3
3.3000+03	0.82766	0.33302	0.11090	3
3.4500+03	0.83762	0.34050	0.11594	3
3.6000+03	0.84696	0.34783	0.12098	3
3.7500+03	0.85572	0.35500	0.12602	3
3.9000+03	0.86394	0.36203	0.13106	3
4.0500+03	0.87166	0.36893	0.13611	3
4.2000+03	0.87892	0.37570	0.14115	3
4.3500+03	0.88575	0.38235	0.14619	3
4.5000+03	0.89218	0.38888	0.15123	3
4.6500+03	0.89823	0.39531	0.15627	3
4.8000+03	0.90393	0.40163	0.16131	3
4.9500+03	0.90930	0.40786	0.16635	3

$(Dt/A^2)$ =DIFFUSION COEFFICIENT D TIMES TIME (T) DIVIDED BY THE  
RADIUS (A) SQUARED.

$(Dt/A^2)^{0.5}$ =SQUARE ROOT OF  $(Dt/A^2)$

$M_t/M_\infty$ =COMPOSITION OF GAS AS A FUNCTION OF TIME

$Q=CS/K$  THE DIFFUSION COEFFICIENT TIMES THE RATIO OF THE SURFACE TO  
VOLUME RATIO (3/A) AND THE RATE CONSTANT OF SURFACE REACTION

VALUES OF F,  $Dt/A^2$ , AND Q ARE ASSUMED TO BE KNOWN

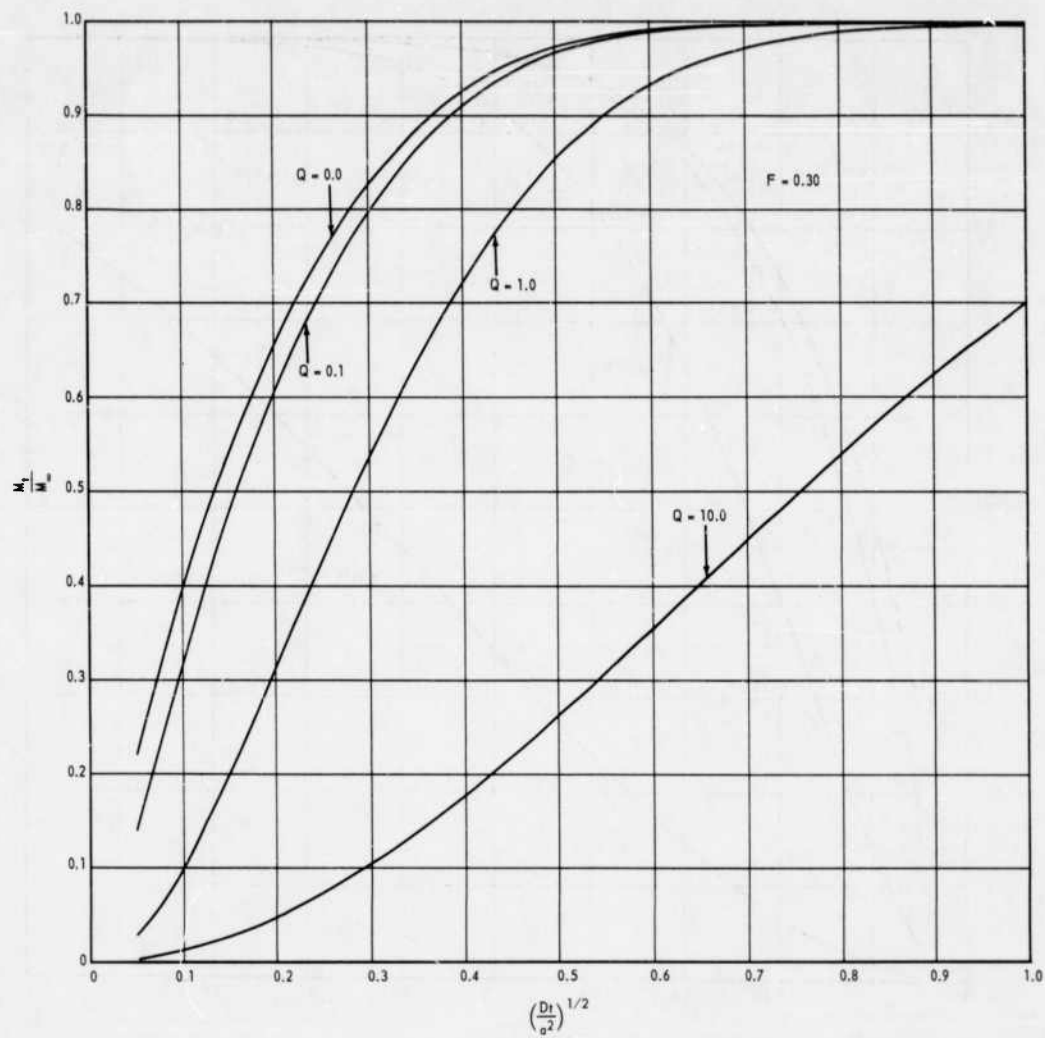


Fig. 26 - Behavior of Equation (I-117) for  $F = 0.30$  and various values of  $Q$

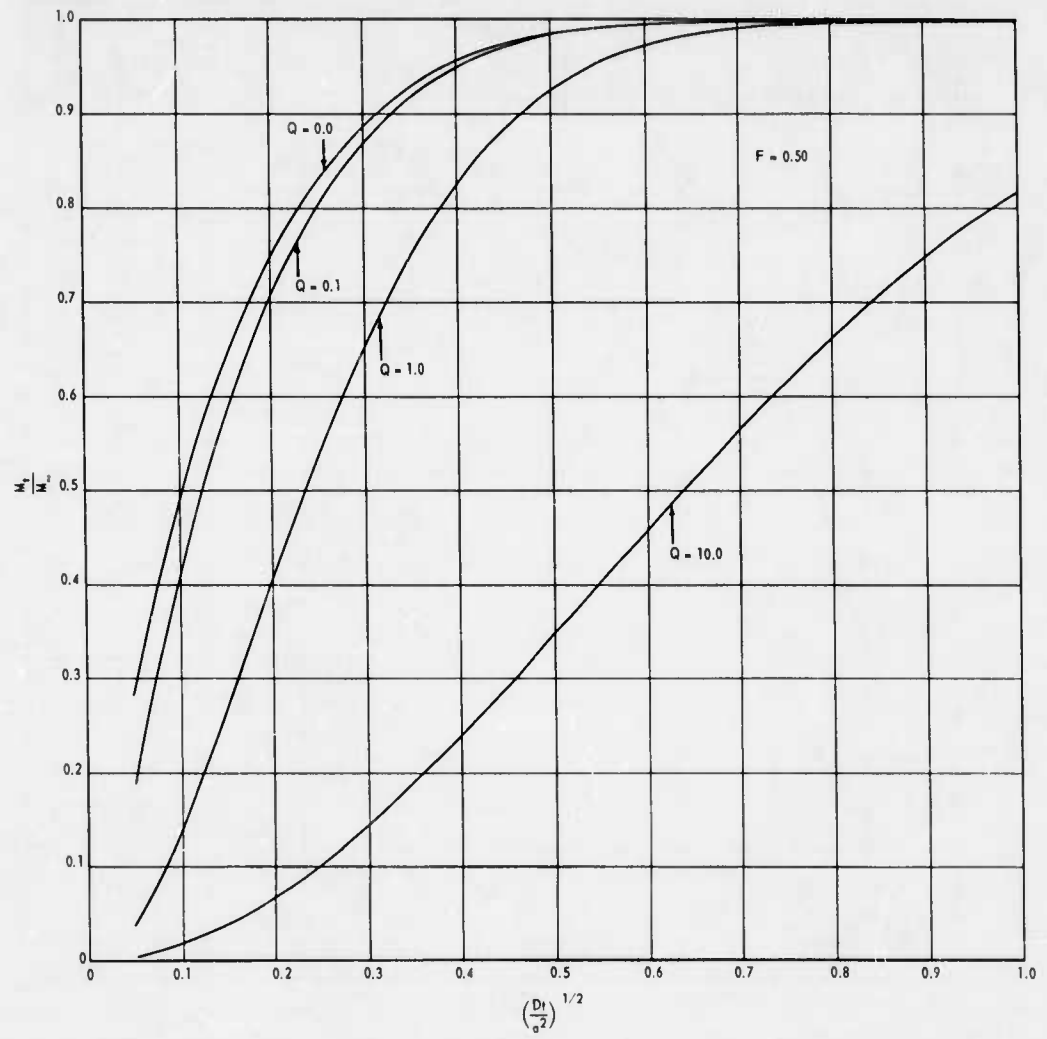


Fig. 27—Behavior of Equation (I-117) for  $F = 0.50$  and various values of  $Q$

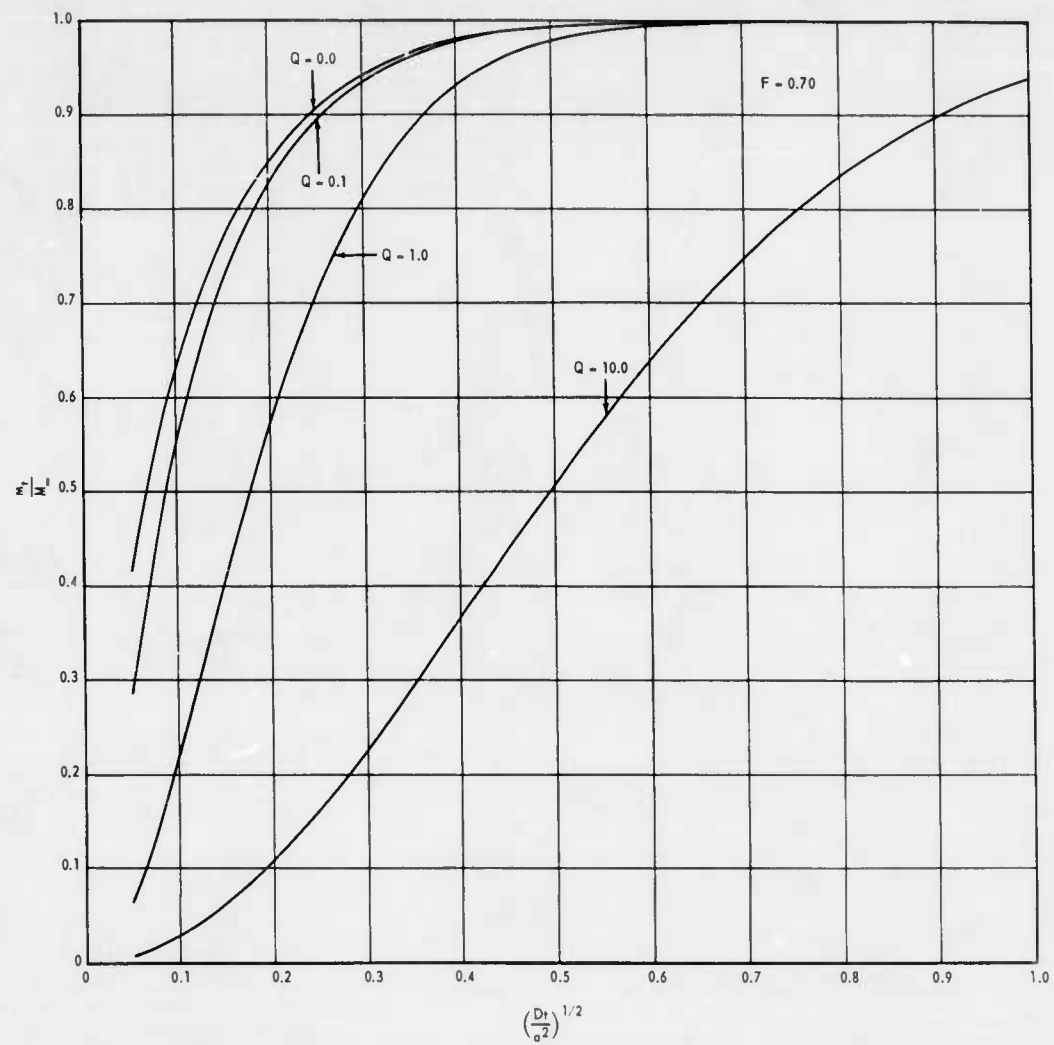


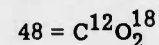
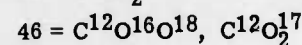
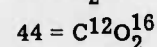
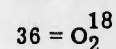
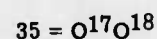
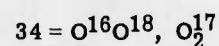
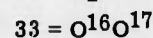
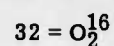
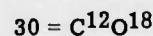
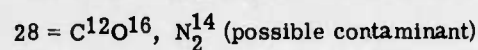
Fig. 28—Behavior of Equation (I-117) for  $F = 0.70$  and various values of  $Q$

## APPENDIX V

### REDUCTION OF MASS SPECTROMETER DATA

The output of the mass spectrometer is recorded on a standard strip chart. Typical curves for the three gases used,  $O_2$ ,  $CO$ , and  $CO_2$ , are shown in Figures 29, 30, and 31, respectively.

An oxygen gas sample gives rise to peaks at mass numbers 28, 30, 32, 33, 34, 35, 36, 44, 46, 47, 48. These peaks are caused by the following molecular species:

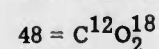
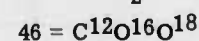
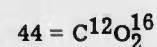
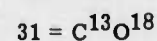
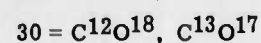
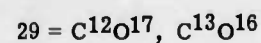
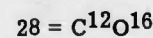


Possibly some  $CO$  and  $CO_2$  are synthesized from oxygen and hydrocarbon grease during exchange experiments, however, most of the  $CO$  and  $CO_2$  are made in the mass spectrometer; both  $CO$  and  $CO_2$  are observed in pure  $O_2$  samples. The amount of  $CO$  and  $CO_2$  made in the mass spectrometer varies somewhat from day to day and sample to sample; however, in all cases it is less than 2 percent of the total gas.

The oxygen isotopic distribution in the  $CO$  and  $CO_2$  was found to be the same as that of the oxygen gas and therefore the peaks at 28, 30, 44, 46, and 48 can be neglected in the calculation of the oxygen isotopic distribution; only the peaks at 32, 33, 34, 35, and 36 then need to be considered. The  $O^{17}$  concentration was less than 0.5 percent, therefore almost all the  $O^{17}$  was present as  $O^{16}O^{17}$  and/or  $O^{17}O^{18}$  and the contribution of  $O_2^{17}$  to the peak at 34 can be neglected.

The  $O^{18}$  isotope concentration was then calculated as  $O^{18}/(O^{16} + O^{18})$ , where  $O^{18}$  is equal to the sum of  $1/2 h_{34} + 1/2 h_{35} + h_{36}$ , and  $O^{16}$  is equal to the sum of  $h_{32} + 1/2 h_{33} + 1/2 h_{34}$ , where the  $h$ 's stand for peak heights.

When  $O^{18}$ -enriched  $CO$  was used as the source of the oxygen gas, the following peaks were observed:



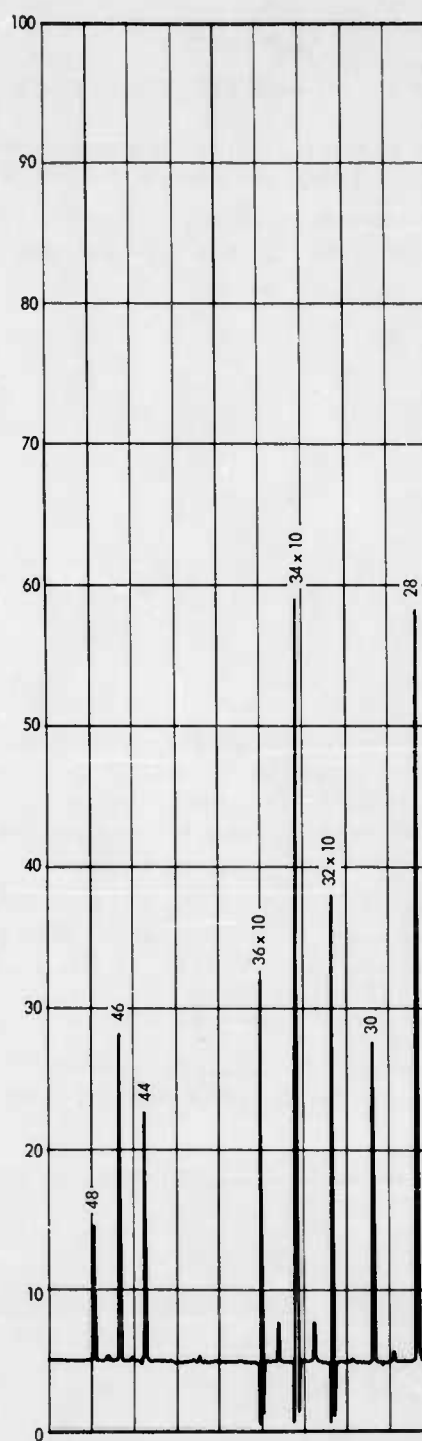


Fig. 29— Typical mass spectrometer trace for enriched O<sub>2</sub> gas

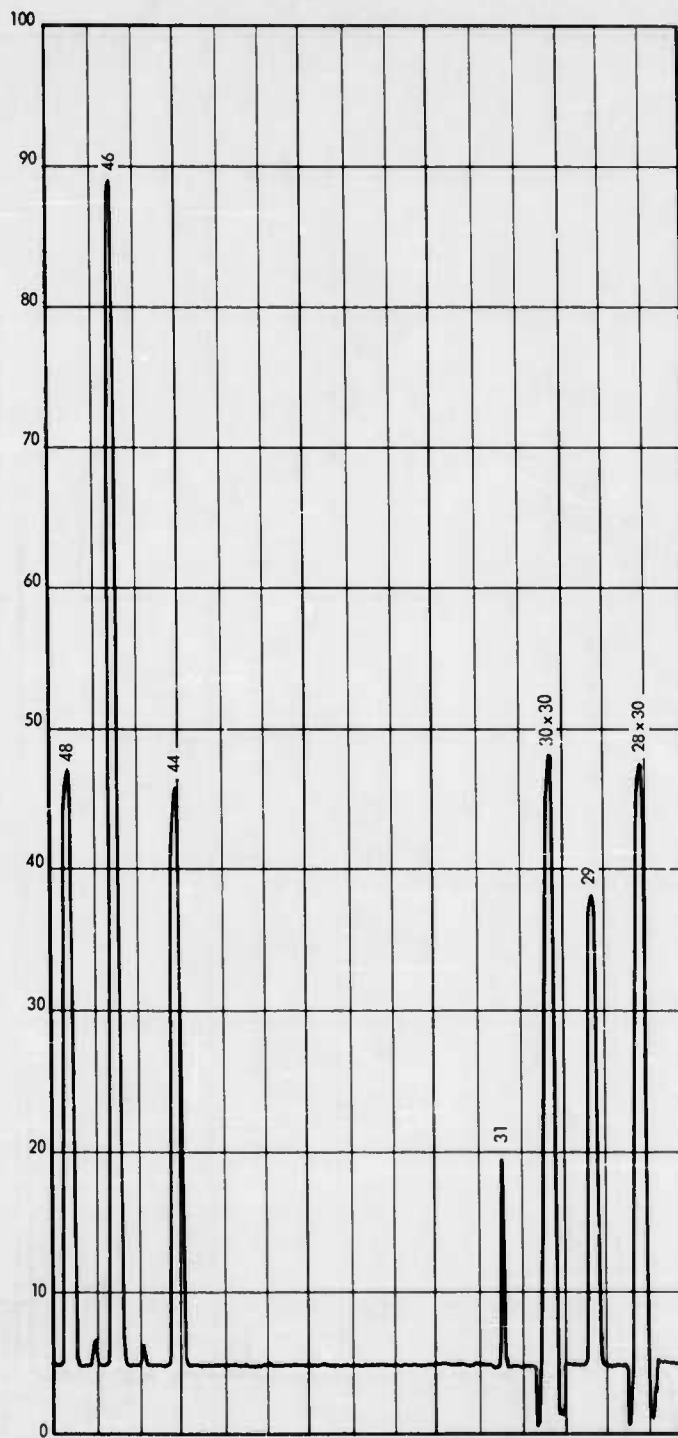


Fig. 30 - Typical mass spectrometer trace for enriched CO gas

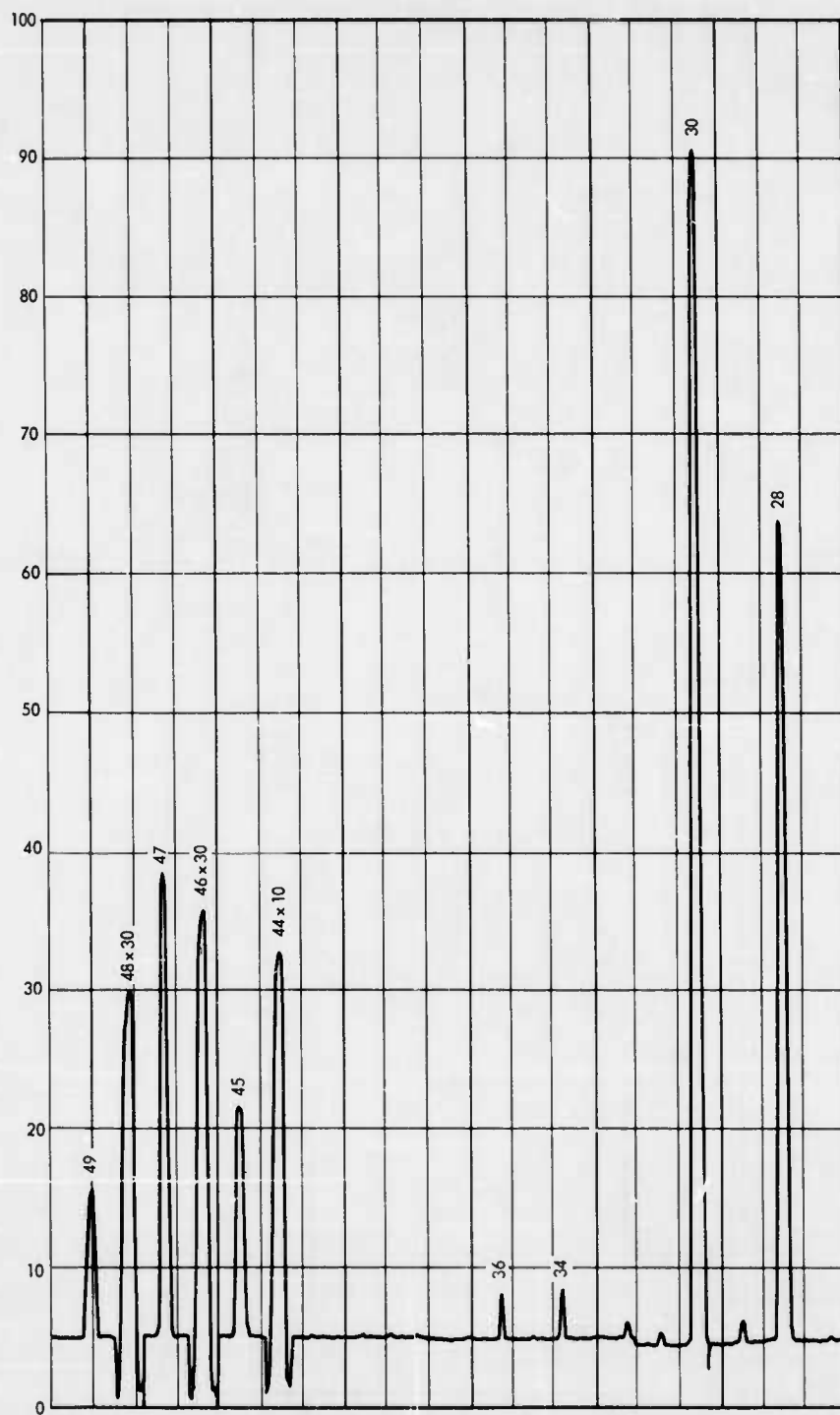


Fig. 31 - Typical mass spectrometer trace for enriched CO<sub>2</sub> gas



$C^{13}$  enrichment was 1.1 percent and  $O^{17}$  enrichment was 0.76 percent maximum in the gas samples used. Therefore the contribution of the  $C^{13}O^{17}$  species to the peak at 30 is very small and can be neglected. A correction for the  $O^{17}$  contribution to the peak at 29 can be made; since the  $C^{12}/C^{13}$  ratio is known, the  $C^{13}O^{16}$  contribution to the peak at 29 can be calculated from the  $C^{12}/C^{13}$  ratio and the height of the peak at 28. Correcting for the  $O^{17}$  concentration in the gas lowered the calculated diffusion coefficient by 1 to 5 percent, therefore it was deemed unnecessary to correct for the  $O^{17}$  gas present. The  $O^{18}$  concentration was then calculated from the mass spectra as  $O^{18}/(O^{16} + O^{18})$ , where  $O^{18}$  is equal to the sum of  $h_{30} + h_{31} + h_{46} + 2 h_{48}$ , and  $O^{16}$  is equal to the sum of  $h_{28} + h_{29} + 2 h_{44} + h_{46}$ .

The  $O^{18}$ -enriched  $CO_2$  gas gave rise to the following peaks of the mass spectrometer:

$$28 = C^{12}O^{16}$$

$$30 = C^{12}O^{18}$$

$$44 = C^{12}O_2^{16}$$

$$45 = C^{12}O^{16}O^{17}, C^{13}O_2^{16}$$

$$46 = C^{12}O^{16}O^{18}, C^{13}O^{16}O^{17}, C^{12}O_2^{17}$$

$$47 = C^{12}O^{17}O^{18}, C^{13}O^{16}O^{18}, C^{13}O_2^{17}$$

$$48 = C^{12}O_2^{18}, C^{13}O^{17}O^{18}$$

$$49 = C^{13}O_2^{18}$$

The  $O^{17}$  concentration in this gas sample could not be determined exactly from these peaks. However, almost all of the  $O^{17}$  will appear as  $C^{12}O^{16}O^{17}$  and  $C^{12}O^{17}O^{18}$ , and therefore a comparison of the ratio of 44/45 peaks and 46/47 peaks with the ratio of the 48/49 peaks gives us the  $O^{17}$  contribution to these peaks. From these data it was calculated that the  $O^{17}$  concentration was less than 1 percent. As was shown in the experiments with CO, neglecting the  $O^{17}$  results in only a small error in the calculated diffusion coefficient.

The  $O^{18}$  concentrations were then calculated from the mass spectra as  $O^{18}/(O^{16} + O^{18})$  where  $O^{18}$  is equal to the sum of  $1/2 h_{30} + 1/2 h_{46} + 1/2 h_{47} + h_{48} + h_{49}$ , and  $O^{16}$  is equal to  $1/2 h_{28} + h_{44} + 1/2 h_{45} + 1/2 h_{46}$ .

The mass spectra of the various samples can then be used to calculate the oxygen isotopic distributions. The disappearance of the desired oxygen isotope from the gas phase and therefore the diffusion into the solid phase can be observed from the change in concentration.

A sample set of gas enrichments calculated from the mass spectrometer peaks is shown in Table 27.

TABLE 27  
SAMPLE GAS-ENRICHMENT CALCULATION FOR EXPERIMENT NO. 38

Sample No.	Mass Number										$O^{16} = 2 \times 32 + 33 + 34$	$O^{18} = 34 + 35 + 36 \times 2$	$O^{16} + O^{18}$	% O <sup>18</sup>
	28	30	32	33	34	35	36	44	46	48				
B	57.7	11.9	605	4.1	444	1.0	81.9	-	-	-	1658	609	2267	26.86
	57.6	13.0	651	4.2	475	1.0	84.9	29.7	19.7	3.5	1781	646	2447	26.40
	56.7	11.6	591	4.0	433	0.9	78.1	-	-	-	1619	590	2209	26.71
	56.5	12.7	645	4.2	470	0.9	83.9	-	-	-	1764	639	2413	26.48
	60.4	12.5	630	4.0	462	0.9	83.4	-	-	-	1726	630	2356	26.74
														av: 26.64
A	71.7	20.2	331	2.6	509	2.4	269.5	-	-	-	1174	1051	2225	47.24
	70.1	19.8	324	2.5	488	2.3	246.4	-	-	-	1139	983	2122	-
	71.0	20.1	329	2.6	505	2.4	267.1	15.5	19.0	7.7	1166	1042	2208	47.19
	68.8	19.9	321	2.5	490	2.5	262.0	-	-	-	1135	1017	2152	47.26
	68.3	19.7	319	2.5	490	2.5	263.4	-	-	-	1131	1019	2150	47.39
C	54.1	22.6	379	2.9	594	2.9	319	-	-	-	1355	1235	2590	47.68
	53.3	22.6	375	2.8	586	2.7	316	17.6	23.3	9.6	1339	1221	2560	47.70
	51.3	21.5	365	2.8	571	2.7	308	-	-	-	1304	1190	2494	47.71
														A + C av: 47.48
D	58.1	16.4	535	2.7	542	1.3	135.0	26.7	25.0	6.2	1615	813	2428	33.48
	57.3	16.1	534	2.8	543	1.2	135.4	-	-	-	1614	815	2429	33.55
	57.5	16.1	530	2.7	528	1.2	133.9	-	-	-	1591	797	2388	33.38
	56.3	15.9	524	2.7	530	1.2	132.7	-	-	-	1581	797	2378	33.52
														av: 33.48
14	60.5	13.3	658	2.6	480	1.0	86.8	-	-	-	1799	655	2454	26.69
	59.9	13.0	650	2.5	474	1.0	85.6	32.0	24.0	4.6	1777	646	2423	26.66
	59.0	12.7	636	2.5	465	1.0	84.4	-	-	-	1740	635	2375	26.74
														av: 26.70

APPENDIX VI

DETERMINATION OF DIFFUSION COEFFICIENTS WITH CONSIDERATION  
OF A PHASE BOUNDARY REACTION

Reprint of an article by Haul, Dümbgen, and Just.

## Bestimmung von Diffusionskoeffizienten unter Berücksichtigung einer Phasengrenzreaktion

Von

R. HAUL, G. DÜMBGEN<sup>1</sup> und D. JUST<sup>1</sup>

Institut für Physikalische Chemie der Universität Bonn

Mit 1 Abbildung im Text

(Eingegangen am 4. Juli 1961)

### Zusammenfassung

Bei heterogenen Isotopen-Austauschversuchen zur Bestimmung von Diffusionskoeffizienten in Festkörpern kann eine Hemmung beim Durchtritt durch die Phasengrenzfläche auftreten. Für den Fall der Diffusion aus einer endlichen, jederzeit homogenen Phase in einen Festkörper wird eine Lösung angegeben und das Auswertungsverfahren beschrieben. In dieser Weise ist es möglich, sowohl Diffusionskoeffizienten als auch Geschwindigkeitskonstanten der Phasengrenzreaktion zu ermitteln.

### Einleitung

In den letzten Jahren ist wiederholt der gas/fest Isotopenaustausch zur Ermittlung von Selbstdiffusionskoeffizienten in Kristallen, insbesondere zur Untersuchung der Anionendiffusion verwendet worden<sup>2</sup>. Hierbei ist entweder das Gas oder der Festkörper mit einem zwischen beiden Phasen austauschbaren, geeigneten stabilen oder radioaktiven Isotop markiert. Bei endlicher Gasmenge können aus der zeitlichen Änderung der Isotopenkonzentration im Gas auf einfache Weise

<sup>1</sup> Teil der Dissertationen Universität Bonn 1961.

<sup>2</sup> C. WAGNER, siehe K. E. ZIMMERS, Ark. Kemi Mineralog. Geol. Ser. A 20 Nr. 18 (1945); 21 Nr. 16 (1946); 21 Nr. 17 (1946). Lit. siehe R. HAUL, D. JUST and G. DÜMBGEN, 4th Int. Symp. on Reactivity of Solids, Amsterdam 1960, in "Reactivity of Solids", J. H. DE BOER u. a., Elsevier Publ. Comp., Amsterdam 1961, S. 65.

Diffusionskoeffizienten bestimmt werden, ohne daß es notwendig ist, die Konzentrationsverteilung im Festkörper etwa mit Hilfe der „Schichten-Technik“ zu ermitteln. In analoger Weise war bereits früher der Stofftransport in porösen Festkörpern untersucht worden, wobei der Fortschritt der Sorption durch Messungen des Gasdruckes verfolgt wurde<sup>3</sup>. Ebenso kann die Diffusion aus Lösungen auf Grund von Konzentrationsmessungen in der Flüssigkeit untersucht werden. In allen diesen Fällen ist das Diffusionsproblem dadurch gekennzeichnet, daß eine zeitliche Änderung der Konzentration bzw. des Isotopenverhältnisses in der Festkörperoberfläche eintritt.

Unter der Voraussetzung, daß zu allen Zeiten an der Phasengrenze zwischen Festkörper und Gas bzw. Flüssigkeit das Gleichgewicht eingestellt ist, wurden von CARMAN und dem einen von uns<sup>4</sup> handliche Lösungen des Diffusionsproblems angegeben. Bei der Untersuchung der Sauerstoffdiffusion in Oxyden mit Hilfe des Isotopenaustausches von Sauerstoff-18 zeigte sich jedoch, daß diese Annahme nicht zutreffend ist<sup>5</sup>. Vielmehr ist der Diffusion im Festkörper eine mit endlicher Geschwindigkeit ablaufende Austauschreaktion an der Phasengrenze vorgelagert. Auf diese Komplikation bei heterogenen Isotopenaustauschversuchen hatte bereits BERTHIER<sup>6</sup> hingewiesen. Lösungen von Diffusionsgleichungen bei Vorhandensein eines „Oberflächenwiderstandes“ sind für eine Reihe von Randbedingungen in der Literatur angegeben<sup>7</sup>. Speziell den vorliegenden Fall der Diffusion aus einem begrenzten Volumen einer intensiv durchmischten fluiden Phase haben CARSLAW und JAEGER<sup>7</sup> in Form des analogen Wärmeleitungsproblems behandelt. Allerdings erwies sich die angegebene Lösung für die Auswertung von heterogenen Isotopenaustauschversuchen, wie später noch gezeigt wird, als praktisch nicht geeignet. Daher wird im folgenden ein einfacheres Verfahren beschrieben, das sich

<sup>3</sup> R. HAUL und F. R. L. SCHÖNING, *Naturwissenschaften* **40** (1953) 507; P. C. CARMAN, „Flow of Gases through Porous Media“, Butterworth Sci. Publ., London 1956.

<sup>4</sup> P. C. CARMAN und R. HAUL, *Proc. Roy. Soc. [London]* **222** (1954) 109.

<sup>5</sup> R. HAUL, D. JUST und G. DÜMBGEN, I. c.

<sup>6</sup> G. BERTHIER, *J. Chim. physique* **49** (1952) 527.

<sup>7</sup> H. S. CARSLAW und J. C. JAEGER, „Conduction of Heat in Solids“, 2. Aufl. Oxford 1948; R. M. BARRER, „Diffusion in and through solids“, University Press, Cambridge 1951; W. Jost, „Diffusion in Solids, Liquids, Gases“, Academic Press, New York 1951; „Diffusion“, Steinkopf Verlag, Darmstadt 1957; J. CRANK, „The Mathematics of Diffusion“, Clarendon Press, Oxford 1956.

zur gleichzeitigen Ermittlung von Festkörper-Diffusionskoeffizienten und Geschwindigkeitskonstanten der Phasengrenzreaktion bewährt hat.

### Liste der Symbole

$D$	= Diffusionskoeffizient [cm <sup>2</sup> /sec]
$k$	= Geschwindigkeitskonstante der Phasengrenzreaktion [sec <sup>-1</sup> ]
$d_0$	= Dicke der mit dem Gas direkt austauschenden Grenzschicht [cm]
$K$	= Konstante der Phasengrenzreaktion $K = k \cdot d_0$ [cm/sec]
$t$	= Zeit [sec]
$p$	= Isotopengehalt (Molenbruch des zur Markierung verwendeten Isotops) im Gas zur Zeit $t$
$p_0$	= Isotopengehalt im Gas zur Zeit $t = 0$
$p_1$	= Isotopengehalt im Festkörper zur Zeit $t$
$n_g$	= Mole der austauschfähigen Atomart im Gas
$n_s$	= Mole der austauschfähigen Atomart im Festkörper
$\lambda$	= $n_g/n_s$
$x$	= Ortskoordinate im plattenförmigen Festkörper
$l$	= $\frac{L}{2}$ = halbe Dicke des plattenförmigen Festkörpers [cm]
$a$	= Radius des kugelförmigen Festkörpers [cm]
$S$	= Spezifische Oberflächengröße (Diffusionsquerschnitt) [cm <sup>2</sup> /cm <sup>3</sup> ]

$$= \frac{1}{l} \text{ bzw. } \frac{3}{a}$$

$V_0$  = Volumen der Grenzschicht [cm<sup>3</sup>]

$V_s$  = Volumen des Festkörpers [cm<sup>3</sup>]

$s$  = Parameter des Laplace-Integrals  $\int_0^\infty e^{-st} p(t) dt = \bar{p}(s)$

### Diffusion in eine ebene Platte

Zur Lösung des Diffusionsproblems, das bei der Bestimmung von Selbstdiffusionskoeffizienten durch heterogenen Isotopenaustausch auftritt, ist es zweckmäßig, im 2. Fickschen Gesetz die Konzentration durch den Isotopengehalt zu ersetzen:

$$\frac{\partial p_s}{\partial t} = D \frac{\partial^2 p_s}{\partial x^2} \quad (1)$$

Weiterhin gelten nachstehende Anfangs- und Randbedingungen, wenn der Isotopenaustausch zwischen einer endlichen, jederzeit homo-

genen Gasmenge und den beiden Grundflächen eines plattenförmigen Festkörpers erfolgt:

$$1. \text{ Anfangsbedingung: } p = p_1 \text{ für } t = 0. \quad (2)$$

$$2. \text{ Anfangsbedingung: } p_s = p_1 \text{ für } t = 0 \text{ und } 0 \leq x \leq l. \quad (3)$$

$$1. \text{ Randbedingung: } \frac{\partial p_s}{\partial x} = 0 \text{ für } t \geq 0 \text{ und } x = 0. \quad (4)$$

Hierbei ist an der Oberfläche der Platte  $x = l$  und in deren Mitte  $x = 0$ .

Für den Isotopenaustausch an der Phasengrenze ergibt sich unter Vernachlässigung eines Isotopieeffektes entsprechend einer Reaktion erster Ordnung:

$$-n_g \frac{dp}{dt} = k n_0 (p - p_s). \quad (5)$$

Die Geschwindigkeitskonstante  $k$  dieser Reaktion gibt den Bruchteil der Mole  $n_0$  in der Oberflächenschicht an, die in der Zeiteinheit mit der Gasphase austauscht. Nimmt man für diese Grenzschicht die gleiche Dichte wie für das Innere des Festkörpers an, so gilt:

$$\frac{n_0}{V_s} = \frac{n_s}{V_s}. \quad (6)$$

und

$$n_0 = n_s \frac{d_0}{l}. \quad (7)$$

Führt man an Stelle der halben Dicke der Platte  $l$  die spezifische Oberflächengröße  $S = \frac{1}{l}$  ein, so ergibt sich aus (5) mit  $n_g/n_s = \lambda$

$$2. \text{ Randbedingung: } -\lambda \frac{dp}{dx} = k d_0 (p - p_s) \text{ für } t > 0 \text{ und } x = l. \quad (8)$$

Faßt man die Phasengrenzreaktion lediglich als einen „Oberflächenwiderstand“ auf, so ist die aus dem Gas verschwindende Isotopenmenge gleich derjenigen, die in das Innere des Festkörpers eindiffundiert:

$$k n_0 (p - p_s) = n_s S D \frac{\partial p_s}{\partial x}$$

bzw.

$$3. \text{ Randbedingung: } k d_0 (p - p_s) = D \frac{\partial p_s}{\partial x} \text{ für } t > 0 \text{ und } x = l. \quad (9)$$

Dieser Ansatz verlangt, daß für  $D = 0$  auch die linke Seite von (9) den Wert Null annimmt. Dies bedeutet, daß der ausschließliche mit der

Phasengrenzschicht erfolgende Austausch und die dadurch bedingte Änderung des Isotopengehaltes im Gas vernachlässigbar sein muß. Diese Bedingung ist bei hinreichend kleiner Oberfläche des Festkörpers erfüllt.

Unter Verwendung analoger Randbedingungen ist das Wärmeleitungsproblem von CARSLAW und JAEGER<sup>7</sup> behandelt worden. Formuliert man die dort angegebene Lösung für den Fall der Diffusion und setzt

$$K = k \cdot d_0, \quad (10)$$

so erhält man

$$\begin{aligned} \frac{p - p_1}{p_1 - p_1} &= \frac{\lambda}{1 + \lambda} \\ &+ \frac{2 K^2}{\lambda S^2 D^2} \sum_{n=1}^{\infty} \frac{\exp(-q_n^2 S^2 D t)}{q_n^4 + q_n^2 \left( \frac{K^2}{S^2 D^2} + \frac{2 K}{S D} \right) + \frac{K^2}{S^2 D^2} \left( 1 + \frac{1}{\lambda} \right)}, \end{aligned} \quad (11)$$

wobei  $q_n$  die positiven, von Null verschiedenen Wurzeln der Gleichung

$$\tan(q) = \frac{q}{\frac{S D}{K} q^2 - \frac{1}{\lambda}}$$

sind.

Mit Hilfe der Gl. (11) ist es bei Kenntnis von  $K$ ,  $D$ ,  $S$  und  $\lambda$  möglich, die zeitliche Änderung der Isotopenzusammensetzung der Gasphase zu berechnen. Liegt umgekehrt die zeitliche Änderung der Isotopenzusammensetzung der Gasphase vor und sollen daraus  $K$  und  $D$  ermittelt werden, so wäre es erforderlich, die Funktionswerte für alle in Frage kommenden Parameterkombinationen zu tabellieren. Mit Rücksicht auf die Vielzahl der Kombinationsmöglichkeiten ist dies jedoch praktisch nicht durchführbar. Wenn ferner der Exponent  $(q_n^2 S^2 D t)$  kleiner als eins ist, was bei Selbstdiffusion in Festkörpern im allgemeinen zutrifft, würde bei Anwendung von Gl. (11) zusätzlich noch die Schwierigkeit auftreten, daß die Summe schlecht konvergiert. Andererseits bietet gerade dieser Fall die Möglichkeit, eine einfachere Lösung mit Hilfe der Laplace-Transformation zu gewinnen, da im Unterbereich

$$\sin h \left( l \sqrt{\frac{s}{D}} \right) = \cos h \left( l \sqrt{\frac{s}{D}} \right) \quad (12)$$

gesetzt werden kann. Man erhält so an Stelle von Gl. (11)

$$\frac{p - p_1}{p_1 - p_1} = \frac{(1 + \beta)}{2 \beta} \operatorname{erfc} \left\{ (1 - \beta) \alpha \sqrt{t} \right\} - \frac{(1 - \beta)}{2 \beta} \operatorname{erfc} \left\{ (1 + \beta) \alpha \sqrt{t} \right\}, \quad (13)$$

wobei

$$\alpha = \frac{K}{2\sqrt{D}}$$

$$\beta = +\sqrt{1 - \frac{4DS'}{\lambda K}}$$

und unter Benutzung der Fehlerfunktion  $\operatorname{erf}(x)$  folgende Bezeichnungen verwendet wurden:

$$\begin{aligned}\operatorname{erfc}(x) &= \exp(x^2) \operatorname{erfc}(x) \\ \operatorname{erfc}(x) &= 1 - \operatorname{erf}(x).\end{aligned}$$

Für den Fall  $\beta = 0$  ergibt sich folgende Lösung: \*

$$\frac{p-p_1}{p_1-p_2} = \left(1 - \frac{Kt}{2D}\right) \operatorname{erfc}\left(\frac{K\sqrt{t}}{2\sqrt{D}}\right) + \frac{K\sqrt{t}}{\sqrt{\pi D}}. \quad (14)$$

#### Numerischer Vergleich der Lösungen für das Plattenmodell

Zur Beurteilung der Leistungsfähigkeit der in Gl. (13) und (14) gewonnenen Lösung wurde ein numerischer Vergleich mit der Summenformel (11) vorgenommen.

Unter Zugrundelegung von typischen Werten für  $D$ ,  $K$ ,  $S$  und  $\lambda$ , wie sie z.B. bei Isotopenaustauschversuchen zwischen gasförmigem Sauerstoff und Sauerstoff und Oxyden vorliegen, wurden die in Tab. 1 aufgeführten

Tabelle 1. Numerischer Vergleich für das Plattenmodell zwischen Gl. (11) und (13) bzw. (14)

$\sqrt{t}$	Gl. (11) Gl. (14)	$D = 10^{-13}$ $K = 10^{-6}$ $\lambda = 10^{-1}$ $l = 5 \cdot 10^{-4}$ $\beta = 0$	$D = 10^{-13}$ $K = 10^{-6}$ $\lambda = 10^{-1}$ $l = 5 \cdot 10^{-4}$ $\beta = 0,4472$ $\alpha = 0,01581$	$D = 10^{-14}$ $K = 10^{-8}$ $\lambda = 10^{-1}$ $l = 5 \cdot 10^{-4}$ $\beta = 0,9592$ $\alpha = 0,05$	$D = 10^{-14}$ $K = 10^{-8}$ $\lambda = 4 \cdot 10^{-1}$ $l = 5 \cdot 10^{-4}$ $\beta = 0,9592$ $\alpha = 0,025$	Gl. (11) Gl. (13)	Gl. (11) Gl. (13)
60	0,749	0,749	0,764	0,892	0,892	0,950	0,950
120	0,525	0,525	0,551	0,790	0,790	0,892	0,892
240	0,308	0,308	0,334	0,634	0,634	0,790	0,790
300	0,253	0,25	0,277	0,574	0,574	0,745	0,745
600	0,132*	0,13	0,146*	0,381	0,381	0,574*	0,574
	$^*w/w_\infty: 0,95$		0,94	0,88		0,80	

\* Anmerkung bei der Korrektur: Gl. (13) gilt auch für den Fall imaginärer  $\beta$ -Werte. Funktionswerte können bisher allerdings nur für  $\beta \leq i$  berechnet werden.

Werte für  $p - p_1/p_2 - p_1$  in Abhängigkeit von der Zeit berechnet. In der Tabelle ist ferner für den Endwert der Austauschgrad  $w/w_\infty$  angegeben, d. h. das Verhältnis der zur Zeit  $t$  und nach vollständigem Austausch aufgenommenen Isotopenmenge

$$w/w_\infty = (1 + \lambda) \left(1 - \frac{p-p_1}{p_1-p_2}\right). \quad (15)$$

Man erkennt eine ausgezeichnete Übereinstimmung zwischen Gl. (11) und den Gln. (13) und (14) bis zu hohen Austauschgraden. Auch für andere Werte von  $D$ ,  $K$ ,  $S$  und  $\lambda$  ist eine Übereinstimmung zu erwarten, sofern die Summe in Gl. (11) schlecht konvergiert.

#### Auswertungsverfahren

Zur Ermittlung von Diffusionskoeffizienten  $D$  und Konstanten  $K$  der Phasengrenzreaktion aus Gl. (13) ist es erforderlich, die Funktionswerte  $p - p_1/p_2 - p_1$  für eine Reihe von Versuchszeiten  $(\sqrt{t})$  in Abhängigkeit von geeignet gewählten  $\alpha$ - und  $\beta$ -Werten zu tabellieren. Mit Hilfe einer elektronischen Rechenmaschine wurden die Funktionswerte für folgende Zeiten berechnet:

$$\sqrt{t} = 30, 60, \dots, 600,$$

wobei  $\beta$  folgende Werte durchlief:

$$\beta = 0,050, 0,100, \dots, 0,500, 0,525, \dots, 0,650, 0,660, \dots, 0,990.$$

Zu jedem  $\beta$  wurden 40  $\alpha$ -Werte berechnet:

$$\alpha = 0,001, 0,002, \dots, 0,040.$$

Liegen derartig ausführliche Tabellen vor, so bereitet es keine Schwierigkeiten, durch Vergleich der experimentell gefundenen Werte von  $p - p_1/p_2 - p_1$  mit den Tabellenwerten diejenigen  $\alpha$  und  $\beta$  zu finden, die den Verlauf des Austauschvorganges beschreiben. Bei Kenntnis von  $S$  und  $\lambda$  können dann die Diffusionskoeffizienten und Konstanten der Phasengrenzreaktion bestimmt werden.

Bereitet die Aufstellung der Tabellen in dem oben angegebenen Umfang Schwierigkeiten, so ist es prinzipiell ausreichend, für jedes  $\beta$  den zeitlichen Funktionsverlauf in Abhängigkeit von nur einem, geeignet gewählten  $\alpha$  zu berechnen. Wie man aus Gl. (13) ersieht, ist nämlich bei gegebenem  $\beta$  der Funktionswert gleich, sofern  $\alpha \cdot \sqrt{t}$  konstant ist. Betrachtet man beispielsweise zwei Kurven, die dem gleichen



$\beta$ -Wert, aber verschiedenen  $\alpha$ -Werten ( $x_1$  und  $x_2$ ) zugeordnet sind, so zeigt sich, daß für jeden Funktionswert  $p - p_1/p_2 - p_1$  das Verhältnis der zugehörigen Zeiten ( $\sqrt{t_1}$  und  $\sqrt{t_2}$ ) konstant ist:

$$\sqrt{\frac{t_1}{t_2}} = \frac{\alpha_2}{\alpha_1} \quad (16)$$

Mit dieser Beziehung ist es möglich, für das jeweilige  $\beta$  aus dem für einen  $\alpha$ -Wert bekannten Funktionsverlauf denjenigen für andere  $\alpha$ -Werte zu berechnen. In Tab. 2 ist daher für eine verhältnismäßig dichte Folge von  $\beta$ -Werten jeweils nur ein  $\alpha$  berücksichtigt, das so gewählt ist, daß die Funktionswerte im Bereich von 0,5 bis 1 erfaßt wurden. Liegt der experimentell bestimmte Verlauf von  $p - p_1/p_2 - p_1$  in Abhängigkeit von  $\sqrt{t}$  vor, so geht man bei der Auswertung beispielsweise in folgender Weise vor. Man entnimmt Tab. 2 für einen  $\beta$ -Wert zwei Funktionswerte etwa in der Nähe von 0,9 und 0,7 mit den zugehörigen Zeiten. Aus der experimentellen Kurve liest man für die gleichen Funktionswerte die zugehörigen Zeiten ab. Dann bildet man in für beide Funktionswerte das Verhältnis  $\sqrt{t_{\text{exp}}/t_{\text{kor}}}$ . Erhält man in

Tabelle 2. Auszug aus den Tabellen der Funktionswerte

$\sqrt{t}$	$\beta: 0,10$	0,20	0,30	0,40	0,50	0,55	0,60	0,65	0,68	0,71
$\alpha: 0,003$	0,003	0,003	0,003	0,004	0,004	0,004	0,005	0,005	0,005	0,006
30	0,993	0,993	0,994	0,990	0,991	0,992	0,988	0,990	0,990	0,988
60	0,975	0,976	0,977	0,966	0,969	0,971	0,962	0,965	0,968	0,960
90	0,951	0,952	0,955	0,933	0,940	0,944	0,928	0,935	0,939	0,926
120	0,922	0,924	0,928	0,897	0,908	0,914	0,891	0,901	0,907	0,890
150	0,891	0,894	0,899	0,860	0,874	0,882	0,853	0,866	0,875	0,854
180	0,859	0,863	0,869	0,822	0,839	0,850	0,816	0,832	0,843	0,818
210	0,827	0,832	0,839	0,786	0,806	0,818	0,781	0,799	0,811	0,784
240	0,795	0,801	0,810	0,751	0,773	0,787	0,747	0,767	0,781	0,752
270	0,764	0,770	0,781	0,718	0,742	0,757	0,715	0,737	0,752	0,721
300	0,735	0,741	0,752	0,686	0,712	0,729	0,684	0,708	0,724	0,692
330	0,706	0,713	0,725	0,656	0,684	0,701	0,656	0,681	0,698	0,665
360	0,679	0,687	0,699	0,628	0,658	0,676	0,629	0,655	0,673	0,640
390	0,653	0,661	0,674	0,602	0,633	0,651	0,604	0,631	0,650	0,616
420	0,629	0,637	0,651	0,578	0,609	0,628	0,580	0,608	0,627	0,593
450	0,606	0,614	0,628	0,555	0,586	0,606	0,558	0,587	0,606	0,572
480	0,584	0,592	0,607	0,533	0,565	0,585	0,538	0,566	0,586	0,552
510	0,563	0,572	0,587	0,513	0,545	0,566	0,518	0,547	0,567	0,533
540	0,544	0,552	0,567	0,494	0,527	0,547	0,500	0,529	0,549	0,515
570	0,525	0,534	0,549	0,476	0,509	0,530	0,483	0,512	0,532	0,498
600	0,508	0,516	0,532	0,460	0,492	0,513	0,466	0,496	0,516	0,482

Tabelle 2 (Fortsetzung)

$\sqrt{t}$	$\beta: 0,74$	0,77	0,80	0,83	0,86	0,89	0,92	0,95	0,97	0,99
$\alpha: 0,006$	0,006	0,007	0,007	0,009	0,010	0,013	0,017	0,027	0,040	0,040
30	0,989	0,987	0,988	0,984	0,984	0,981	0,978	0,973	0,972	0,991
60	0,963	0,958	0,963	0,953	0,954	0,946	0,943	0,934	0,936	0,978
90	0,932	0,924	0,932	0,917	0,919	0,909	0,906	0,896	0,901	0,965
120	0,899	0,888	0,900	0,880	0,885	0,873	0,870	0,860	0,869	0,953
150	0,865	0,852	0,868	0,845	0,851	0,838	0,836	0,826	0,837	0,940
180	0,832	0,818	0,836	0,810	0,818	0,805	0,804	0,794	0,808	0,928
210	0,800	0,785	0,806	0,778	0,788	0,773	0,773	0,764	0,780	0,916
240	0,770	0,753	0,777	0,747	0,758	0,744	0,745	0,736	0,754	0,905
270	0,741	0,724	0,750	0,718	0,731	0,716	0,718	0,710	0,729	0,893
300	0,713	0,696	0,724	0,691	0,705	0,690	0,693	0,685	0,706	0,882
330	0,687	0,670	0,699	0,666	0,680	0,665	0,669	0,661	0,683	0,871
360	0,663	0,645	0,675	0,641	0,657	0,642	0,646	0,639	0,662	0,860
390	0,640	0,621	0,653	0,619	0,635	0,620	0,625	0,618	0,642	0,850
420	0,618	0,600	0,632	0,597	0,614	0,599	0,604	0,598	0,623	0,840
450	0,597	0,579	0,612	0,577	0,594	0,580	0,585	0,579	0,605	0,830
480	0,577	0,559	0,593	0,558	0,576	0,561	0,567	0,561	0,587	0,820
510	0,559	0,541	0,575	0,540	0,558	0,544	0,550	0,544	0,571	0,810
540	0,541	0,523	0,558	0,523	0,541	0,527	0,534	0,528	0,555	0,800
570	0,524	0,507	0,541	0,507	0,525	0,511	0,518	0,513	0,540	0,791
600	0,508	0,491	0,526	0,491	0,510	0,496	0,503	0,498	0,526	0,782

beiden Fällen den gleichen Wert, dann ist bereits der gesuchte  $\beta$ -Wert ermittelt, sofern sich das gleiche Verhältnis auch für andere Funktionswerte ergibt. Stimmen die Verhältnisse nicht überein, so muß das gleiche Verfahren mit anderen  $\beta$ -Werten wiederholt werden. Mit einiger Übung läßt sich der richtige  $\beta$ -Wert in dieser Weise rasch ermitteln.  $\alpha$  folgt dann für das betreffende Experiment aus:

$$\alpha_{\text{exp}} = \alpha_{\text{kor}} \sqrt{\frac{t_{\text{kor}}}{t_{\text{exp}}}} \quad (17)$$

### Einfluß der Geschwindigkeit der Phasengrenzreaktion auf den Austauschvorgang

Es ist nicht beabsichtigt, im Rahmen dieser Arbeit experimentelle Ergebnisse zu diskutieren, es soll lediglich an Hand von Abb. 1 der Einfluß der Phasengrenzreaktion auf den zeitlichen Verlauf des Isotopenaustausches und damit auf die Bestimmung von Diffusionskoeffizienten veranschaulicht werden. Hierbei sind typische Werte für  $D$ ,  $S$  und  $\lambda$ , wie sie bei den Sauerstoff-Austauschversuchen auf-



treten, angenommen worden. Die Kurve  $D$  gibt den Verlauf für den Fall wieder, daß sich das Isotopengleichgewicht an der Oberfläche beliebig schnell einstellt. Zur Berechnung diente folgende Gleichung\*:

$$\frac{p - p_1}{p_2 - p_1} = \operatorname{erfc} \left( \frac{S\sqrt{Dt}}{\lambda} \right). \quad (18)$$

Läuft dagegen die Phasengrenzreaktion mit endlicher Geschwindigkeit ab, so tritt eine Verzögerung des Isotopenaustausches ein, die um

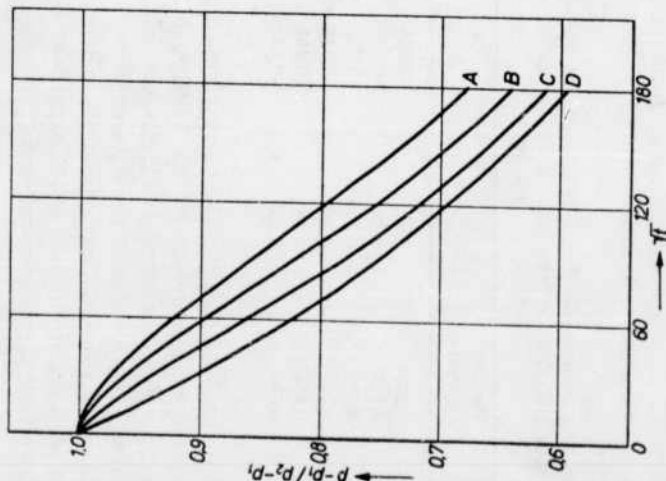


Abb. 1. Einfluß der Geschwindigkeit der Phasengrenzreaktion auf den Austauschvorgang.  $D = 10^{-14} \text{ cm}^2/\text{sec}$ ;  $S = 3 \cdot 10^3 \text{ cm}^2/\text{cm}^2$ ;  $\lambda = 10^{-1}$ ; Kurve A:  $K = 1,21 \cdot 10^{-3} \text{ cm}^2/\text{sec}$ ;  $\beta = 0,100$ . Kurve B:  $K = 2,00 \cdot 10^{-4}$ ;  $\beta = 0,625$ . Kurve C:  $K = 5,00 \cdot 10^{-5}$ ;  $\beta = 0,870$ . Kurve D:  $K = \infty$ ;  $\beta = 1,000$

so größer ist, je kleiner  $K$  wird (Kurven A, B und C). Als Maß für diesen Einfluß kann die Größe  $\beta$  angesehen werden, die für  $K = \infty$  den Wert

\* Vgl. CARMAN und HAUL<sup>4</sup> Gl. (17a) der dortigen Arbeit, wobei zu berücksichtigen ist, daß  $S = \frac{z}{l}$  ist.

eins annimmt. Die Bestimmung von  $K$  wird um so genauer, je kleiner  $\beta$  ist.

Zur Auswertung von Diffusionsmessungen unter Verwendung von Gl. (18) wäre es prinzipiell ausreichend, einen einzigen Meßpunkt zu bestimmen. Der Einfluß einer mit endlicher Geschwindigkeit ablaufenden Phasengrenzreaktion läßt sich jedoch nur erkennen, wenn die Änderung der Isotopenzusammensetzung des Gases zu verschiedenen Zeiten gemessen und eine Auswertung nach Gl. (13) vorgenommen wird. Diese ermöglicht nicht nur erst die Bestimmung der wahren Diffusionskoeffizienten, sondern gleichzeitig auch die Ermittlung von Geschwindigkeitskonstanten der Phasengrenzreaktion.

### Diffusion in eine Kugel

Mit den analogen Randbedingungen und Vereinfachungen, die im linearen Fall zu Gl. (13) führen, ergibt sich für das kugelsymmetrische Problem folgende Lösung\*:

$$\begin{aligned} \frac{p - p_1}{p_2 - p_1} = & \left[ \frac{z_1^2 - z_1 \left( \frac{S\sqrt{D}}{3} - \frac{K}{\sqrt{D}} \right)}{(z_1 - z_2)(z_1 - z_3)} \right] \operatorname{erfc}(-z_1/\sqrt{t}) \\ & + \left[ \frac{z_2^2 - z_2 \left( \frac{S\sqrt{D}}{3} - \frac{K}{\sqrt{D}} \right)}{(z_1 - z_2)(z_3 - z_1)} \right] \operatorname{erfc}(-z_2/\sqrt{t}) \\ & + \left[ \frac{z_3^2 - z_3 \left( \frac{S\sqrt{D}}{3} - \frac{K}{\sqrt{D}} \right)}{(z_3 - z_1)(z_3 - z_2)} \right] \operatorname{erfc}(-z_3/\sqrt{t}) \end{aligned} \quad (19)$$

wobei  $z_1$ ,  $z_2$  und  $z_3$  die Wurzeln der kubischen Gleichung

$$z^3 + z^2 \left( \frac{K}{\sqrt{D}} - \frac{S\sqrt{D}}{3} \right) + z \left( \frac{KS}{\lambda} \right) - \frac{KS^2\sqrt{D}}{3\lambda} = 0 \quad (20)$$

sind. Bei Kenntnis von  $D$ ,  $K$ ,  $S$  und  $\lambda$  ist es mit Gl. (19) möglich, den zeitlichen Verlauf von  $p - p_1/p_2 - p_1$  zu berechnen. Eine Tabellierung der Funktion, die zur Auswertung von Diffusionsmessungen erforderlich wäre, ist jedoch praktisch nicht durchführbar, da neben  $\sqrt{t}$  mehr als zwei Parameter auftreten und die Zahl möglicher Kombinationen zu groß ist. Außerdem treten besondere Schwierigkeiten auf, wenn die Wurzeln der kubischen Gleichung komplex sind.

\* Diese Gleichung tritt an die Stelle von Gl. (19) der Arbeit von CARMAN und HAUL<sup>4</sup>, die für den Fall unendlicher schneller Phasengrenzreaktion gilt, wobei  $S = \frac{z}{l}$  ist.

Für ein Beispiel wurde der Funktionsverlauf mit folgenden Werten berechnet:  $D = 10^{-14} \text{ cm}^2/\text{sec}$ ,  $K = 10^{-8} \text{ cm/sec}$ ,  $S = 3 \cdot 10^3 \text{ cm}^{-1}$  und  $\lambda = 0,1$ . In Tab. 3 sind in Abhängigkeit von der Zeit die erhaltenen  $p - p_1/p_2 - p_1$ -Werte aufgeführt und denjenigen gegenübergestellt, die sich aus Gl. (13) für ein Plattenmodell ergeben. Man erkennt hieraus, daß der Austausch nach gleicher Versuchsdauer bei kugelförmigen weniger weit fortgeschritten ist als bei plattenförmigen Teilchen. Dies ist dadurch bedingt, daß mit zunehmender Eindringtiefe bei einer Kugel der Diffusionsquerschnitt mit dem Quadrat des Radius abnimmt, dagegen bei einer Platte konstant bleibt.

Tabelle 3. Numerischer Vergleich zwischen Platten- und Kugelmodell  
Gl. (13) und (19)  $D = 10^{-14} \text{ cm}^2/\text{sec}$ ;  $K = 10^{-8} \text{ cm/sec}$ ;  $S = 3 \cdot 10^3 \text{ cm}^2/\text{cm}^3$ ;  
 $\lambda = 10^{-1}$

$\sqrt{t}$	Platte Gl. (13)	$w/w_\infty$	Kugel Gl. (19)	$w/w_\infty$
30	0,926	0,081	0,926	0,081
60	0,845	0,171	0,846	0,169
90	0,773	0,250	0,775	0,248
120	0,709	0,320	0,712	0,317
150	0,654	0,381	0,658	0,376
180	0,606	0,433	0,611	0,428

Sofern der Austauschgrad nicht zu groß ist, d.h. die Eindringtiefe im Vergleich zum Durchmesser der Teilchen hinreichend klein ist, stimmen die Funktionswerte für Kugel und Platte nahezu überein, wie man aus Tab. 3 erkennt. Diese Übereinstimmung ist für einen vorgegebenen Austauschgrad um so besser, je kleiner  $\lambda$  ist. Für praktische Zwecke ist es daher in vielen Fällen ohne Bedeutung, welches Modell der Auswertung zugrunde gelegt wird.

Die Berechnung und Tabellierung der Funktion (13) wurde mit Hilfe einer elektronischen Rechenanlage (ER 56, Universität Bonn) durchgeführt. Den Herren Dr. P. F. MÜLLER und Dr. F. KRÜCKEBERG vom Institut für Instrumentelle Mathematik an der Universität Bonn möchten wir für ihre bereitwillige Unterstützung und wertvolle Diskussionen unseren besonderen Dank aussprechen.

Der Deutschen Forschungsgemeinschaft und dem Fonds der Chemischen Industrie danken wir für die Bereitstellung von Mitteln.

## REFERENCES

1. Kingery, W. D. (Editor), Kinetics of High Temperature Processes, Technology Press, Cambridge, Massachusetts, 1959, pp. 37-61.
2. Garner, W. E. (Editor), Chemistry of the Solid State, Butterworths Scientific Publications, London, 1955, pp. 20-57.
3. Kubaschewski, O., and Hopkins, B. E., Oxidation of Metals and Alloys, Butterworths Scientific Publications, London, 1953, pp. 26-36.
4. Crank, J., The Mathematics of Diffusion, Clarendon Press, Oxford, 1956, pp. 84-98.
5. Wilson, A. H., "A Diffusion Problem in which the Amount of Diffusing Substance is Finite," Philosophical Magazine, Volume 39, 1948, p. 48.
6. Carman, P. C., and Haul, R.A.W., "Measurement of Diffusion Coefficients," Proceedings of the Royal Society of London, Volume 222A, 1954, p. 109.
7. Haul, R., Dumbgen, G., and Just, D., "Bestimmung von Diffusionskoeffizienten unter Berücksichtigung einer Phasengrenzreaktion," Zeitschrift für Physikalische Chemie (Neue Folge), Volume 31, 1962, pp. 309-320.
8. Kingery, W. D., et al., "Oxygen Ion Mobility in Cubic  $Zr_{0.85}Ca_{0.15}O_{1.85}$ ," Journal of American Ceramic Society, Volume 42, 1954, p. 393.
9. Auskern, A. B., and Belle, J., "Self-Diffusion of Oxygen in Uranium Dioxide," Journal of Chemical Physics, Volume 28, 1958, p. 171.
10. Reed, T. B., "Induction-Coupled Plasma Torch," Journal of Applied Physics, Volume 32, 1961, p. 821.
11. Reed, T. B., "Growth of Refractory Crystals Using the Induction Plasma Torch," Journal of Applied Physics, Volume 32, 1961, p. 2534.
12. Reed, T. B., "Plasma Torches," International Science and Technology, June 1962, pp. 42-48.
13. Campbell, I. E. (Editor), High-Temperature Technology, John Wiley and Sons, Inc., New York, 1956.
14. Schwarzkopf, P., and Kieffer, R., Refractory Hard Metals - Borides, Carbides, Nitrides, and Silicides, The Macmillan Company, New York, 1953, pp. 271-315.
15. Samsonov, G. V., and Umanskiy, Ya. S., "Hard Compounds of Refractory Metals," NASA Translation, NASATT-F-102, June 1962.
16. Krikorian, O. H., "Thermal Expansion of High Temperature Materials," AEC, UCRL-6132, September 1960.
17. Lambertson, W. A., Mueiler, M. H., and Gunzel, F. H., Jr., "Uranium Oxide Phase Equilibrium Systems," Journal of American Ceramic Society, Volume 36, 1953, pp. 397-399.
18. Geller, R. F., and Yavorsky, P., "Effects of Some Oxide Additions on the Thermal Length Changes of Zirconia," Journal of Research of the National Bureau of Standards, Volume 35, 1945, pp. 87-110.
19. Glaser, F. W., "Contribution to the Metal-Carbon-Boron Systems," Journal of Metals, Volume 4, 1952, pp. 391-396.
20. United States Borax Research Corporation, Technical Data Sheet 3-B, November 1961.

21. "Materials Symposium," Aeronautical Systems Division, U.S. Air Force, ASD 61-322, July 1961, p. 681.
22. The Carborundum Company, New Products Branch, Technical Data Sheet.
23. Moers, K., Zeitschrift für Anorganische und Allgemeine Chemie, Volume 198, 1931, pp. 262-275.
24. Polty, A. E., Margolin, H., and Nielsen, J. P., "Titanium - Nitrogen and Titanium-Boron Systems," Transactions of American Society of Metals, Volume 46, 1954, p. 312.
25. American Potash and Chemical Corporation, Bulletin No. DB-28.
26. Schwarzkopf, P., and Glaser, F., Zeitschrift Metallkunde, Volume 44, 1953, pp. 353-358.
27. National Carbon Company, Bulletin No. 106EB.
28. The Norton Company, Technical Bulletin 515, November 1951.
29. Glaser, F., and Post, B., "System Zirconium-Boron," Journal of Metals, Volume 5, 1953, pp. 1117-1118.
30. Glaser, F., Moskowitz, D., and Post, B., "A Study of Some Binary Hafnium Compounds," Journal of Metals, Volume 5, 1953, pp. 1119-1120.
31. Honak, E. R., Thesis, Technische Hochschule, Graz, 1951.
32. Ham, J. L., "An Introduction to Arc-Cast Molybdenum and its Alloys," American Society of Mechanical Engineers, Transactions, Volume 73, 1951, pp. 723-732.
33. Steinitz, R., Binder, I., and Moskowitz, D., "System Molybdenum-Boron and Some Properties of the Molybdenum-Borides," Journal of Metals, Volume 4, 1952, pp. 983-987.
34. Steinitz, R., "The System Molybdenum-Boron," Journal of Metals, Volume 4, 1952, p. 148.
35. Gilles, P., and Pollock, B., "The Molybdenum-Boron System," Journal of Metals, Volume 5, 1953, pp. 1537-1538.
36. Brewer, L., Sawyer, D. L., Templeton, D. H., and Dauben, C. H., "A Study of the Refractory Borides," Journal of the American Ceramic Society, Volume 34, 1951, pp. 173-179.
37. American Potash and Chemical Corporation, Bulletin No. TD-5.
38. Lafferty, J. M., "Boride Cathodes," The Physical Review, Volume 79, 1950, p. 1012.
39. Feisel, D. H., "Some Metallurgical Observations of the Transition Metal Borides," Program of the 1962 Fall Meeting of Metallurgical Society of AIME, p. 20.
40. Popper, P. (Editor), Special Ceramics, Academic Press, Inc., New York, 1960, Chapter 18, Jackson, J. S., and Palmer, P. F., "Hot Pressing Refractory Hard Materials," p. 318.
41. Wood, A. A. R., Borax Consolidated Limited, Surrey, England, (Private Communication).
42. Chown, J., and Deacon, R. F., "Boride and Carbide Coatings on Graphite," Part II of report by Chown, Deacon, Singer, and White, "Refractory Coatings on Graphite with Some Comments on the Ultimate Oxidation Resistance of Coated Graphite," Morganite Research and Development, Limited, The British Ceramic Research Association - Symposium on Special Ceramics, July 1962.
43. Churchill, R. V., Modern Operational Mathematics in Engineering, McGraw-Hill, New York, 1944.
44. McLachlan, N. W., Complex Variable Theory and Transform Calculus, Second Edition, Cambridge University Press, Cambridge, 1955.
45. Carslaw, H. S., and Jaeger, J. C., Operational Methods in Applied Mathematics, Second Edition, Oxford University Press, Oxford, 1948. (Also available from Dover Publications, Inc., 1963).
46. Carslaw, H. S., and Jaeger, J. C., Conduction of Heat in Solids, Second Edition, Oxford University Press, Oxford, 1959.
47. Wagner, C., "Zur Kinetik Heterogenen Austauschreaktionen," Arkiv für Kemi Mineralogi och Geologi, Volume 20A, 1945, p. 14.

Aeronautical Systems Division, AF Materials Laboratory, Metals & Ceramics Division, Wright-Patterson AFB, Ohio.  
Rpt. No. ASD-TDR-63-635. THORIUM OXIDE-DIFFUSION OF OXYGEN, COMPATIBILITY WITH BORIDES, AND FEASIBILITY OF COATING BORIDES BY PYROLYSIS OF METAL HALIDES. Final report, July 63, 142 pp. incl. illus., tables, 47 refs.

Measurements of self-diffusion of oxygen in ThO<sub>2</sub> were complicated by slow exchange at the surface. The measured values of the diffusion coefficient, D, range from 1.8 x 10<sup>-13</sup> cm<sup>2</sup>/sec at 800°C to 3.5 x 10<sup>-3</sup> cm<sup>2</sup>/sec at 1500°C. The rate constant of the surface reaction, K, ranged from 6.8 x 10<sup>-10</sup> cm/sec at 800°C to 1.3 x 10<sup>-4</sup> cm/sec at 1500°C. The results may be expressed by equations in the form of  
D = 4.4 exp (-65,800/RT) cm<sup>2</sup>/sec and  
K = 7.6 x 10<sup>3</sup> exp (-63,800/RT) cm/sec.

( over )

Attempts to deposit dense impervious layers of ThO<sub>2</sub> on selected solid borides by pyrolysis of ThCl<sub>4</sub> were essentially unsuccessful. The main problem was attack of the borides by O<sub>2</sub> in the coating gas. The pyrolysis technique might prove to be an economical way to build up a coating of ThO<sub>2</sub> that had been started by another method.

The commercially available boride samples which were tested reacted with ThO<sub>2</sub> at temperatures in the range 2400° to 2600°C. The boride samples also reacted with graphite in the temperature range of 2400° to 2700°C. Because of these reactions, a graphite-boride-thoria system will be useful for only limited times at temperatures above 2400°C. While pure borides were not investigated, it is expected that their behavior would be similar to that of the commercial samples examined in this work.

1. Thoria
2. Coating studies
3. Diffusion studies
4. High-temperature compatibility
- I. AFSC Project 7350, Task 735001
- II. Contract No. AF 33 (657)-8470
- III. General Electric Co., Nuclear Materials and Propulsion Operation, Evendale, Ohio
- IV. H. S. Edwards, A. F. Rosenberg, and J. T. Bittel
- V. Avail fr OTS
- VI. In ASTIA collection

Aeronautical Systems Division, AF Materials Laboratory, Metals & Ceramics Division, Wright-Patterson AFB, Ohio.  
Rpt. No. ASD-TDR-63-635. THORIUM OXIDE-DIFFUSION OF OXYGEN, COMPATIBILITY WITH BORIDES, AND FEASIBILITY OF COATING BORIDES BY PYROLYSIS OF METAL HALIDES. Final report, July 63, 142 pp. incl. illus., tables, 47 refs.

Measurements of self-diffusion of oxygen in ThO<sub>2</sub> were complicated by slow exchange at the surface. The measured values of the diffusion coefficient, D, range from 1.8 x 10<sup>-13</sup> cm<sup>2</sup>/sec at 800°C to 3.5 x 10<sup>-3</sup> cm<sup>2</sup>/sec at 1500°C. The rate constant of the surface reaction, K, ranged from 6.8 x 10<sup>-10</sup> cm/sec at 800°C to 1.3 x 10<sup>-4</sup> cm/sec at 1500°C. The results may be expressed by equations in the form of  
D = 4.4 exp (-65,800/RT) cm<sup>2</sup>/sec and  
K = 7.6 x 10<sup>3</sup> exp (-63,800/RT) cm/sec.

( over )

Attempts to deposit dense impervious layers of ThO<sub>2</sub> on selected solid borides by pyrolysis of ThCl<sub>4</sub> were essentially unsuccessful. The main problem was attack of the borides by O<sub>2</sub> in the coating gas. The pyrolysis technique might prove to be an economical way to build up a coating of ThO<sub>2</sub> that had been started by another method.

The commercially available boride samples which were tested reacted with ThO<sub>2</sub> at temperatures in the range 2400° to 2600°C. The boride samples also reacted with graphite in the temperature range of 2400° to 2700°C. Because of these reactions, a graphite-boride-thoria system will be useful for only limited times at temperatures above 2400°C. While pure borides were not investigated, it is expected that their behavior would be similar to that of the commercial samples examined in this work.

1. Thoria
2. Coating studies
3. Diffusion studies
4. High-temperature compatibility
- I. AFSC Project 7350, Task 735001
- II. Contract No. AF 33 (657)-8470
- III. General Electric Co., Nuclear Materials and Propulsion Operation, Evendale, Ohio
- IV. H. S. Edwards, A. F. Rosenberg, and J. T. Bittel
- V. Avail fr OTS
- VI. In ASTIA collection

<p>1. Thoria</p> <p>2. Coating studies</p> <p>3. Diffusion studies</p> <p>4. High-temperature compatibility</p> <p>I. AFSC Project 7350, Task 735001</p> <p>II. Contract No. AF 33 (657)-8470</p> <p>III. General Electric Co., Nuclear Materials and Propulsion Operation, Evendale, Ohio</p> <p>IV. H. S. Edwards, A. F. Rosenbergs, and J. T. Bittel</p> <p>V. AVAL fr OTS</p> <p>VI. In ASTIA collection</p>	<p>Aeronautical Systems Division, AF Materials Laboratory, Metals &amp; Ceramics Division, Wright-Patterson AFB, Ohio.</p> <p>Rpt. No. ASD-TDR-63-635. THORIUM OXIDE-DIFFUSION OF OXYGEN, COMPATIBILITY WITH BORIDES, AND FEASIBILITY OF COATING BORIDES BY PYROHYDROLYSIS OF METAL HALIDES. Final report, July 63, 142 pp. incl. illus., tables, 47 refs.</p> <p>Unclassified Report</p> <p>Measurements of self-diffusion of oxygen in ThO<sub>2</sub> were complicated by slow exchange at the surface. The measured values of the diffusion coefficient, D, range from 1.8 x 10<sup>-13</sup> cm<sup>2</sup>/sec at 800°C to 3.5 x 10<sup>-8</sup> cm<sup>2</sup>/sec at 1500°C. The rate constant of the surface reaction, K, ranged from 6.8 x 10<sup>-10</sup> cm/sec at 800°C to 1.3 x 10<sup>-4</sup> cm/sec at 1500°C. The results may be expressed by equations in the form of</p> <p><math>D = 4.4 \exp (-65,800/RT) \text{ cm}^2/\text{sec}</math> and</p> <p><math>K = 7.6 \times 10^3 \exp (-63,800/RT) \text{ cm}/\text{sec}.</math></p> <p>( over )</p>	<p>1. Thoria</p> <p>2. Coating studies</p> <p>3. Diffusion studies</p> <p>4. High-temperature compatibility</p> <p>I. AFSC Project 7350, Task 735001</p> <p>II. Contract No. AF 33 (657)-8470</p> <p>III. General Electric Co., Nuclear Materials and Propulsion Operation, Evendale, Ohio</p> <p>IV. H. S. Edwards, A. F. Rosenbergs, and J. T. Bittel</p> <p>V. AVAL fr OTS</p> <p>VI. In ASTIA collection</p>	<p>Aeronautical Systems Division, AF Materials Laboratory, Metals &amp; Ceramics Division, Wright-Patterson AFB, Ohio.</p> <p>Rpt. No. ASD-TDR-63-635. THORIUM OXIDE-DIFFUSION OF OXYGEN, COMPATIBILITY WITH BORIDES, AND FEASIBILITY OF COATING BORIDES BY PYROHYDROLYSIS OF METAL HALIDES. Final report, July 63, 142 pp. incl. illus., tables, 47 refs.</p> <p>Unclassified Report</p> <p>Measurements of self-diffusion of oxygen in ThO<sub>2</sub> were complicated by slow exchange at the surface. The measured values of the diffusion coefficient, D, range from 1.8 x 10<sup>-13</sup> cm<sup>2</sup>/sec at 800°C to 3.5 x 10<sup>-8</sup> cm<sup>2</sup>/sec at 1500°C. The rate constant of the surface reaction, K, ranged from 6.8 x 10<sup>-10</sup> cm/sec at 800°C to 1.3 x 10<sup>-4</sup> cm/sec at 1500°C. The results may be expressed by equations in the form of</p> <p><math>D = 4.4 \exp (-65,800/RT) \text{ cm}^2/\text{sec}</math> and</p> <p><math>K = 7.6 \times 10^3 \exp (-63,800/RT) \text{ cm}/\text{sec}.</math></p> <p>( over )</p>
<p>Attempts to deposit dense impervious layers of ThO<sub>2</sub> on selected solid borides by pyrohydrolysis of ThCl<sub>4</sub> were essentially unsuccessful. The main problem was attack of the borides by CO<sub>2</sub> in the coating gas. The pyrohydrolysis technique might prove to be an economical way to build up a coating of ThO<sub>2</sub> that had been started by another method.</p> <p>The commercially available boride samples which were tested reacted with ThO<sub>2</sub> at temperatures in the range 2400° to 2600°C. The boride samples also reacted with graphite in the temperature range of 2400° to 2700°C. Because of these reactions, a graphite-boride-thoria system will be useful for only limited times at temperatures above 2400°C. While pure borides were not investigated, it is expected that their behavior would be similar to that of the commercial samples examined in this work.</p>	<p>Attempts to deposit dense impervious layers of ThO<sub>2</sub> on selected solid borides by pyrohydrolysis of ThCl<sub>4</sub> were essentially unsuccessful. The main problem was attack of the borides by CO<sub>2</sub> in the coating gas. The pyrohydrolysis technique might prove to be an economical way to build up a coating of ThO<sub>2</sub> that had been started by another method.</p> <p>The commercially available boride samples which were tested reacted with ThO<sub>2</sub> at temperatures in the range 2400° to 2600°C. The boride samples also reacted with graphite in the temperature range of 2400° to 2700°C. Because of these reactions, a graphite-boride-thoria system will be useful for only limited times at temperatures above 2400°C. While pure borides were not investigated, it is expected that their behavior would be similar to that of the commercial samples examined in this work.</p>	<p>Attempts to deposit dense impervious layers of ThO<sub>2</sub> on selected solid borides by pyrohydrolysis of ThCl<sub>4</sub> were essentially unsuccessful. The main problem was attack of the borides by CO<sub>2</sub> in the coating gas. The pyrohydrolysis technique might prove to be an economical way to build up a coating of ThO<sub>2</sub> that had been started by another method.</p> <p>The commercially available boride samples which were tested reacted with ThO<sub>2</sub> at temperatures in the range 2400° to 2600°C. The boride samples also reacted with graphite in the temperature range of 2400° to 2700°C. Because of these reactions, a graphite-boride-thoria system will be useful for only limited times at temperatures above 2400°C. While pure borides were not investigated, it is expected that their behavior would be similar to that of the commercial samples examined in this work.</p>	<p>Attempts to deposit dense impervious layers of ThO<sub>2</sub> on selected solid borides by pyrohydrolysis of ThCl<sub>4</sub> were essentially unsuccessful. The main problem was attack of the borides by CO<sub>2</sub> in the coating gas. The pyrohydrolysis technique might prove to be an economical way to build up a coating of ThO<sub>2</sub> that had been started by another method.</p> <p>The commercially available boride samples which were tested reacted with ThO<sub>2</sub> at temperatures in the range 2400° to 2600°C. The boride samples also reacted with graphite in the temperature range of 2400° to 2700°C. Because of these reactions, a graphite-boride-thoria system will be useful for only limited times at temperatures above 2400°C. While pure borides were not investigated, it is expected that their behavior would be similar to that of the commercial samples examined in this work.</p>



1. Thoria
2. Coating studies
3. Diffusion studies
4. High-temperature compatibility
- I. AFSC Project 7350, Task 735001
- II. Contract No. AF 33 (657)-8470
- III. General Electric Co., Nuclear Materials and Propulsion Operation, Evendale, Ohio
- IV. H. S. Edwards, A. F. Rosenberg, and J. T. Bittel
- V. Avail fr OTS
- VI. In ASTIA collection

Aeronautical Systems Division, AF Materials Laboratory, Metals & Ceramics Division, Wright-Patterson AFB, Ohio.  
Rpt. No. ASD-TDR-63-635. THORIUM OXIDE-DIFFUSION OF OXYGEN, COMPATIBILITY WITH BORIDES, AND FEASIBILITY OF COATING BORIDES BY PYROLYSIS OF METAL HALIDES. Final report, July 63, 142 pp. incl. illus., tables, 47 refs.

Unclassified Report  
Measurements of self-diffusion of oxygen in ThO<sub>2</sub> were complicated by slow exchange at the surface. The measured values of the diffusion coefficient, D, range from 1.8 x 10<sup>-13</sup> cm<sup>2</sup>/sec at 800°C to 3.5 x 10<sup>-8</sup> cm<sup>2</sup>/sec at 1500°C. The rate constant of the surface reaction, K, ranged from 6.8 x 10<sup>-10</sup> cm/sec at 800°C to 1.3 x 10<sup>-4</sup> cm/sec at 1500°C. The results may be expressed by equations in the form of  $D = 4.4 \exp(-65,800/RT) \text{ cm}^2/\text{sec}$  and  $K = 7.6 \times 10^3 \exp(-63,800/RT) \text{ cm}/\text{sec}$ .

( over )

Attempts to deposit dense impervious layers of ThO<sub>2</sub> on selected solid borides by pyrohydrolysis of ThCl<sub>4</sub> were essentially unsuccessful. The main problem was attack of the borides by CO<sub>2</sub> in the coating gas. The pyrohydrolysis technique might prove to be an economical way to build up a coating of ThO<sub>2</sub> that had been started by another method.

The commercially available boride samples which were tested reacted with ThO<sub>2</sub> at temperatures in the range 2400° to 2600°C. The boride samples also reacted with graphite in the temperature range of 2400° to 2700°C. Because of these reactions, a graphite-boride-thoria system will be useful for only limited times at temperatures above 2400°C. While pure borides were not investigated, it is expected that their behavior would be similar to that of the commercial samples examined in this work.

1. Thoria
2. Coating studies
3. Diffusion studies
4. High-temperature compatibility
- I. AFSC Project 7350, Task 735001
- II. Contract No. AF 33 (657)-8470
- III. General Electric Co., Nuclear Materials and Propulsion Operation, Evendale, Ohio
- IV. H. S. Edwards, A. F. Rosenberg, and J. T. Bittel
- V. Avail fr OTS
- VI. In ASTIA collection

Aeronautical Systems Division, AF Materials Laboratory, Metals & Ceramics Division, Wright-Patterson AFB, Ohio.  
Rpt. No. ASD-TDR-63-635. THORIUM OXIDE-DIFFUSION OF OXYGEN, COMPATIBILITY WITH BORIDES, AND FEASIBILITY OF COATING BORIDES BY PYROLYSIS OF METAL HALIDES. Final report, July 63, 142 pp. incl. illus., tables, 47 refs.

Unclassified Report  
Measurements of self-diffusion of oxygen in ThO<sub>2</sub> were complicated by slow exchange at the surface. The measured values of the diffusion coefficient, D, range from 1.8 x 10<sup>-13</sup> cm<sup>2</sup>/sec at 800°C to 3.5 x 10<sup>-8</sup> cm<sup>2</sup>/sec at 1500°C. The rate constant of the surface reaction, K, ranged from 6.8 x 10<sup>-10</sup> cm/sec at 800°C to 1.3 x 10<sup>-4</sup> cm/sec at 1500°C. The results may be expressed by equations in the form of  $D = 4.4 \exp(-65,800/RT) \text{ cm}^2/\text{sec}$  and  $K = 7.6 \times 10^3 \exp(-63,800/RT) \text{ cm}/\text{sec}$ .

( over )

Attempts to deposit dense impervious layers of ThO<sub>2</sub> on selected solid borides by pyrohydrolysis of ThCl<sub>4</sub> were essentially unsuccessful. The main problem was attack of the borides by CO<sub>2</sub> in the coating gas. The pyrohydrolysis technique might prove to be an economical way to build up a coating of ThO<sub>2</sub> that had been started by another method.

The commercially available boride samples which were tested reacted with ThO<sub>2</sub> at temperatures in the range 2400° to 2600°C. The boride samples also reacted with graphite in the temperature range of 2400° to 2700°C. Because of these reactions, a graphite-boride-thoria system will be useful for only limited times at temperatures above 2400°C. While pure borides were not investigated, it is expected that their behavior would be similar to that of the commercial samples examined in this work.

<p>Aeronautical Systems Division, AF Materials Laboratory, Metals &amp; Ceramics Division, Wright-Patterson AFB, Ohio.</p> <p>Rpt. No. ASD-TDR-63-635. THORIUM OXIDE-DIFFUSION OF OXYGEN, COMPATIBILITY WITH BORIDES, AND FEASIBILITY OF COATING BORIDES BY PYROHYDROLYSIS OF METAL HALIDES. Final report, July 63, 142 pp. incl. illus., tables, 47 refs.</p> <p>Unclassified Report</p> <p>Measurements of self-diffusion of oxygen in ThO<sub>2</sub> were complicated by slow exchange at the surface. The measured values of the diffusion coefficient, D, range from <math>1.8 \times 10^{-13}</math> cm<sup>2</sup>/sec at 800°C to <math>3.5 \times 10^{-3}</math> cm<sup>2</sup>/sec at 1500°C. The rate constant of the surface reaction, K, ranged from <math>6.8 \times 10^{-10}</math> cm/sec at 800°C to <math>1.3 \times 10^{-4}</math> cm/sec at 1500°C. The results may be expressed by equations in the form of <math>D = 4.4 \exp(-65,800/RT)</math> cm<sup>2</sup>/sec and <math>K = 7.6 \times 10^3 \exp(-63,800/RT)</math> cm/sec.</p>	<p>1. Thoria</p> <p>2. Coating studies</p> <p>3. Diffusion studies</p> <p>4. High-temperature compatibility</p> <p>I. AFSC Project 7350, Task 735001</p> <p>II. Contract No. AF 33 (657)-8470</p> <p>III. General Electric Co., Nuclear Materials and Propulsion Operation, Evendale, Ohio</p> <p>IV. H. S. Edwards, A. F. Rosenbergs, and J. T. Bittel</p> <p>V. Aval fr OTS</p> <p>VI. In ASTIA collection</p>	<p>1. Thoria</p> <p>2. Coating studies</p> <p>3. Diffusion studies</p> <p>4. High-temperature compatibility</p> <p>I. AFSC Project 7350, Task 735001</p> <p>II. Contract No. AF 33 (657)-8470</p> <p>III. General Electric Co., Nuclear Materials and Propulsion Operation, Evendale, Ohio</p> <p>IV. H. S. Edwards, A. F. Rosenbergs, and J. T. Bittel</p> <p>V. Aval fr OTS</p> <p>VI. In ASTIA collection</p>	<p>Attempts to deposit dense impervious layers of ThO<sub>2</sub> on selected solid borides by pyrohydrolysis of ThCl<sub>4</sub> were essentially unsuccessful. The main problem was attack of the borides by CO<sub>2</sub> in the coating gas. The pyrohydrolysis technique might prove to be an economical way to build up a coating of ThO<sub>2</sub> that had been started by another method.</p> <p>The commercially available boride samples which were tested reacted with ThO<sub>2</sub> at temperatures in the range 2400° to 2600°C. The boride samples also reacted with graphite in the temperature range of 2400° to 2700°C. Because of these reactions, a graphite-boride-thoria system will be useful for only limited times at temperatures above 2400°C. While pure borides were not investigated, it is expected that their behavior would be similar to that of the commercial samples examined in this work.</p>	<p>Attempts to deposit dense impervious layers of ThO<sub>2</sub> on selected solid borides by pyrohydrolysis of ThCl<sub>4</sub> were essentially unsuccessful. The main problem was attack of the borides by CO<sub>2</sub> in the coating gas. The pyrohydrolysis technique might prove to be an economical way to build up a coating of ThO<sub>2</sub> that had been started by another method.</p> <p>The commercially available boride samples which were tested reacted with ThO<sub>2</sub> at temperatures in the range 2400° to 2600°C. The boride samples also reacted with graphite in the temperature range of 2400° to 2700°C. Because of these reactions, a graphite-boride-thoria system will be useful for only limited times at temperatures above 2400°C. While pure borides were not investigated, it is expected that their behavior would be similar to that of the commercial samples examined in this work.</p>	<p>( over )</p>	<p>( over )</p>
--	--	--	--	--	-----------------	-----------------



1. Thoria
2. Coating studies
3. Diffusion studies
4. High-temperature compatibility
- I. AFSC Project 7350, Task 735001
- II. Contract No. AF 33 (657)-9470
- III. General Electric Co., Nuclear Materials and Propulsion Operation, Evendale, Ohio
- IV. H. S. Edwards, A. F. Rosenberg, and J. T. Bittel
- V. Aval fr OTS
- VI. In ASTIA collection

Aeronautical Systems Division, AF Materials Laboratory, Metals & Ceramics Division, Wright-Patterson AFB, Ohio.  
Rpt. No. ASD-TDR-63-635. THORIUM OXIDE-DIFFUSION OF OXYGEN, COMPATIBILITY WITH BORIDES, AND FEASIBILITY OF COATING BORIDES BY PYROLYSIS OF METAL HALIDES. Final report, July 63, 142 pp. Incl. illus., tables, 47 refs.

Unclassified Report  
Measurements of self-diffusion of oxygen in ThO<sub>2</sub> were complicated by slow exchange at the surface. The measured values of the diffusion coefficient, D, range from  $1.8 \times 10^{-13}$  cm<sup>2</sup>/sec at 800°C to  $3.5 \times 10^{-3}$  cm<sup>2</sup>/sec at 1500°C. The rate constant of the surface reaction, K, ranged from  $6.8 \times 10^{-10}$  cm/sec at 800°C to  $1.3 \times 10^{-4}$  cm/sec at 1500°C. The results may be expressed by equations in the form of  $D = 4.4 \exp (-65,800/RT)$  cm<sup>2</sup>/sec and  $K = 7.6 \times 10^3 \exp (-63,800/RT)$  cm/sec.

( over )

Attempts to deposit dense impervious layers of ThO<sub>2</sub> on selected solid borides by pyrohydrolysis of ThCl<sub>4</sub> were essentially unsuccessful. The main problem was attack of the borides by CO<sub>2</sub> in the coating gas. The pyrohydrolysis technique might prove to be an economical way to build up a coating of ThO<sub>2</sub> that had been started by another method.

The commercially available boride samples which were tested reacted with ThO<sub>2</sub> at temperatures in the range 2400° to 2600°C. The boride samples also reacted with graphite in the temperature range of 2400° to 2700°C. Because of these reactions, a graphite-boride-thoria system will be useful for only limited times at temperatures above 2400°C. While pure borides were not investigated, it is expected that their behavior would be similar to that of the commercial samples examined in this work.

Aeronautical Systems Division, AF Materials Laboratory, Metals & Ceramics Division, Wright-Patterson AFB, Ohio.  
Rpt. No. ASD-TDR-63-635. THORIUM OXIDE-DIFFUSION OF OXYGEN, COMPATIBILITY WITH BORIDES, AND FEASIBILITY OF COATING BORIDES BY PYROLYSIS OF METAL HALIDES. Final report, July 63, 142 pp. Incl. illus., tables, 47 refs.

Unclassified Report  
Measurements of self-diffusion of oxygen in ThO<sub>2</sub> were complicated by slow exchange at the surface. The measured values of the diffusion coefficient, D, range from  $1.8 \times 10^{-13}$  cm<sup>2</sup>/sec at 800°C to  $3.5 \times 10^{-3}$  cm<sup>2</sup>/sec at 1500°C. The rate constant of the surface reaction, K, ranged from  $6.8 \times 10^{-10}$  cm/sec at 800°C to  $1.3 \times 10^{-4}$  cm/sec at 1500°C. The results may be expressed by equations in the form of  $D = 4.4 \exp (-65,800/RT)$  cm<sup>2</sup>/sec and  $K = 7.6 \times 10^3 \exp (-63,800/RT)$  cm/sec.

( over )

Attempts to deposit dense impervious layers of ThO<sub>2</sub> on selected solid borides by pyrohydrolysis of ThCl<sub>4</sub> were essentially unsuccessful. The main problem was attack of the borides by CO<sub>2</sub> in the coating gas. The pyrohydrolysis technique might prove to be an economical way to build up a coating of ThO<sub>2</sub> that had been started by another method.

The commercially available boride samples which were tested reacted with ThO<sub>2</sub> at temperatures in the range 2400° to 2600°C. The boride samples also reacted with graphite in the temperature range of 2400° to 2700°C. Because of these reactions, a graphite-boride-thoria system will be useful for only limited times at temperatures above 2400°C. While pure borides were not investigated, it is expected that their behavior would be similar to that of the commercial samples examined in this work.

1. Thoria
2. Coating studies
3. Diffusion studies
4. High-temperature compatibility
- I. AFSC Project 7350, Task 735001
- II. Contract No. AF 33 (657)-9470
- III. General Electric Co., Nuclear Materials and Propulsion Operation, Evendale, Ohio
- IV. H. S. Edwards, A. F. Rosenberg, and J. T. Bittel
- V. Aval fr OTS
- VI. In ASTIA collection

Aeronautical Systems Division, AF Materials Laboratory, Metals & Ceramics Division, Wright-Patterson AFB, Ohio.  
Rpt. No. ASD-TDR-63-635. THORIUM OXIDE-DIFFUSION OF OXYGEN, COMPATIBILITY WITH BORIDES, AND FEASIBILITY OF COATING BORIDES BY PYROLYSIS OF METAL HALIDES. Final report, July 63, 142 pp. Incl. illus., tables, 47 refs.  
Unclassified Report  
Measurements of self-diffusion of oxygen in ThO<sub>2</sub> were complicated by slow exchange at the surface. The measured values of the diffusion coefficient, D, range from  $1.8 \times 10^{-13}$  cm<sup>2</sup>/sec at 800°C to  $3.5 \times 10^{-5}$  cm<sup>2</sup>/sec at 1500°C. The rate constant of the surface reaction, K, ranged from  $6.8 \times 10^{-10}$  cm/sec at 800°C to  $1.3 \times 10^{-4}$  cm/sec at 1500°C. The results may be expressed by equations in the form of  $D = 4.4 \exp(-65,800/RT)$  cm<sup>2</sup>/sec and  $K = 7.6 \times 10^3 \exp(-63,800/RT)$  cm/sec.

( over )

Attempts to deposit dense impervious layers of ThO<sub>2</sub> on selected solid borides by pyrohydrolysis of ThCl<sub>4</sub> were essentially unsuccessful. The main problem was attack of the borides by CO<sub>2</sub> in the coating gas. The pyrohydrolysis technique might prove to be an economical way to build up a coating of ThO<sub>2</sub> that had been started by another method.

The commercially available boride samples which were tested reacted with ThO<sub>2</sub> at temperatures in the range 2400° to 2600°C. The boride samples also reacted with graphite in the temperature range of 2400° to 2700°C. Because of these reactions, a graphite-boride-thoria system will be useful for only limited times at temperatures above 2400°C. While pure borides were not investigated, it is expected that their behavior would be similar to that of the commercial samples examined in this work.

1. Thoria  
2. Coating studies  
3. Diffusion studies  
4. High-temperature compatibility  
I. AFSC Project 7350, Task 735001  
Contract No. AF 33 (657)-0470  
III. General Electric Co., Nuclear Materials and Propulsion Operation, Evendale, Ohio  
IV. H. S. Edwards, A. F. Rosenberg, and J. T. Bittel  
V. Aval fr OTS  
VI. In ASTIA collection

Aeronautical Systems Division, AF Materials Laboratory, Metals & Ceramics Division, Wright-Patterson AFB, Ohio.  
Rpt. No. ASD-TDR-63-635. THORIUM OXIDE-DIFFUSION OF OXYGEN, COMPATIBILITY WITH BORIDES, AND FEASIBILITY OF COATING BORIDES BY PYROLYSIS OF METAL HALIDES. Final report, July 63, 142 pp. Incl. illus., tables, 47 refs.  
Unclassified Report  
Measurements of self-diffusion of oxygen in ThO<sub>2</sub> were complicated by slow exchange at the surface. The measured values of the diffusion coefficient, D, range from  $1.8 \times 10^{-13}$  cm<sup>2</sup>/sec at 800°C to  $3.5 \times 10^{-5}$  cm<sup>2</sup>/sec at 1500°C. The rate constant of the surface reaction, K, ranged from  $6.8 \times 10^{-10}$  cm/sec at 800°C to  $1.3 \times 10^{-4}$  cm/sec at 1500°C. The results may be expressed by equations in the form of  $D = 4.4 \exp(-65,800/RT)$  cm<sup>2</sup>/sec and  $K = 7.6 \times 10^3 \exp(-63,800/RT)$  cm/sec.

( over )

Attempts to deposit dense impervious layers of ThO<sub>2</sub> on selected solid borides by pyrohydrolysis of ThCl<sub>4</sub> were essentially unsuccessful. The main problem was attack of the borides by CO<sub>2</sub> in the coating gas. The pyrohydrolysis technique might prove to be an economical way to build up a coating of ThO<sub>2</sub> that had been started by another method.

The commercially available boride samples which were tested reacted with ThO<sub>2</sub> at temperatures in the range 2400° to 2600°C. The boride samples also reacted with graphite in the temperature range of 2400° to 2700°C. Because of these reactions, a graphite-boride-thoria system will be useful for only limited times at temperatures above 2400°C. While pure borides were not investigated, it is expected that their behavior would be similar to that of the commercial samples examined in this work.

1. Thoria  
2. Coating studies  
3. Diffusion studies  
4. High-temperature compatibility  
I. AFSC Project 7350, Task 735001  
Contract No. AF 33 (657)-0470  
III. General Electric Co., Nuclear Materials and Propulsion Operation, Evendale, Ohio  
IV. H. S. Edwards, A. F. Rosenberg, and J. T. Bittel  
V. Aval fr OTS  
VI. In ASTIA collection